Theses and Dissertations

Theses, Dissertations, and Senior Projects

January 2016

Effect Of Silica Supported Platinum Catalyst On The Performance And Durability Of PEM Fuel Cells

Jivan N. Thakare

Follow this and additional works at: https://commons.und.edu/theses

EFFECT OF SILICA SUPPORTED PLATINUM CATALYST ON THE
PERFORMANCE AND DURABILITY OF PEM FUEL CELLS

By

Jivan N Thakare

B.S. in Polymer Technology, Amravati University, India, 2002

M. S. in Chemical Engineering, Texas A&M University, Kingsville, USA, 2009

A Dissertation

Submitted to the Graduate Faculty

of the

University of North Dakota

in partial fulfillment of the requirements

for the degree of

Doctor of Philosophy

Grand Forks, North Dakota

August

2016

This dissertation, submitted by Jivan N Thakare in partial fulfillment of the requirements for the Degree of Doctor of Philosophy from the University of North Dakota, has been read by the Faculty Advisory Committee under whom the work has been done and is hereby approved.

Dr. Michael Mann, Chairperson
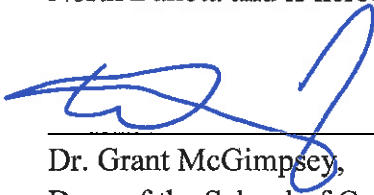
Dr. Brian Tande

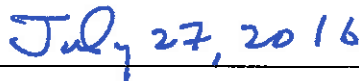Dr. Frank Bowman

Dr. Hossein Salehfar

Dr. Julia Zhao

This dissertation is being submitted by the appointed advisory committee as having met all of the requirements of the School of Graduate Studies at the University of North Dakota and is hereby approved.

Dr. Grant McGimpsey,
Dean of the School of Graduate Studies

July 27, 2016

Date

iii

PERMISSION

Title	Effect of Silica Supported Platinum Catalyst on the Performance and Durability of PEM Fuel Cells
Department	Chemical Engineering
Degree	Doctor of Philosophy

In presenting this dissertation in partial fulfillment of the requirements for a graduate degree from the University of North Dakota, I agree that the library of this University shall make it freely available for inspection. I further agree that permission for extensive copying for scholarly purposes may be granted by the professor who supervised my dissertation work or, in their absence, by the chairperson of the department or the dean of the School of Graduate Studies. It is understood that any copying or publication or other use of this dissertation or part thereof for financial gain shall not be allowed without my written permission. It is also understood that due recognition shall be given to me and to the University of North Dakota in any scholarly use which may be made of any material in my dissertation.

Name: Jivan N Thakare

Date: 20th July 2016

iv

TABLE OF CONTENTS

LIST OF FIGURES

xv

xvi

LIST OF TABLES

NOMENCLATURE

Abbreviations	
3-D	Three-dimensional
AFC	Alkaline Fuel Cell
ARH	Anode Side Relative Humidity
AST	Accelerated Stress Tests
CCG	Catalyst Coated GDL
CCM	Catalyst Coated Membrane
CCM-DS	Catalyst Coated Membrane - Direct Wet-Spray
CCM-DS	Catalyst Coated Membrane - Decal Transfer Technique
CE	Counter Electrode
CHP	Combined Heat and Power
CO_2	Carbon Dioxide
CRH	Cathode Side Relative Humidity
CV	Cyclic Voltammetry
DHE	Dynamic Hydrogen Electrode
DI	Deionized
DMFC	Direct Methanol Fuel Cell
DOE	Department of Energy
ECASA	Electrochemical Active Surface Area
EPDM	Ethylene Propylene Diene Monomer

EW	Equivalent Weight
FC	Fuel Cell
GDE	Gas Diffusion Electrode
GDL	Gas Diffusion Layer
GDM	Gas Diffusion Media
H_2	Hydrogen
H_2O	Water
H_2O_2	Hydrogen Peroxide
HOR	Hydrogen Oxidation Reaction
ICE	Internal Combustion Engine
In-situ	Experiments that are performed in a unit-cell PEMFC
IPA	Isopropyl Alcohol
IV Test	Polarization Test
MCFC	Molten Carbonate Fuel Cell
MEA	Membrane Electrode Assembly
MPL	Microporous Layer
N_2	Nitrogen
N-115	Nafion 115
NBA	Normal Butyl Acetate
NFP	Nafion Percentage
NP	Nanoparticle
O_2	Oxygen

OCV	Open Circuit Voltage
ORR	Oxygen Reduction Reaction
PAFC	Phosphoric Acid Fuel Cell
PEM	Polymer Electrolyte Membrane
	Proton Exchange Membrane
PEMFC	Polymer Electrolyte Membrane Fuel Cell
	Proton Exchange Membrane Fuel Cell
PFSA	Perfluorosulphonic Acid
PGM	Platinum Group Metal
Pt	Platinum Catalyst
Pt/Carbon	Carbon-Supported Platinum Catalyst
Pt/Silica	Silica Supported Platinum Catalyst
PTFE	Poly Tetra Fluoro Ethylene
RE	Reference Electrode
RH	Relative Humidity
RHE	Reversible Hydrogen Electrode
rpm	Rotation Per Minute
Ru	Ruthenium
SEM	Scanning Electron Microscopy
SHE	Standard Hydrogen Electrode
SOFC	Solid Oxide Fuel Cell
TEOS	Tetraethylorthosilicate

Type-A MEA	In-house fabricated MEA with commercial Pt/Carbon Catalyst	
Type-B MEA	In-house fabricated MEA with commercial Pt/Silica Catalyst	
Type-BB MEA	In-house fabricated MEA with "Pt/Silica + Carbon Powder" Catalyst	
Type-C MEA	Commercial MEA with Pt/Carbon Catalyst	
UND	University of North Dakota	
WE	Working Electrode	
XRF	X-Ray Fluorescence	
ZRA	Zero Resistance Ammeter	
Symbols		
A_{CL}	Area of the catalyst layer or active area of MEA	cm^2
A_S	Specific activity of the catalyst	$A/m^2{}_{Pt}$
A_w	Catalyst mass activity	A/mg_{pt}
$i_{0.9}$	Current density in A/cm^2 at 0.9 V	A/cm^2
L_{Naf}	Fraction of Nafion in the catalyst per gram of catalyst	%
Ld_{Carbon}	Carbon Loading	%
Ld_{Pt}	Actual Pt loading in the catalyst layer of an MEA	mg/cm^2
$Ld_{Targeted}$	Targeted Pt loading in the catalyst layer of an MEA	mg/cm^2
M_{Cat}	Mass of catalyst in the ink	mg
M_{GDE}	Actual weight of GDE after over drying	mg
M_{GDL}	Actual weight of GDL after over drying	mg
M_{Naf}	Mass of Nafion ionomer in the ink	%

M_{Pt}	The amount of catalyst	mg
$T_{Humidifier}$	Humidifier Temperature	°C
T_{cell}	Cell Temperature	°C
W_{Pt}	Mass fraction of Pt catalyst in the catalyst	%
λ	Stoichiometric ratio	-

ACKNOWLEDGEMENTS

It is my pleasure and honor to express my sincere gratitude to all who inspired me and supported, and contributed either directly or indirectly during my doctoral study and made this dissertation possible.

First, I would like to express my deepest gratitude to my advisor, Dr. Michael Mann, for his constant encouragement, excellent guidance, and patience. This work would not have been possible without his support. I am forever grateful to him for shaping me into the scientific researcher that I am today. I would like to express my deepest gratitude to all my advisory committee members Dr. Brian Tande, Dr. Frank Bowmen, Dr. Hossein Salehfar and Dr. Julia Zhao, for taking the precious time to serve on my committee and for their guidance and support during the completion of this dissertation.

I am most grateful to Dr. Aize Li (former graduate student, Chemistry Department, UND) and Nenny Fahruddin (former research assistant, Chemistry Department, UND) for the development and fabrication of the Pt/Silica catalyst. Without their help, this work would not have been completed. I want to thank my former labmates, Dr. Samir Dahal and Dr.Tahee Han for their friendship, support, and assistance in the lab.

Last, I would like to thank my fellow graduate students (especially Reddy and Shankar), staff (Connie and Joe) and faculty of Chemical Engineering Department, UND for their support throughout my doctoral studies.

Dedication

This dissertation is dedicated to my beloved father

ABSTRACT

Proton exchange membrane fuel cells (PEMFCs) have a unique property of zero (ultra-low) emission and provide significant technical and overall cost advantages compared to other types of fuel cells. As a result, PEMFCs have attracted considerable attention as an alternative power source for stationary and mobile applications. However, the PEMFCs are yet to realize mass-market commercialization hindered mainly by its poor durability. Therefore, numerous research efforts have been devoted to studying the durability of PEMFCs, motivated by the desire to improve its lifetime without unduly increasing cost or compromising performance.

The catalyst support largely determines the stability of supported platinum group metal (PGM) catalysts, overall electrochemical activity and durability of the catalyst layer in PEMFCs. This research was motivated by the desire to improve the stability and durability of the PEMFCs by utilizing the novel silica supported platinum (Pt/Silica) catalyst support. The purpose of this study was to develop a membrane electrode assembly (MEA) from Pt/Silica catalyst and to investigate/analyze the effects of Pt/Silica on the performance and durability of PEMFC. The primary hypothesis of this work is that *the Pt/Silica catalyst would enhance the performance and durability of PEMFCs compared to state $-$ of $-$ the $-$ art carbon-supported platinum (*Pt/Carbon)* catalysts.

In this dissertation work, two types of MEA's were prepared using a hot-pressed GDE method. Type-A MEA was prepared using a $state-of-the-art$ Pt/Carbon commercial catalyst and serve as a baseline MEA. Type-B MEA was prepared using novel Pt/Silica in-house fabricated catalyst, and was used as the basis to prove the hypothesis of this work. Finally, the MEA prepared during this research work were mounted in a 25 cm^2 unit-cell PEMFC fixture for its $in-situ$ evaluation. The evaluation of both of Type-A and Type-B MEA was performed using Polarization (IV) and Cyclic Voltammetry (CV) electrochemical techniques. The performance and durability data was then compared to test the hypothesis of this research.

The maximum power density of Pt/Silica catalyst was found to be 52 % of the commercial Pt/Carbon catalyst under the identical experimental setup and operating conditions. Similar results were demonstrated in CV testing, where the calculated ECASA of Pt/Silica catalyst was found to be 75 % of the commercial Pt/Carbon catalyst. Electrode flooding and low conductivity of silica support were experimentally found as the cause of the reduced performance of the Pt/Silica catalyst. When operated under conditions to eliminate flooding for Pt/Silica, its performance improved, with its maximum power density found to be 62 % of the commercial Pt/Carbon catalyst. When operated under the conditions to eliminate flooding for Pt/Silica, its performance improved, with its maximum power density found to be 62 % of the commercial Pt/Carbon catalyst. When the conductivity of Pt/Silica-based MEA was improved by adding carbon black in the catalyst ink, and operated under the conditions to eliminate

flooding for Pt/Silica, its performance improved, with its maximum power density found to be 82 % of the commercial Pt/Carbon catalyst.

The durability study showed that the loss in ECASA of the novel Pt/Silica catalyst at the end of the 24-hour potential hold test was 27 % from its baseline condition. The corresponding loss in commercial Pt/Carbon catalyst was found to be 55 %. The Pt/Carbon catalyst deterioration was also more severe during 10,000-cycle potential cycling durability test compared to the baseline ECASA. The Pt/Carbon catalyst was able to retain only 27 % of the active Pt surface area compared to 68 % retained by the Pt/Silica catalyst after the 10,000-cycle test.

CHAPTER 1

INTRODUCTION

The chapter starts with a background of fuel cells and its types, followed by a detailed description of the polymer electrolyte membrane fuel cells (PEMFCs) with its components and operating principle.

1.1   General Background

Ever-increasing energy consumption, growing awareness of the need for environmental protection and the existing nature of fossil fuel has given rise to significant research efforts focused on alternative/renewable energy sources. Electrochemical cells are one of the most practical candidates for the next generation, cleaner, and potentially fossil fuel independent energy source.

Electrochemical cells are the devices that can convert chemical energy directly into electrical energy at high efficiency and without combustion (A. V. D. Rosa, 2009). Since electrochemical cells work on an electrochemical principle, to convert chemical energy directly into electrical energy without the intermediate degradation into heat, electrochemical cells are not restricted by the Carnot efficiency (Cengel & Boles, 2006). As a result, electrochemical cells can achieve higher efficiency than the energy source limited by the Carnot efficiency such as an internal combustion engine (ICE). The

1

traditional ICE converts chemical energy to thermal energy; this heat is then converted to mechanical energy and then to electrical energy by complex machinery (Barbir, 2005). Since energy conversions of the electrochemical type bypass cumbersome and inefficient steps, they yield both significantly higher efficiency (~60%) and environmentally safer by-products (only water when pure hydrogen is used as fuel, CO_2 and water, when hydrocarbon fuels are used) compared to the current combustion technologies (Minh & Takahashi, 1995). The comparison of energy conversion pathways between electrochemical cells and ICE is illustrated in Figure 1-1.
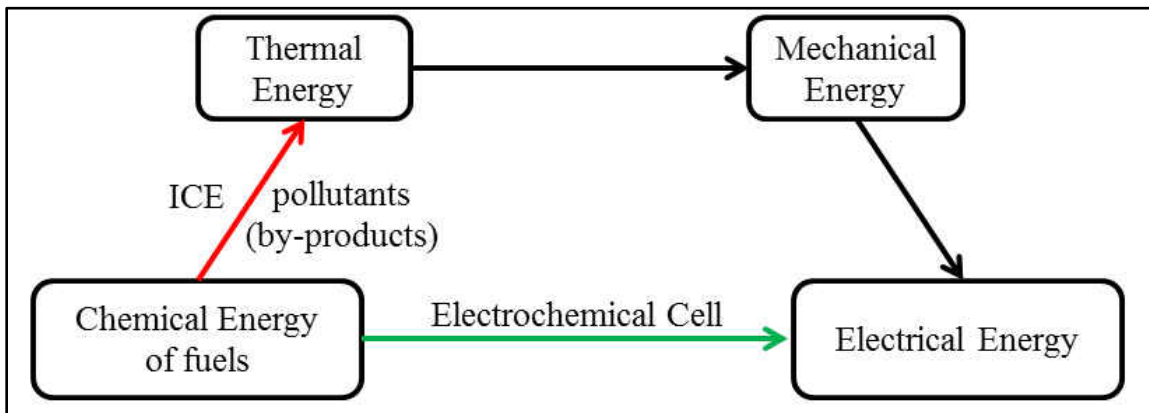
Figure 1-1 A comparison of energy conversion pathways between Electrochemical Cell and an Internal Combustion Engine (ICE)

Electrochemical cells are broadly categorized as expendable or nonexpendable; the former cannot be preserved after its first discharge while the latter is considered as reusable. The non-expendable cells can be further sub-categorized as either rechargeable (battery), i.e., an electrical charging can restore their activity, or refuelable (fuel cells), which deliver a sustained output (A. V. D. Rosa, 2009).

Fuel cells produce electricity via an electrochemical reaction like that of a battery, but unlike batteries, fuel cells use a continuous supply of fuel from an external storage

2

tank. Fuel cell systems have the potential to deal with the most challenging problems associated with the now existing battery systems, namely their insufficient energy at a given weight (specific energy density) or volume (volumetric energy density).

A fuel cell is an old innovation, but for a long time, it was hardly more than a curiosity in the field of energy technology. However, several fundamental technological breakthroughs have been achieved during the past two decades, and fuel cells are now rapidly approaching commercialization in many applications. This development in fuel cells is catalyzed by the fact that the global energy use is increasing steadily, environmental problems related to energy production, and transportation is growing. At the same time, the efficiencies of conventional energy conversion processes are approaching their thermodynamic limits.

1.1.1 Fuel Cells

Fuel cells are energy conversion devices that convert chemical energy into electrical energy via an electrochemical reaction involving a fuel source (e.g. any hydrogen-containing gas) and an oxygen source (e.g. air, pure oxygen or some intermediate) (Minh & Takahashi, 1995). In the most basic form, a fuel cell is composed of four parts: anode, cathode, electrolyte and an external circuit. The electrolyte is sandwiched between two electrodes, e.g., anode and cathode, which are connected to an external circuit as showed in Figure 1-2. Reactions occur on either side of a semi-permeable electrolyte, where fuel is oxidized catalytically at the anode, and an oxidant is reduced at the cathode. These reactions, and the subsequent flow of ions through the

electrolyte, and electrons through an external circuit, generate electricity. Fuel cells have many unique characteristics that make them attractive (Barbir, 2005):

The promise of high efficiency: - Fuel cells are more efficient than ICE and not limited by the Carnot cycle efficiency, particularly at the low temperature. This is further explained in section 1.1.
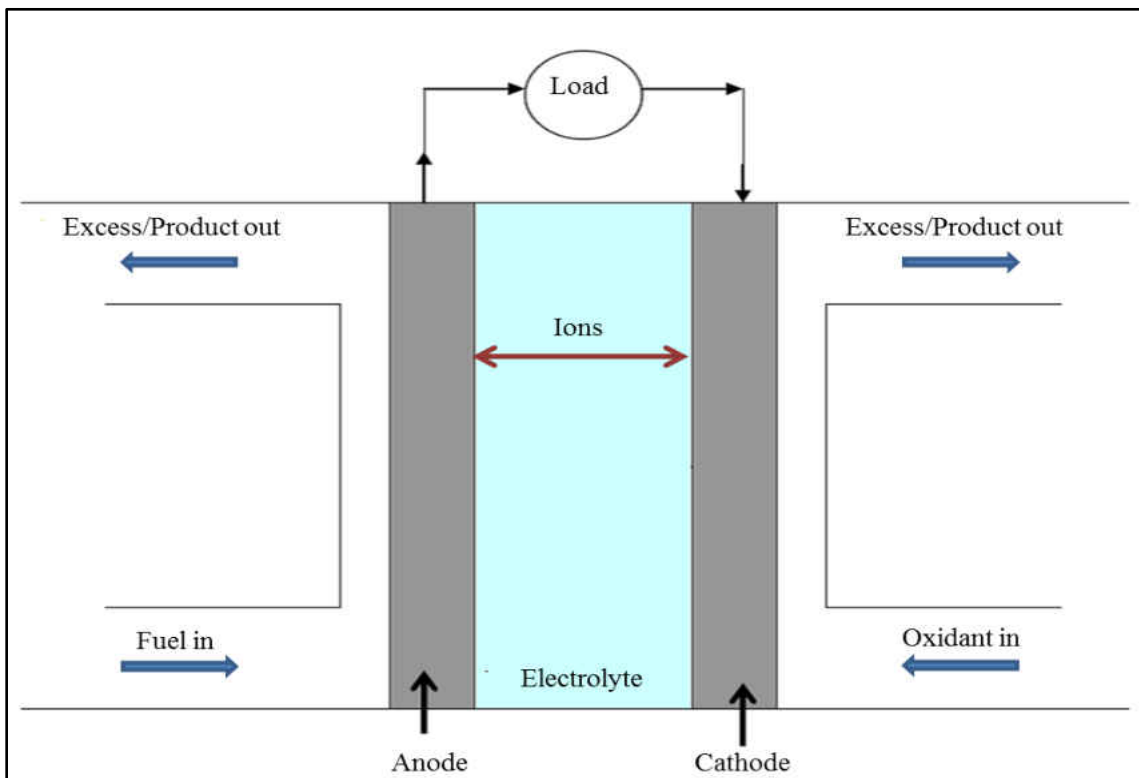
Figure 1-2 Schematic of Basic Form of a Fuel Cell

The promise of low or zero greenhouse emission: - a fuel cell operating on hydrogen generates zero emissions, and its only by-product is water. Even though hydrogen is not readily available in its pure molecular state, it can be produced using renewable sources such as electrolyzer, powered by wind turbines or solar photovoltaics.

The promise of long life: - Unlike batteries, the fuel cells are capable of producing electrical energy as long as the reactants are supplied to the electrodes.

Quiet and mechanically ideal system: - Fuel cells are mechanically ideal since they do not have moving parts. This yields the potential for a highly reliable, efficient and silent systems.

Modular: - Fuel cells can be made from microwatt to megawatt sizes. Such an advantage makes them useful in a variety of applications, from powering electronic devices to provide electricity to the grid.

1.1.2 Types of Fuel Cells

Fuel cells are commonly classified according to their ion transport medium i.e. electrolyte used in them (Kirubakaran, Jain, & Nema, 2009). The electrolyte determines the type of chemical reactions that take place in the cell, the catalysts required and the operating temperature of the cell as listed in Table 1-1. These characteristics, in turn, affect the efficiency and applications for which these cells are most suitable. There are six major types of fuel cell (U. S. D. o. E. E. E. a. R. Energy, 2011):

- Alkaline fuel cell (AFC)

- Phosphoric acid fuel cell (PAFC)

- Solid oxide fuel cell (SOFC)

- Molten carbonate fuel cell (MCFC)

- Proton exchange membrane fuel cell (PEMFC)

- Direct methanol fuel cell (DMFC)

5

Table 1-1 Types of Fuel Cells (U. S. D. o. E. E. E. a. R. Energy, 2011)

Fuel Cell	Common Electrolyte	Catalyst	Operating Temperature (°C)	Electrode Reactions
Polymer Electrolyte Membrane Fuel Cell (PEMFC)	Solid polymer membrane	Platinum is the most common	30-80	Anode: $H_2 \rightarrow 2H^+ + 2e^-$ Cathode: $\frac{1}{2}O_2 + 2H^+ + 2e^- \rightarrow H_2O$ Cell: $H_2 + \frac{1}{2}O_2 \rightarrow H_2O$
Alkaline Fuel Cell (AFC)	Potassium hydroxide solution in water	Can use non-precious metal catalysts	90-100	Anode: $H_2 + 2OH^- \rightarrow H_2O + 2e^-$ Cathode: $\frac{1}{2}O_2 + H_2O + 2e^- \rightarrow 2OH^-$ Cell: $H_2 + \frac{1}{2}O_2 \rightarrow H_2O$
Phosphoric Acid Fuel Cell (PAFC)	Liquid phosphoric acid ceramic in a lithium aluminum oxide matrix	Carbon-supported platinum catalyst	175-200	Anode: $H_2 \rightarrow 2H^+ + 2e^-$ Cathode: $\frac{1}{2}O_2 + 2H^+ + 2e^- \rightarrow H_2O$ Cell: $H_2 + \frac{1}{2}O_2 \rightarrow H_2O$
Molten Carbonate Fuel Cell (MCFC)	Alkali (Na & K) carbonates retained in a ceramic matrix of LiHO2	Lower-cost non-platinum group catalysts	600-1,000	Anode: $H_2 + CO_3{}^{2-} \rightarrow H_2O + CO_2 + 2e^-$ Cathode: $\frac{1}{2}O_2 + CO_2 + 2e^- \rightarrow CO_3{}^{2-}$ Cell: $H_2 + \frac{1}{2}O_2 + CO_2 \rightarrow H_2O + CO_2$
Solid Oxide Fuel Cells (SOFC)	A solid ceramic, typically yttria-stabilized zirconia (YSZ)	Lower-cost non-platinum group catalysts	600-1,000	Anode: $H_2 + O^{2-} \rightarrow H_2O + 2e^-$ Cathode: $\frac{1}{2}O_2 + 2e^- \rightarrow O^{2-}$ Cell: $H_2 + \frac{1}{2}O_2 \rightarrow H_2O$

Table 1-2 Overview of Different Types of Fuel Cells (U. S. D. o. E. E. a. R. Energy, 2011)

Fuel Cell Type	Combined Heat and Power (CHP) Efficiency (%)	Advantages	Disadvantages	Applications
Polymer Electrolyte Membrane Fuel Cell (PEMFC)	70-90% (low-grade waste heat)	▪ Low temperature ▪ Quick start-up ▪ Reduced corrosion and electrolyte management problem	▪ Expensive catalyst ▪ Sensitive to fuel impurities	▪ Backup power ▪ Portable Power ▪ Small distributed generation ▪ Transportation ▪ Specialty Vehicles
Alkaline Fuel Cell (AFC)	>80% (low-grade waste heat)	▪ Low cost components ▪ Faster cathode reaction leads to high performance	▪ Sensitive to CO_2 ▪ Electrolyte management	▪ Military ▪ Space
Phosphoric Acid Fuel Cell (PAFC)	>40%	▪ Higher temperature enables CHP ▪ Increased tolerance to fuel impurities	▪ Platinum catalyst ▪ Long start up time ▪ Low current and power	▪ Distributed generation
Molten Carbonate Fuel Cell (MCFC)	>80%	▪ High efficiency ▪ Fuel flexibility ▪ Can use variety of catalysts ▪ Suitable for CHP	▪ High-temperature corrosion and breakdown of cell components ▪ Long start of time ▪ Low power density	▪ Electric utility ▪ Large Distributed generation
Solid Oxide Fuel Cells (SOFC)	<90%	▪ High efficiency ▪ Fuel flexibility ▪ Can use variety of catalysts ▪ Solid electrolyte ▪ Suitable for CHP	▪ High-temperature corrosion and breakdown of cell components ▪ High-temperature operation requires long start up time and limits	▪ Auxiliary power ▪ Electric utility ▪ Large distributed generation

A comparison of these six major types of fuel cells, based on their efficiency, advantages, limitations, and potential applications is listed in Table 1-2. The fuel cells are further classified based on their operating temperature. The low operating temperature is in the range of 50–250 °C for PEMFC, AFC and PAFC, and high operating temperature in the range of 650–1,000 °C like MCFC and SOFC.

Among these various types of fuel cells, PEMFCs have been extensively studied over the last two decades or so and have emerged as one of the potential systems, which offer not only clean energy but also commercial viability (e.g. Ballard and Smart Fuel Cells). Numerous successful applications of PEMFCs like passenger vehicles, generators, chargers and other portable and hand-held devices including mobile phones and laptops are now commercially available (Agnolucci, 2007; Andújar & Segura, 2009; Gencoglu & Ural, 2009).

PEMFCs offer the advantages of low weight and volume, as the electrolyte is a solid polymeric membrane. It is theoretically the simplest of fuel cells, and potentially the easiest to manufacture with the low-temperature operation, around 80 °C. PEMFCs also has a unique property of zero (ultra-low) emission along with a high power density, which offers the possibility of increased energy security. As a result, in recent years PEMFCs are in the forefront stage, drawing much attention to both fundamental research and industrial applications in recent years (Mert, Dincer, & Ozcelik, 2012) as an alternative power source for stationary and mobile applications. They are particularly attractive due to their quick start-up, low-temperature operation, and high power densities (de Bruijn, 2005).

8

The success of PEMFCs in these applications will depend on reductions in cost and improvements in a lifetime without compromising its performance. Since improvements in catalyst durability can both reduce the cost and increase the lifetime of PEMFCs, it has been and continued to be a focus for research.

1.2   PEM Fuel Cells

The polymer electrolyte membrane fuel cell (PEMFC), as its name suggests, uses a polymer electrolyte membrane (PEM), which selectively allows protons to pass through it. Therefore, PEMFC is also known as proton exchange membrane (PEM) fuel cells. PEMFC use hydrogen and oxygen to create electrical power through an electrochemical reaction, and a water-based, acidic polymer membrane as its electrolyte between the anode and cathode electrodes as showed in Figure 1-3.
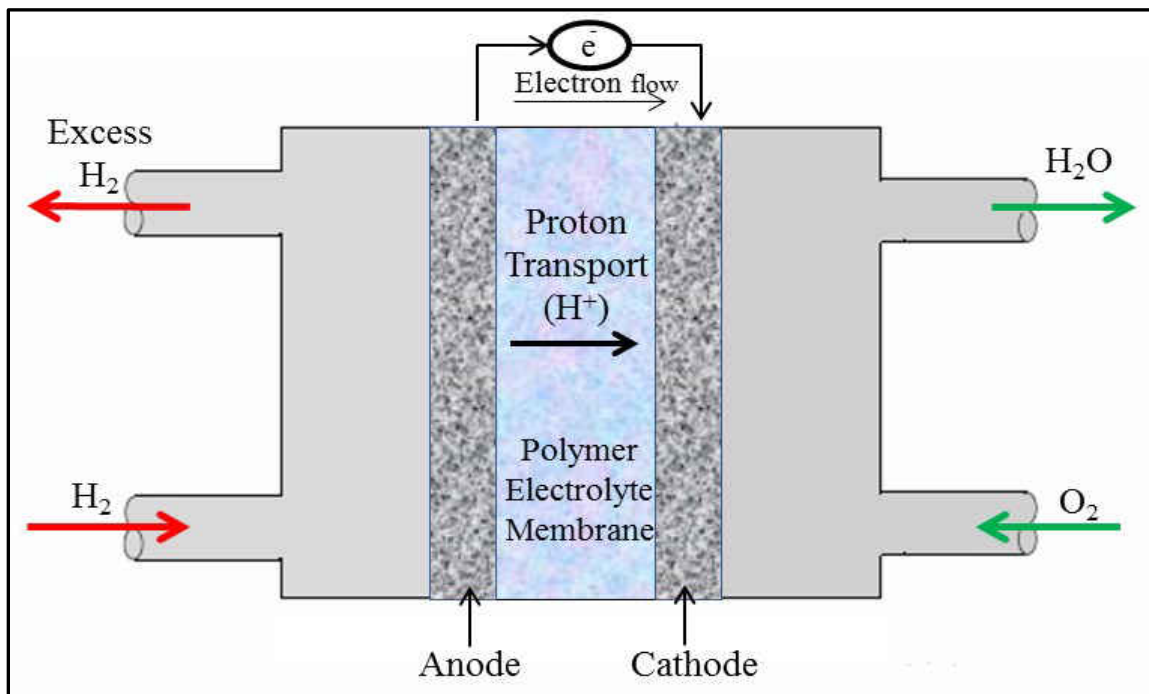
Figure 1-3 Structure of PEMFC in its Basic Form

9

The sandwich structure of a catalyzed membrane and the backing layers is called a membrane electrode assembly (MEA). Each electrode has a porous and electrically conductive backing layer to supply the reactant gas to the active area where the noble metal catalyst is in contact with the ionic and electronic conductor. Typically, the anode and cathode each consist of platinum catalyst supported on a porous, electrically conductive carbon backing layer (usually carbon paper or cloth). PEMFC operate at relatively low temperatures (below 100°C), and can tailor its electrical output to meet dynamic power requirements.

The low-temperature operation allows a PEMFC to start quickly (less warm-up time) and results in less wear on system components, resulting in better durability. However, it requires precious metal-based (typically platinum) electrodes for its electrochemical reaction to take place at low-temperature. Due to the relatively low temperatures and the use of precious metal-based electrodes, these cells must operate on pure hydrogen. The use of precious metal-based electrodes and pure hydrogen makes PEMFC expensive. However, PEMFC provides significant technical and overall cost advantages compared to other types of fuel cells. The preference for the PEMFC is due to the reasons listed below:

1 High power density

2 High efficiency

3 Clean operation

4 Relatively quick start up

5 Rapid response to the varying load

6 Lower operating temperatures

7 Solid non-corrosive electrolyte

8 Insensitive to differential pressures

9 No carbonate formation

10 Long life

11 Potable liquid product water

12 Ease of design and adaptable size

Because PEMFCs are lightweight, have such high power density, and cold start capability, they qualify for many applications, such as stationary power, portable power, transport and application in space. PEMFC can obtain a net power density of over 1 kW/liter, which makes them competitive with the internal combustion engine for transportation applications (LI, 2005). They are also the most convenient type of fuel cell for automotive applications due to their low operative temperature (40-80°C), quick start-up, high power density, high efficiency, excellent transient response, the absence of corrosive liquid electrolytes, and potential compact design (Larminie & Dicks, 2000; Weaver, 2002).

1.3 PEM Fuel Cell Components

A typical unit-cell PEMFC consists of several parts that work together to perform the necessary electrochemistry. A schematic diagram of an open unit-cell PEMFC with its components is shown in Figure 1-4. A typical unit-cell PEMFC consists of 11 components, two current collector plates, two flow channel plates, two gaskets, two gas

diffusion layers, two catalyst layers and an electrolyte membrane. The PEMFC is symmetric around the electrolyte membrane, which is located between two catalyst layers; the gas diffusion layer (GDL) supports the catalyst layer. The 5-layered structure of gas diffusion layers, anode and cathode catalyst layer, and a proton exchange membrane is called as an MEA. An MEA is placed between two flow field plates commonly made of graphite, which is supported by two current collector plates. A rubber gasket is used between the MEA and a graphite flow field plate to secure a seal to prevent leakage of reactants and products. A silicon sheet heater can also be placed on the outer side of the current collector plate or on an end plate to provide an external heating to the fuel cell if required.
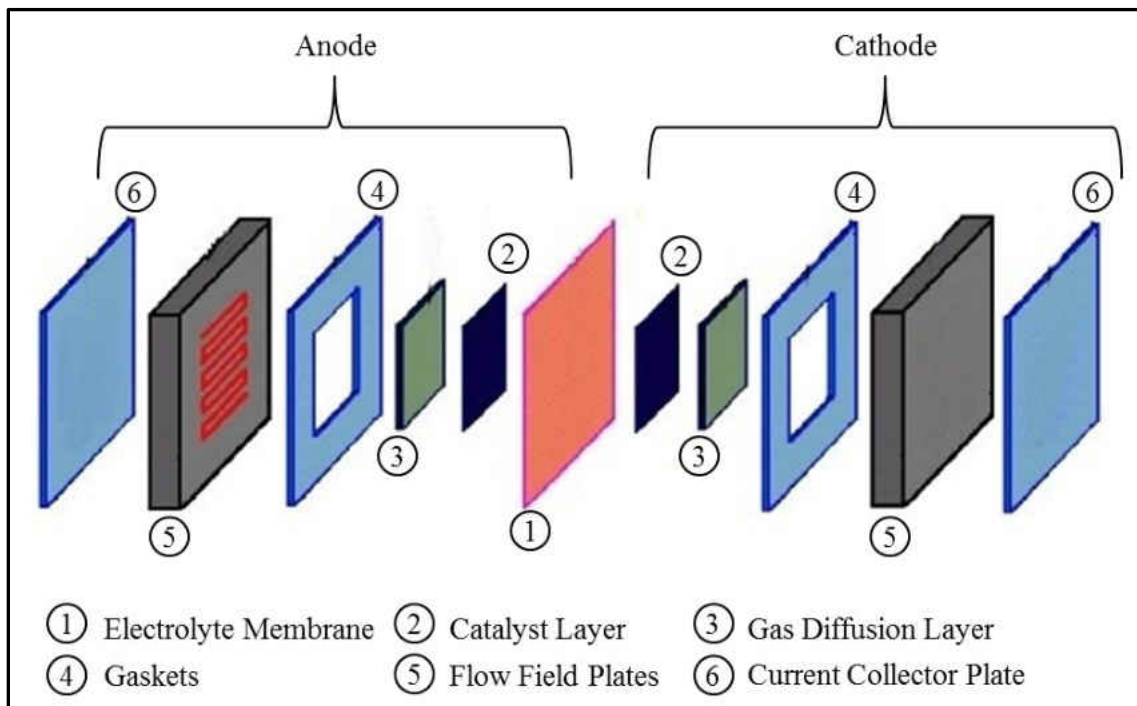
Figure 1-4 Unit-cell PEMFC Components

The anode is the negative electrode of the fuel cell and consists mainly of catalyst particles where the hydrogen oxidation reaction takes place. The cathode is the positive

electrode of the fuel cell and consists primarily of catalyst particles where the oxygen reduction reaction takes place. PEMFCs currently use Pt and Pt alloys as the catalyst both at the cathode and at the anode. All these components of PEMFC are enlisted with their primary functions in Table 1-3.

Table 1-3 Primary Functions of the main Components of a PEMFC

Component	Number on Figure	Typical Thickness	Function	Common Types
Polymer Electrolyte Membrane	1	50-200 microns	Enables transfer of proton from anode to cathode	Nafion 112, 115, 117
Catalyst Layer	2	2-20 microns	On the anode catalyst layer, hydrogen splits into positive hydrogen ions (protons) and negatively charged electrons On the cathode catalyst layer, oxygen combines with the protons and the electrons to form water and heat	Both anode and cathode catalyst layers have Platinum catalyst on carbon support
Gas Diffusion Layer	3	100-500 microns	Allows fuel and oxidant to travel through the porous layer while collecting electrons	Carbon cloth or carbon paper
Gasket	4	10 mil	Prevent fuel leak, and help distribute pressure evenly on an MEA	Silicon, Teflon
Flow Field Plate	5	40-60 mm	Distributes the fuel and oxidant to the gas diffusion layer	Graphite, stainless
Current Collector Plate	6	10 mm	Efficiently collects the current generated in the fuel cell, and also holds main components of a PEMFC in place	Gold plated stainless steel

The typical dimensions of the cell components vary from 10-30 microns thin catalyst layers to 50 mm thick flow field plates. The polymer electrolyte membrane and

the GDLs have thicknesses ranging in 50-100 microns and 200-300 microns, respectively.

The reaction-transport processes in PEMFCs are highly coupled, and a constituent material property influences its overall performance. A description of the key components of a PEMFC and their functionality is discussed in section 3.1 of this dissertation.

1.4 Basic Operation Principle of a PEM Fuel Cell

A PEMFC, as described earlier, consists of an electrolyte membrane sandwiched between two porous electrodes, an anode, and cathode. The anode is the negative electrode, and the cathode is the positive electrode of the fuel cell. The anode and cathode electrodes are located on left half and right half of the PEMFC respectively in the schematic shown in Figure 1-5.

Hydrogen passes through the anode electrode and oxygen over the cathode electrode generating electricity, water, and heat. This electrochemical energy conversion is achieved through two reactions that occur at the anode and cathode of the fuel cell.

At the anode catalyst layer, hydrogen is electrochemically oxidized into protons and electrons in a reaction called hydrogen oxidation reaction (HOR):

$$\text{Anode Reaction:} \quad 2\,H_2 \quad \rightarrow \quad 4\,H^+ + 4\,e^- \qquad\qquad E^\circ = 1.229\,V \qquad\qquad (1.1)$$
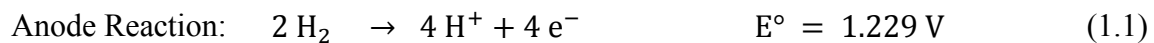
At the cathode catalyst layer, the electrons react with oxygen and electrons in a reaction called oxygen reduction reaction (ORR):

Cathode Reaction: $O_2 + 4H^+ + 4e^- \rightarrow 2H_2O$ $E° = 0.000$ V   (1.2)
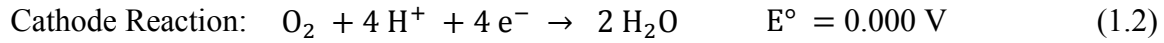
The overall reaction produces water and heat as by-products:

Overall Reaction: $2H_2 + O_2 \rightarrow 2H_2O$ $E°_{Cell} = 1.229$ V   (1.3)
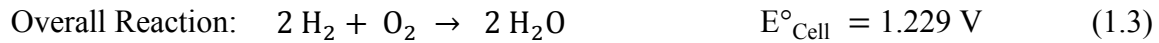
The net result of these simultaneous reactions is the flow of electrons through an external circuit, i.e., direct electrical current. A schematic of the PEMFC processes, components, and flow paths and basic operations are shown in Figure 1-5. The steps involved in PEMFC operation are:

1   Reactants delivery on anode and cathode side

2   Electrochemical reaction at anode

3   Electrochemical reaction at cathode

4   Ionic conduction through the electrolyte and electronic conduction through the external circuit

5   Product removal from the fuel cell

1. **Reactants delivery**: humidified hydrogen gas is fed to the fuel cell anode through flow field plates while humidified oxygen gas is channeled to the fuel cell cathode. These reactants are then diffused through gas diffusion layers to the catalyst on their respective sides of the MEA.
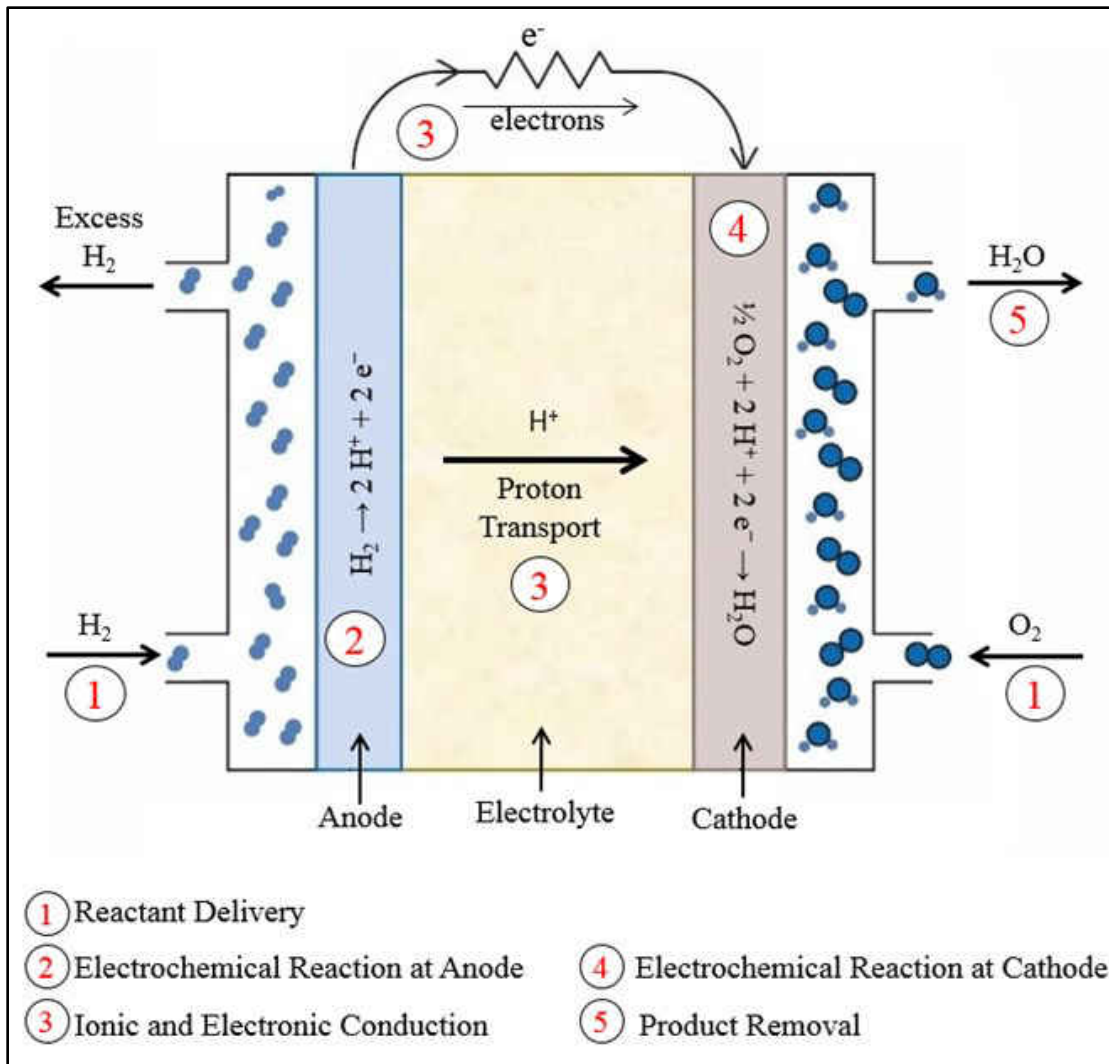
Figure 1-5 Basic Operation Principal of PEM Fuel Cell

2. **Electrochemical reaction at the anode**: Immediately after the delivery of humidified reactants, the electrochemical reactions occur at the surface of the catalyst as the schematic configuration and basic operating principles in Figure 1-5. At the anode, a platinum catalyst causes the hydrogen to split into positive hydrogen ions (protons) and negatively charged electrons (Equation 1.1).

3. **Ionic and electronic conduction**: Ions and electrons produced at the anode electrode must be consumed at the cathode electrode. The electrons and ions must be

16

transported from the place they are produced to the place they are consumed, in order to maintain charge balance. The Proton Exchange Membrane (PEM) allows only the positively charged ions to pass through it to the cathode. The negatively charged electrons must travel along an external circuit to the cathode, creating an electrical current.

4. **Electrochemical reaction at the cathode:** Meanwhile, at the cathode, oxygen reacts with protons and electrons to form water and heat (Equation 1.2).

5. **Product Removal**: The fuel cells produce electricity, water, and heat. The water and heat are the byproducts of the fuel cell reaction and need to be removed continuously from the fuel cell for its efficient performance. The water is removed from the other side of the cathode while the heat can be removed by the convection in the flow channels, and conduction in the solid portion of the catalyst layers, the gas diffusion media and bipolar plates.

In a PEMFC, the total amount of current generated is directly related to the geometrical surface area of the catalyst layer by the current density of the cell in A/cm^2. In addition, the product of current density and cell voltage gives the power density in W/cm^2 of a unit-cell, which is often shown via the polarization curve.

1.5   PEM Fuel Cell Stack

Typical a unit-cell fuel cell operates at a voltage ranging from $0.6 - 0.8$ V and produces a current of 0.2 to 1 A/cm^2 per active area (current density). As a result, it generates only a small amount of power —far from enough for any practical application.

Therefore, to obtain the desired amount of electrical voltage and power, several individual fuel cells are combined in a cascaded series and parallel form to increase its power capacity. This assembly of the combined cells is called a fuel cell stack, or just a stack. The potential power generated by a fuel cell stack depends on the number and size of the individual fuel cells that form the stack. Increasing the number of cells in a stack increases its total voltage while increasing the surface area of the cells increases its total current.
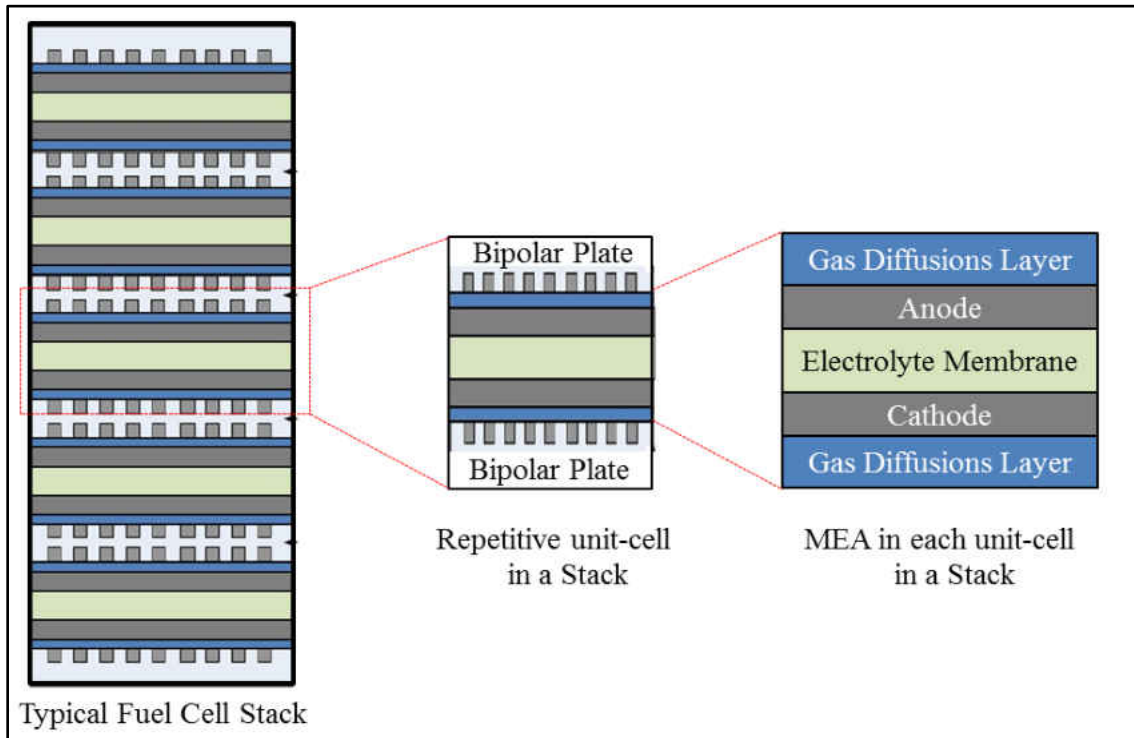
Figure 1-6 Typical fuel cell stack configuration (a five-cell stack), exploded view of one unit-cell in a stack

The most common fuel cell stack configuration is shown in Figure 1-6. A PEMFC stack is made up of bipolar plates, MEAs, and end plates. In a fuel cell stack, many cells are connected in series, and the cathode of one cell is connected to the anode of the next

cell. Bipolar plates are made of electrically conductive; gas-impermeable materials are used to combine individual fuel cell into a series of fuel cell stacks.

Bipolar plates in the fuel cell stacks contain machined flow fields on both sides to decrease the number of flow fields that reduce the weight and size of the fuel cell stack. Bipolar plates separate one cell from the next and prevent the mixing of fuel and oxidants of each fuel cell. Produced electrons from each fuel cell are transported through the end plate.

Each cell (MEA) in the stack is separated by a bipolar plate with flow fields to distribute the fuel and oxidant. The majority of fuel cell stacks are of this configuration regardless of fuel cell size, type or fuel used. A high-power stack may also contain cooling plates and other features not appearing in the illustration Figure 1-6. The development of stacks was outside the scope of the present work.

1.6   Dissertation Outline

The dissertation contains eight chapters. Following this introduction, Chapter 2 presents the proposed research work with its overview. A brief summary of the research approach and scope of the dissertation is also presented in this chapter in addition to the significance and limitations of this research.

Chapter 3 presents a review of the literature on the topics most pertinent to the dissertation work. These include a description of PEMFC components, MEA fabrication details, and theories for electrochemical techniques used for fuel cell evaluation.

Chapter 4 explains the MEA fabrication and experimental methods used for the $in-situ$ evaluation. This chapter also highlights the $in-situ$ diagnostic techniques and accelerated stress tests (AST) used to study the performance and durability of the catalysts.

Chapter 5 discusses the experimental design and setting used for conducting the experiments. Therefore this section is treated separately from the experimental methods presented in Chapter 4.

Chapter 6 explains the major findings of this study and the possible causes of performance loss using analytical and experimental methods in comparison to theoretical expectations and literature backgrounds.

Chapter 7 contains the exploratory work performed during this research study, which includes a study to evaluate the effects of freezing cycle on a fuel cell performance and MEA durability, and a novel accelerated conditioning method for PEMFC MEAs.

Chapter 8 is the final chapter, which summarizes the contributions of the dissertation work, and some personal opinions and suggestions for future work.

CHAPTER 2

2   PROPOSED RESEARCH

This chapter presents the proposed research work with its overview. The chapter starts with a general background for the proposed work, followed by a discussion of the motivation and rationale for this study. A brief summary of the research approach and scope of the dissertation is also presented in this chapter. The significance and limitations of this research is also discussed.

2.1   Research Background

In recent years, PEMFCs have been demonstrated to be feasible energy converters that convert the chemical energy of fuels directly into electrical energy with high power density, high efficiency, and near-zero emissions. Their applications have been identified in the power demanding areas such as portable, transportation, as well as stationary. PEMFC has also been shown to be competitive with conventional energy conversion devices such as internal combustion engines and batteries, and therefore is expected to be a major energy technology for the future (Vogel, 2008).

However, since the PEMFCs operate at low temperature, it requires a precious metal catalyst to provide the requisite activity at that low temperature. The use of these precious metal catalysts makes the PEMFC technology very expensive compared to the

other energy conversion devices. Currently, Pt and Pt alloys are widely used as anode and cathode catalysts in PEMFCs. Pt offers (a) highest catalytic activity, (b) chemical stability, (c) high exchange current density, and (d) superior work function for PEMFC (Chen et al., 2006; Halder, Sharma, Hegde, & Ravishankar, 2009; Kua & Goddard, 1999; Lin, Cui, Yen, & Wai, 2005).

The reactions in PEMFC are catalytic in nature; therefore, these reactions only take place on the surface of the catalyst, and the extent of such regions is obviously very limited in a catalyst layer. As a result, a significant portion of the expensive noble metal catalyst is unused and unavoidably wasted (Cheng et al., 1999).

Therefore, it was envisioned that if nano-sized particles of the precious metal are dispersed on a low-cost material as shown in Figure 2-1, a high surface-to-volume ratio of catalyst particles would be achieved, and the surface area of the catalysts available for the reaction would be maximized. The low-cost material on which the precious catalyst is dispersed is called as a catalyst support.
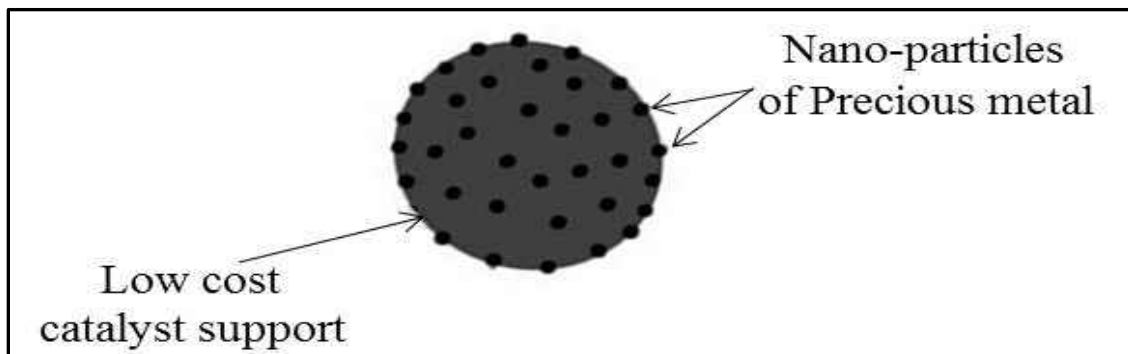
Figure 2-1 Nano-particles of precious metal catalyst deposited on a low-cost support

The catalyst support should have several important properties to achieve a high performing fuel cell catalyst including excellent electronic conductivity, high corrosion resistivity, uniform particle size distribution, large surface area, strong cohesive force to catalyst particles, and easy formation of a uniform dispersion of catalyst particles on their surface.

Conventionally, highly conductive carbon blacks (especially Vulcan XC-72) are the most commonly used supports for Pt and Pt-alloy catalysts to ensure large electrochemical reaction surfaces. The high surface area ($250 \text{ m}^2/\text{g}$ for Vulcan XC-72), low cost and easy availability of carbon blacks help reduce the overall cost of the fuel cell.

The use of carbon black as a catalyst support has significantly cut the platinum requirements. Typical platinum loadings in the electrode today are about 0.2-0.6 mg/ cm^2, which is significantly lower than 25 mg/cm^2 with early platinum catalysts without the support (Chunzhi He, Sanket Desai, & Garth Brown, and Srinivas Bollepalli, 2005). Although dramatic reduction of Pt loading has been achieved in the past decade, the current level of Pt loading still approaches or exceeds 0.2 mg/cm^2, which is almost twice the US Department of Energy (DOE) technical target of 0.125 mg/cm^2 for 2017.

2.2   Motivation for this Study

Despite its many significant advantages, the state $-$ of $-$ the $-$ art PEMFC is yet to realize mass-market commercialization hindered mainly by its poor durability (Gittleman C, DM, Jorgensen S, Waldecker J, Hirano S, Mehall M, 2010). Numerous

23

research efforts have been devoted to studying the durability of PEMFCs, motivated by the desire to improve its lifetime without unduly increasing cost or compromising performance.

Studies have shown that, although the electro-chemical interactions, transport losses and lack of ideal water management affect the durability of PEMFCs, catalyst degradation is the major cause for low durability of PEMFCs (Minh & Takahashi, 1995), which greatly reduces its lifetime and performance. The corrosion of carbon support materials has been identified to be the major contributor to the catalyst degradation (Kangasniemi, Condit, & Jarvi, 2004; Roen, Paik, & Jarvi, 2004; Siroma et al., 2005), in particular for Pt-based catalysts, which results in Pt dissolution, sintering, as well as agglomeration (Ferreira et al., 2005; Yasuda, Taniguchi, Akita, Ioroi, & Siroma, 2006).

The corrosion of carbon support has a significant impact on catalyst degradation rates, dramatically decreasing the electrochemically active surface area (ECASA); corrosion also has a profound effect on the electrode morphology. As a result, the catalyst support material exhibits great influence on the durability of PEMFCs in addition to its cost and performance.

Since it is commonly recognized that the catalyst support largely determines the stability of supported PGM nanoparticles, overall electrochemical activity and durability of the catalyst layer in the fuel cells (Lee, Zhang, Wang, & Wilkinson, 2006; Lim, Lee, Wheldon, Macy, & Smyrl, 2010). Pt-based catalyst in the form of nanoparticles dispersed on carbon black supports are still the most practical catalysts for PEMFC at the current

state of the technology (Y. Wang, Wilkinson, & Zhang, 2011). This research is motivated by the desire to improve the stability and durability of the PEMFC by utilizing the novel catalyst support to improve PEMFC lifetime without unduly increasing its cost or compromising performance.

2.3   Rationale for Silica as Catalyst Support

At the $state - of - the - art$ PEMFC technology, carbon black is the most efficient and practical support for the Pt-based catalyst. However, these carbon supports are not stable enough for the practical Pt-based catalysts, and as catalyst support material presents some disadvantages. Porous electrically conductive carbon blacks do not exhibit adequate resistance to corrosion caused by electrochemical oxidation in the PEMFCs operating conditions, which include high acidity, high potential, high humidity, and high oxygen concentration (Borup, Davey, Garzon, Wood, & Inbody, 2006; Kangasniemi et al., 2004; J. Wang et al., 2007). Generally, carbon blacks have the high specific surface area, which contributes mostly with micro-pores of less than 1 nm, which are therefore more difficult to be fully accessible. When the average diameter of the pores is less than 2 nm, the supply of the fuel to the surface may not occur smoothly, and as a result, the activity of the catalyst may be limited (Antolini, 2009). In the same way, the presence of a high amount of micropores results in a low accessible surface area for the deposition of metal particles. In addition, carbon particles generally contain sulfur groups, and that may cause Pt particle aggregation.

In addition, during fuel cell operation in particular at conditions of dynamic load operation, the cathode catalyst will experience high electrode potential at low to zero load during load-cycling (Mark F Mathias, Rohit Makharia, Hubert A Gasteiger, Jason J Conley, Timothy J Fuller, Craig J Gittleman, Shyam S Kocha, Daniel P Miller, Corky K Mittelsteadt, Tao Xie, SG Van, Paul T Yu, 2005; Yasuda et al., 2006), which results in oxidation of the carbon support to produce CO_2. For the anode catalyst, the carbon support can also be oxidized in the situation of fuel (hydrogen) starvation (Paul T. Yu, Wenbin Gu, Jingxin Zhang, Rohit Makharia, Frederick T. Wagner, Hubert A. Gasteiger, 2009). In addition, Pt catalysts seem to accelerate the rate of carbon support oxidation (Roen et al., 2004). These instabilities of carbon support result in the loss of electrochemical active surface area caused by both platinum nanoparticle dissolution/loss and platinum nanoparticle aggregation (Shui & Li, 2009); these effects are depicted in Figure 2-2.
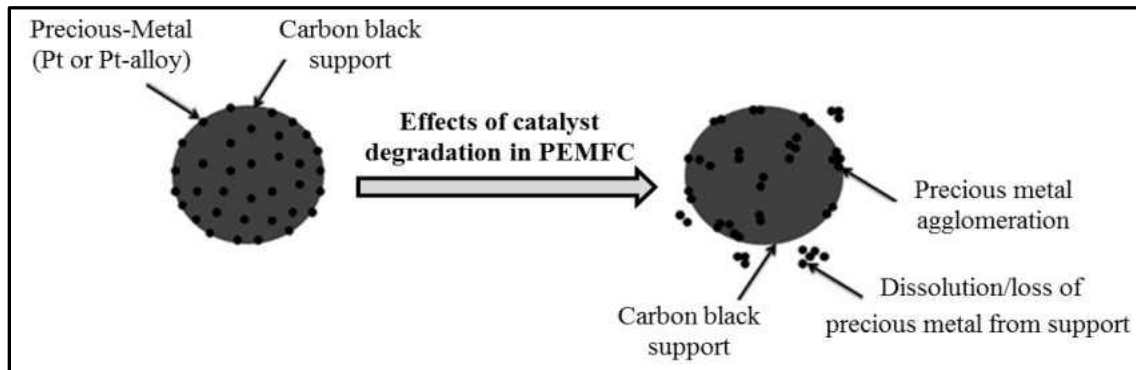
Figure 2-2 Effects of catalyst degradation in PEMFC

These separated Pt particles would become electronically isolated, leading to a low Pt utilization as well as degraded fuel cell performance due to increased kinetics polarization loss. This leads to the exploration of new support materials with

higher/better stability in corrosive conditions for PEMFC's applications to improve its durability.

Therefore, various alternative catalyst supports are being investigated. However, little research has been performed to date on the use of non-carbon catalyst supports. Ordered silica is an interesting material, which is receiving attention as fuel cell catalyst support due to their high surface area and high amount of mesopores, which allow high metal dispersion and good reactant flux.

Silica nanoparticles constitute a relatively new support material for noble metal catalysts. The large pore size of their structures makes them particularly well suited to many catalysis applications. In addition, their consistent spherical shape allows for well-defined and readily accessible catalytic sites compared to amorphous supports, such as silica gels, polymers or carbon powders. Moreover, silica has a rigid structure that does not deform upon heating and does not swell in solvents; hence, it can withstand a wide variety of reaction media, and it can be used at high temperatures (A. Li, Zhao, & Pierce, 2010). Because of its various advantages over carbon as a potential support material, ordered silica needs to be explored as a support material for PGM catalyst for its application in PEMFC.

Thus, silica nanoparticle's large pore size, consistent spherical shape, rigid structure, and its higher catalytic activity and reduced CO poisoning in $ex-situ$ methanol oxidation lead to the rational that it would be the ideal candidate as a support

for Pt catalyst in PEMFC applications. Therefore, this proposed research aims to evaluate the performance and durability of Pt/Silica catalyst in a PEM fuel cell.

2.4   Research Hypothesis

The primary hypothesis of this work is that silica-supported Pt catalyst will enhance the performance and durability of PEM fuel cell compared to carbon-supported catalysts. The following sub-hypothesis will be examined to test the primary hypothesis.

1. The Pt/Silica catalyst will achieve an equivalent power density of a Pt/Carbon catalyst in PEMFCs.

2. The ECASA loss based on the AST test (potential hold and potential cycling) will be reduced for a Pt/Silica catalyst as compared to Pt/Carbon catalyst and thereby enhance the durability of PEMFCs.

2.5   Research Objectives

In order to tests the hypothesis stated above (section 2.4), four primary research objectives were established; 1) to design and fabricate a test station; 2) to develop an MEA fabrication method; 3) to evaluate the in-situ performance of Pt/Silica catalyst and 4) to evaluate the in-situ durability of Pt/Silica catalyst. More specifically, the four primary objectives of this work are the following

1. Design and fabricate a test station for controlled unit-cell characterization. This objective will be accomplished by fabricating test-stand with:

a. dedicated humidification system for both the anode and cathode side of the unit-cell

b. a precise temperature control and monitoring of the unit-cell

c. a precise reactant flow control, and a liquid water trap (water collection bottles) downstream the unit-cell to eliminate water entering into the venting system

d. diagnostic equipment (DC load, potentiostat, etc.) suitable for unit-cell study

2. Develop an MEA fabrication method to fabricate reproducible and high performing MEA in-house. This objective will be accomplished through experiments designed to:

a. determine the consistency and/or accuracy of achieving the targeted catalyst loading

b. determine the reproducibility of the results of the fabricated MEAs, and

c. compare the performance of in-house fabricated MEA with the commercial MEA of similar specifications

3. Design and conduct the performance tests to evaluate Pt/Silica catalyst $in-situ$ in an MEA using a unit-cell PEMFC. This objective will be accomplished through experiments designed to

a. determine the IV characteristic curves of the Pt/Silica-based MEA, and compare it with the Pt/Carbon-based MEA

b. determine the ECASA of the Pt/Silica-based MEA using a CV test, and compare it with the Pt/Carbon-based MEA

4. Design and conduct the durability tests to evaluate Pt/Silica catalyst $in-situ$ in an MEA using a unit-cell PEMFC. This objective will be accomplished through experiments designed to

    a. determine the IV-performance loss and ECASA loss of the Pt/Silica-based MEA during potential hold AST test, and compare it with the Pt/Carbon-based MEA

    b. determine the IV-performance loss and ECASA loss of the Pt/Silica-based MEA during potential cycling AST test, and compare it with the Pt/Carbon-based MEA

2.6 Approach

Much of the current research on the catalyst's durability for PEMFCs can be classified into three categories (Li et al., 2011):

1. Modifying primary Pt catalyst - lowering platinum content and improving its activity by changing catalyst particle size, morphology, and crystal structure; even alloy Pt with less expensive metals such as Fe, Co, Mn, Ni, Cu and others

2. Looking for the novel support - such as novel carbon supports, alternative carbon structures, and non-carbon supports

3. Developing non-precious metal oxygen reduction reaction (ORR) catalyst

The catalyst support largely determines the stability of supported PGM nanoparticles in additon to the overall electrochemical activity and durability of the

catalyst layer in the PEMFCs. Therfore this research focuses on the second approach of optimizing the electrode structure using novel non-carbon support.

In this work, in − situ evaluation of the catalyst was performed by integrating it into a 5-layered MEA, and then evaluating its performance and durability in a 25 cm^2 unit-cell PEMFC fixture. The in − situ testing provides valuable information about the true properties of a catalyst under real PEMFC operating conditions. Unit-cell PEMFC provides relatively uniform operating conditions that allow for more straightforward analysis of electrochemical performance of a novel support, and also conserve the catalyst material (particularly total weight of catalyst) since unit-cells utilize only one MEA at a time.

Two different catalysts were used in this research work, in-house fabricated Pt/Silica catalyst and, Pt/Silica catalyst which was procured from Fuel Cell Store Inc. A carbon-free silica support for Platinum (Pt/Silica) catalyst used in this work was fabricated in-house at Dr.Zhao's lab in Chemistry Department at the University of North Dakota (UND). The MEAs prepared using the novel Pt/Silica catalyst are labeled as Type-B MEA, and the MEAs prepared using conventional Pt/Carbon catalyst are labeled as Type-A MEA. The catalyst coated gas diffusion layer (CCG) method was used to fabricate both Type-A and Type-B MEA.

To fabricate the MEA from a catalyst, the catalyst ink was first prepared using silica-supported Pt (Pt/Silica) catalyst and applied to the gas diffusion layer (GDL) by hand brush to form the gas diffusion electrode (GDE). Then, these electrodes were

31

assembled with the electrolyte membrane (PEM) by a hot press to form a Type-B MEA. The same procedure was also used to prepare Type-A MEAs using the $state-of-the-art$ Pt/Carbon. The MEA fabrication method used for this research work was not extensively optimized, as the goal was simply to obtain consistent MEA performance to enable comparison of the Pt/Silica catalyst with the state-of-the-art Pt/Carbon catalyst.

Finally, the MEA prepared during this research work were mounted in a 25 cm^2 unit-cell PEMFC fixture for its $in-situ$ evaluation. The evaluation of both of Type-A and Type-B MEA was performed using electrochemical techniques at a different combination of H_2 and O_2, fuel cell temperatures and humidity levels. Finally, the performance and durability data was compared to prove the hypothesis of this research.

The purpose of this study was to develop a Type-B MEA from Pt/Silica catalyst and to investigate/analyze effects of Pt/Silica on the performance and durability of PEMFC. We hypothesized that the Pt/Silica catalyst would enhance the durability and utilization of Pt catalyst for PEMFC, which will eventually improve the performance of PEMFC.

2.7 Research Scope

This study was mainly focused on $in-situ$ characterization of a novel non-carbon support for platinum group metal (PGM) catalyst used in a PEMFC. The scope of this research work was related to improving the durability and lifetime, which will results in reducing the cost of the PEMFC technology.

The stability of the conventional catalyst support materials is limited during lifetime operation at temperatures around 80 °C. At elevated temperatures, the degradation is accelerated further, becoming even more critical. In addition, the direct contact of platinum (Pt) and carbon has been shown to contribute to carbon degradation. In this work the possibility of reducing catalyst support degradation by depositing Pt onto silica while maintaining the same performance is explored by studying Pt/Silica catalyst for both anode and cathode.

Since the hypothesis of this research was focused on the enhanced performance and durability of MEAs with novel Pt/Silica catalyst, compared to the MEAs with the state-of-the-art Pt/Carbon catalyst, two types of MEAs Type-A (with Pt/Carbon catalyst) and Type-B (with Pt/Silica catalyst) were fabricated using CCG method. The in-situ evaluation of both Type-A and Type-B MEA is carried out in a 25 cm^2 unit-cell PEMFC fixture.

The project focusses on the development of a GDE method to prepare a key component of the PEFCs, the MEA. The focus is therefore on understanding and identifying the key steps in the preparation process and deriving a reproducible procedure. Even though in the study some parameter variation is performed during the MEA fabrication process, optimization of the developed method falls outside the scope of this project.

2.8   Significance of the Study

Through this research work, we are exploring silica as a novel support for the platinum group metal (PGM) catalyst to enhance the performance and durability of PEMFC. Being chemically and thermally stable, carbon-free silica support would enhance the durability of the PEMFC. Because of its large pore size, the supply of fuel to the surface will not be hampered, and thus, enhance the activity of the catalyst. This would be beneficial in retarding PGM migration and inhibiting PGM coalescence versus PGM catalysts on a traditional carbon support caused by degradation of support material. Apparently, both consequences directly affect PEMFC lifetime, cost and performance through enhanced durability for both stationary and automotive applications.

Since silica is a neutral compound without any reactive group, this novel support could also be used for catalysts other than PGM, and could have potential applications in other electrochemical systems in addition to PEMFC.

The results of this work will improve the understanding of the characteristics of the non-carbon support, an area of study that is lacking. Furthermore, this study will add to the growing body of literature to meet the long-term goal of our research team: to generate detailed fundamental data that will result in the optimization of renewable power production systems allowing the nation to establish a renewable hydrogen fuel cell power production system as a promising and efficient technique. This goal is consistent with others searching for solutions to our nation's energy security and environmental problems.

2.9   Limitations

There are many different reasons for degradation in a PEMFC. However, the tests in this dissertation were only aimed to analyze the degradation induced by potential hold and potential cycling. The only part of the fuel cell that was regarded in this project was the Membrane Electrode Assembly (MEA), specifically the anode and cathode catalyst layers. Degradation is present on all the components of the fuel cell. The degradation in other components except MEA are assumed to be negligible, and these were not investigated and are not discussed further in this report. The only performed measurements to evaluate the degradation were $in-situ$ methods.

CHAPTER 3

3   LITERATURE SEARCH

This chapter presents a review of the literature on the topics most pertinent to the dissertation work. These include a description of PEMFC components, MEA fabrication details, and theories for electrochemical techniques used for fuel cell evaluation.

3.1   PEM Fuel Cell Components and their Functionality

As mentioned earlier (section 1.3) PEMFC is consists of several parts that work together to perform the necessary electrochemistry. A description of all these key components of a PEMFC and their functionality is discussed here.

3.1.1   Membrane Electrode Assembly (MEA)

The membrane electrode assembly (MEA) is the heart of PEMFCs and determines its performance and durability. The MEA components material, structure and fabrication methods play important roles in determining PEMFCs performance. Therefore, understanding the structure and the components of the MEA is necessary to gain a thorough understanding of how MEAs work.

MEA is an elegant design; combining five different layers. The five layers include a polymer electrolyte membrane (PEM), two porous catalyst layers and two gas diffusion layers (GDLs). PEM is sandwiched between two catalyst layers, which are again

sandwiched between the two GDLs. A schematic of a cross-sectional view of the five-layer MEA is shown in Figure 3-1.
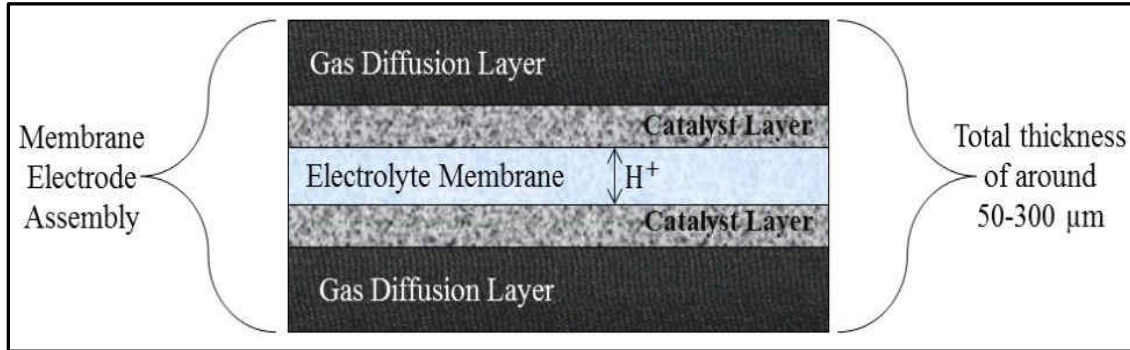
Figure 3-1 Schematic cross-sectional View of Five-layer Membrane Electrode Assembly

The surface area of the electrolyte membrane is about four times bigger than the area of catalyst layers and GDL. Both catalyst layers and GDLs have the same surface area and are located at the center of the electrolyte membrane as shown in Figure 3-2.
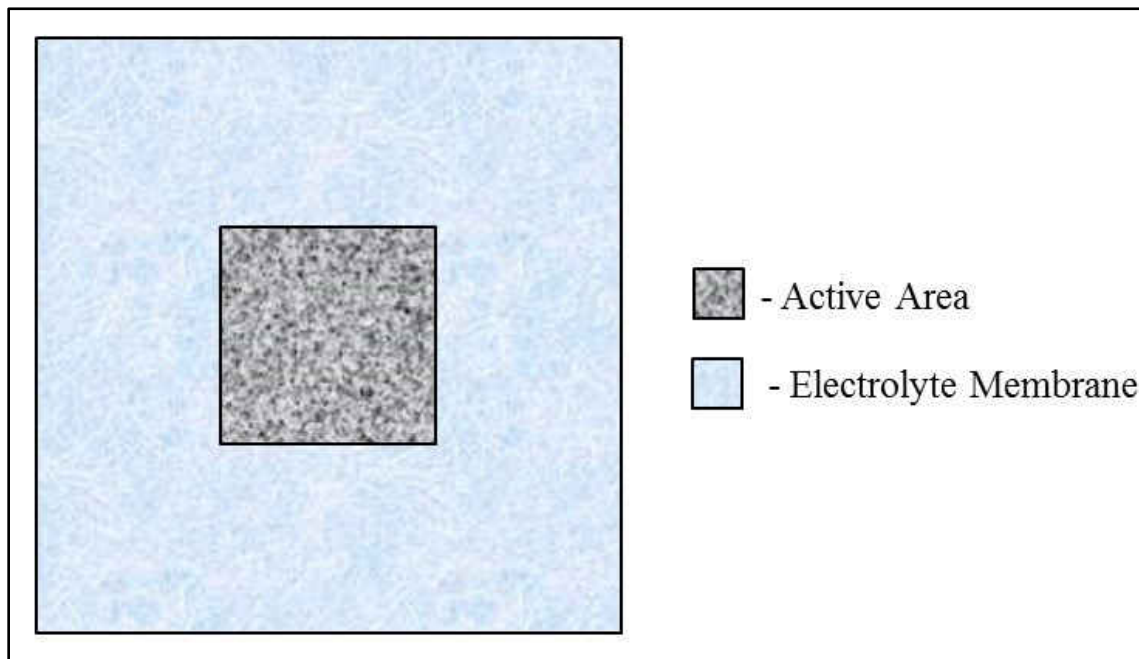
Figure 3-2 MEA Schematic with position of catalyst layers and GDLs on it

The electrolyte membrane separates the reduction and oxidation half-reactions but allows the protons to pass through to complete the overall reaction while forcing the electrons to pass through an external circuit. The anode catalyst layer stimulates oxidation half reaction, while the cathode catalyst layer stimulates reduction half-reaction. The GDL further improves the efficiency of the system by allowing direct and uniform access of reactant gasses to the catalyst layers.

These principal components of the MEA are described in the following sections as to their purpose within the MEA, as well as the impact each has on the MEA performance.

Polymer Electrolyte Membrane (PEM)

The polymer electrolyte membrane (PEM) has been a key component, enabling fuel cell miniaturization for portable applications. It is an elegant design, combining the requirement of physical and electrical isolations of the reactants and ion transport all in one structure. Electrolyte membrane refers to a thin layer of a particular type of polymer membrane (usually ~50–200 μm thick), which allows only protons to pass through. Because of its proton conducting property, it is also referred to as a proton exchange membrane (PEM). This unique property of the PEM itself makes PEMFC possible. The electrolyte membrane helps separate the reduction and oxidation half-reactions by separating two electrodes. It is a critical component of the PEMFC, which must exhibit high protonic conductivity, a barrier to the mixing of fuel and reactant gasses, and chemical and mechanical stability within the fuel cell environment.

There are different types of PEMs and are categorized as perfluorinated, partially-perfluorinated, non-perfluorinated, and non-perfluorinated composites. The most commonly employed electrolyte for PEMFCs is a DuPont product - Nafion, which is a semi-permeable perfluorinated sulfonic acid-based ionomer (PFSA), which is also the one considered in this project.

PFSA consists of three regions: (1) a polytetrafluoroethylene (PTFE, a.k.a. DuPont's Teflon^{TM}) - like backbone, (2) side chains of $--O--CF_2--CF--O--CF_2--CF--$ which connects the molecular backbone to the third region, and (3) ion clusters consisting of sulfonic acid ions. When the membrane becomes hydrated, the proton conductivity results from hydrophilic sulfonic groups bonded to the polymer chain. The sulfonic groups create tunnels and protons can jump between fixed ionic groups under the influence of a voltage gradient.

There are two advantages to the use of PFSA membranes in PEMFC. First, because the structure is based on PTFE backbone, PFSA membranes are relatively robust and stable in both oxidative and reductive environments. It has been reported that the PFSA membrane is durable up to 60,000 h (Fang, Qiao, Wilkinson, & Zhang, 2007). Second, the protonic conductivities achieved in a well-humidified PFSA membrane can be as high as $0.2 \, S/cm^2$ at PEMFC operating temperatures. This translates to a cell resistance as low as $0.05 \, \Omega - cm^2$ for a $100 \, \mu m$ thick membrane with voltage loss of only 50 mV at $1.0 \, A/cm^2$ (Litster & McLean, 2004).

Given these advantages, there are several disadvantages to the use of PFSA membranes in PEMFC. In addition to the membrane material being expensive, disadvantages can be categorized as those related to supporting equipment requirements and temperature-related limitations. Because PFSA membranes must be kept hydrated to retain proton conductivity, the operating temperature of the cell must be maintained below the boiling point of water.

The initial Nafion membranes were N-115 and N-117 with a film thickness of 127 μm and 177 μm respectively. Unfortunately, with time when the electrode platinum loadings were reduced and the current density was increased, the resistance of thick membranes caused a decrease in performance and water management problems. Thus, new thinner, extrusion cast membranes, N-105 (a lower equivalent weight (EW), 127 μm), N-1135 and N-1035 (standard and low EW versions with 90 μm thick), N-112 (50 μm) were made (Nafion® material specification sheet.2001).

Catalyst Layer/Electrode

The catalyst layer is in direct contact with the gas diffusion layer on one side, and electrolyte membrane on the other side. An MEA has two different catalyst layers, anode catalyst layer and cathode catalyst layer and is located on both sides of the electrolyte membrane. Catalyst layer facilitates the electrochemical reactions and provides pathways for the transport of reactants, electrons, protons, and products for the efficient working of the MEA. Therefore, its material and structure have a major influence on its performance.

In order to catalyze the fuel cell reactions, catalyst particles must have contact with the protonic and electric conductors. There also must be passages for reactants to reach catalyst sites and for reaction products to exit from the catalyst layer. The contact point of the reactant gas, catalyst, and the electrolyte membrane is conventionally referred to as the three-phase interface. The reactions in the catalyst layers are exothermic; therefore, the catalyst layer must be able to transport the heat out of the cell. The heat can be removed by conduction from the solid portion of the catalyst layer, GDLs and flow field plates, and by convection from the flow channels.

The catalyst layer is a three-dimensional (3-D) porous structure composed of a network of (1) metal catalyst (2) catalyst-support material with metal catalyst particles dispersed on it, and (3) proton ionomer. A simplified structure of the catalyst layer in an MEA is depicted in Figure 3-3.
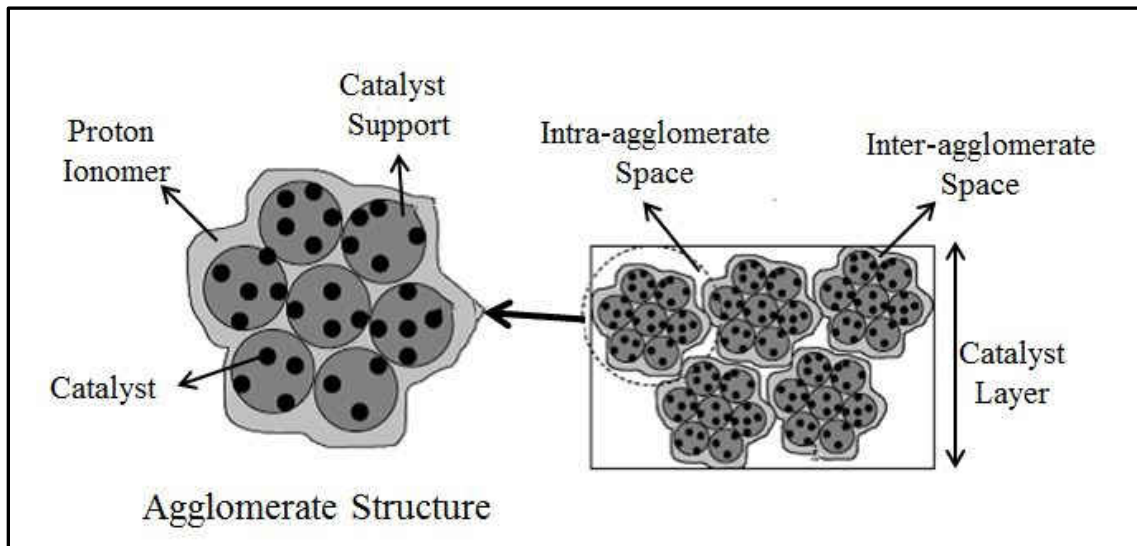
Figure 3-3 Simplified structure of the catalyst layer in an MEA

The function of the catalyst is to increase the reaction rates. The catalyst plays a critical role in reducing the reaction activation barrier by providing the reaction with an alternative path that has lower activation energy as compared to the uncatalysed reaction. In order to achieve acceptable reaction rates, the effective area of active catalyst sites must be several times higher than the geometrical area of the electrode.

Platinum (Pt) is the most commonly used catalyst in PEMFCs. Other catalysts have been successfully used, the most common one being a ruthenium (Ru). Pt-Ru alloys have been successfully used and are less prone to catalyst poisoning due to carbon monoxide than pure Pt. Pt and several of its alloys (Pt–Co, Pt–Ni, Pt–Fe, Pt–V, Pt–Mn and Pt–Cr) also exhibit suitable catalyst kinetics (Appleby & Foulkes, 1993; Fernandez, Walsh, & Bard, 2004; Pharkya, Alfantazi, & Farhat, 2005; Yu, Pemberton, & Plasse, 2005).

The catalyst support is used to ensure maximum activity of the catalyst (Appleby & Foulkes, 1993). The requirements of the support material are that it is electronically conductive, stable and has a sufficiently high surface area to allow effective dispersion of the catalyst particles. A commonly used support is Vulcan XC-72 that has a specific surface area of about 250 m^2/g (Lázaro et al., 2011).

During the MEA fabrication, proton ionomers are included in the catalyst layer. These ionomers act as (i) proton conductors to expand the electrochemically active region into the bulk catalyst layer, (ii) binding material to impart mechanical stability and (iii) hydrophilic agent to retain moisture and prevent membrane dehydration. The amount of

the proton ionomer in the catalyst layer is very critical in determining the performance of the MEA. If the amount of proton ionomer is insufficient to form a three-dimensional network, protons cannot access every part of the catalyst layer. Therefore, only part of the catalyst can be utilized as active sites for electrochemical reactions. In contrast, if an MEA contains too much ionomer, electronic conduction paths (Pt/Carbon) and gas transport channels (pores) in the catalyst layers will be blocked by either the ionomer or flooded water inside the hydrophilic pores, particularly at a high current density (Lee et al., 1998; Passalacqua, Lufrano, Squadrito, Patti, & Giorgi, 2001; Sasikumar, Ihm, & Ryu, 2004a; Sasikumar, Ihm, & Ryu, 2004b; Uchida, Aoyama, Eda, & Ohta, 1995).

Gas Diffusion Layers

The gas diffusion layer (GDL) is often integrated as part of the MEA acting both as the functional as well as a support structure and is one of the vital components. In a unit-cell fuel cell, there are two pieces of GDLs, located between the catalyst layer and the flow field plates on each side of the electrolyte membrane. GDL play multiple roles: (1) electronic connection between the bipolar plate and the electrode, (2) passage for gaseous reactants transport and heat/water removal, (3) mechanical support to the MEA, and (4) protection of the catalyst layer from corrosion or erosion caused by flows or other factors (Larminie & Dicks, 2000).

Usually, a GDL is a dual layer structure made up of a backing layer or gas diffusion media (GDM) and a microporous layer (MPL). The first layer is made of either carbon paper or carbon cloth; with a thickness in the range of 100-300 μm. Carbon cloth

performs better than paper at high current density ($>0.5\,\text{A/cm}^2$) with internal humidification (Ralph et al., 1997). The second layer of the GDL, in contact with the catalyst layer, is a thinner microporous layer consisting of carbon black and PTEF (hydrophobic agent) to ensure efficient water removal. This allows reactant gasses and water vapor to pass through the pores of the catalyst while still preventing the GDLs from becoming saturated by liquid water. An ideal GDL is required to transport the gas reactants effectively to the catalyst layer, have a surface that enhances electronic contact, and have proper hydrophobicity.
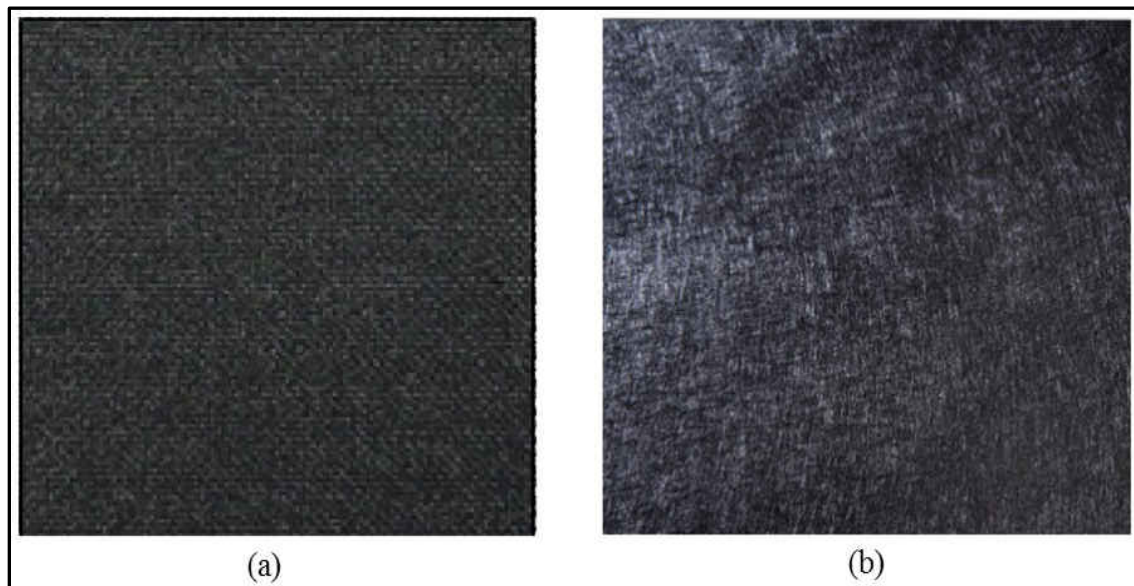
Figure 3-4 Gas Diffusion Layer (a) Carbon Cloth (b) Carbon Paper

3.1.2 Gasket

Gaskets are used in PEMFCs or stacks to prevent leaking of reactant gasses and the liquid products from the cell. The gasket provides a seal around the peripherals of the cell between the plates and the MEA and is exposed to acidic, humid gasses, mechanical compressive pressure and cyclic temperature (Lin et al., 2011). Typical

sealing materials utilized in PEMFCs include ethylene propylene diene monomer (EPDM) rubber, and silicone for a low-temperature fuel cell, and Teflon for the high-temperature fuel cell. The thickness of the gasket is crucial since it has to be thick enough to prevent leaks; however, it cannot be too thick, as that would hinder electrical contact between the plate and the MEA.

Normally, a silicone rubber is used as the material of choice for a gasket due to their elasticity and heat resistance. However, the environment the gaskets endure within the PEMFCs is acidic and as a result, the gaskets are degraded over time. If any gasket degrades, the reactant gasses (hydrogen and oxygen) can leak or mix each other directly during operation, and the anode and the cathode side of the fuel cell will be in electrical contact with each other. This will affect the overall operation and performance of the fuel cell. Therefore, the gaskets are regularly replaced to avoid a decrease in PEMFC's performance.

3.1.3   Flow Field Plates

The flow field plate has gas-flow channels curved on one side of the plate and performs many roles in fuel cells. In a fuel cell stack with more than one cell, a bipolar plate is used in place of a flow field plate. Bipolar plates have flow channels curved on both sides, forming the anode compartments of one cell and cathode compartments of the adjacent cell of the stack on the opposing sides of the bipolar plate. It also used to separate the individual cells in the stack and form the supporting structure of the fuel cell.

In a fuel cell, the main purpose of the flow field and the bipolar plate is to distribute fuel and oxidant within the cell and provide current and heat conductions. In order to simultaneously perform these functions, specific plate materials and designs are used. Commonly used designs can include single serpentine, multiple serpentines, parallel and interdigitated flow fields. These flow designs in depicted in Figure 3.5.
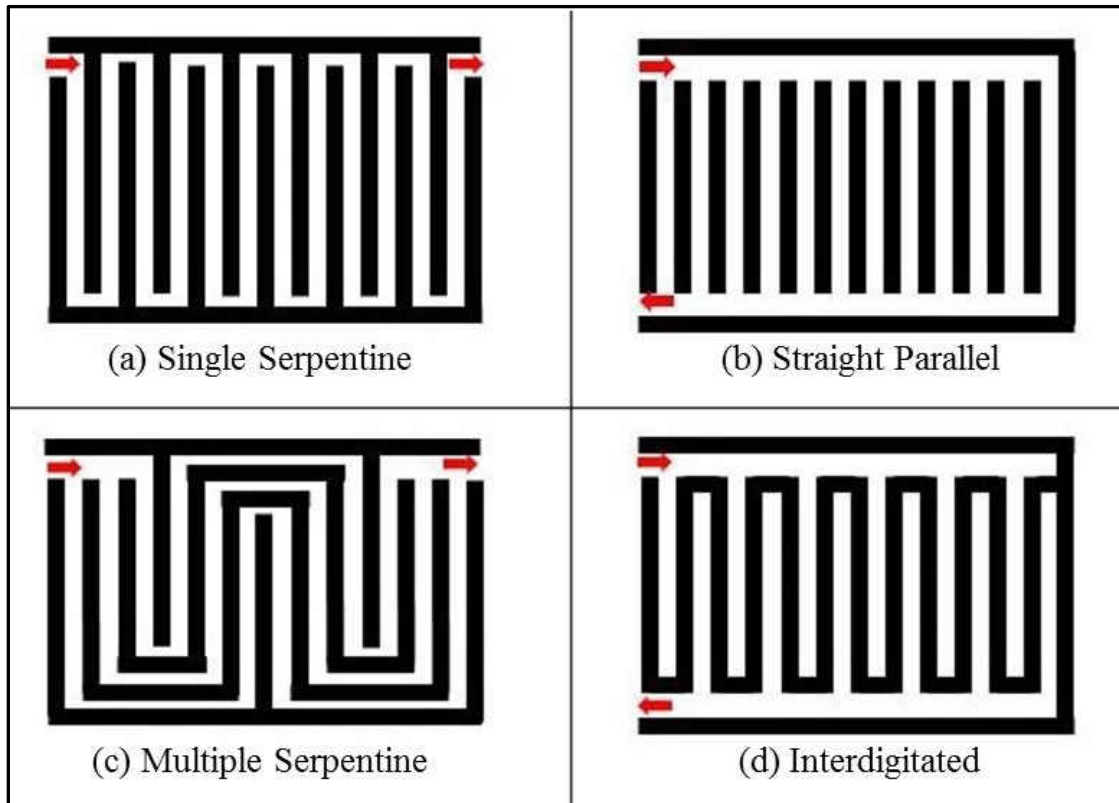
Figure 3-5 Different Flow Field Plate Design (a) Single Serpentine (b) Straight Parallel (c) Multiple Serpentine (d) Interdigitated

The requirements for a flow field plate and a bipolar plate material are chemical compatibility in both oxidizing and reducing conditions, resistance to corrosion, cost, density, electronic conductivity, gas diffusivity/impermeability, manufacturability, material strength, and thermal conductivity. It should also be cheap and well suited for high-volume manufacturing methods. The materials most often used are stainless steel,

titanium, nonporous graphite, and doped polymers. Several composite materials have been researched and are beginning to be mass-produced.

3.1.4   Current Collector Plates

A current collector is a plate attached to a flow field plate to collect the current generated by fuel cell reaction. Sometimes, metal flow field plates/bipolar plates can also serve as a current collector in a unit-cell PEMFCs or a stack. The current collectors collect current and transport the electrons via the external circuit from the anode to the cathode proving electrical power to the external device.

The material used for the current collector should have an excellent electronic conductivity, strong electrochemical and mechanical stability, low cost, and a lightweight to reduce the weight of the fuel cell stack. To increase the electronic conductivity, its surface is usually coated with another metal (e.g. gold-coated copper and gold-coated aluminum).

3.2   MEA Fabrication

MEA fabrication is the most complicated multi-step process of all the components in a fuel cell. It is mainly because MEA is not a single component but a series of components, which need to be bonded together in a precise way. Therefore, to produce a high performing MEA that is durable, and to gain a thorough understanding and necessary competence, a rigorous literature review was conducted to acquire an understanding and guidance in designing the MEA fabrication process, which could be replicated and improved in the laboratory settings.

MEA is the core component of a PEMFC's system, and consists of an electrolyte membrane, catalyst layers, and GDLs, with these components typically prepared individually, then pressed together at high pressures and temperatures to strengthen their interfacial contact (Larminie & Andrew, 2003).

MEA fabrication methods are categorized according to how the catalyst layers of the MEA are formed which is depicted in Figure 3.6, and described in details in section 3.1.2 of this dissertation.
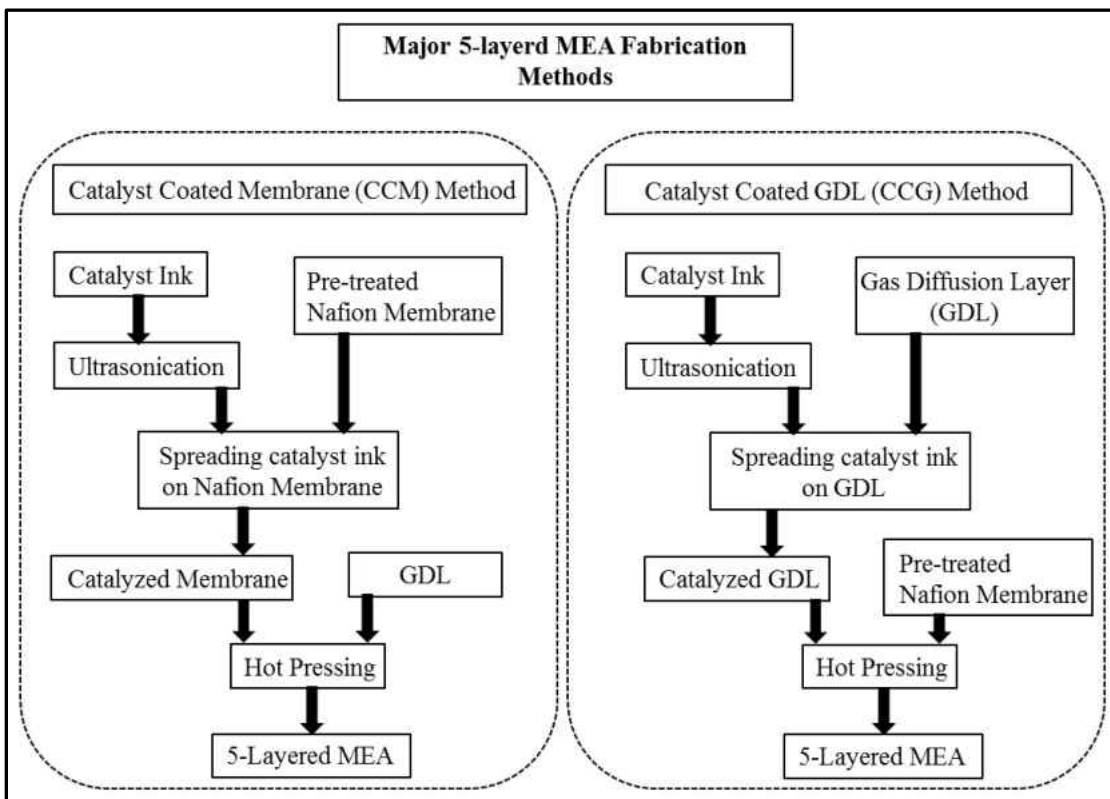
Figure 3-6 Major 5-layerd MEA fabrication methods

As described earlier, MEA fabrication is a multi-step process, as presented as a flowchart in Figure 3-7 is divided into three different steps that include (Frey & Linardi, 2004a):

1   Catalyst-ink preparation

2   Catalyst spreading to prepare fuel cell electrodes - which is spreading the catalyst ink either on an electrolyte membrane or on a gas diffusion layer

3   Hot pressing - in which the electrolyte membrane, electrodes and gas diffusion layers are pressed together under heat and pressure to form an MEA

MEA Preparation Flowchart

Catalyst Ink Preparation
- Mixing catalyst, deionized water, nafion ionomer, and solvent
- Making a homogeneous ink of the mixture using a sonicator or magnetic stirrer

Catalyst Spreading
- Application of catalyst ink to prepare a fuel cell electrodes using either a CCM or CCG method
- Repeat the ink application and drying of electrodes alternatively to achieve a targeted metal loading

Hot Pressing
- Hot pressing the 2 electrodes onto two sides of the electrolyte membrane and sandwiching it between 2 GDLs at a pressure and temperature to make good interfacial contact between them

Figure 3-7 Flowchart for MEA fabrication

3.2.1   Catalyst Ink Preparation

Depositing the catalyst into an MEA for $in-situ$ evaluation requires the creation of catalyst ink, which contains the catalyst, Nafion ionomer solution, and a solvent. Dispersing the catalyst into an ink solution allows for ease of its application onto a GDL or membrane through painting or spraying. The presence of a Nafion ionomer in

the ink enhances the bonding between membrane and electrodes; it also facilitates a better transfer of protons between the membrane and catalyst particles to the electrodes. A required amount of solvent was added to the mixture to keep the ink in solution form.

Effect of Nafion Content

Ticianelli et al. (Ticianelli, Derouin, Redondo, & Srinivasan, 1988) examined the effect of Nafion loading for various ranges of current density. In the low current density region (mA/cm^2), the cell performance increases within Nafion loading. This can be explained by an increased active area in the electrodes. For the high current density region (300-600 mA/cm^2), the increase of Nafion content has a positive impact only up to 33% of Nafion, after which the performance starts to decrease rapidly. In the high current density region, low Nafion loading leads to the poor internal electrolytic conductivity that accounts for the poor cell performance. With increased Nafion loading, the conductivity increases, but a thicker layer of Nafion ionomer inside the pores of the electrode introduces mass transport problems either by retarding the access of gasses to the active sites or by encouraging flooding. Thus, for the high current density region, Ticianelli found that a Nafion content of about 33 % appears to be optimum for minimizing both ohmic and mass transport limitations.

Paganin et al. (Paganin, Ticianelli, & Gonzalez, 1996) ascertained that in their thin-film catalyst layer when the Nafion loading was increased from 0.87 to 1.75 mg/cm^2 the performance improved significantly. Moreover, the performance deteriorated at higher current densities when the Nafion loading was increased beyond

2.2 mg/cm^2, which is equivalent to an optimum Nafion percentage of 33 % of the catalyst layer weight. These values have been supported by several other recent studies (Gamburzev & Appleby, 2002; Qi & Kaufman, 2003). The effect of Nafion loading, as found by QK (Qi & Kaufman, 2003), is presented in Figure 3-8.
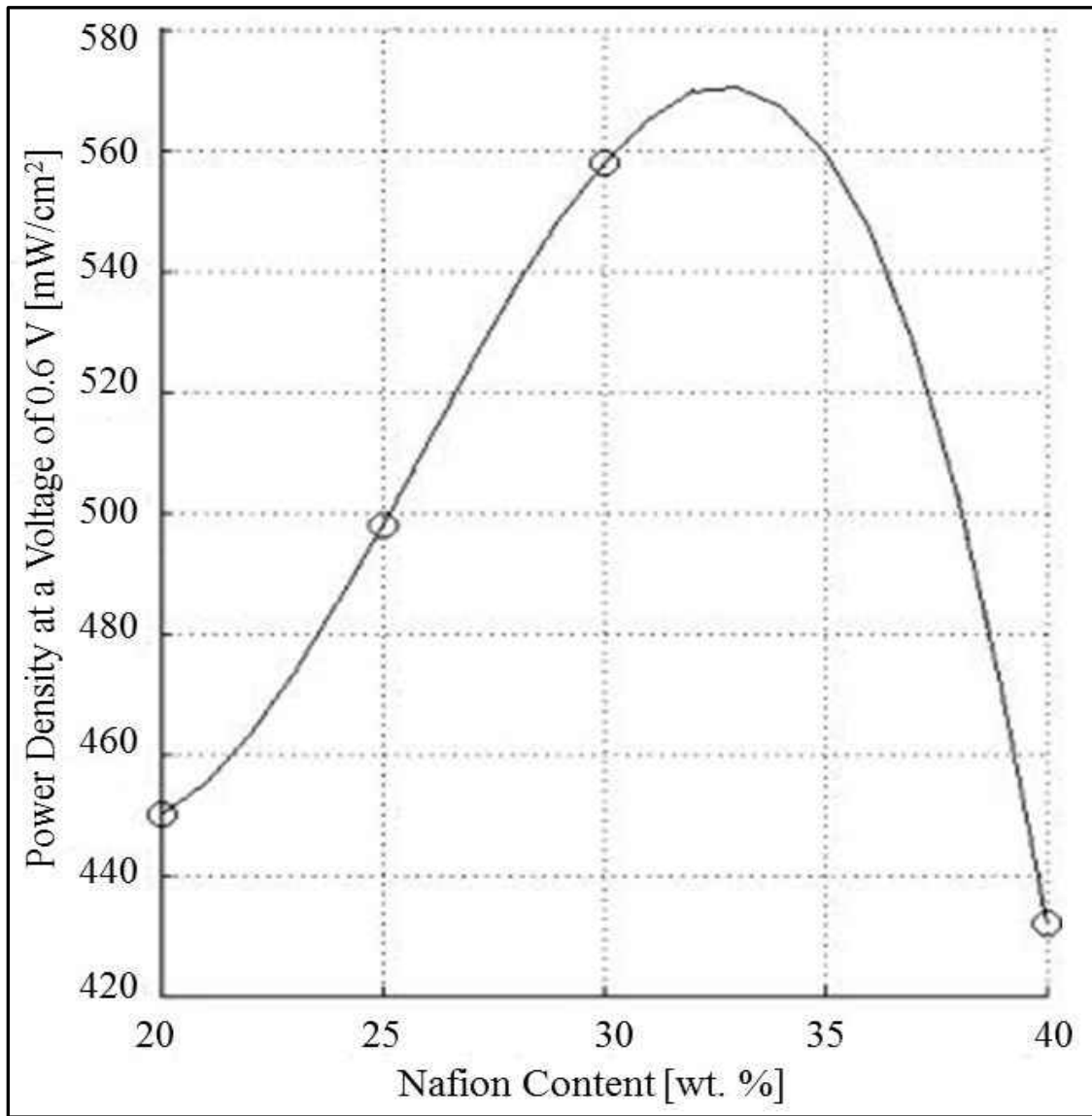
Figure 3-8 Effect of Nafion Ionomer content in the catalyst layer on performance E-TEK 20% Pt/Carbon, 35/45/45 °C (Qi & Kaufman, 2003)

Figure 3-9 is a schematic of the catalyst layer that depicts the effect of Nafion loading. Passalacqua et al. (Passalacqua et al., 2001) offer similar explanations who assert that at low Nafion content, some catalyst particles are not connected to the membrane by a Nafion bridge. However, too much Nafion in the catalyst layer creates a complex pathway for electron transport and increases the electronic resistance. At the optimal Nafion content in the catalyst layer, all the catalyst particles are properly connected for both ionic and electronic conduction.
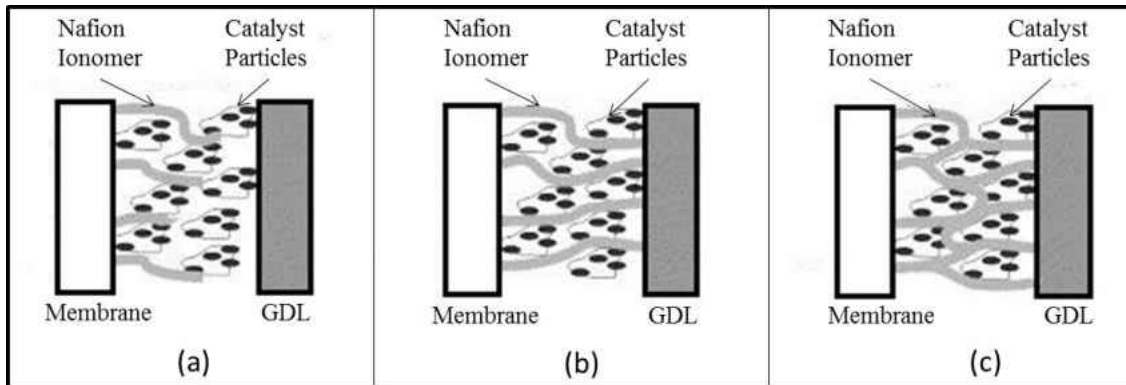
Figure 3-9 Schematic representation of the catalyst layer (a) the content of Nafion too low: not enough catalyst particles with an ionic connection to the membrane. (b) Optimal Nafion content: electronic and ionic connections well balanced. (c) The content of Nafion too high: catalyst particles electronically isolated from diffusion layer Reproduced from (Passalacqua et al., 2001)

Passalacqua and coworkers (Passalacqua et al., 2001) defined a parameter called NFP, which is the weight percentage of Nafion in the catalyst layer and found that the optimal NFP is 33 %. They used 20 % Pt on Vulcan XC-72 carbon at a Pt loading of 0.1 mg/cm^2. In addition, Ticianelli and coworkers (Ticianelli et al., 1988) found their best NFP is 33 %. They used 20 % Pt on carbon catalyst with a Pt loading of 0.35 mg/cm^2.

Effects of Solvent

Solvent plays a vital role in preparing a high-performance electrode, which has high catalyst utilization, as well as low contact and mass-transfer resistance. The solvent determines how well the catalyst ink adheres to the membrane, how even the catalyst layer can be applied, as well as how homogenously the catalyst ink is mixed. The solvent must be such that it does not interact with the membrane at all but instead serves as a means to apply the catalyst. In addition, a solvent not only affects the formation of the proton conduction network but also influences the intimate contact between the catalyst layer and the membrane due to the swelling property of the membrane during the coating or hot-press process (Therdthianwong, Ekdharmasuit, & Therdthianwong, 2010).

From the literature, it was found that the boiling point and dielectric constant value of a solvent plays a major role in determining a suitable solvent for preparing efficient and homogeneous catalyst ink. The higher the boiling point, the longer the solvents take to vaporize, and more solvent is left on the membrane to contribute to an adverse reaction. In contrast, the lower the boiling point of the solventless solvent and catalyst mixture adheres to the membrane. The appropriate range of boiling points must be examined. Finally, the catalyst ink's ability to form a homogeneous mixture is determined by the solvent, as the solvent is present in the greatest volume. The catalyst ink is typically composed of a 5% Nafion, in water. Thus, the solvents ability to mix with water would directly affect its ability to prepare a homogeneous catalyst ink.

The dielectric constant (ε) of a solvent also plays a critical role in determining the state of the Nafion ionomer in the catalyst ink solution, which consequently has an impact on the MEA performance during cell operation. The solvent with $10<\varepsilon$ makes the catalyst ink in solution form, $3<\varepsilon<10$ makes the catalyst ink in colloids form, and $\varepsilon<3$ makes it in precipitated form (Shin et al., 2002; Uchida, Fukuoka, Sugawara, Ohara, & Ohta, 1998). It is said that Nafion ionomers in the colloidal form are absorbed more homogeneously on the Pt/C than in the solution form. This would then aid in the development of a uniform three-phase interface, which must be optimized to increase performance. Shin et al. (Shin et al., 2002) compared the power output of MEAs made from two different catalyst inks. One using isopropyl alcohol (IPA, $\varepsilon=18.3$) and the other using normal butyl acetate (NBA, $\varepsilon=5.01$) as a solvent. The MEA with NBA solvent had higher power output than the MEA with IPA solvent. NBA solvent created an aggregated ionomer that created large pores (~736 nm) for better mass transfer and proton conducting network in the catalyst layer than those created by solution phase ionomer. The influence of solvent type on electrode performance was different for different MEA fabrication methods (Therdthianwong et al., 2010).

3.2.2 Catalyst Spreading

MEA fabrication methods are broadly categorized according to how the catalyst layers of the MEA are formed : the catalyst coated membrane (CCM) method and catalyst coated gas-diffusion-layer (CCG) method. Both of these methods have been successfully demonstrated on a commercial scale.

Catalyst Coated Membrane (CCM) Method

The catalyst-coated membrane (CCM) method involves direct (in the form of catalyst ink) or indirect (through a decal transfer) application of the catalyst layer to the Nafion membrane, then assembly with the anode side and cathode side gas-diffusion-layers (Tang, Wang, Jiang, & Pan, 2007). Primarily, there are two different fabrication techniques to prepare MEA by the CCM method, decal transfer technique (CCM-DT) and direct wet-spray onto the electrolyte membrane (CCM-DS).

In CCM-DS techniques, a catalyst ink is directly applied to the membrane (Sun, Ran, Wang, & Shao, 2008), while in an alternative CCM-DT technique, the catalyst layers are primarily formed over the decal substrates such as Teflon, and are subsequently transferred onto dry membranes surface during hot-pressing of MEA (usually 160–210 ℃) (Sun, Ran, & Shao, 2010). The catalyst coated membrane (CCM) method is depicted in Figure 3-10.
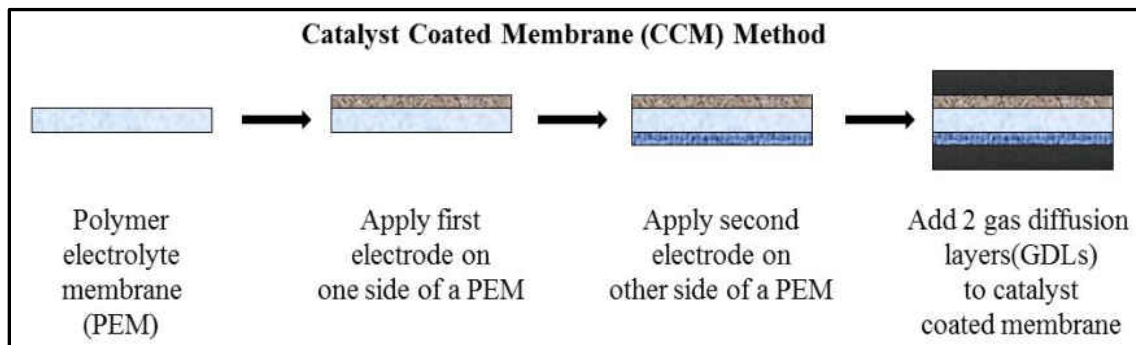
Figure 3-10 Schematic of catalyst-coated membrane (CCM) method

Catalyst Coated GDL (CCG) Method

In the CCG-based method, a catalyst layer is directly applied onto the GDL in the form of catalyst ink to prepare gas diffusion electrodes (GDEs) before hot-pressing with the membrane (Fernández, Ferreira-Aparicio, & Daza, 2005). The catalyst-coated GDL (CCG) method is depicted in Figure 3-11.
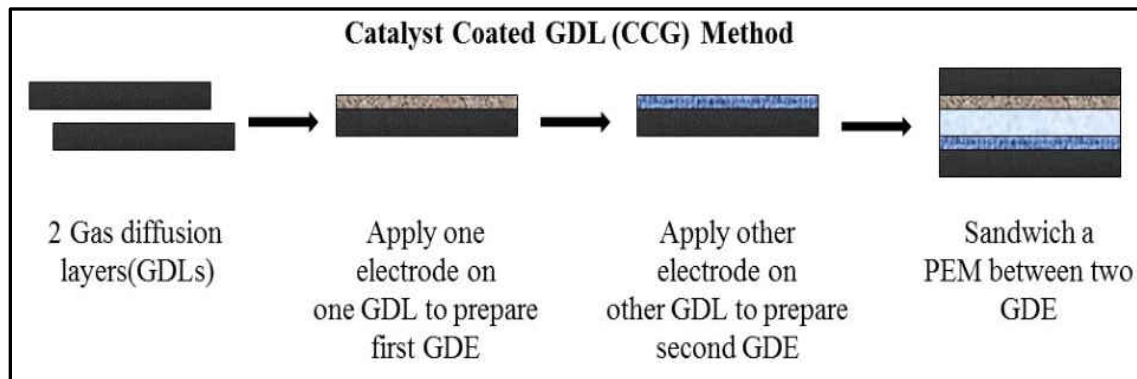
Figure 3-11 Schematic of catalyst-coated GDL (CCG) method

Thanslip and Hunsom (Thanasilp & Hunsom, 2010) showed that the contact resistance between the catalyst layer and membrane was less for the CCM method, which results in improved MEA performance. However, Song et al. (Song, Suzuki, Uchida, & Watanabe, 2006) improved the catalyst utilization using the CCG method. Literature gives many examples of both methods being applied; examples of the CCM method include Millington et al. (Millington, Du, & Pollet, 2011) Rodgers et al. (Rodgers, Mohajeri, Bonville, & Slattery, 2012) and Debe (Debe, 2011).

Even though the CCM method produces a better MEA performance due to a strong attachment of catalyst layers on the membrane than the CCG method (Xiong & Manthiram, 2005), the CCG method by brushing/coating catalyst ink onto the GDL was

selected as the MEA fabrication method for this work. The CCG method is relative simple in the number of ingredients and fabrication steps and easy to replicate in the laboratory, it also has some advantages over CCM methods. The main drawback of CCM is the tendency to serious swelling, wrinkling and cracking of the membrane when spraying/applying catalyst ink directly on the Nafion membrane during the fabrication process (Sun et al., 2008). The deformed electrolyte membrane never relaxed back to its original shape, which gives rise to the deformation of the catalyst layer by quick volume changes of the membrane. In addition, drying during and after catalyst spreading step results in a brittle membrane. The CCG-based method has the advantage that the catalyst loading can be adjusted very precisely by simply weighing the gas diffusion layer before and after the coating process (Frey & Linardi, 2004b).

3.2.3 Hot Press of MEA

Hot pressing is an important and necessary process for the preparation of MEA using the CCG method. It is an efficient and simple way to assemble an MEA with a good interfacial contact between the electrodes and electrolyte membrane. During the hot pressing process, inner structure and porosity of the electrodes can be changed (Küver, Vogel, & Vielstich, 1994). It can also cause the dehydration of the Nafion membrane, which may lead to an irreversible performance loss of the MEA (Zawodzinski, Springer, Uribe, & Gottesfeld, 1993). Therefore hot-pressing conditions, such as temperature, pressure, and pressing duration, influence the performance and durability of the resulting MEA (Guilminot, Corcella, Charlot, Maillard, & Chatenet, 2007; Mennola, Mikkola,

Noponen, Hottinen, & Lund, 2002; Yoda, Uchida, & Watanabe, 2007; Yoshida, Kinumoto, Iriyama, Uchimoto, & Ogumi, 2007).

Effect of Hot Press Temperature:

The temperature of the hot-press process plays a major role in MEA performance. For Nafion-based membrane, the hot-pressing temperature is usually limited by its glass transition temperature (T_g ~128 C). At a lower temperature than T_g, the Nafion resin in both the catalyst layer and the membrane will not melt and can result in poor ionic contact between catalyst layer and the membrane, which leads to low catalyst utilization and higher ionic resistance. In contrast, a temperature much higher than the T_g may lead to a loss of the water retention property of Nafion, and acidic group degradation in the ionomer.

Hot-press is used for adhesion and transfer of catalyst on the membrane to obtain good interfacial contact between electrolyte membrane and gas diffusion electrodes. This is essential because it creates a good continuity of Nafion between the membrane and the catalyst that will allow quick transport of the protons from the anode to the cathode side.

The impact of hot pressing conditions on the performance of PEMFCs appear to be minor (Wilson & Gottesfeld, 1992). Hot pressing is a very critical step in the preparation of MEA using the GDL-based method. The procedure and method for the fabrication of the MEA play a major role in the efficiency and catalytic activity of the catalysts, with direct consequences for the fuel cell performance.

Therefore, the temperature, time span, and pressure are all key parameters when hot pressing the membrane and the catalyst.

Effect of Hot-pressing Pressure:

The hot pressing is related to the mechanical strength, porosity, and thickness of the electrode. Normally, this porosity decreases with increasing pressure, which can restrict the mass transport of the gas. Moreover, the carbon fibers are prone to be crushed under high pressure, which shortens the mass transportation pathway. A study (Guilminot et al., 2007) showed that a lower hot pressure could result in a better fuel cell performance than a higher hot-pressing pressure.

Effect of Hot Press Duration:

Hot pressing time is another important parameter that affects the contacts between the membrane and the electrode, as well as the electrode porosity. It is recognized that with an increase in hot-pressure time, the ionic conductivity and the three-phase reaction in hot-pressing condition area in the catalyst layer can be first increased and then decreased, and the electrode porosity can also be decreased.

3.3   Theory/ Electrochemical Techniques

Electrochemical techniques, such as the polarization curve and cyclic voltammetry (CV), have been popularly employed in the characterization/evaluation of PEMFCs. The theories behind these electrochemical techniques are described herein

3.3.1 Polarization Curves of Fuel Cells

A polarization curve is plotted to characterize the performance of a fuel cell and visualize voltage losses. A polarization curve represents the performance of a fuel cell by plotting the cell voltage behavior against its operating current. It is important to emphasize that the polarization curve is an overall effect of numerous transports (electron and ion conduction, chemical species diffusion/convection, mass convection), and electrochemical reactions (oxygen reduction reaction and hydrogen evolution reaction). It yields information on the performance losses in the cell and, is especially a useful tool for comparison of the performance of the cell.
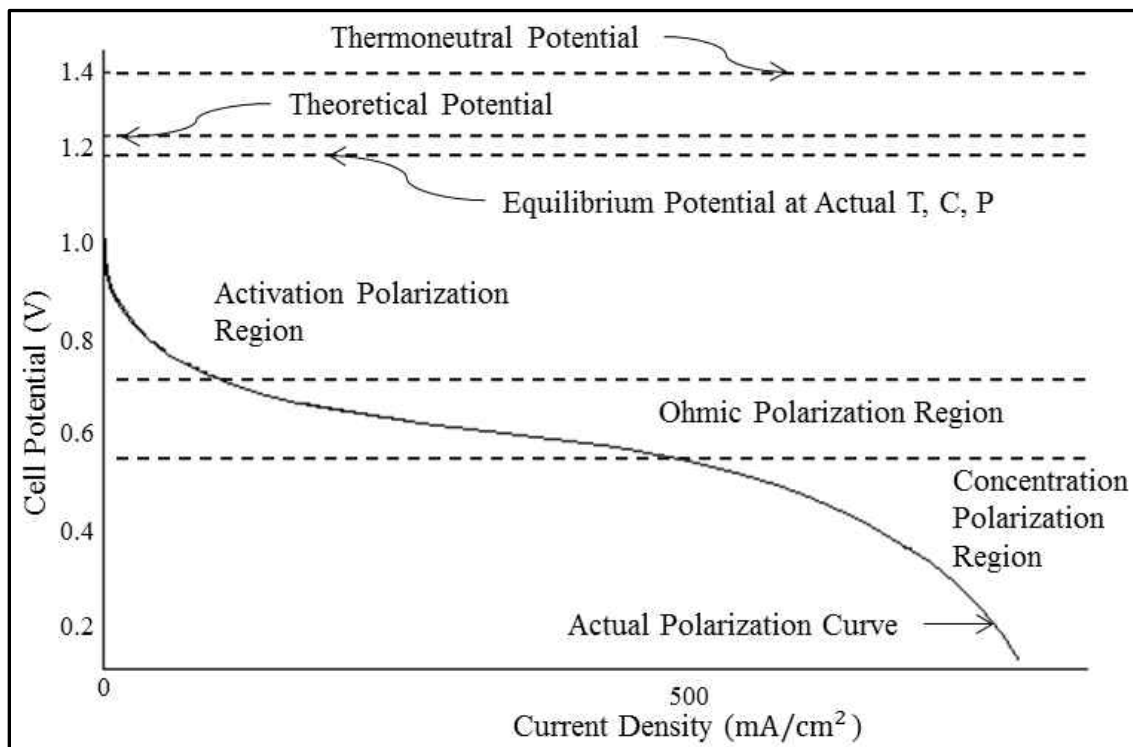
Figure 3-12 Generalized polarization curve of a fuel cell showing regions dominated by different types of loss (adapted from Larminie & Dicks, 2000)

The ideal polarization curve for a unit-cell PEMFC has three major regions, which are shown in Figure 3-12 (Barbir, 2005). These three majors regions are known as

activation polarization, ohmic polarization and concentration polarization. The cell potential drops sharply at low current densities (the region of activation polarization), due to oxygen reduction reaction's (ORR) sluggish kinetics (Barbir, 2005). At intermediate current densities (the region of ohmic polarization), the voltage loss caused by ohmic resistance becomes significant, which results mainly from resistance to the flow of ions in the electrolyte and electrons through the electrode. In this region, the cell potential decreases nearly linearly with current density, while the activation overpotential reaches a relatively constant value (Barbir, 2005). At high current densities (the region of concentration polarization), mass transport effects dominate due to the transport limit of the reactant gas through the pore structure of the gas diffusion layers (GDLs) and catalyst layers, and cell performance drops drastically. From Figure 3-12 it can also be seen that the difference between the theoretical cell potential (1.23 V) and the thermoneutral voltage (1.4 V) represents the energy loss under the reversible condition (the reversible loss) (LI, 2005). The theoretical reasons behind those losses during cell operation are discussed in the following sections.

Activation Polarization Losses

A certain portion of energy is needed to start the chemical reaction in a fuel cell, which results in a non-linear voltage drop in the activation polarization region. This voltage loss is known as activation polarization loss. Activation loss occurs on both anode and cathode catalysts. Since ORR is much slower than HOR, it produces a much larger activation polarization loss. The activation losses usually occur in the low current density (~1 to 100 mA/cm^2) region and caused by the sluggish nature of the reaction

kinetics taking place on the electrode surface (Barbir, 2005). For a single reaction the voltage loss due to activation polarization can be described by the Tafel equation:

$$V = A \cdot \ln\left(\frac{i}{i_o}\right)$$
(3.1)

Where,

    V - is the activation overpotential,

    A - is constant representing the reactivity of electrochemical reaction,

    i - is the current density of the fuel cell, and

    i_o - is the exchange current density of the fuel cell

For PEM fuel cells, the constant A in Equation 3.1 is given as

$$A = \frac{R \cdot T}{2 \cdot \propto \cdot F}$$
(3.2)

Where,

    R - is the universal gas constant,

    T - is the absolute cell temperature,

    F - is the Faraday constant, and

    α - is the charge transfer coefficient

Based on Equation 3.1 and 3.2 the polarization loss increases as A increases which mean that the reaction is slow. The exchange current density (i_o) and charge transfer coefficient (α) are dependent on the types of reaction involved and materials of the catalyst and electrolyte. Therefore, the activation loss can be lowered only if new catalyst materials and electrolyte can be developed.

Ohmic Polarization Loss

The voltage loss in the ohmic polarization region is due the resistive losses which are caused by the resistance to the ionic and electronic flows. The ionic resistance is the resistance to the flow of ions through the electrolyte membrane. The electronic resistance includes the resistance to the flow of electrons through the material of the electrodes (Catalyst layers, MPLs, GDLs,) and the interconnections (gas distributors, flow field plates and current collectors). Similar to most of the electronic circuitry, the voltage drop is linearly proportional to current density. The effects of ohmic losses are most pronounced at intermediate current densities (~100 to 500 mA/cm^2). The over-potential of ohmic loss can be represented by Ohm's Law:

$$V = i \cdot R \tag{3.3}$$

Where,

i - is the current density of the cell, and

R - is the overall area specific resistance (Ω./cm^2) within the cell

The electric resistance of the material of the electrodes and the interconnections can be considered constant with respect to current and temperature. Therefore, any change in the ohmic losses is only dependent on membrane resistance which is a function of membrane water concentration and membrane temperature (Springer, Zawodzinski, & Gottesfeld, 1991).

Concentration or Mass Transport polarization Loss

At high current densities ($>500 \, \text{mA/cm}^2$) the diffusion rate of the reactants cannot keep up with the rate of reaction. One more time the limiting side is the cathode side since the diffusivity of oxygen through the GDL, and the MPL is about 5 times less than the diffusivity of hydrogen, and as a result, the concentration of oxygen on the cathode is lower. This voltage loss is often described as concentration polarization loss. The concentration reduction of the reactants is the result of the concentration gradient required to transport sufficient reactant to the electrode surface. Therefore, it's also called as mass transport polarization loss. Sometimes this type of loss is also called "Nernstian" because this is related to the concentration of the fuel and the Nernst equation used to model the effects of concentration.

This polarization loss usually occurs at high current density densities ($>500 \, \text{mA/cm}^2$) regions because of the high demand of the reactants and only limited amount of reactants can be transported to electrode surfaces. The current density at which zero reactant concentration reaches is called the limiting current density (i_l). Considering this

64

relationship between reactant mass transport and current density, the mass transport losses can be expressed as (Barbir, 2005):

$$V = -B \cdot \ln\left(1 - \frac{i}{i_l}\right) \tag{3.4}$$

Where,

B - is a constant that depends on the fuel cell and its operating state, and

i - is the current density, and

i_l- is the limiting current density

The theoretical value of B is different for different reactants

for hydrogen $\qquad B = \dfrac{R \cdot T}{2 \cdot F}$ $\hspace{4cm}$ (3.5)

and

for oxygen $\qquad B = \dfrac{R \cdot T}{4 \cdot F}$ $\hspace{4cm}$ (3.6)

If the limiting current density of one electrode is reached, the voltage falls rapidly to zero, irrespective of the limiting current density at the other electrode.

3.3.2 Cyclic Voltammetry

Cyclic voltammetry (CV) is a commonly used electrochemical characterization technique for the study of electroactive species and electrode surfaces. It is a fast and

reliable technique to characterize fuel cell catalyst activity. It is a powerful tool for determining redox potentials, detecting chemical reactions that precede or follow an electrochemical reaction, and evaluating electron transfer kinetics (Greef, Peat, Peter, Pletcher, & Robinson, 1985). In a standard CV measurement, the potential of a system is swept forward (positive going) and reversed (negative going) directions between two voltage limits while monitoring the resulting current of the system. The voltage sweep is linear with time, and the plot of the resulting current versus voltage is called a cyclic voltammogram and gives information about reactions and processes occurring on the surface of the electrode (Kumpulainen et al., 2002). A typical cyclic voltammogram for a Pt/Carbon electrode is shown in Figure 3-13.
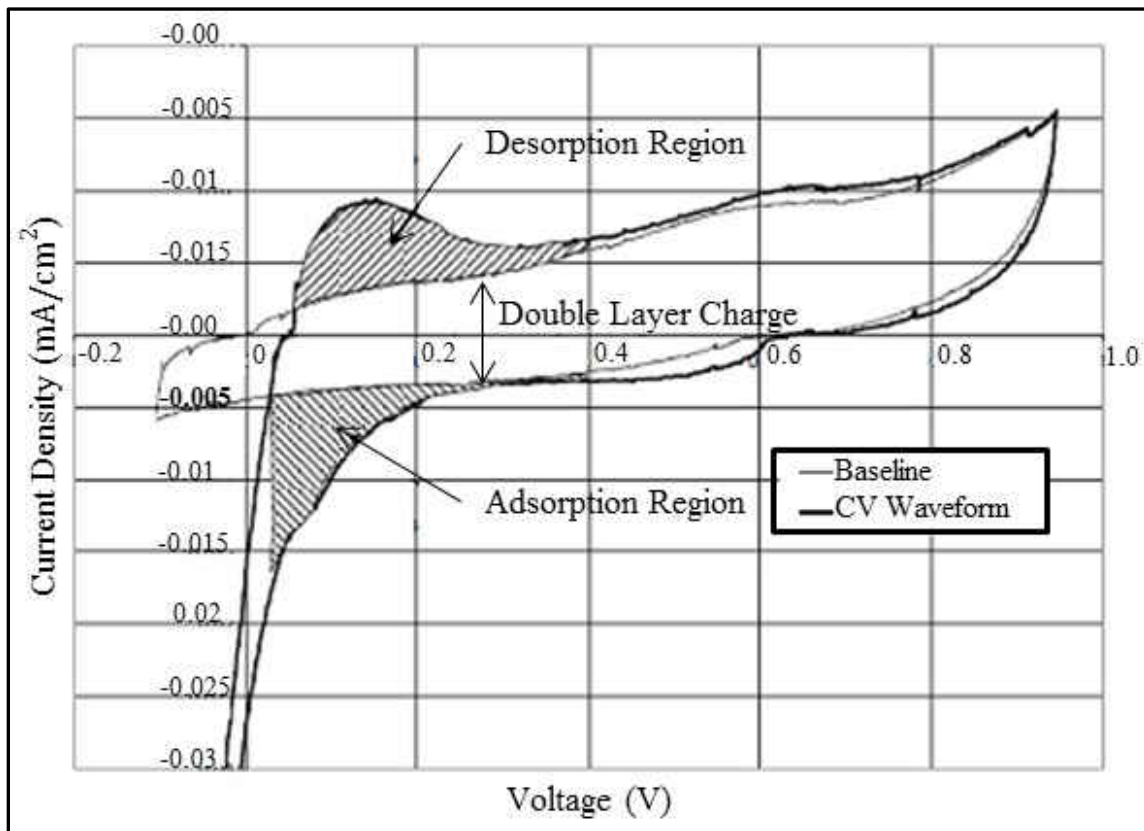
Figure 3-13 Typical Cyclic Voltammetry curve for a Pt/Carbon electrode

The characteristic shape of the cyclic voltammogram is a result of different processes taking place at the working electrode surface. Following the common convention, the positive-going scan currents are denoted as anode currents and the negative-going scan currents as cathode currents (Hamman, Hamnett. A., & Vielstich, 1998).

At the start of the test, hydrogen adsorption on the Pt occurs because of the applied potential. As the voltage increases, hydrogen desorption from the Pt begins (equation 3.7), and the hydrogen is oxidized as electrons leave the electrode (equation 3.8). The electrons that leave the electrode during this process comprise the desorption-charge. During the reverse sweep, the hydrogen is reduced (equation 3.9) and re-adsorbed to the Pt (equation 3.10) as electrons are supplied to the electrode. The electrons supplied during this process comprise the adsorption charge.

$$H_{ads} = H \tag{3.7}$$

$$H = H^+ + e^- \tag{3.8}$$

$$H^+ + e^- = H \tag{3.9}$$

$$H = H_{ads} \tag{3.10}$$

To provide a baseline, the test is also conducted with nitrogen gas flowing through both sides of the cell. Again, the current was recorded during the last of three voltage cycles. This baseline indicates the charge double-layer that builds up across the electrolyte during the test. This charge double-layer is due to the capacitive nature of the

cell and the rapid changes in voltage imposed during the test and is independent of the processes described in equations 3.7 through 3.10.

CV uses a three electrodes configuration; consisting of a working, a reference, and a counter electrode. The working electrode can be seen as a medium whose reductive or oxidative force can be remotely adjusted by the magnitude of the applied potential. As the applied potential is increased or decreased linearly with time, it becomes a stronger oxidant or reductant, respectively. Therefore, the working electrode, which is usually comprised of an inert conductive material, for example, Pt, acts as a contributor or acceptor of electrons participating in the general electrode reaction.

To do a similar experiment in a fuel cell with two electrodes, the reference and counter electrode are clamped together. Hydrogen is flushed into the electrode chamber and due to the low overpotential, the potential could be seen as constant. Since the hydrogen reaction is reversible, the electrode is used as the counter electrode at both cathodic and anodic sweeps.

The potential is measured across the reference and working electrodes, and the current is measured between the working and counter electrodes. The reference electrode keeps the potential between itself and the working electrode constant. A counter electrode is employed to allow accurate measurements between the working and reference electrodes. The counter electrode ensures that the current does not flow through the reference electrode since it would change the reference electrodes potential.

CV tests can be performed in both $in-situ$ and $ex-situ$ experiments. In $ex-situ$ experiments (half-cell experiments) the properties of the catalyst are investigated using a standard three-electrode configuration, where the working electrode consists of a catalyst-coated glass carbon disk electrode while the counter electrode is usually a Pt wire, graphite, Au or other highly conductive materials with good resistance to redox environments. $In-situ$ CV experiments normally employ a two-electrode configuration in which the working electrode is the electrode of interest and the other serves as both a counter electrode and a pseudo-reference electrode (Wang, Yuan, & Li, 2011). When the experiment is performed to investigate the properties of the cathodic electrode, the fuel cell anode is used as the counter/reference electrode, with the assumption that its polarization is small in comparison with the one imposed on the fuel cell cathode (working electrode). In this configuration, hydrogen is fed at the anode that acts as a dynamic hydrogen electrode (DHE). The cathode is fed with inert an gas nitrogen or argon and acts as working electrode. It is preferable to limit the maximum of the potential sweep to 1 V (vs. DHE) in order to avoid carbon oxidation.

CHAPTER 4

EXPERIMENTAL METHOD

This chapter explains the MEA fabrication and experimental methods used for the $in-situ$ evaluation. The first part of this chapter lists the material used in this study, and details the fabrication procedure for the Pt/Silica catalyst, which was fabricated in-house at UND. The second part of this chapter describes the design and fabrication of the test stand, procedures and equipment used to conduct $in-situ$ tests. Finally, this chapter highlights the $in-situ$ diagnostic techniques and accelerated stress tests (AST) used to study the performance and durability of the catalysts.

4.1   Chemicals, Gasses, and Materials

The following materials, chemicals, and gasses were procured and used in this research work. All chemicals and materials were used as received without further purification, except the Nafion membrane and catalysts.

Materials:

The novel silica-supported platinum (Pt/Silica) catalyst (10% Pt on silica), was fabricated in-house and provided by UND's Chemistry Department. The carbon supported platinum (Pt/Carbon) catalyst (10% Pt on Vulcan XC-72), carbon black

(Vulcan XC-72) and 5-layer MEAs (25 cm^2 active area, 0.3 mg/cm^2, size 10 cm x 10 cm) were purchased from ElectroChem, Inc. Nafion membrane (N-115), a gas diffusion layer (carbon cloth, size 30 cm × 30 cm), and silicon gaskets were purchased from the Fuel Cell Store.

Both Nafion membrane (N-115) and catalysts (Pt/Silica and Pt/Carbon) were pretreated before its use. The pretreatment procedure is described in section 4.3.2 and section 4.3.3 of this dissertation.

Chemicals:

Nafion solution (Aqueous, 5 wt%, 1100 EW) was purchased from Fuel Cell Store. HPLC grade Cyclohexane, H_2O_2 (3%) and H_2SO_4 were purchased from Fischer Scientific. Hexanol (99%) and Triton X-100 were purchased from Alfa Aesar. Tetraethylorthosilicate (TEOS, 98%), hydrogen hexachloroplatinate ($H_2PtCl_6 \cdot 6H_2O$, 99.9% purity) and sodium borohydride ($NaBH_4$, 98+% purity) were purchased from Acros Organics. Ammonium Hydroxide (EM Science, GR), and (3-Aminopropyl) Triethoxysilane (APTS, 99%) were purchased from Sigma-Aldrich. Other chemicals were procured from either Sigma-Aldrich or Fisher Scientific.

Gasses:

Industrial grade hydrogen (H_2), oxygen (O_2), nitrogen (N_2), and air bottled tanks were purchased from Praxair, Grand Forks, North Dakota.

4.2   Pt/Silica Catalyst Formation

Pt/Silica nanoparticles were synthesized in-house at UND's Chemistry Department using a relatively simple template synthesis method that can control the size, spatial distribution and composition of deposited Pt nanocatalysts on silica NPs. The catalyst formation method is described previously by Aize et al. (Li, Zhao, & Pierce, 2010) and is reviewed briefly here.

4.2.1   Preparation of Amine-functionalized Silica NP Supports

Silica nanoparticles (NPs) with uniform sizes were prepared by a reverse microemulsion method. A mixture of 7.5 ml cyclohexane (Fischer Scientific, HPLC grade), 1.8 ml hexanol (Alfa Aesar, 99%), and 1.77 ml Triton X-100 (Alfa Aesar) was well mixed in a vial to form the microemulsion. Spherical silica NPs were formed by adding 100 μl of tetraethylorthosilicate (TEOS, Acros, 98%), 60 μL of ammonium hydroxide (EM Science, GR) and stirring 24 hours. The NPs were post-coated with amine functional groups by adding 50 μL of TEOS and 50 μL 3-Aminopropyltriethoxysilane (APTS, Aldrich, 99%) and allowing the hydrolysis to proceed for another 24 hours. An addition of acetone was used to break the microemulsion, and the NPs were separated from the solution by centrifugation. The amine-functionalized NPs were washed with ethanol two times to remove the surfactant and then dried under ambient conditions. Assuming that the hydrolysis of APTS with the NPs was quantitative, the amine group density of the post-coated NPs was close to 3.6 mmol/g NP or $4.63 \cdot 10^{-18}$ mol per NP.

4.2.2 Preparation of Silica-supported Pt Catalysts

For Pt nanocatalysts, amine-functionalized NPs (60 mg) were suspended in 10 ml hydrochloric acids (pH-2) to protonate the functional groups (~214 μmol estimated). An aqueous solution of hydrogen hexachloroplatinate ($H_2PtCl_6 \cdot 6H_2O$), Acros Organics, 99.9% purity) was added dropwise to the NP solution and stirred for 1 hour to completely adsorb the metal precursor. To make silica NP-supported Pt nanocatalysts with a 10 wt. % loading of Pt, $H_2PtCl_6 \cdot 6H_2O$ solution was slowly introduced to the NP solution. To reduce the adsorbed metal precursor, a solution of 0.05 M sodium borohydride ($NaBH_4$, Acros Organics, 98+% purity) and 0.025 M Na_2CO_3 was added slowly to the NP suspension and allowed to stir for 5 hours. The amount of borohydride solution was adjusted to ensure a 10-fold excess of $NaBH_4$ to metal ions. The metal-coated nanoparticles were collected by centrifugation and washed twice with water.

4.3 MEA Fabrication Process

The most realistic technique to study the performance of a new catalyst for PEMFCs is by catalyst integration into a membrane electrode assembly (MEA), and evaluation of its $in-situ$ performance in a unit-cell PEMFC. The experimental understanding of the various factors involved in the fabrication of MEA was developed by conducting a thorough literature review (section 3.2). With this background, and from experimental observations made during the earlier MEA fabrication (section 6.1.1) during this research work, the proposed methodology to fabricate reproducible MEA was developed.

Several different techniques are used to fabricate PEMFCs MEA as discussed in section 3.2 of this dissertation. In this research, MEAs were fabricated in-house using a catalyst coated GDL (CCG) method, whereby the catalyst layer was applied using a hand brush to form a thin uniform layer of a prepared catalyst ink onto the GDL. The CCG method for the fabrication of MEA is explained in section 3.2 of this dissertation.

The procedure for the development of the MEA fabrication method involved the replication of MEA fabrication procedures from the literature reported to give a good performance, followed by a critical evaluation of the parameters said to affect the performance. The understanding that was developed, based on theoretical and experimental investigation of the various aspects, was used to propose methodologies for fabrication of a high-performance MEA.

Since the hypothesis of this research was focused on the enhanced performance and durability of MEA with novel Pt/Silica catalyst, compared to the MEA with the state-of-the-art Pt/Carbon catalyst, two types of MEAs, Type-A and Type-B were fabricated in-house using CCG method. Both Type-A and Type-B MEAs were fabricated using identical steps and same recipe, except Type-A MEA uses a Pt/Carbon catalyst and Type-B MEA uses Pt/Silica. Table 4-1 summarizes the components utilized for the Type-A and Type-B MEA fabrication using CCG method.

In addition, a Type-C MEA, a commercial MEA made by ElectroChem Inc, was also used in some experiments in this research. These MEAs were made on Nafion-115

membrane with 0.3 mg/cm^2 catalyst loading but detail information about the commercial

MEA was not disclosed by the vendor due to proprietary reasons.

Table 4-1 Components used for the fabrication of Type-A and Type-B MEA

Component	Manufacturer	Description
Pt/Carbon Catalyst	ElectroChem Inc.	10% Pt on Vulcan XC-72, used in Type-B MEA
Pt/Silica Catalyst	In-house at UND's Chemistry department	10% Pt on silica, used in Type-B MEA
Gas Diffusion Layer	Fuel Cell Store	Teflon treated carbon cloth
Electrolyte Membrane	Du Pont	Nafion 115 (thickness: 125μm)
Ionomer solution	Ion power	5 wt% Nafion solution (1100 EW)
Solvent	Alfa Aesar	Iso-propanol

Type-A MEA:

Type-A MEA reported in this study was fabricated using Pt/Carbon as the catalyst for both the anode and cathode electrode. This was used to develop the baseline to which compare the performance and durability of Type-B MEA using novel Pt/Silica catalyst.

Although high-quality MEAs with the $state-of-the-art$ catalyst could be purchased from many vendors such as E-Tek, Gore, Fuel Cell Store or ElectroChem Inc. the commercial MEA cannot be used for developing the baseline in this project, since

very little information is usually disclosed about the electrodes and the MEA fabrication method due to proprietary reasons.

Type-B MEA:

The Type-B MEA was prepared using Pt/Silica as the catalyst for both the anode and cathode electrode in this study. The Type-B MEA was used as the basis to prove the hypothesis of this work.

Since the performance of the Type-B MEA will be evaluated relative to the performance of their corresponding Type-A MEA, the MEA fabrication method, the catalyst ink mixture, and Pt loading ratios were not extensively optimized in this study. The goal was simply to obtain consistent performance to enable comparison.

Dimensions of the MEAs used in this work are depicted in Figure 4-1. The active area of 25 cm² (5 cm

Figure 4-1 Dimensions of the MEAs used in this work
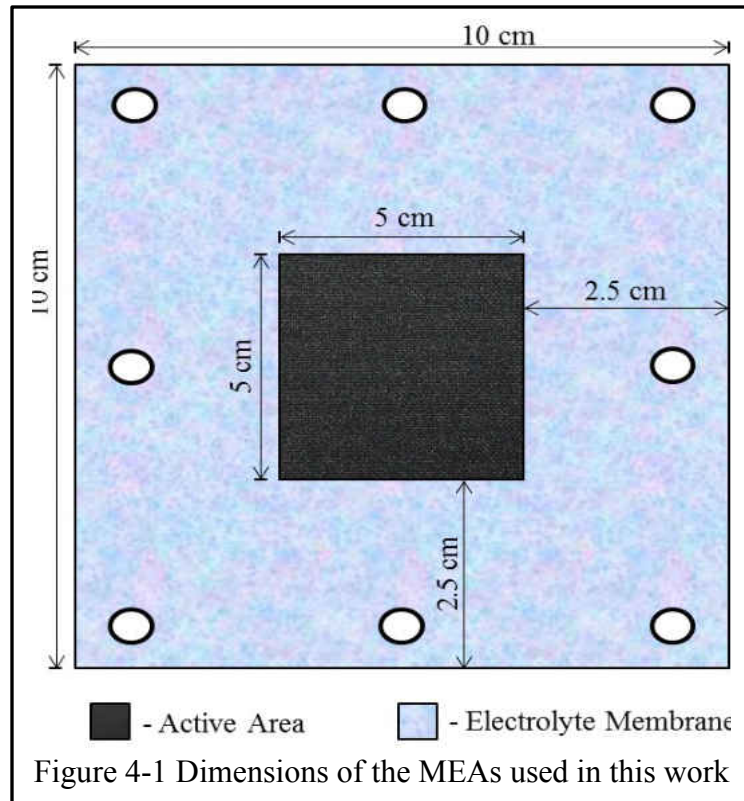
x 5 cm) was located at the center of the polymer electrolyte membrane of 100 cm² (10 cm x 10 cm). Thinner membranes have a lower resistance to protons which results in

76

better performance (Kocha, 2003; Kordesch & Simader, 1996), but since a hot press method was used for MEA fabrication, a thicker membrane was used for this study. Nafion-115 (thickness: 125μm) membrane was used as the polymer electrolyte membrane for both Type-A and Type-B MEA. The diffusion layer backing can be either carbon paper or carbon cloth. For this study, Teflon treated carbon cloth was used as a GDL since hot-pressing pressure can easily damage the carbon paper.

As mentioned earlier (section 3.2), MEA fabrication using CCG method is a multi-step process. All the steps involved in the fabrication of an MEA using the CCG method for this research work are explained in the following section.

4.3.1   Cutting Appropriate Size Membrane and GDL

A plastic template shown in Figure 4-2 was used to cut the membrane and GDL. The plastic template reflects the exact dimensions of the MEA and fuel cell hardware,
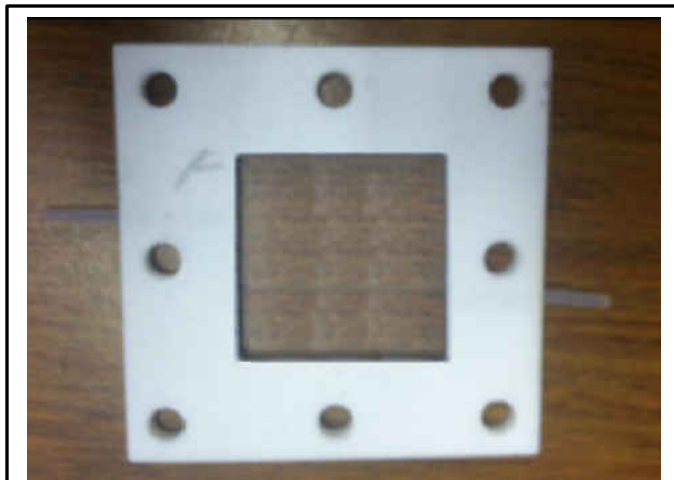
Figure 4-2 Plastic templet for membrane, GDL, and gasket cutting

including its flow field and eight holes on the edges and corner for the bolts for fixing the fuel cell. The Nafion membrane was cut into a square size with the help of a razor blade with each side measuring 10 cm using the plastic template shown in Figure 4-2. The membrane was also cut with eight holes on the edges using the same plastic template for the bolts for fixing the fuel cell hardware. GDLs were cut to the required size of 5cm x 5

77

cm using the inner square of the same plastic template. The membrane and GDL after cutting to the appropriate size are shown in Figure 4.3 (a) and (b) respectively.
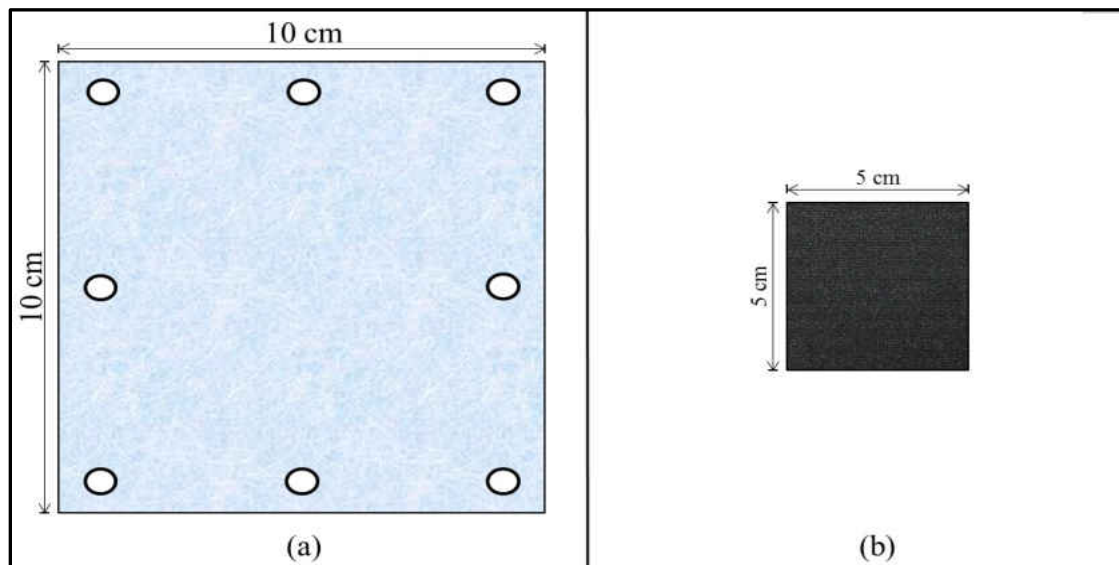
Figure 4-3 Dimensions of (a) electrolyte membrane and (b) gas diffusion layer

4.3.2 Membrane Pretreatment

Membrane pretreatment involves cleaning the Nafion membrane. Since the electrolyte membrane was not protected from organic contaminants, the membrane needs to be cleaned by pre-treatment to remove all the organic/inorganic impurities and to increase its protonic conductivity.

The pre-treatment of the Nafion membrane was accomplished by successively treating the membrane in a sequence mentioned in Table 4-2. First; it was boiled in deionized water for 30 mins, followed by boiling in 500 ml of 3 wt. % hydrogen peroxide for 60 mins and then again in deionized water for 30 mins to remove any traces of hydrogen peroxide in the membrane. This step helps removes all the organic/inorganic impurities from the membrane. The membrane was then converted to proton conductive

form by boiling in 0.5M sulfuric acid for 60 mins, and then cleaned by boiling in deionized water for another 30 mins to remove any traces of sulfuric acid in the membrane. Finally, the membrane was rinsed three times in lightly boiling deionized water. Electrolyte membrane pretreatment sequence is depicted in Figure 4-4.

Table 4-2 Nafion membrane pre-treatment sequence

Step #	Process	Time
1	Deionized Water	30 mins
2	3 wt. % Hydrogen Peroxide (H_2O_2)	60 mins
3	Deionized Water	30 mins
4	0.5M Sulfuric Acid	60 mins
5	Deionized Water	30 mins
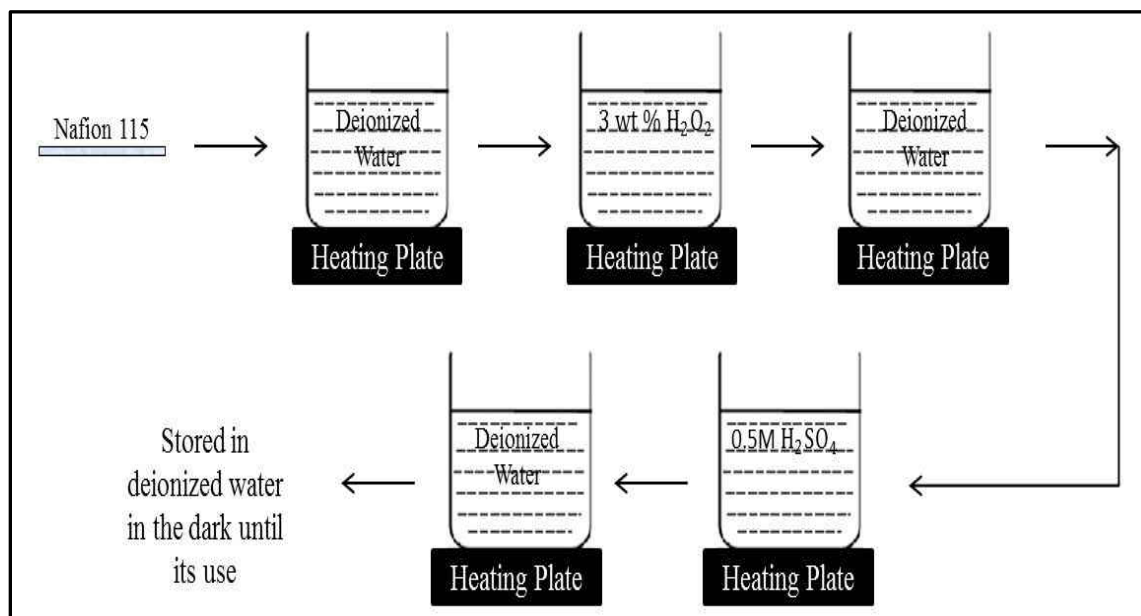
Figure 4-4 Nafion Membrane pretreatment procedure

This pretreated membrane was then stored in deionized water in the dark until its use. The deionized water was refreshed every week to keep membrane proton-active. It

79

should be noted that boiling denotes a gentle boiling, vigorous boiling could damage the membrane surface.

4.3.3   Catalyst Pre-treatment

Both Pt/Silica and Pt/Carbon catalysts were dried at 100° C for 60 mins in an oven to remove the moisture absorbed by the catalyst from the atmosphere. These dried catalysts were then stored in the desiccators. This is a good precaution since catalyst can absorb water. Alternatively, one may use the catalyst as is and determine a correction factor later by weighing

Figure 4-5 Catalysts stored in a desiccator after pretreatment

catalyst as received and determining the mass fraction of water lost.
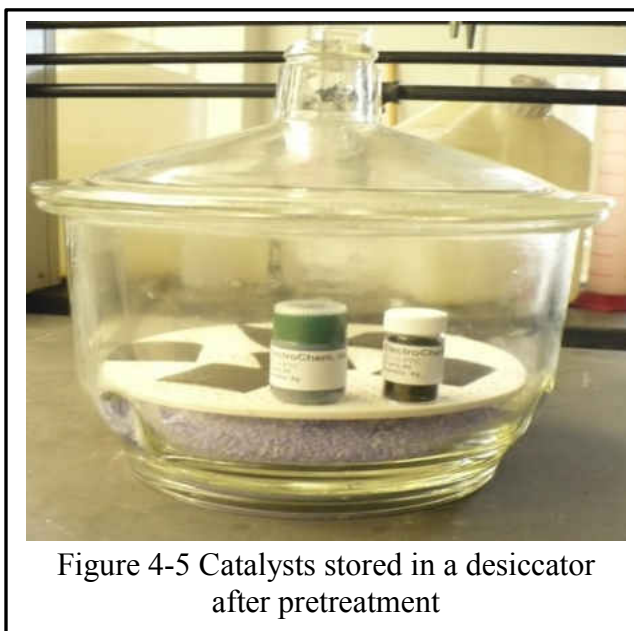
4.3.4   Catalyst Ink Preparation

In this study, two separate catalyst inks were prepared for fabricating Type-A and Type-B MEA using Pt/Carbon catalyst and Pt/Silica catalyst respectively. The ink was prepared by mixing catalyst, deionized water, Nafion solution, and a solvent; the mixture was then sonicated in a Misonix® Sonicator 3000 for 15 mins. For this study Nafion loading in the ink was set to be 33 (wt.) %, and the targeted catalyst loading was set to be 0.3 mg/cm^2.

Catalyst Loading (Ld_{Pt} in mg/cm^2):

Catalyst loading is the amount of catalyst metal of the catalyst layer. The symbol for loading is Ld_{Pt} which has a unit of $mg - metal/cm^2$. The catalyst loading is always with respect to the metal catalyst content; therefore, one must know the mass fraction of metal on catalyst support in the catalyst to calculate it. In this research, $0.3mg/cm^2$ was chosen for both Type-A and Type-B MEA's as representative Pt loading. The amount of catalyst (M_{Pt}) required in mg to prepare a catalyst ink with a targeted catalyst loading can be calculated using equation 4.1.

$$M_{Pt} = \frac{Ld_{Targeted} \times A_{CL}}{w_{Pt}}$$
(4.1)

Where,

$Ld_{Targeted}$ – Targeted Pt loading in the catalyst layer of an MEA in mg /cm^2

A_{CL} — Area of the catalyst layer or active area of MEA in cm^2

w_{Pt} — Mass fraction of Pt catalyst in the catalyst

Nafion Loading (L_{Naf} in mg/cm^2): Nafion loading is the weight percentage of Nafion in the catalyst layer per cm^2 of the electrode area, and is calculated by equation 4.2. It is generally denoted by L_{Naf}.

$$L_{Naf}(\%) = \frac{M_{Naf}}{M_{Naf} + M_{Cat}} \times 100 \qquad (4.2)$$

Where,

M_{Naf} — Mass of Nafion ionomer in the ink

M_{Cat} — Mass of catalyst in the ink

First, a desired amount of the catalyst was determined using equation 4.1, and 20 % additional catalyst was weighed into a vial using an analytical balance. The additional 20% of catalyst would compensate with the waste amount of ink during catalyst layer application on the brush and to the vial. A small amount of deionized water was then added to the catalyst using a micropipette. Deionized water helps remove air bubbles from the catalyst, and also prevents combustion upon the addition of alcohol on the catalyst. In order to efficiently transport the protons from anode to cathode to complete the electrochemical reactions in equation 1.3 (see section 1.4), a continuous path of the ionomer is required between the catalyst layer and electrolyte membrane. Therefore, a Nafion ionomer solution was also added to provide an ionic conduction path for protons to transport from anode to cathode. The amount of Nafion in catalyst ink is an important parameter, in this study, Nafion in the ink was set to be 33 (wt.) % based on the literature value. A required amount of the Nafion solution was determined using equation 4.2 and a solvent was then added to the catalyst.

The catalyst ink composition for both Type-A and Type-B MEA is given in Table 4-3. Each GDE has a catalyst loading of 0.3 mg/cm² for a 25 cm² of an active area of

MEA. For every mg of catalyst, the stock solution contained 9.85 mg of 5% Nafion solution, 40 mg of isopropanol, and around 4-6 mg of water.

Table 4-3 Catalyst Ink Composition for Type-A and Type-B MEA

Components	Type-A MEA Ink (for each electrode)	Type-B MEA Ink (for each electrode)
Catalyst ($Ld_{Targeted}$ 0.3 gm/cm2)	75 mg Pt/Carbon	75 mg Pt/Silica
Deionized water	As required to make catalyst wet (usually 4-5 drops total)	As required to make catalyst wet (usually 4-5 drops total)
Ionomer Solution (33 wt.% Loading)	0.74 g of Nafion Ionomer	0.74 g of Nafion Ionomer
Solvent	3.0 g of isopropanol	3.0 g of isopropanol

The resulting mixture was then sonicated for 15 mins at room temperature to prepare a homogeneous ink. The sonication probe was placed at the center of the vial and approximately 2-3 mm below the surface. The sonicator was started and the output power shown on the screen of the generator was monitored. Care was taken to ensure that overheating of the catalyst did not occur during mixing by keeping the vial in an ice-cold water bath during sonicating. The ideal catalyst ink suspends the catalyst particles in a colloidal suspension while minimizing agglomeration of the catalyst particles. Ideally, the catalyst suspension will have a uniform consistency that remains stable throughout the catalyst application process. A successful catalyst ink formula and preparation method

ensures the creation of a uniform catalyst layer and allows for consistency between separate MEAs.

4.3.5   Catalyst Layer Application

The fabrication of the gas diffusion electrode (GDE) includes forming the reactive catalyst layer on GDL by coating a catalyst ink on top of the microporous GDL. The coating technique is very critical for the uniform distribution of catalyst. Before starting the coating process, the actual weight of each GDL (M_{GDL}) was determined and noted after drying the GDL at 110 °C for 15 mins to remove any moisture from GDL. This weight was then used to determine the actual loading of catalyst in a fabricated MEA in section 4.3.6.

In this work, the GDEs (anode and cathode electrode) were fabricated by hand painting the catalyst ink on the GDLs (5 cm x 5cm) using a small paintbrush. The same procedure was followed for preparing both the anode and cathode GDEs, with a

Figure 4-6 Illustration of GDE formation from GDL using hand painting
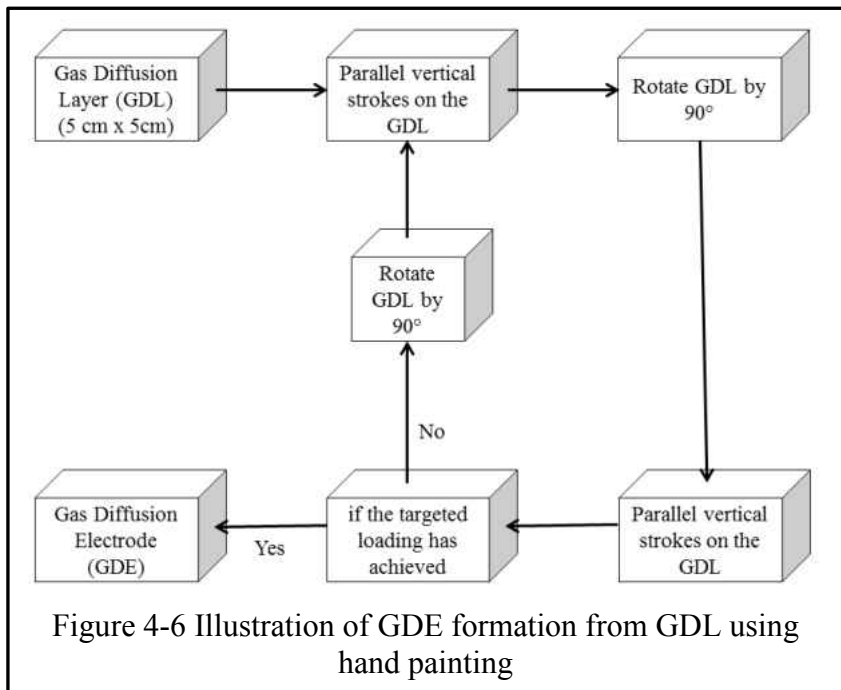
targeted loading of 0.3 mg/cm² for both electrodes, which is also depicted in Figure 4-6.

The coating process takes place on a heated hot plate at 60 °C so that the ink can be dried very fast and cannot diffuse through the carbon cloth. The use of heated hot place was used to avoid the diffusion of catalyst ink through the GDL to the other side, which was observed during preliminary experiments in section 6.1.2.

The vial with the desired catalyst ink was placed in a beaker filled with ice to avoid solvent evaporation. A paintbrush was dipped into the catalyst ink and pressed against the side of the vial to remove excess liquid before each coat was applied. The catalyst ink was then applied by successive parallel vertical strokes on the GDL. The GDL was rotated 90° between each coat for even distribution of the catalyst. The catalyst ink was repeatedly applied on GDL to obtain a targeted loading of 0.3 mg/cm². In order to achieve accurate Pt loading of each electrode, the weight of the electrode was recorded after each coat until the total weight of the electrode reached its intended weight. Depending on the ink, 10–15 layers were required to achieve the targeted metal loading. When the desired loading was obtained, the GDE were then oven dried at 120 °C for 20 mins to remove solvent from the catalyst layer. These GDL – electrodes are then stored in desiccators at room temperature until needed.

4.3.6   Calculation of Actual Catalyst Loading in GDE

After drying the GDE to remove solvents, the dried GDE was then weighed (M_{GDE}) to determine the actual weight of the catalyst layer on the GDL by subtracting the actual weight of the uncoated GDL (M_{GDL}), which was determined before the catalyst coating.

$$Ld_{Pt} = \frac{(M_{GDE} - M_{GDL}) \times (1 - L_{Naf}) \times w_{Pt}}{A_{CL}} \qquad (4.3)$$

Where,

Ld_{Pt} — Actual loading of Pt in the GDE in mg/cm^2

M_{GDL} — Weight of GDL in mg

M_{GDE} — Actual weight of GDE in mg

L_{Naf} — fraction of Nafion in the catalyst per gram of catalyst

w_{Pt} — Mass fraction of Pt catalyst in the catalyst

A_{CL} — Area of the catalyst layer or active area of MEA in cm^2

4.3.7   Hot Pressing

Finally, the pretreated Nafion membrane was sandwiched between the anode and cathode GDEs and hot pressed to form an MEA. The hot-pressing method promotes a good contact within the three-phase region, which lowers the resistance of the MEA by allowing a smooth flow of protons from catalyst layer to the membrane.

Two separate thin (1 mm thick, 15 cm x 15 cm) stainless steel plates were used for aligning the MEA components, and then it was placed in the hot press. These external plates were used to avoid the displacement of MEA components after alignment if the

MEA components are directly aligned in the hot-press, which was observed during preliminary experiments in section 6.1.2.

To form the MEA, first, an aluminum foil about 15 cm x 15 cm sizes was wrapped on both external plates to eliminate sticking of MEA to it. The aluminum foil was kept wrapped around the plates during the entire hot pressing process. Then a pretreated Nafion membrane square stored in deionized water was dried using a Kim-wipe and flattened between hot press plates for 10 mins without heat or pressure.

The alignment of MEA components starts with placing the first metal plate with aluminum foil wrapped around it on a flat surface. Then cathode GDL was carefully placed at the center of the metal plate with a catalyst layer facing up. The dried and flattened membrane was then aligned on top of the cathode GDL so that the cathode GDL is located at the center of the membrane. If the membrane was warped, then the edges of the membrane could be taped to flatten the membrane. Then the anode GDL was placed on top of the membrane with the catalyst layer facing the membrane. It is vital that the two GDLs are aligned completely together to ensure proper sealing and even distribution of the reactants to the catalyst and removal of the unwanted products from the catalyst. Once the GDLs are aligned, the second metal plate was placed on the top. Then the MEA components aligned between the two external metal plates was placed in the hot press, and the hot press were allowed to warm up for 5 mins without compression at 100 °C. Figure 4-7 showed the aligned MEA components between two thin metal plates and inserted into the hot press.

87
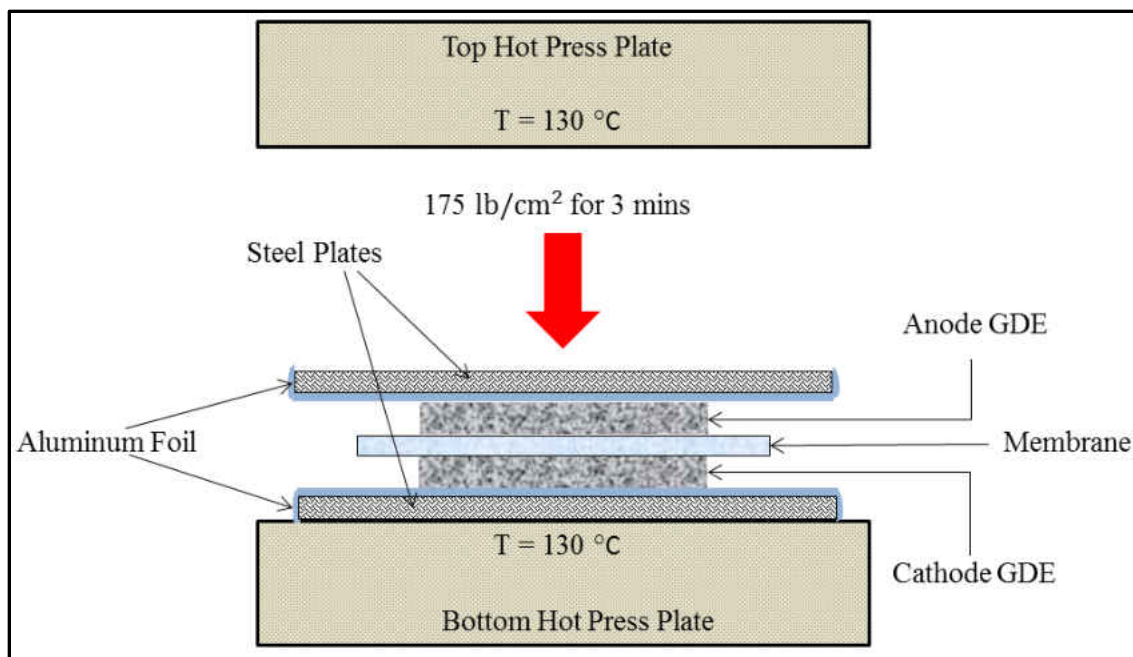
Figure 4-7 Schematic of hot pressing of membrane electrode assembly

The temperature of the hot-press was set at the glass transition temperature of Nafion, which is 130 ºC. The hot pressing procedure above the glass transition temperature of Nafion® causes the ionic polymer phase to flow and provides good contact between the catalyst layers and the membrane. For hot pressing a pressure of 175 lb/cm² electrodes are used for a carbon cloth as GDL (Zhang, Yin, Wang, Lai, & Cai, 2007). However, lower hot press pressure is applied when using a carbon paper as a GDL since it has a risk of breaking down under high pressure.

Table 4-4 Conditions for MEA hot press

Hot Press Condition	Set Point
Temperature (°C)	130
Pressure (lb/cm²)	175
Time (s)	180

After hot pressing under the conditions mentioned in Table 4-4, the hot press pressure was released, and the heat was turned down. The MEA was allowed to cool in the hot press for 30 mins. The MEA was then removed from the press still held between the two flat metal plates and further allowed to cool on the bench top. The MEA was removed from metal plates after cooling it for 60 mins at room temperature.

4.4 Pt/Silica Catalyst Performance Improvement

The $in-situ$ performance of Pt/Silica catalyst investigated in section 5.3 (results are presented in section 6.3) was very poor compared to the Pt/Carbon catalyst. The poor performance of Pt/Silica catalyst was thought to be as a result of low conductivity of silica. As mentioned earlier, an effective MEA must have the Pt metal accessible with both protonic and electronic path. The protonic path is achieved by the Nafion ionomer in the MEA, and the electric path is obtained by the combination of catalyst and support. Silica is less electronically conducting due to its low conductivity around $\sim 10^{-7}$ S/cm (Feng, Yao, & Zhang, 2004), which has drastically reduced the electron flow path in the catalyst layer.

Therefore, to further improve the electronic path in the catalyst layer carbon black powder was added to the catalyst ink. An appropriate amount of carbon power is needed to improve the electric path in the MEA. Adding an excess amount of carbon power could lead to decreased protonic conductivity. Both can influence the accessibility to the Pt metal. Therefore a method was developed to prepare modified Type-B MEA, and this modified MEA was labeled as Type-BB MEA.

The Type-BB MEA was prepared using the same method described in section 4.3, except the catalyst ink preparation (section 4.3.4) part. The catalyst ink recipe for Type-BB MEA was modified by adding the carbon-powered to the desired amount of amount of catalyst to achieve the targeted Pt loading. The formula for calculating NFP (equation 2.3) was modified to compensate for the added amount of carbon powder as follows.

$$L_{Naf}(\%) = \frac{M_{Naf}}{M_{Naf} + M_{Cat+CP}} \times 100 \tag{4.3}$$

Where,

M_{Naf} − Mass of Nafion ionomer in the ink

M_{Cat+CP} − Mass of catalyst and carbon powder in the ink

With the experimental observation made during the earlier Type-BB MEA fabrication (section 6.1.2) method development work, the appropriate Nafion loading was found to be 37%, and the experimental study was performed to determine the effect of carbon powder inclusion in the catalyst ink on the performance and durability of Type-BB MEA.

For this study the Nafion loading was not optimized, 37 % Nafion loading was found to be the minimum required amount of Nafion in the ink to make a compact and workable MEA (section 6.1.2).

4.5   Laboratory Equipment used for MEA Fabrication

As described in the previous section (section 4.3.7), a Carver hot press and Misonix S3000 Sonicator® was used in this work for MEA fabrication.

4.5.1   Hot-Press:

A Carver standard heated press was used to assemble the MEA under high temperature and pressure. It is a laboratory bench-top manual press with two 6 inch x 6 inch electrically heated steel plates. Each plate with a 700 Watts heater has a temperature range up to 400 °C and an analog gauge for its temperature control. It also has 12 ton, manual, two-column hydraulic lab press with 0-24,000 lb. analog pressure gauge, reading in 200 lb. increments, and daylight opening adjustable to 15 inches. The picture of the Carver standard bench top laboratory hot press used in this study is shown in Figure 4-8-a.

4.5.2   Sonicator

A Misonix S3000 Sonicator® (Figure 4-8-b), was used for the dispersion of catalyst nanoparticles in this work. A sonicator uses sound waves to agitate the nanoparticles in a solution to make a homogeneous mixture. The ultrasonicator uses a probe tip that transmitted ultrasonic energy into the Nanofluid. The available ultrasonication power settings were from 6 Watts to 42 Watts in 3 Watt increments with no alternate output power setting possible. During ultrasonication, the temperature of the Nanofluid was monitored using a thermocouple. For this study, the catalyst ink was sonicated for 15 mins at 6 Watts setting.
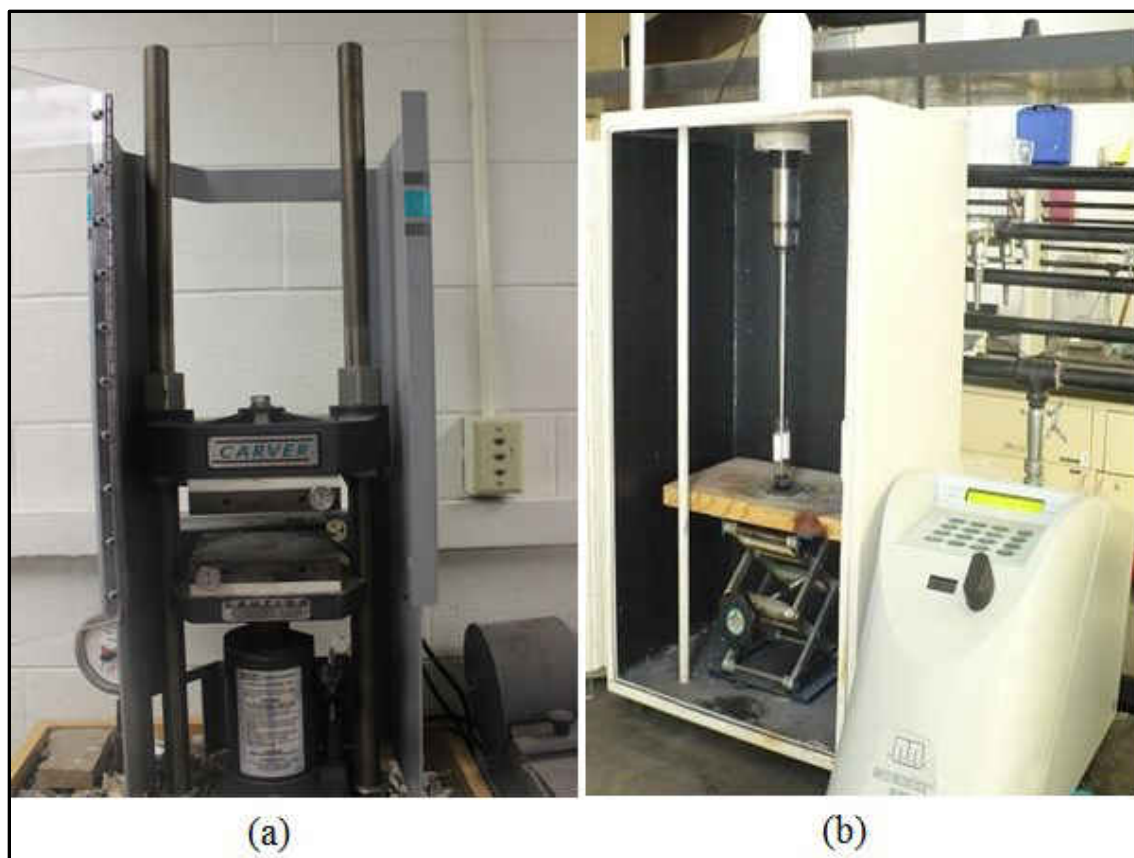
Figure 4-8 Laboratory equipment used for MEA fabrication (a) CARVER hot press (b) Misonix S3000 Sonicator®

4.6   Experimental Setup (Unit-cell Test Stand)

The test stand used in this work was designed and constructed in-house. Extensive experiments were conducted to develop the test stand. At the beginning of the work, the laboratory was equipped with an in-house built measurement system, which was designed for the primary characterization of fuel cell stacks and water electrolyzer stacks. In its original configuration, the system was best suited for the measurement of small fuel cell stacks with air supply by free convection. However, for a controlled unit-cell measurement; a forced cathode gas supply was needed, and the system was therefore modified to include gas supply from a pressurized bottle.

Initial experiments with the unit-cell highlighted the importance of controlled humidification of the reactant gasses and better temperature and gas flow rate control of the cell. The experience gathered from the old measurement system and expanding measurement needs suggested that a dedicated measurement and temperature monitoring system was required for controlled unit-cell performance and durability measurements; therefore, a test stand was designed and built in-house for this research work.

The test station components were regularly calibrated. The test station also has some built-in safety features that allow the station to be shut down either manually or automatically under dangerous situations, specifically hydrogen gas leakage. Preliminary tests with a commercial (Type-C) MEA and the experiments conducted on the sample (Type-A and Type-B) MEAs demonstrated that the test stand could reliably provide consistent conditions suitable for high-performance fuel cell operation and can reliably collect data.

The test stand has four main components: a unit-cell fixture, a control system, a gas feed system and a diagnostic system. A schematic diagram of the test stand is shown in Figure 4-9, and a picture is shown in Figure 4-10.
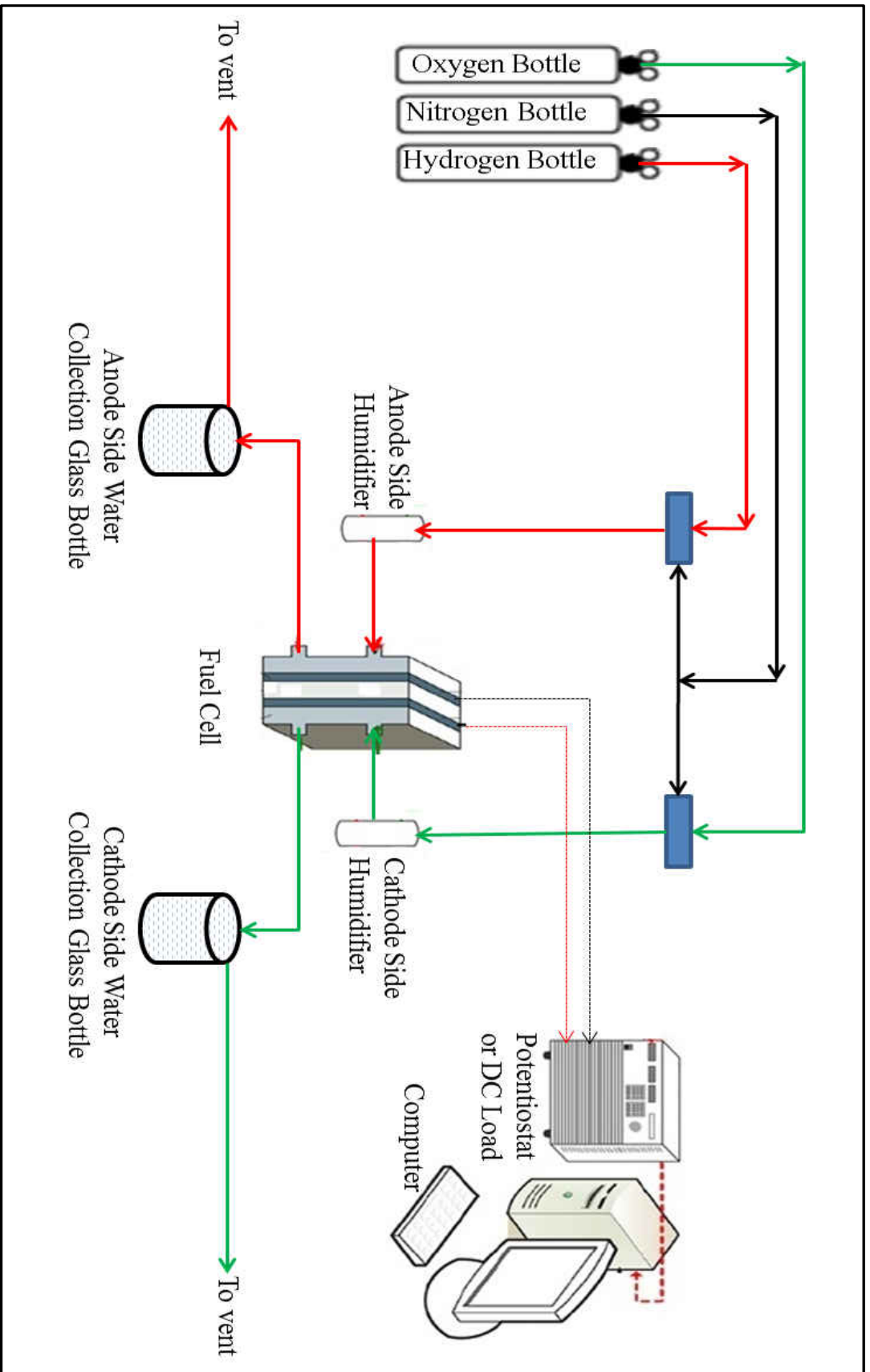
Figure 4-9 Schematic of the In-house Built Fuel Cell Test Stand (Flow Diagram)

94
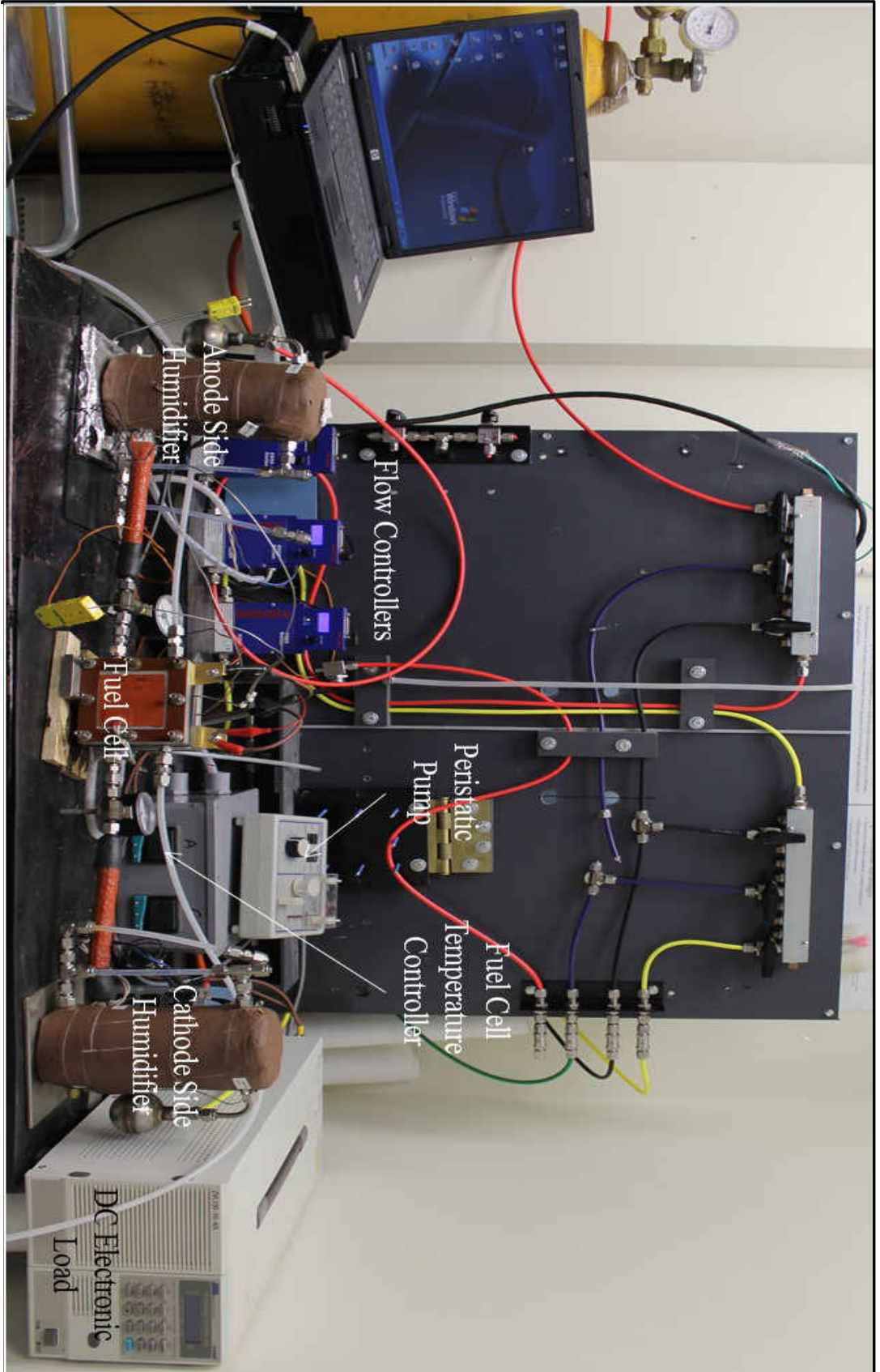
Figure 4-10 Picture of the in-house Built Fuel Cell Test Stand

4.6.1 Unit-Cell Fixture

The unit-cell PEMFC fixture used in this study is designed by HEPHASE Energy to test and evaluate MEA's in a consistent operating environment. The external size of the fixture is about 10 cm x 10 cm x 6 cm with an active area of 25 cm^2 (5 cm x 5 cm). This fuel cell fixture could be used for both hydrogen and methanol MEA's, and rated to operate up to 40-psi pressures and 120 °C temperature. The cell is was insulated from the metal endplates by hard Teflon® plates on both sites, to prevent an electrical shortage

The fuel cell test fixture is composed of 10 pieces: two flow field plates, two current collector plates, two end plates, two Teflon plates and two sheet heaters. All these fuel cell pieces are held together using eight compression bolts, and for that eight quarter-inch boltholes are located on the edge of all the fuel cell plates. A picture of the unit-cell fixture with its components is shown in Figure 4-11.

The flow field plates used in the test cell are natural fuel cell grade graphite (Figure 4-12-a),
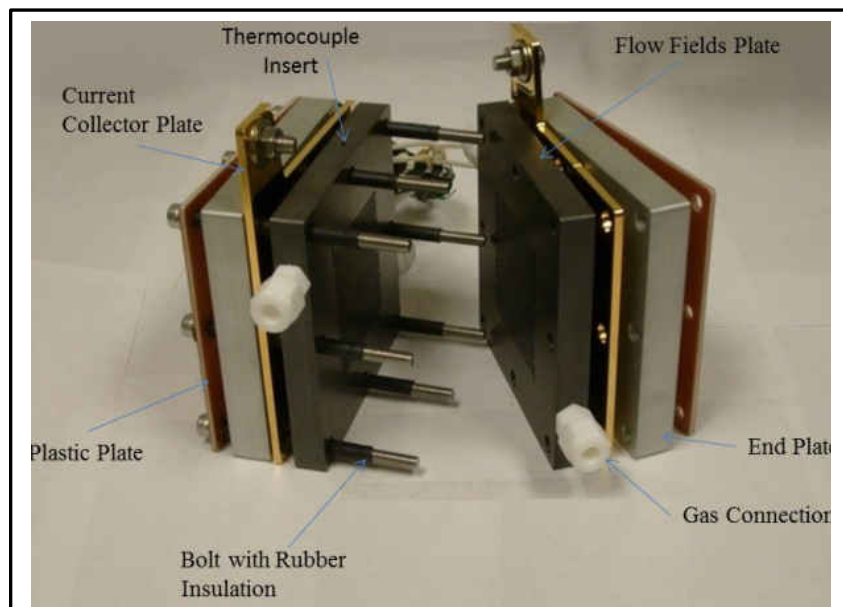
Figure 4-11 Unit-cell fixture with its components

which has engraved triple channel serpentine flow field winding back and forth across the active area. The flow field plates have connections for gas supply lines for the reactants

and products. Each flow field plate also has a hole to insert thermocouple at center the active area for precise monitor and control of cell temperature.
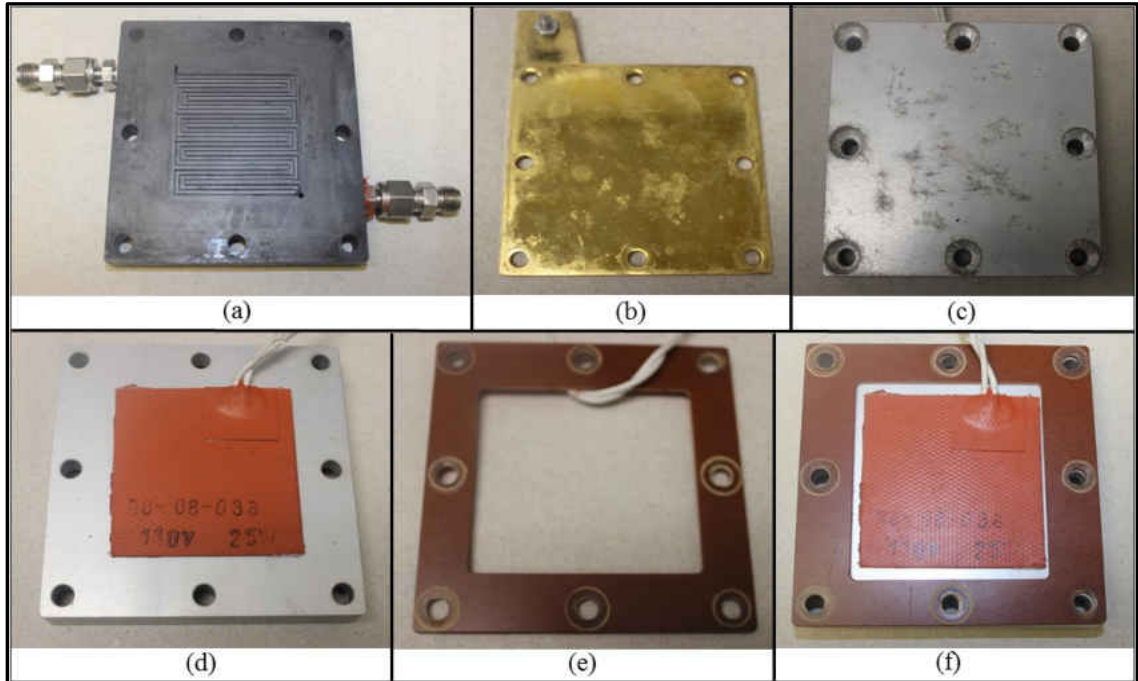
Figure 4-12 Images of the unit-cell fixture components (a) Graphite flow field with serpentine pattern (b) Gold plated current collector (c) Aluminum end plate (d) Silicon rubber sheet heater (e) Teflon plates (f) Outer side of end plate with Teflon plate and sheet heater attached to it

The current collectors (Figure 4-12-b) are gold-coated stainless steel plates; these plates enable the efficient measurement of the current and the voltage generated during the electrochemical reaction in a fuel cell. The aluminum endplates (Figure 4-12-c) serve as a clamp that holds all of the components of the cell together. The temperature of the cell is measured using thermocouples and maintained by external silicon rubber sheet heaters (Figure 4-12-d) located on the outside surface of the end plates. The Teflon plates (Figure 4-12-e) avoid any electrical short that could be caused by the bolts. The Teflon

plate and silicon sheet heater are attached on the outer side of the end plate (Figure 4-12 –

f). The components specifications of the unit-cell fixture are listed in Table 4.5.

Table 4-5 Specifications of the components of the unit-cell PEMFC fixture

Component	Specifications
Flow Field Plates	12 mm thick fuel cell grade graphite plate with triple channel serpentine flow field
Thermocouple Insert Holes	2 mm diameter hole in the flow field plate to insert thermocouple at center the active area for precise monitor and control of cell temperature
Current Collector Plates	3 mm thick gold plated plates with corrosion resistance
End Plates	15 mm thick stainless steel plates (70x70) mm
Heaters	6 cm x 6cm silicon rubber sheet heaters, 110 V, and 25 W
Compression Bolts	5 mm diameter and 75 mm long, eight steel bolts covered with plastic insulators

This fuel cell fixture is held together using 5 mm diameter and 75 mm long, eight steel bolts; these bolts were insulated with a shrinking tube to prevent an electrical short-circuit
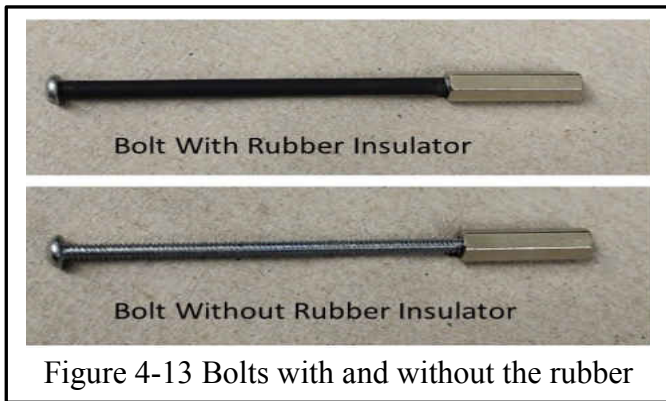
Figure 4-13 Bolts with and without the rubber

between anode and cathode side. A picture of one of the bolts with and without the plastic insulator is shown in Figure 4-13.

4.6.2   Control System

The control system controls and measures the operating conditions of the unit-cell fixture. The control system can control cell temperature, cell voltage, cell current as well as temperature, flow rate and humidity for both anode and cathode reactant gas streams.

Heating of the humidifiers, the tubes leading to the fuel cell and the unit-cell was accomplished using heat tapes, and temperatures of the feed streams and fuel cell are maintained using temperature controllers. The temperature controllers for the fuel cell heating elements and humidification bottles are also located on the fuel cell stand. The test stand also has a computer to control the diagnostic components remotely using an acquisition card.

4.6.3   Gas Feed System

The gas feed system is for humidifying and supplying the fuel and oxidant gas to the cell. The gas feed system provides industrial grade high-purity (>99.5%) reactants (hydrogen, oxygen/air) to the fuel cell; using a manually controlled digital mass flow controller Brooks 4800 series. The anode side feed stream can be switched between hydrogen and nitrogen gas, and the cathode side feed stream can be switched between oxygen, air, and nitrogen gas. Nitrogen gas was used for purging both the anode and cathode side when needed, and during diagnostic testing. Effluents from both the anode and the cathode side of the fuel cell are first run through the liquid collection bottle where

water is collected, and the gasses vented to a hood for safety purposes. The laboratory was equipped with a specially built ventilating system to ensuring safety while working with hydrogen gas.

The gas sub-system contains humidification bottles before the fuel cell and liquid collection bottles after the fuel cell. Humidification of the feed streams is necessary to keep the electrolyte membrane hydrated to retain its proton conductivity. The humidification can be bypassed if dry gas feed into the cell is desired. Anode side feeds supplied from a pressurized cylinder is sent through the heated anode humidifier before being fed through heated tubes to the anode side of the fuel cell. Similarly, cathode side feed is supplied from a pressurized cylinder and sent to the heated cathode humidifier before being fed through heated tubes to the cathode side of the fuel cell.

Both anode and cathode gas feeds (dry gas) are fed through a humidifier, which is simply a sparger (porous frit) bottle, heated by a heating jacket and filled with deionized water. In a humidifier, dry gas is dispersed into the water by a porous metal rod and the bubbles pick up moisture and leave the bottle carrying water vapor. The gas lines from the humidifiers to the cell assembly were wrapped in heat tape set an additional 5 °C above the humidifier temperature to prevent water condensation.

Humidification Unit

The humidification unit was used to provide humidification to the reactant gas by controlling the moisture content of the inlet gas stream. The bottle-type humidification system (HSA^{TM}) used in this work was procured from ElectroChem, Inc. The

humidification system is a stand-alone, with separate humidification unit for the anode and cathode side. Each humidification unit has a 500 ml stainless still water container with stainless steel gas channels. The container was placed in a heating pad, thus allowing the temperature of the water to be adjusted. The system also includes four temperature controllers, two for controlling the temperature of the gas humidifiers, and two other for controlling the temperature of gas transfer lines between the humidification unit and the test cell.

Figure 4-14 Humidification System used for reactants humidification

The picture of the humidification unit with its temperature controller is shown in Figure 4-14. The humidification system provides 100 % humidification with gas flow rates up to 2,000 ml/min, and can operate at a maximum operating pressure of 50 psi.

Bottle-type humidifiers are simple and cost-effective and are based on passing the gas to be humidified through a heated water bath. Water vapor is absorbed by the gas, as the bubbles rise through the water. Water uptake by the gas is a function of the water-gas interfacial area, and therefore, a sparger (porous frit) is commonly used to produce fine bubbles thereby increasing the humidification efficiency. The schematic of the humidification unit with its components is shown in Figure 4-15.
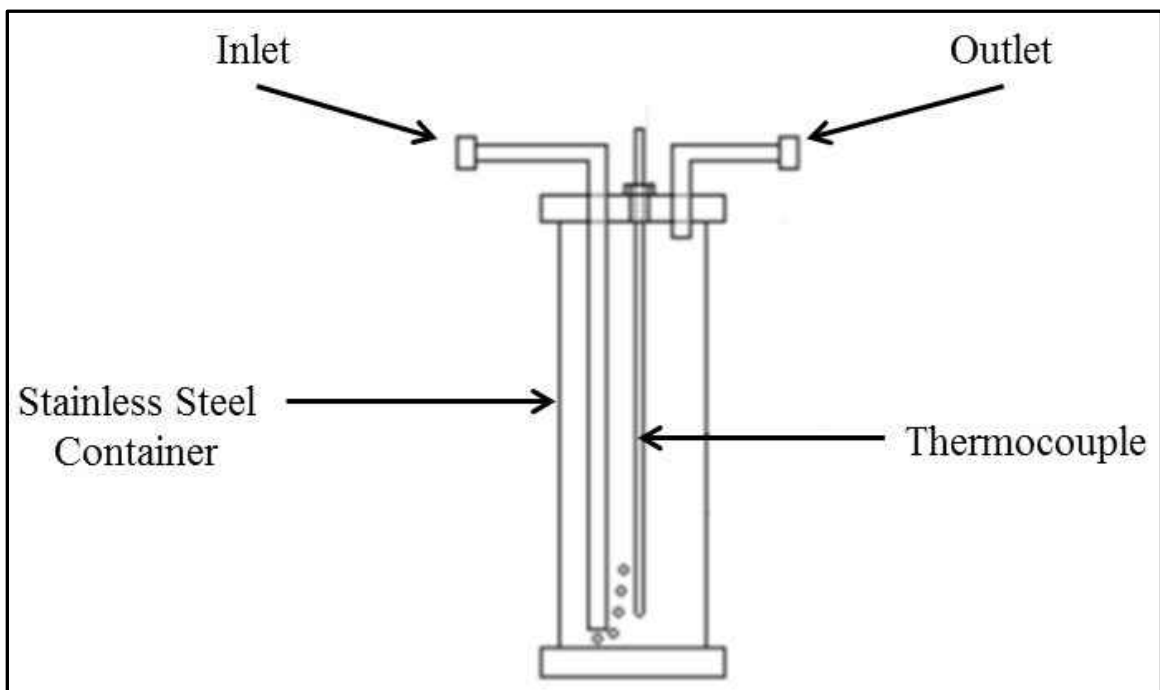
Figure 4-15 Schematic of humidification Unit

The relative humidity of the flowing reactant gasses was controlled by varying the temperature of the humidifiers and the temperature of the cell. The relative humidity at the fuel cell inlet is determined by the dew point temperature of the gas leaving the humidifier (T_{dp}) and the temperature of the gas entering the cell (T_{cell}) using equation 4.4.

$$\text{Relative Humidity} = \frac{p_{H_2O}}{P^*_{H_2O}} = \frac{p_{H_2O\ (T_{humidifier})}}{P^*_{H_2O}(T_{cell})} = \frac{P_{sat}(T_{dp})}{P_{sat}(T_{cell})} \quad (4.4)$$

Where, P_{sat} is a saturation pressure at a temperature. This pressure can be found using tables or calculated using equation 4.5, which is a curve fit proposed by Springer et al. (Springer, Zawodzinski, & Gottesfeld, 1991):

$$\log P_{sat}(T) = -2.1794 + 0.02953 \cdot T - 9.1837 \cdot 10^{-3} \cdot T^2$$

$$(4.5)$$

$$+1.4454 \cdot 10^{-7} \cdot T^3$$

Where, the partial pressure of water P_{H_2O} is equal to the vapor pressure of water, $P^*_{H_2O}$ at the temperature of the humidifier $T_{humidifier}$. The denominator is the vapor pressure of water at the temperature of the cell T_{cell}.

During the experiments, both humidifiers were controlled by thermocouples placed just above the water level. The small capacity of the humidifier (500 ml) enabled a constant temperature of 90 °C to be applied for no longer than 6 hours. After this time, the chamber ran out of the water. The humidifier was refilled with cold water, and consequently, it took 15 to 20 mins to stabilize the temperature.

Liquid Collection Bottles

The liquid collection bottles were used downstream of the fuel cell on both the anode and cathode side. During the fuel cell operation, water is generated on cathode side, which also needed to be collected before releasing the unreacted gasses to the

ventilation system. Also, humidification of both reactants results in condensed water in both anode and cathode line after the fuel cell. In order to prevent the water from the fuel cell from entering into the venting system, it is collected in the liquid collection bottles on anode and cathode sides. The picture of one of the liquid collection bottles used in this study is shown in Figure 4-16.
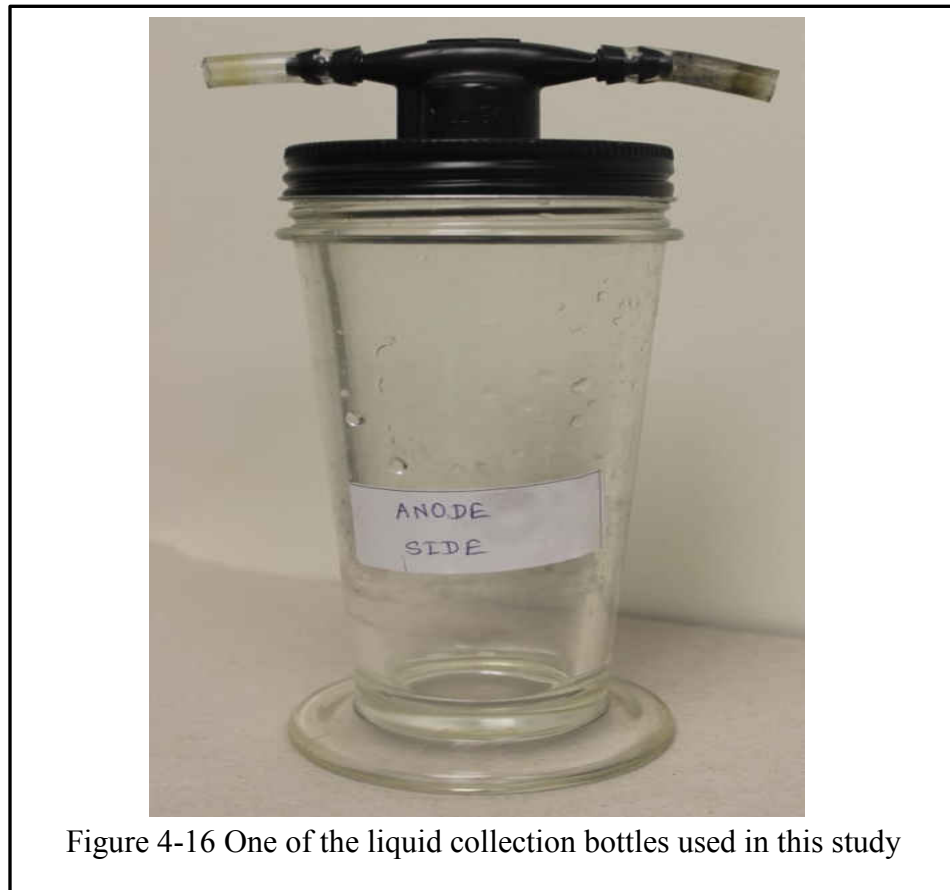
Figure 4-16 One of the liquid collection bottles used in this study

4.6.4 Diagnostic System

The test stand is integrated with several diagnostic components to evaluate PEMFC performance, which consists of two main components: a DC electronic load and

a potentiostat. The electronic load and potentiostat were used to characterize the performance and durability of the fuel cell under various conditions.

Programmable DC Load

AMREL's ZVL Series of Zero-volt Programmable DC Electronic Loads (Figure 4-17) are specifically designed for zero-volt load applications and offers the industry's highest current rating for "zero-Volt" operation. Custom-tailored voltage and current ratings make ZVL100-10-40L zero-
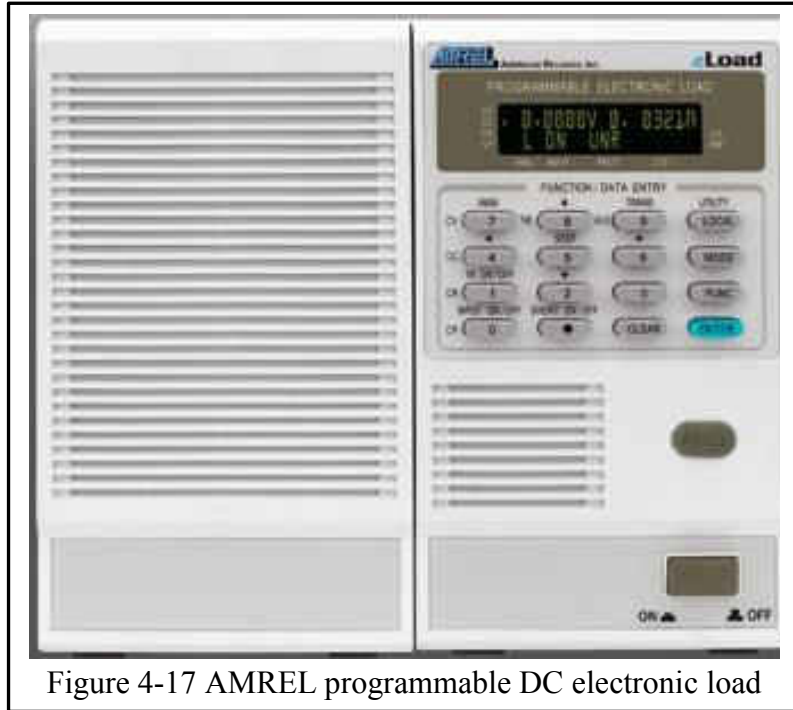
Figure 4-17 AMREL programmable DC electronic load

volt loads perfect for unit-cell fuel cell applications, which is rated at 40 W.

The load is air-cooled, and can be used in various increments to simulate the real-time load and drive the current flow from the fuel cell. The control system is designed to operate the eLoad in four modes – constant current mode, constant resistance mode, constant power mode and constant voltage mode. It has several safety features to prevent damage to the load and the fuel cell. Both current and voltage of the load are limited to

105% of the selected range, and the power is limited to 40 Watts. The load operates to control the voltage, current, or power within the ranges given in Table 4-6.

Table 4-6 Range of operation for eLoad

Parameter	Range
Voltage (V)	0-10
Current (A)	0-100
Power (W)	0-40

The load can be controlled manually from its front panel or remotely using the acquisition software. The software is a product of Scriber Associates Inc. and has a variety of monitoring, data logging, and display features. The software allows real-time visualization and is also able to log information in the form of excel files.

Potentiostat

In this work, Solartron Analytical 1287 (Figure 4.18) and Gamry G750 (Figure 4.19) potentiostats were used for the fuel cell performance and durability evaluation. Both potentiostats could run both as a current controlled system (galvanostatic mode) and a voltage controlled system (potentiostatic mode), and as a potentiostat, a galvanostat, or a ZRA (zero resistance ammeter).

Figure 4-18 Picture of Solartron Analytical 1287

The potentiostat regulates the potential difference between the reference electrode and the working electrode, and the current response is measured through the counter electrode and the working electrode. A potentiostat uses a feedback circuit to control the potential between the working electrode and reference electrode. The input voltage is set through communication with a software program. The amplifier controls the potential difference
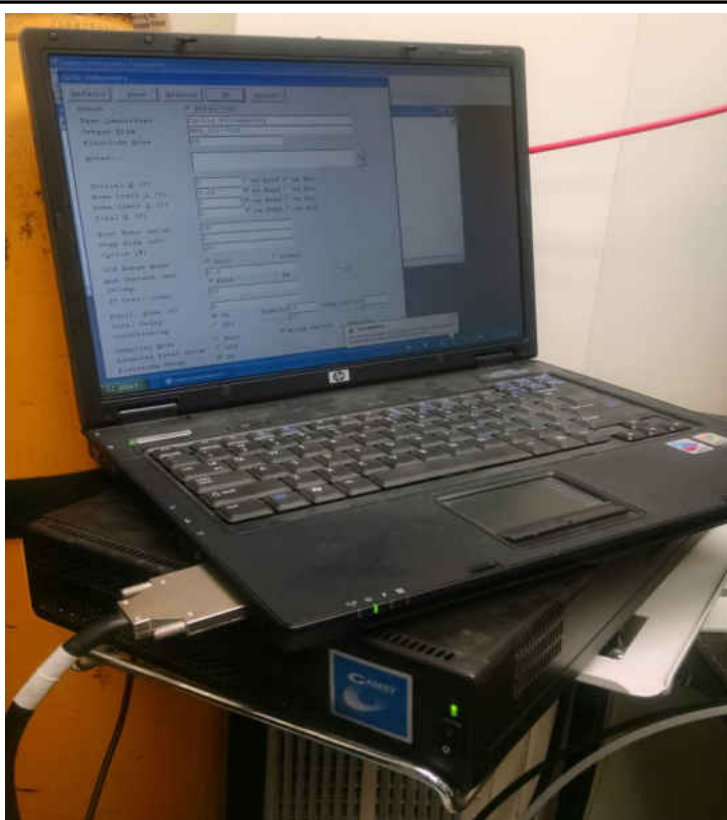
Figure 4-19 Picture of Gamry G750 potentionstat

between the working electrode and the reference electrode by varying the output current, which is measured between the counter and working electrodes. In the case of a unit-cell PEMFC, the reference, and the counter electrodes are the same.

4.7   Assembly of the MEA in the Unit-cell

The $in-situ$ electrochemical evaluation of the fabricated MEA was done by mounting it in unit-cell fuel cell hardware. Before the fuel cell was assembled, all the parts of the fuel cell hardware were cleaned using alcohol to ensure minimal contact resistance within the hardware and to achieve the best cell performance. After the MEA

was mounted in a unit-cell, pre-test integrity tests were performed to assure for the proper functioning of the test equipment and to warrant the test effort.

Once the unit-cell was assembled and pretested, the MEA was conditioned, and the electrodes were activated so that the MEA reached its peak performance before it is electrochemically tested.

4.7.1 MEA Mounting

The fabricated MEA was mounted in unit-cell fuel cell hardware along with a gasket for its electrochemical evaluation. Two 15 mils thick gaskets were cut with a razor blade using the same plastic template shown in Figure 4.2 (in section 4.3.1) that reflects the dimensions of the MEA and the fuel cell hardware. The middle square piece of each gasket is taken out so that it properly fits around each GDE while extending past the edges of the Nafion membrane, so that when compressed they formed a tight seal surrounding edges of the of the MEA by exactly matching the MEA and gasket with the fuel cell hardware. Just like the membrane, gaskets are also cut with eight holes on the edges for the bolts for fixing the fuel cell hardware.

First, the cathode-side end plate with the Teflon plate and silicon heater attached to it and all the bolts inserted in it was placed horizontally on a flat surface (Figure 4-20 – a). The cathode side current collector plate was then carefully aligned on the cathode-side end plate (Figure 4-20–b). The cathode side flow field plate was then carefully aligned on it with the cathode flow field facing up (Figure 4-20–c), and then the gasket was carefully placed on top of flow field plate so that the flow field shows through the gasket opening (Figure 4-20–d). The MEA was then aligned on top of the gasket in a way that the

cathode electrode is facing the cathode plate through the gasket opening (Figure 4-20–e). The second gasket is then aligned on top of the MEA so that the anode electrode shows through the gasket opening (Figure 4-20–f). The fuel cell anode plate is then aligned on top of the second gasket with the flow field facing down (Figure 4-20–g), and anode side current collector plate was placed horizontally on the top (Figure 4-20–h). Finally, the anode-side end plate was placed on the top(Figure 4-20–i), and the bolts were tightened in a cross pattern by hand using a torque wrench.
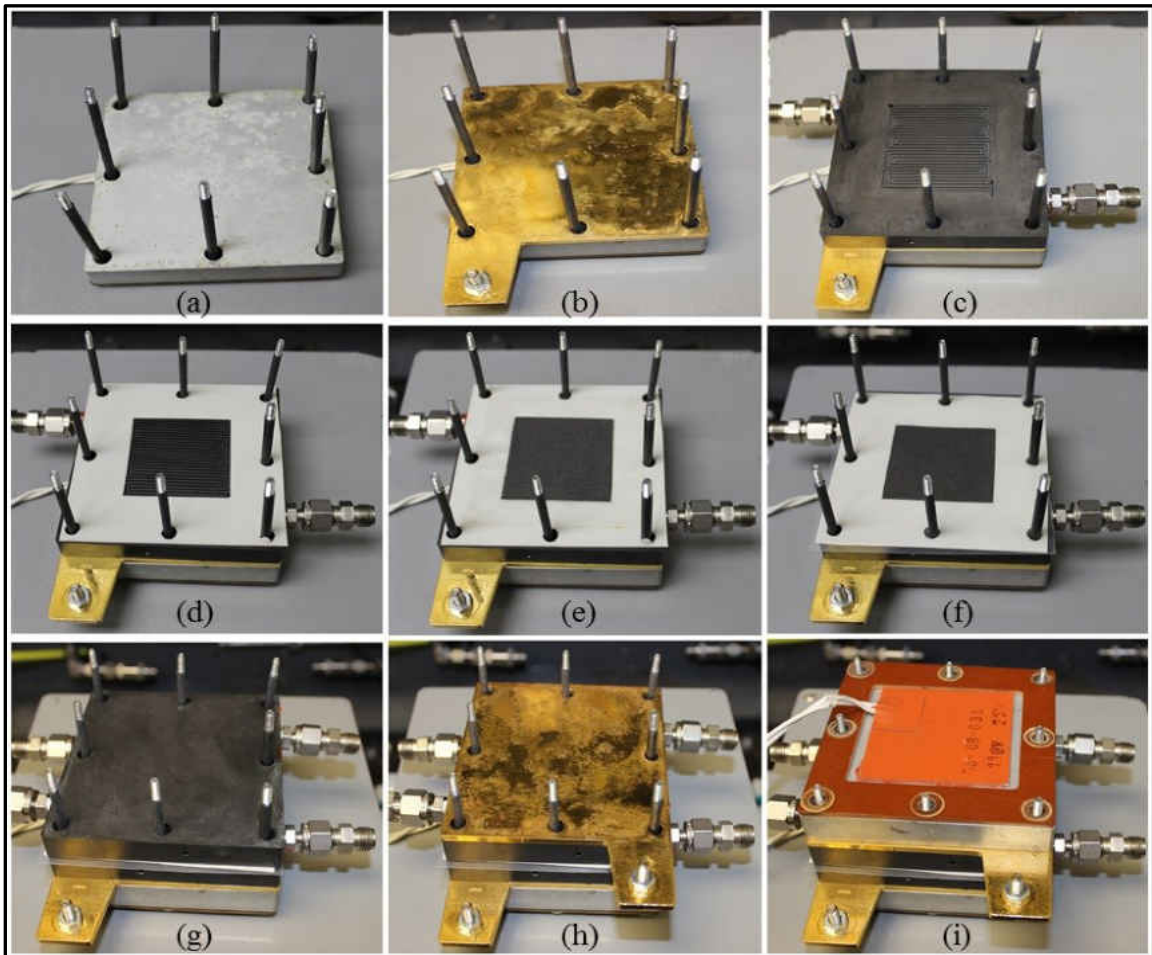
Figure 4-20 Sequence of MEA mounting in the unit-cell fixture

The cross tightening pattern of the bolts gives a uniform pressure distribution across the MEA. The bolts were tightened incrementally in a cross pattern at 07 foot-pounds per increment and were tightened to a final torque of 35 foot-pounds each. The torque wrench has a range of 05 - 80 foot-pounds torque with 16 hex head adapters to fit the fuel cell stack nuts.

4.7.2   Pretest Integrity Test

After the cell is mounted on the test stand, the leak tests and the resistance tests for the cell were done to validate proper functioning of test equipment and cells. The pre-tests were performed with dry nitrogen gas in the following order.

Checking Gas Flow, Cross-over, and Leakage

The leak test was conducted to make sure that gasses enter and exit the fuel cell system properly. First, dry nitrogen was fed at 200 ml/min to the anode-side inlet at 20 psi while the cathode side inlet and outlet were closed. The end of a tube, which was connected to the anode-side outlet, was held into the water in a beaker to confirm the gas flow. The same procedure was done with the cathode side while the anode side was closed also using nitrogen as the testing gas.

For checking for the gas crossover from the anode to cathode side or vice versa, nitrogen gas was again fed at 200 ml/min to the anode-side inlet at 20 psi, while closing the anode-side outlet and cathode-side inlet. The end of a tube, which was connected to the cathode-side outlet, was held into a beaker of water. The same check was done on the cathode side. Gas bubbles would represent air crossing over from anode to cathode for

110

the first case and the second instance crossing over from cathode to anode. This could have several reasons, assuming the MEA is correctly centered on the flow fields and covers them completely. The first reason would be an insufficient compression force so that the gas channels between the gaskets and the membrane to the other side. Applying 05 lb. more pressure stepwise might solve that problem. The second reason could be a hole in the membrane, which would result in discarding the MEA. Gas leakage was also checked by spraying soapy water on the gas connectors to the fuel cell.

Checking for Electrical Short-circuit

The fuel cell fixture further has to be checked for an electrical short-circuits. To test the fuel cell system for electrical short-circuits a voltmeter is switched to ohm mode, and each probe is contacted with one current collector. The ohmmeter should show a fluctuating value in the range of kilo-ohms (KΩ) which would be typical for the electrolyte membrane. If one observes a low, stable reading on the ohmmeter, there is a short between the anode and cathode side. That means that the current collectors or the gas distributors or in the worst case the catalyst layer are contacting each other.

The gaskets between the MEA and flow field plates prevent any electrical short. Also, the insulating shrinking tubes around the compression bolts make sure that there is no short if the bolts happen to touch any extraneous conductive material. For the first problem checking the compression bolts for direct contact with the current collectors and fixing the shrinking tube might help. The second issue can be eliminated by changing the gaskets. The most severe problem, a direct contact of both catalyst layers would mean a

hole in the membrane and a too high compression force, in this case, the MEA would have to be discarded.

4.7.3 MEA Conditioning

The basic principle of MEA conditioning is to hydrate the electrolyte membrane to improve its ionic conductivity since the hot-press MEA fabrication will cause the electrolyte membrane to dehydrate. As a result, the electrolyte membrane has very low ionic conductivity for ionic transport. Therefore, the MEA needs to be conditioned to increase its ionic conductivity. In addition, the conditioning process also removes the oxide layer on the catalyst; which helps improve the catalytic activity of the catalyst.

In this work a one-step (Bi, Gray, & Fuller, 2007) conditioning process was used after mounting the MEA and performing the pretest integrity test. In a one-step electrochemical conditioning, dry MEA was exposed to fully humidified hydrogen on the anode side and fully humidified oxygen on the cathode side, followed by controlling the cell voltage at fuel cell operating condition until a steady state performance is achieved. Murthy et al. (Yuan, Zhang, Sun, & Wang, 2011) recommended monitoring a fuel cell's output current density at 0.6 V and recording it as a function of time during the application of a given conditioning procedure.

The cell was first purged with fully humidified nitrogen at 500 ml/min on both anode and cathode side for 15 min while heating the cell to reach 60 °C. Once the set operating conditions were reached, nitrogen flow was switched to hydrogen and oxygen to the anode and cathode respectively, and the cell was operated at 0.6 V until a steady

state current was reached. It usually takes 15-20 hours for a newly mounted MEA to fully hydrate and reach to steady state current. The feed gas specifications for MEA conditioning are summarized in the Table 4-7.

Table 4-7 Feed gas specifications for MEA conditioning

	Anode	Cathode
Gas	Hydrogen	Oxygen
Cell Temperature (°C)	60	60
Stoichiometric Ratio (λ)	2.0	3.0
Relative Humidity (%)	100	100

4.8　In-situ Diagnostic Techniques

$In - situ$ evaluation using a unit-cell is used to validate the catalyst performance in MEA under practical cell operating conditions. The diagnostic techniques used for the $in - situ$ characterization of MEAs were polarization curves (IV), cyclic voltammetry (CV) and IV test is the MEA performance test, which establishes the relationship between its current density, voltage and power. CV tests determine the electrochemical characteristics of MEA such as electrochemically active surface area (ECASA).

The $in - situ$ characterization of the MEAs was performed using the same unit-cell text fixture mentioned in section 4.6.1 of this dissertation. The adopted measuring procedure in this study was based on the experience from a series of measurements during these preliminary experiments.

4.8.1 Polarization Curves

The polarization curve (often referred to as an IV curve) is the most common method of representing the performance of a fuel cell. Polarization measurements record voltage as a function of current (or current density in A/cm^2) generated in a fuel cell MEA. The IV curve is helpful in explaining the chemistry and physics associated with fuel cell operation, since current represents the rate of chemical reaction, and voltage represents the driving force for that reaction in a fuel cell.

IV curves are measured by exposing the anode side to hydrogen and cathode side to oxygen or air at a various relative humidity of the reactant gas, cell temperature, and cell pressure. When using the humidifier, anode and cathode line temperatures between the cell and humidifier were set at 5 ºC higher than the cell temperature. The polarization curve depends strongly on the operating conditions, such as the temperature, pressure, relative humidity and gas flow rates. Therefore, it is important to keep these parameters constant when comparing different catalysts.

There are two ways to measure the polarization curve: first setting the current density drawn from the fuel cell and measure the resulting cell voltage (galvanostatic); second setting the cell voltage and measure the resulting current density (potentiostatic) (Wu et al., 2008). After collecting the series of data, the cell voltage is plotted as a function of current or current density. The current density is simply the actual current divided by the electrode area. A power curve can also be immediately obtained by multiplying voltage and current ($P = V \cdot I$) of the same polarization measurement and by plotting current as a function of power (or power density W/cm^2). When plotted on a

114

current density basis, the resulting IV curve and power curve can be used to compare the performance of different MEAs with varying composition and operating parameters of interest.

In this study, the fuel cell polarization (IV) tests were measured in a constant voltage (potentiostatic) mode and were recorded at various times during the performance and durability evaluation of a catalyst in MEA. IV curves obtained right after the completion of MEA conditioning were used for its performance evaluation, and the curves obtained before and after the AST durability tests were used to investigate the catalyst degradation.

4.8.2 Cyclic voltammetry

Cyclic voltammetry (CV) refers to a repetitive cycling of the potential between chosen low initial and high final points, and recording the current response in the potential cycling region. This current response can give information about the adsorption and desorption of hydrogen. The resulting plot of potential versus current is called a voltammogram. Figure 4-21 shows a typical response of current density as a function of the applied voltage recorded during the CV tests. CV provides a method for quantifying the ECASA of the Pt catalyst in each MEA.

The $in-situ$ cyclic voltammograms were obtained using a two-electrode configuration. The electrode under study is purged by an inert gas (nitrogen) while the other electrode is purged by hydrogen gas so as to form a reversible hydrogen electrode (RHE). The counter electrode also served as the reference electrode due to its negligible

overpotential. In this manner, the surface processes taking place on both the anode and cathode side of the MEA could be measured and evaluated. The sweeping of the potential is carried out linearly, and the sweeping rate can be controlled in a wide range.
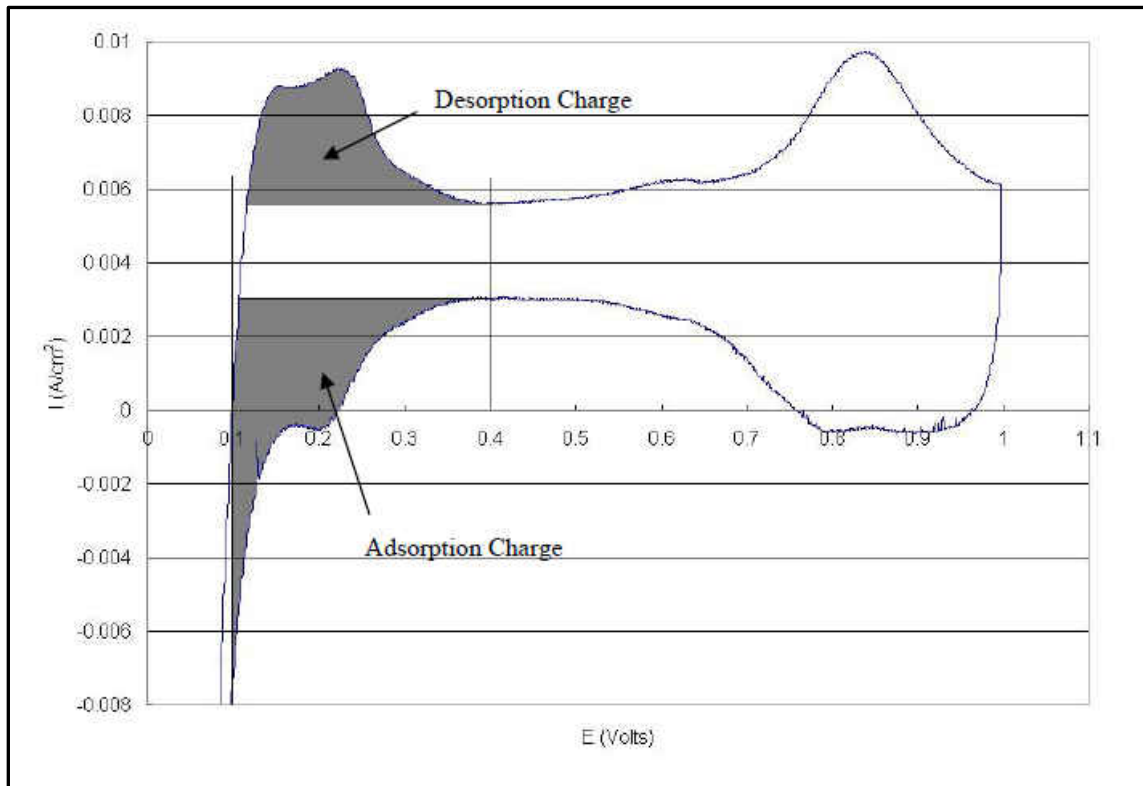
Figure 4-21 Typical Cyclic Voltammograms

In this research the $in-situ$ cyclic voltammetry (CV) test was conducted to determine the ECASA and the catalyst utilization of the catalyst in a MEA. ECASA and catalyst utilization are critical performance metrics for catalyst and membrane electrode assembly (MEA). Like polarization tests CV tests, were also conducted when a new MEA was conditioned as well as periodically during AST tests for fuel cell electrode degradation.

116

Electrochemically Active Surface Area (ECASA) Determination

It is well known that the electrical current generated in a fuel cell is directly proportional to the real surface area of the MEA electrode, which is larger than the geometric area due to the presence of surface rugosities due to steps, holes, kinks, and terraces. In electrochemistry, the term "real surface area" means the ECASA under working conditions. Therefore, ECASA of the electrode(s) is a more crucial factor in determining its performance than catalyst loading. Determination of the real surface area is necessary to normalize activities of different MEAs to the same number of reactive surface sites.

Both $In-situ$ and $ex-situ$ CV has been proven to be a valid technique for the measurement of ECASA of the catalyst in PEMFCs. The ECASA is calculated by means of Equation 4.6, after determining the charge associated with the adsorption and desorption of hydrogen. Each of these charges is obtained by integrating the cell current over time. Typically integration was performed approximately between the potentials of 0.1 and 0.4 V. Ideally, the adsorption and desorption charges would be the same. In practice, they differ somewhat, and the average of the two charges is taken as the charge transferred during the adsorption/desorption of a hydrogen monolayer. The ECASA of the electrode can thus be calculated using equation 4.6

$$\text{ECASA}\left[\frac{cm^2}{mg_{pt}}\right] = \frac{Q_{a/dH}\ [\mu C]}{Q_m\left[\frac{\mu C}{cm^2}\right] \times m_{pt}[mg_{Pt}]} \qquad (4.6)$$

Where,

$Q_{a/d}$ - is the average of the adsorption/desorption charges in μC

Q_m - is hydrogen adsorption charge on a smooth Pt electrode in $μC/cm^2$

Ld_{pt} - Total Pt metal loading in the electrode in mg_{pt}

The hydrogen adsorption charge on a smooth Pt electrode has been measured to be 210 $μC/cm^2$ of Pt loading in the catalyst layer (O'Hayre, Lee, Cha, & Prinz, 2002), and is denoted by Q_m.

4.8.3   Catalyst Mass Activity

The mass activity (A_w) is the current generated per gram of Pt in the sample. Catalyst mass activity (A/g_{pt}) was calculated by dividing the current density (A/cm^2) by catalyst loading (g_{pt}/cm^2).

$$A_w = \frac{i_{0.9}}{Ld_{Pt}} \qquad (4.7)$$

Where

A_w - is the catalyst mass activity in A/mg_{pt}

$i_{0.9}$ - is the current density in A/cm^2 at 0.9 V, and

Ld_{Pt} - is the loading of Pt in g_{pt}/cm^2

The value of 0.9 V is chosen to avoid inclusion of any concentration polarization. The mass activity was measured under fully humidified hydrogen and oxygen as the

118

reactants. In order to calculate the mass activity, the polarization curves for a given electrode is established. The current density at 0.9 V is obtained from current-potential data.

4.8.4 Specific Activity

The specific activity is the current produced per square meter of Pt exposed in the sample. Specific activity $(A/m^2{}_{Pt})$ was calculated by dividing mass activity (A/g_{pt}) by the electrochemically active surface area (m^2/g_{Pt}) of the MEA.

$$A_S = \frac{A_w}{ACASA} \tag{4.8}$$

Where,

A_S - is the specific activity of the catalyst in $A/m^2{}_{Pt}$

A_w - is the catalyst mass activity in A/mg_{pt}

ACASA - is the real (accessible) ECASA of the catalyst in the electrode in m^2/g_{Pt}.

4.9 In-situ Performance Test

The electrochemical characterization methods used in this research for $in-situ$ performance evaluation include polarization (IV) and cyclic voltammetry (CV). Specifically, performance was evaluated from polarization tests and CV determined the active catalyst area (ECASA) of each MEA.

4.9.1 Polarization (IV) Test

In this study, the fuel cell polarization (IV) tests were conducted in a constant voltage (potentiostatic) mode and were recorded at various times during the performance and durability evaluation of a catalyst in MEA. IV curves obtained right after the completion of MEA conditioning were used for its performance evaluation, and the curves obtained before, after and during the AST durability tests were used to investigate the catalyst degradation. The experimental setup employed for polarization (IV) test is shown schematically in Figure 4-22.
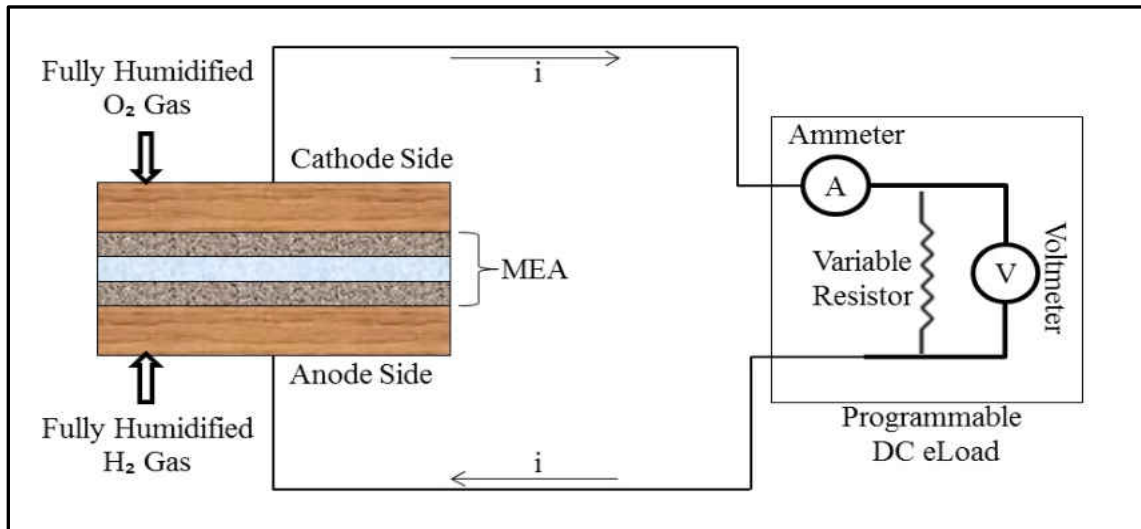
Figure 4-22 Schematic diagram for polarization curve measurements of fuel cell

The key components of the setup are an AMREL's ZVL Series of Zero-volt Programmable DC Electronic Load (Figure 4-17, section 4.6.4), unit-cell PEM fuel cell (Figure 4.11, section 4.6.1) and a software program (Amrel eLoad software). The software program was used to record the polarization data in addition to control either voltage, current or power.

After the completion of MEA conditioning humidified nitrogen at 300 ml/min is introduced to purge the anode and cathode sides of the unit-cell. During the purge, the cell and humidifiers are heated to their respective operating temperatures. When the cell and humidifiers reach the desired temperature, the nitrogen is replaced by hydrogen and oxygen for the anode and cathode, respectively. For the dry reactants case, the gas flow was bypassed from the humidifiers. For humidified reactants case gas flow was run through the humidifying bottle with the line temperature set 5 °C above the cell temperature (T_{Cell}) to eliminate the condensation of humidified reactants in the lines.

The fuel cell was then run with the electrical load disconnected for 15 min to reach steady state open circuit voltage (OCV). OCV is considered as the maximum usable potential of the PEMFC. All the IV curves were recorded after a stable OCV was attained. After a stable OCV had been attained, the IV curve was generated by recording steady state current at different voltages. During experiments, the cell voltage was kept constant while current is measured as a function of time. The cell voltage was switched manually from OCV to 0.2 V with a step of 0.1 V. Polarization data was taken by starting at OCV where I = 0 A, and decreasing the voltage in steps of 0.1 V every 10 min until 0.2 V. The average cell current in the last 3 min during each 5 min testing at each potential is taken as final current at that potential. The current density is obtained by dividing the current by the cell area (25 cm^2).

Approximately 6-7 mins were required to reach steady state for changes in current at constant composition (flow rate and humidity) and temperature; however, it might take 20-30 min to reach steady state for a change in either composition or temperature.

121

4.9.2 Cyclic Voltammetry (CV) Tests

The $in - situ$ CV test was performed after cooling the test fixture down to room temperature, and using a two-electrode potentiostatic measurement circuit as described in section 4.8. In two-electrode potentiostatic measurement one of the electrodes of the fuel cell acts as both a counter electrode and a pseudo-reference electrode. The experimental setup employed for in $-$ situ CV test is shown schematically in Figure 4-23.

The key components of the setup are the Gamry PCI4G-750 Potentiostat, seen in Figure 4-19, unit-cell PEMFC seen in Figure 4-11 (section 4.6.1) and a software program (Gamry Instruments Framework V5.50). The software program was used to record the voltammogram, in addition, to apply and control the potential through potentiostat.
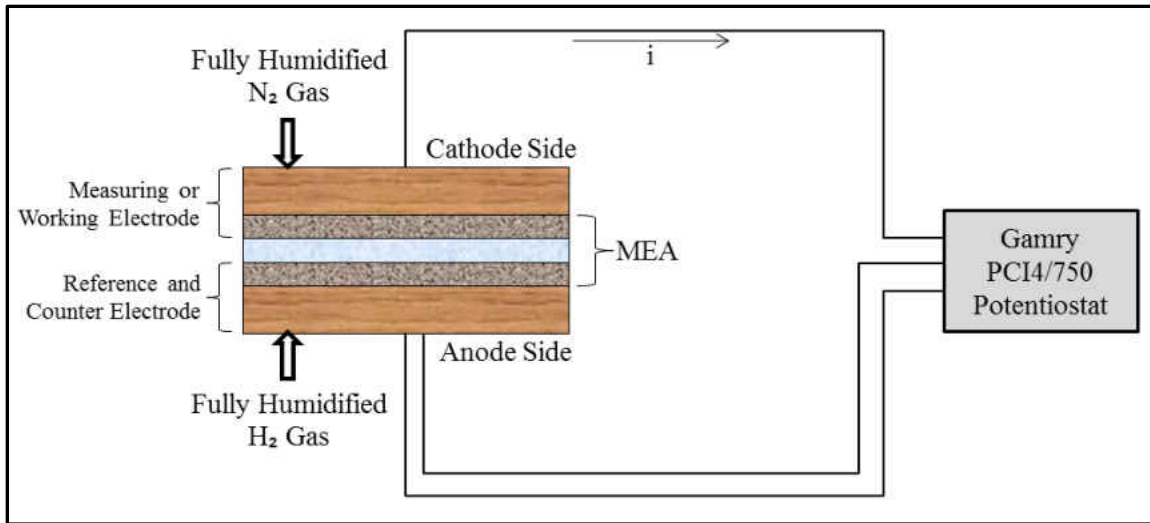
Figure 4-23 $In - situ$ cyclic voltammetry of a unit-cell test Setup

For this study, the cathode electrode was fed with fully humidified (CRH $=$ 100%) nitrogen gas at 250 ml/min, and it acted as a measuring electrode. The anode electrode was supplied with fully humidified (ARH $=$ 100%) hydrogen gas at 250 ml/

min, and it served as a counter electrode. Because of its negligible overpotential, the counter electrode also acts as the reference electrode. The temperature of the humidification ($T_{Humidifier}$) bottles was kept at 40 °C for more efficient humidification, and the cell was kept at room temperature for acceptable measuring results. Table 4.8 lists the CV test operating conditions.

Table 4-8 CV test operating conditions

Variable	Cathode Side (Working Electrode)	Anode Side (Counter/Reference Electrode)
Reactants	Dry Nitrogen	Dry Hydrogen
Reactants flow (ml/min)	250	250
Relative Humidity (%)	100	100
Cell Temperature (T_{cell})	Room Temperature	Room Temperature
Cell Pressure	Atmospheric Pressure	Atmospheric Pressure

Prior to taking the first measurement purging and humidification of the cell was performed using 40 min gas flow time. Thereafter the activating and purifying CV cycles (around 15 cycles) were continued until a constant overlay of voltammetric data was observed. After the scan had been stabilized during the first 15-20 cycles, the CV curve was recorded for three measurement cycles. The actual CV test measurement was then taken from the third cycle. In this work, CV curves were used to estimate the electrochemically active surface area (ECASA).

4.10 In-situ Durability Tests

A conventional method of testing the PEMFC durability requires a fuel cell to run several thousand hours under a realistic cycle. However, this type of testing is expensive with very low output and impractical for evaluation of new materials. Alternatively, accelerated stress test (AST) protocols can be used to induce rapid degradation of cell components and can be applied $in-situ$. It typically involves changing one or more parameters to create specific conditions and trigger specific degradation pathways related to a particular component of the fuel cell based on assumed but widely accepted mechanisms, while minimizing degradation of other components.

4.10.1 Potentiostatic Hold

The potentionstatic hold AST test involved holding the unit-cell at high potentials and measuring both the ECASA and the catalyst activity both before and after the potential holds. Potentiostatic hold at >1.1 V vs. RHE for several hours are usually suggested for testing the durability of the catalyst support, since above 1.1 V, the Pt catalyst is better protected from dissolution (Darling & Meyers, 2005). The purpose of the high potential hold AST is to isolate carbon degradation from Pt degradation.

The potentiostatic holds tests involved testing an MEA at 80 °C cell temperature for 24 hours. The cathode side was supplied with fully humidified nitrogen, and it works as a working electrode. The anode side was provided with fully humidified hydrogen, and it functions as a counter electrode. In this setup, the counter electrode also serves as a hydrogen reference electrode.

4.10.2 Potential Cycling

Potential cycling protocol was designed to simulate multiple transitions from no-load to full-load conditions during fuel cell operation. In the testing procedure proposed by U. S. DOE, the voltage is cycled, but the fuel cell is not in operation since nitrogen is supplied to the cathode. The anode was used as both reference and counter electrodes by introducing the fully humidified hydrogen into the anode-side gas channel, and the potential of the cathode was swept from 0.6 V to 1.0 V, while the anode served as a reversible hydrogen electrode (RHE).
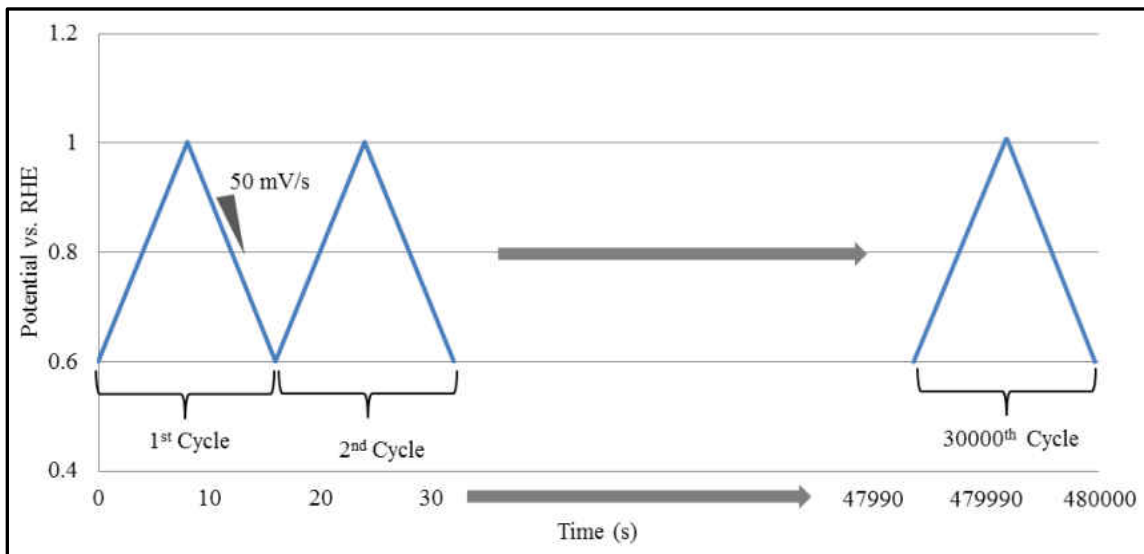
Figure 4-24 DOE catalyst durability triangular load cycling protocol

Triangle-wave potential cycling was introduced as AST for catalyst support corrosion. As shown in Figure 4-24, the AST includes sweeping the potential of the cathode between 0.6 and 1.0 V vs. RHE. The lower scanning voltage of 0.6 V simulates the fuel cell operates in a normal mode, at which the Pt surface is reduced from its oxide coverage and water is produced due to the ORR. The upper scanning voltage was set to

125

1.0 V to simulate OCV, and the current generated is originated from carbon corrosion, oxygen evolution, Pt oxidation and double layer current.

The potential cycling showed much better results in terms of degrading the support in a reasonable amount of time, without some reversible effects observed by the potentiostatic holds. This test was therefore used as the standard AST to screen for durable support. The drawback is of course that the Pt catalyst will no longer be protected by the oxide coverage. Pt will undergo oxidation and reduction during each cycle, increasing Pt dissolution rates. The stability of the support was quantified by measuring the change in ECASA.

CHAPTER 5

5 **EXPERIMENTS**

This section discusses the experimental design/setting used for conducting the experiments. Therefore this section is treated separately from the experimental methods presented in chapter 4.

The description of the experimental work of the dissertation is divided into four main categories: physical characterization of catalyst and MEA fabricated preliminary evaluation, in-situ performance evaluation, and in-situ durability evaluation. All experiments in this work have been performed at the in-house built fuel cell test stand (described in section 4.6) using a unit-cell PEMFC fixture (described in section 4.6.1) with 25 cm^2 of active surface area.

5.1 Physical Characterization

Physical characterization includes the catalyst characterization of in-house-fabricated Pt/Silica catalyst using spectroscopy to verify its composition and visual characterization of MEA during the MEA fabrication method development.

5.1.1 Catalyst Characterization

The Pt/Silica catalyst synthesized and provided by the UND's Chemistry Department for this research was examined using spectroscopy to confirm its elemental

contents, particle size and to verify the Pt spreading on the support. The results of the spectroscopy characterization techniques will help explain the $in-situ$ performance of the catalyst samples using a unit-cell fixture. The samples were characterized by a scanning electron microscopy (SEM) and and X-Ray Fluorescence (XRF) at the Material Characterization Testing laboratory, Institute of Energy Studies, at UND.

5.1.2   MEA Characterization

At the beginning of the MEA fabrication work, an effort was made to replicate the MEA fabrication from literature mentioned in section 3.2, and modification of this method was planned only if these efforts proved unsuccessful in fabricating a fully functional MEA, some modifications were made.

The procedure involved the replication of those MEA fabrication procedures from the literature reported to give a good performance, followed by a critical evaluation of the parameters said to affect the performance. The understanding that was developed, based on theoretical and experimental investigation of the various aspects, was used to propose fabrication methodologies for high-performance MEA.

The results obtained and observations made during this method development work were used as a guide to developing a standardized method for the fabrication of both Type-A and Type-B MEAs, which is mentioned in section 4.3 and section 4.4.

In this work, the catalyst coated gas-diffusion-layer (CCG) method was used for fabricating the membrane electrode assembly (MEA). In the CCG method, the gas-diffusion-electrodes (GDEs) are prepared by coating the catalyst ink directly on the gas-

diffusion-layer (GDL), and then the GDEs were hot-pressed with electrolyte membrane to form an MEA.

The MEA fabrication method used for this research work was not extensively optimized, as the goal was simply to obtain consistent MEA performance to enable comparison of the Pt/Silica catalyst with state-of-the-art Pt/Carbon catalyst.

5.2   Preliminary Evaluation

The preliminary performance results of the in-house fabricated Type-A MEAs are summarized in this section. In the first part, the quality of the MEAs fabricated in-house has been studied by characterizing the MEAs with a reproducibility test. In the second part of this section, the performance of in-house fabricated MEA was compared with a similar commercial MEA to verify if the in-house fabrication method can produce a high performing MEA.

5.2.1   MEA Reproducibility Study

The reproducibility of the MEAs fabricated in-house is very vital, as non-reproducible MEAs cannot be used as a basis for comparison with experimental results. The reproducibility test was conducted by first fabricating four Type-A MEAs with similar Pt loading, catalyst ink composition, and hot-pressing conditions. These Type-A MEAs were then electrochemically tested under the same operation conditions to compare their performance. The purpose was to determine if the fabrication method developed can be used to achieve consistent performance.

Table 5-1 Reproducibility test MEA (Type-A) catalyst ink composition

Components	Type-A MEA Ink
Catalyst	75 mg Pt/Carbon
Deionized water	As required to make catalyst wet (usually 4-5 drops total)
Ionomer Solution	0.739 g of 5 wt.% Nafion Ionomer
Solvent	3.0 g of isopropanol

The composition of the catalyst ink utilized for the reproducibility test is listed in Table 5-1. The MEAs (Type-A) for reproducibility were fabricated using the method outlined in section 4.3 with commercial 10% Pt/Carbon catalyst, and Nafion-115 electrolyte membrane procured from Fuel Cell Store. The Pt loading of 0.3 mg/cm² Nafion loading of 33% was used for both the anode and cathode GDE for all the MEAs fabricated for reproducibility tests. The hot-pressing conditions of temperature, pressure, and duration were same for all the MEAs and are given in Table 5-2.

Table 5-2 Reproducibility test MEA (Type-A) hot-press conditions

Hot Press Condition	Set Point
Temperature (°C)	130
Pressure (lb/cm²)	175
Time (s)	180

These MEAs were then mounted in a unit-cell fixture (described in section 4.7.1) one at a time for their performance evaluation. Before the performance evaluation, each MEA was conditioned using the conditioning method outlined in section 4.7.3 of this dissertation. The reproducibility was determined first by calculating catalyst loadings in

both the anode and cathode electrode of each MEA, and then performing IV test. The polarization tests were conducted under identical operating conditions, with an anode side stoichiometric flow (λ_{H2}) of 2.0 and cathode side stoichiometric flow (λ_{O2}) of 3.0 using the procedure mentioned in section 4.10.1 and operating conditions listed in Table 5.3.

Table 5-3 IV curve operating conditions for Type-A reproducibility test

Variable	Anode Side	Cathode Side
Reactants	Dry Hydrogen	Dry Oxygen
Cell Temperature (°C)	70	70
Relative humidity (%)	100	100
Stoichiometric Flow Rate (λ)	2.0	3.0

The reproducibility study for the experimental MEAs will show not only the reproducibility of the MEA fabrication technique but also the reproducibility of the Pt deposition technique, which is vital for all $in-situ$ fuel cell testing. The results for polarization curves were expected to be identical for all the MEAs with similar composition.

5.2.2 Comparison Test (in-house fabricated MEA *vs.* commercial MEA)

A performance comparison test of the in-house fabricated Type-A MEA and commercial Type-C MEA was carried out. The comparison was performed to verify if the method developed to fabricate in-house MEA could produce a high performing MEA. The MEAs (Type-A) for the performance comparison test were fabricated using the method outlined in section 4.3 with commercial 10% Pt/Carbon catalyst and the Nafion-

115 electrolyte membrane. The Pt loading of 0.3 mg/cm^2 and Nafion loading of 33% was used for both the anode and cathode GDE. The comparison between Type-A and Type-C MEA components is listed in Table 5.4.

Table 5-4 Comparison of Type-A and Type-C MEA components

Components		MEA	
		Type-A	Type-C
Catalyst	Metal	Pt	Pt
	Support	Carbon	Carbon
	wt. %	10	**Not Disclosed**
	Loading (mg/cm^2)	0.3059	0.3
MEA Active Area (cm^2)		25	25
Gas Diffusion Layer		Teflon treated carbon cloth	Teflon treated carbon cloth
Electrolyte Membrane		Nafion 115	Nafion 115
Ionomer solution		5 wt% Nafion solution	**Not Disclosed**
Solvent		Isopropanol	**Not Disclosed**
Hot-press	Temperature (°C)	130	**Not Disclosed**
	Pressure (lb/cm^2)	175	
	Time (s)	180	

The details about the components and fabrication method used for the commercial (Type-C) MEAs could not be obtained from ElectroChem Inc. due to proprietary reasons.

Hence, a detailed comparison of preparation methods, especially for electrode preparation, and hot press condition could not be drawn.

The MEA was mounted in a unit-cell fixture (described in section 4.7.1), and before the performance evaluation, each MEA was conditioned using the conditioning method outlined in section 4.7.3 of this dissertation. The polarization tests for both Type-A and Type-C were was conducted under identical operating conditions. Fully humidified reactants (ARH = CRH = 100 %) with stoichiometric anode flow of two (λ_{H_2}= 2) and stoichiometric cathode flow of 3.0 (λ_{O_2}= 3.0) were supplied to both the anode and cathode sides, and IV curves were recorded at cell temperature (T_{Cell}) of 70 °C.

5.3 Pt/Silica In-situ Performance Test (Hypothesis 01 Testing)

This section compares the performance of Type-A (Pt/Carbon electrodes) with Type-B (Pt/Silica electrodes) MEAs fabricated in-house with same electrolyte membrane (Nafion-115), same GDLs (carbon cloth) and similar catalyst layers. Both MEAs were fabricated using the procedures mentioned in section 4.3.

5.3.1 Pt/Silica (Type-B) MEA performance against Pt/Carbon (Type-A) MEA

A study was designed to investigate the performance of Pt/Silica catalyst in an MEA using an unit-cell, and its performance was compared with the commercial Pt/Carbon catalyst. The comparison was performed to test *the hypothesis of this research that the Pt/Silica catalyst will achieve an equivalent power density of a Pt/Carbon catalyst in PEMFCs*.

133

The MEAs (Type-A) for the performance comparison test were fabricated using the method outlined in section 4.3. Type-A MEA was made with commercial 10% Pt/Carbon catalyst and the Nafion-115 electrolyte membrane. Type-B MEA was made with the in-house fabricated 10 % Pt/Silica catalyst and the Nafion-115 electrolyte membrane. The targeted Pt loading of 0.3 mg/cm^2 and Nafion loading of 33% was used for both the anode and cathode GDE. The comparison between Type-A and Type-B MEA fabricated for this test is listed in Table 5-5.

Table 5-5 Comparison of Type-A and Type-B MEA components

Components		MEA	
		Type-A	Type-B
Catalyst	Metal	Pt	Pt
	Support	Carbon	Silica
	wt. %	10	10
	Loading (mg/cm^2)	0.3070	0.3031

The MEA was mounted in a unit-cell fixture (described in section 4.7.1), and before the performance evaluation, each MEA was conditioned using the conditioning method outlined in section 4.7.3 of this dissertation. The polarization tests for both Type-A and Type-B MEA were conducted under identical operating conditions. Fully humidified reactants (ARH = CRH = 100 %) with stoichiometric anode flow of two (λ_{H_2} = 2) and stoichiometric cathode flow of 3.0 (λ_{O_2} = 3.0) were supplied to both the anode and cathode sides, and IV curves were recorded at cell temperature (T_{Cell}) of 70

°C. Table 5-6 summarized the operating conditions under which the performance of Type-A and Type-B MEAs were determined during the during the in-situ evaluation.

Table 5-6 Operating conditions used for MEA $in-situ$ evaluation

Operating Condition	Anode Side	Cathode Side
Humidity (%)	100	100
Cell Temperature (°C)	70	70
Stoichiometric Flow (λ)	2.0	3.0

5.3.2 Effects of Operating Conditions on Pt/Silica catalyst (Sub-hypothesis 01 Testing)

The performance of the Pt/Silica catalyst was lower than that of Pt/Carbon catalyst. As will be discussed in section 6.3.1, it was suspected that the testing environment (operating conditions) was far better suited to the Type-A MEA which was causing water flooding in the Pt/Silica catalyst layer. Therefore, a study was designed and conducted to test the first sub-hypothesis that- *silica support in the Pt/Silica catalyst was able to retain water in the catalyst layer, which causes the electrode flooding*.

The operating conditions of PEMFCs have a significant influence on the power output of a fuel cell system particularly in a unit-cell fixture since every unit-cell is made of a unique set of components (Colmati, Paganin, & Gonzalez*, 2006; Park, Lee, Sauk, & Son, 2008). The cell temperature, for example, influences the rate of reaction and the rate of water evaporation.

Since the lower performance of Pt/Silica catalyst was suspected due to the hydrophilic nature of the silica support, the tests performed were focused on the water management in PEMFC. Water management is among the key factors in maximizing the performance of PEMFCs since less water could result in the dehydrated membrane and more water results in electrodes flooding. Relative humidity of reactant gasses, the temperature of the unit-cell and stoichiometric flow rates are the most important parameters in maintaining the water balance in PEMFCs. Therefore, it is important to study the effects of these parameters on the $in - situ$ performance of Pt/Silica to test the first sub-hypothesis proposed (section 6.3.2) for the lower performance of Pt/Silica catalyst.

The initial level of each factor was set as what is seen as acceptable levels for Pt/Carbon catalyst and according to normal operating conditions listed in Table 5-6. In order to identify the factors that affect in-situ Pt/Silica catalyst performance, a method of varying only one parameter at a time was adopted. The intention for these tests was to see how the Pt/silica catalyst responds to the PEMFC operating conditions.

5.3.3 Development of "Pt/Silica + Carbon powder" MEA (Sub-hypothesis 02 Testing)

The main objective of developing the "Pt/Silica + Carbon powder" MEA was to test the second hypothesis that *the low electronic conductivity of silica support has caused the non-facile electronic and/or ionic flow path in the catalyst layer*. Therefore, a study was designed to improve the electronic path in the Pt/Silica electrode by incorporating a high conductive nano-material into the electrode. Carbon black is widely

used in the PEMFC's catalyst layer; therefore, an effort was made to determine if the incorporation of highly conductive carbon black powder as an additive in the catalyst ink could enhance the electronic flow path in the catalyst layer of Pt/Silica catalyst.

The catalyst ink preparation process for these experiments involved adding various quantities of carbon powder to compare how varying level of carbon powder affects the performance of Pt/Silica catalyst. Four MEAs were made, each with a different carbon loading (Ld_{Carbon}) in the catalyst ink: 0, 5, 7.5 and 10 wt. %. The Pt loading was 0.3 mg/cm^2 in each MEA and the Nafion content in the ink was 37 % as noticed during the preliminary experiments (section 6.1.2); it was the minimum amount required to make a compact and workable MEA. Finally, each MEA was hot pressed at 130 °C with 175 lb/cm2 pressure for 3 mins.

For each Type-BB MEA fabricated for this section, the initial performance was evaluated by polarization experiments and then the ECASA was determined from CV tests. The effect of carbon powder additive on the performance of Pt/Silica catalyst was monitored under constant voltage operation.

5.3.4 Comparison of Type-A, Type-B and Type-BB MEA at their Peak Performance

Finally the performance of Type-BB (Pt/Silica + Carbon Powder) MEA was compared with Type-A (Pt/Carbon catalyst) and Type-B (Pt/Silica catalyst) MEA. The difference between the comparison studies in this section from the section 4.3 in which both Type-A and Type-B MEAs were tested under same operating conditions, whereas in this section the peak performance of all three MEAs is compared which was obtained at

different operating conditions. The operating conditions for this comparison tests are summered in Table 5-7.

Table 5-7 IV curve operating conditions for the comparison test

Variable	Type-A and Type-B MEA		Type-B and Type-BB MEA at peak performance	
	Anode Side	Cathode Side	Anode Side	Cathode Side
Reactants	Dry Hydrogen	Dry Oxygen	Dry Hydrogen	Dry Oxygen
Cell Temperature (°C)	70	70	70	70
Relative humidity (%)	100	100	100	0
Stoichiometric Flow Rate (λ)	2.0	3.0	3.0	4.5

In order to obtain a peak performance, a study was designed to compensate the flooding effect observed in section 6.3, which was limiting the performance of Type-B MEA. Therefore in this study, Type-B and Type-BB MEAs were tested at partially humidified conditions (ARH = 100% and CRH = 0 %) and at higher stoichiometric conditions (λ_{H_2}= 3.0 and λ_{O_2}= 4.5). Type-A MEA was tested at fully humidified (ARH = CRH = 100%) reactants, anode stoichiometric flow of 2.0 (λ_{H_2}= 2.0) and cathode stoichiometric flow of 3.0 (λ_{O_2}= 3.0). However, the cell temperature was kept constant during the evaluation of all the MEAs since the electrochemical reaction kinetics is dependent on the temperature. CV tests were not performed for this comparison since CV

test could be run only at room temperature with fully humidified (ARH = CRH = 100%) nitrogen and hydrogen at 250 ml/min flow rate each on anode and cathode side respectively. Therefore the ECASA was expected to be same for a particular MEA.

5.4 Pt/Silica In-situ Durability Tests (Hypothesis 02 Testing)

A study was designed to investigate the durability of Pt/Silica catalyst in an MEA using accelerated stress test protocols, and its durability was compared with the commercial Pt/Carbon catalyst. The comparison was performed to test the second hypothesis of this research that *the ECASA loss based on the AST test (potential hold and potential cycling) will be reduced for a Pt/Silica catalyst as compared to Pt/Carbon catalyst and thereby enhance the durability of PEMFCs*.

The two $in-situ$ accelerated stress tests (AST) used in this study are poentiostatic holds and potential cycling to evaluate catalyst support and catalyst stability in an MEA operating in a unit-cell. The fuel cell performance was monitored during the AST tests through the $in-situ$ measurement of polarization (IV) curves and cyclic voltammetry (CV). A fresh new MEA was used in each test to measure the changes occurred during the AST tests. This was necessary to make a comparison between the initial and final state of an MEA through $in-situ$ AST methods. During the AST tests, gas flow rates, cell temperature, and reactant gas humidity were controlled with the test stand, and the potential was controlled using a potentiostat. The change in IV curve performance and the ECASA were used to evaluate the in-situ durability.

All the MEAs used in AST experiments have been assumed to have the same properties before the tests. This assumption was necessary not only to quantify the changes before and after the tests but also to compare the effects on performance and degradation during the two AST tests.

5.4.1   Potentiostatic Hold

In this work, the durability of both Type-A (commercial Pt/Carbon based) and Type-B (novel Pt/Silica-based) MEAs were tested using potentiostatic hold accelerated stress tests (AST) at 1.2 V vs. RHE for 24 hours. Changes in the IV curve performance and ECASA after different load cycles were used to evaluate the catalyst stability potential hold conditions.

A fresh MEA was mounted in a unit-cell as outlined in section 4.7 and conditioned after the pre-integrity tests for this test. The cathode side was supplied with 250 ml/min of fully humidified nitrogen, and it works as a working electrode. The anode side was supplied with 250 ml/min of fully humidified hydrogen, and it works as a counter electrode. In this setup, the counter electrode also serves as a hydrogen reference electrode. The incoming relative humidity (RH) of the gasses was 100 % (ARH = CRH = 100%) and the temperature of the cell (T_{cell}) was 80 °C.

Before exposing the cell to postnetiostaic holds condition, performance tests were performed to establish initial baseline performance. Polarization (IV) curve and CV tests were conducted in the same order to evaluate the performance. After completing the baseline performance test, the unit-cell was switched to the potentiostatic hold test

conditions, and held potentiostatically at 1.2 V for 8 hours at a time. At the completion of each 8-hours subsequent potentiostatic holds, polarization (IV) measurements were performed, followed by ECASA estimation from the CV measurements.

For IV performance of Type-A MEA, the gas on the cathode side was switched from nitrogen to oxygen at a stoichiometric flow rate of 3.0. The hydrogen flow rate on the anode was changed to a stoichiometric flow rate of 2.0. The cell temperature (T_{cell}) was set at 70 °C with fully humidified reactants (ARH = CRH = 100%). IV curve was recorded only after reaching a steady state at OCV using the procedure outlined in section 4.9.1. For IV performance of Type-B MEA, the reactants flow rate was higher than Type-A MEA and dry reactants on the cathode side (ARH = 100% CRH = 0%) to compensate for the electrode flooding. The anode side was at a stoichiometric flow rate of 3.0 ($\lambda_{H_2} = 3.0$).The cathode side was at stoichiometric flow rate of 4.5 ($\lambda_{O_2} = 4.5$).

The test setup was then transferred to the CV measuring arrangement. For CV measurements, the gas on the cathode side was switched from oxygen to nitrogen at 250 ml/min flow rate, and the hydrogen flow was changed to 250 ml/min. The cell temperature (T_{cell}) was decreased from 70 °C to room temperature and humidifier temperature ($T_{Humidifier}$) was set at 40 °C for efficient humidification. The CV was performed between 0.08 V and 1.0 V at a sweep rate of 50 mV/s. The ECASA was then calculated from the hydrogen adsorption and desorption region of the voltammogram.

5.4.2 Potential Cycling

In order to make a more comprehensive evaluation of the Pt/Silica catalyst a harsh AST test of potential cycling between $0.6 - 1.2$ V was designed to simulate catalyst degradation under repeated start-stop cycles. A potential cycling method was applied to the unit-cell to investigate its effect on both Pt/Carbon and Pt/Silica catalyst in an MEA operating in a unit-cell. Measurements of polarization (IV) curves and electrochemical surface area (ECASA) were made $in-situ$ periodically during testing to characterize the performance changing as a function of time. The schematic of the triangle-wave potential cycling used for this test can be seen in Figure 5.1.
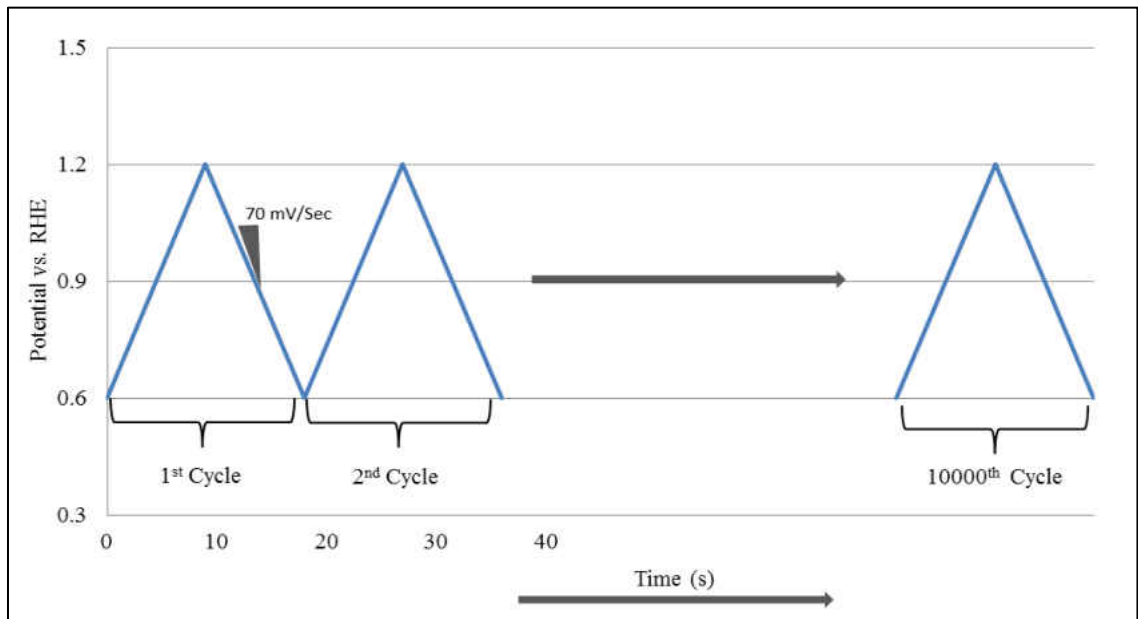
Figure 5-1 Schematic of the Triangular wave potential cycling used in this study

During potential cycling, a fresh MEA was mounted in a unit-cell as described in section 4.6 and conditioned after the pre-integrity tests for this test. The cathode electrode was exposed to fully humidified (CRH = 100 %) nitrogen gas at 250 ml/min, and it acted as a measuring electrode. The anode electrode was exposed to fully humidified (ARH =

100 %) hydrogen gas at 250 ml/min, and it served as a counter electrode. Because of its negligible overpotential, the counter electrode also acts as the reference electrode. The cell temperature (T_{Cell}) was held constant at 80 °C during the potential cycling. The cathode potential was swept linearly with time for 10,000 cycles from an initial voltage of 0.6 to an upper limit voltage of 1.2 V at a rate of 70 mV/s.

The performance of the MEA was measured initially and after 3,000, 6,000 and 10,000 cycles to establish initial baseline performance and subsequent performance changes. Performance tests conducted before exposing the MEA to the potential cycling were used to establish initial baseline performance. After completing the baseline performance test, the unit-cell was switched to the potential cycling test conditions.

Polarization (IV) curve and CV tests were conducted in the same order to evaluate the performance. Changes in the IV curve performance and ECASA after different load cycles were used to evaluate the catalyst stability under load cycling conditions.

For IV performance of Type-A MEA, the gas on the cathode side was switched to at a stoichiometric flow rate of 3.0. The hydrogen flow rate on the anode was changed to a stoichiometric flow rate of 2.0. The cell temperature (T_{cell}) was set at 70 °C with fully humidified reactants (ARH = CRH = 100%). The IV curve was recorded only after reaching a steady state at OCV using the procedure mentioned in section 4.9.1 For IV performance of Type-B MEA; the reactants flow rate was higher than Type-A MEA and dry reactants on cathode side (ARH = 100% CRH = 0%) to compensate for the electrode

flooding. The anode side was at a stoichiometric flow rate of 3.0 (λ_{H_2} = 3.0).The cathode side was at stoichiometric flow rate of 4.5 (λ_{O_2} = 4.5).

The test setup was then transferred to the CV measuring arrangement. Characterization cyclic voltammograms (CV) were performed initially and after 3,000, 6,000 and 10,000 cycles to quantify the ECASA. For CV measurements, the gas on the cathode side was switched from oxygen to nitrogen at 250 ml/min flow rate, and the hydrogen flow was changed to 250 ml/min. The cell temperature (T_{cell}) was decreased from 70 °C to room temperature and humidifier temperature ($T_{Humidifier}$) was set at 40 °C for efficient humidification. The CV was performed between 0.08 V and 1 V at a sweep rate of 50 mV/s. The ECASA was then calculated from the hydrogen adsorption and desorption region of the voltammogram.

CHAPTER 6

6   **RESULTS AND DISCUSSION**

The major findings of this study are presented and discussed in this chapter in comparison to theoretical expectations and literature backgrounds.

6.1   Physical Characterization

The catalysts used in this study and the MEAs fabricated during the study were physically examined and evaluated to confirm they exhibited the desired structure and to obtain a quantitative and qualitative analysis of samples. Catalysts were characterized using spectroscopy characterization techniques while MEAs were visually characterized during the MEA fabrication method development.

6.1.1   Catalyst Characterization

Scanning electron microscopy (SEM), and X-Ray Fluorescence (XRF) were used to verify the size, composition, and nano-architecture of the nanoparticles. Only the in-house fabricated Pt/Silica catalyst was characterized, and the commercial Pt/Carbon was not characterized since the characterization equipment could not detect carbon.

The element contents of the Pt/Silica samples determined by XPF can be seen in Figure 6-1. As can be seen, Al, Na, and K elements coexist within these three samples, and the trace of Fe species appeared in the catalyst sample. In order to qualitatively

measure the amount of Pt in the synthesized catalyst and corroborate the theoretical amount of Pt content in the catalyst, SEM measurements were taken as shown in Figure 6-2.
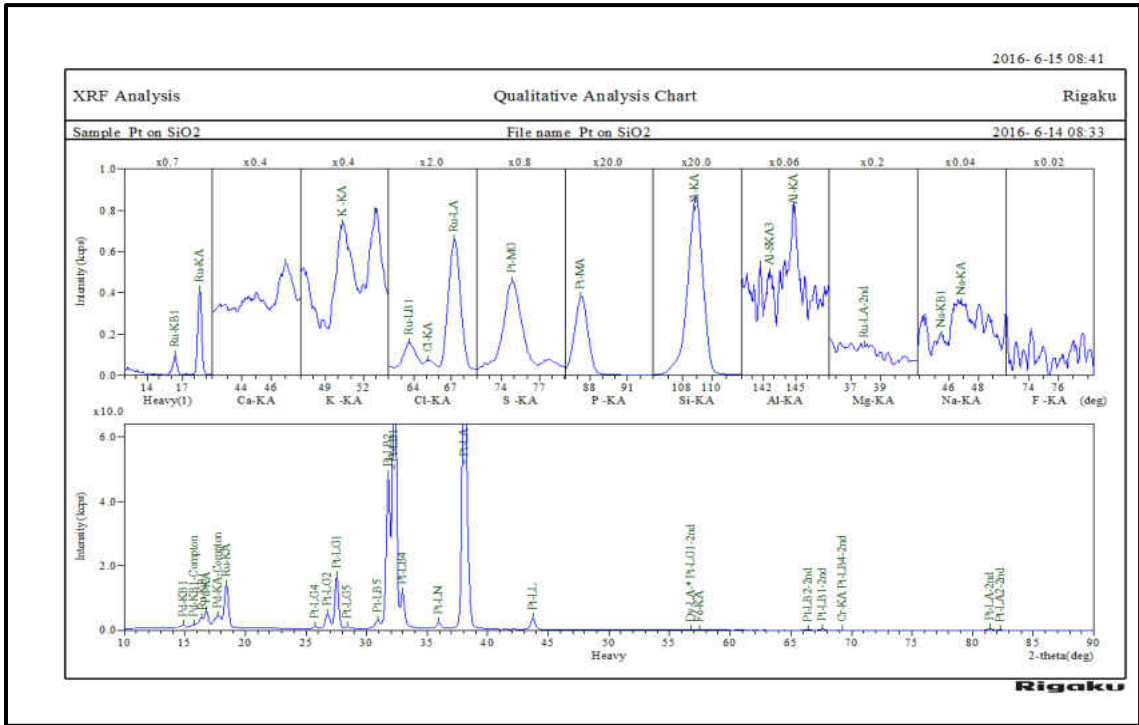
Figure 6-1 XRF analysis chart of Pt/Silica sample
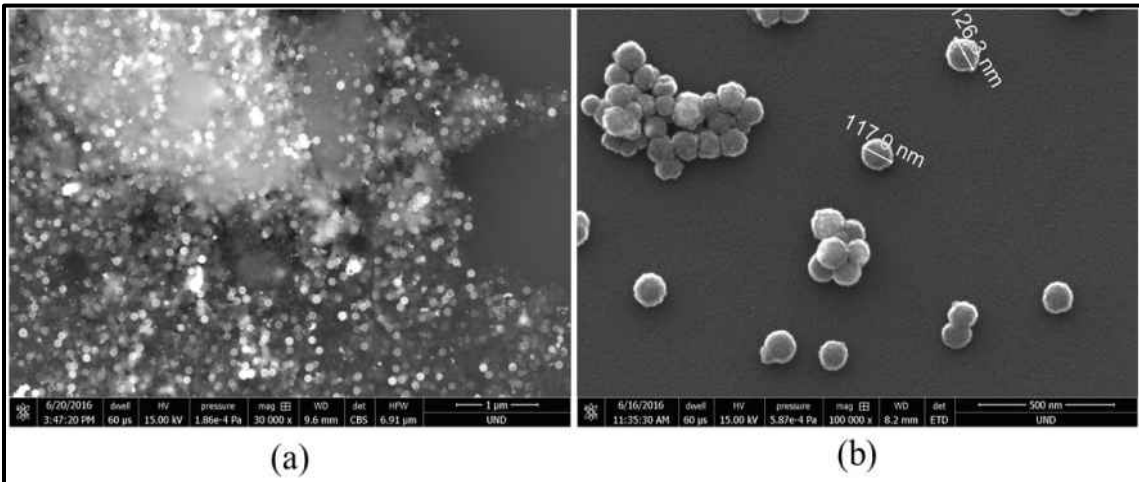
Figure 6-2 SEM image of Pt/Silica sample with (a) corresponding Pt distribution, bright spots are silica support and black spots are Pt particles (b) the corresponding size of Pt/Silica catalyst

146

The amount of the Pt recorded in the catalyst samples was calculated to be 10.30 %. The calculated amount of Pt (i.e. 10 %) in the sample correlates well to the amount of Pt quantified via SEM. The Pt/Silica nanoparticles were found slightly larger at 120 nm across (Figure 6-2-b) and composed of 10% Pt catalyst of the support. Also as can be seen in the SEM image of Figure 6-2-a, Pt particles were less uniformly dispersed on Silica.

6.1.2 MEA Characterization

During this research work, close to 100 MEAs were fabricated in-house using both Pt/Silica and Pt/Carbon catalyst. Out of these MEAs, many were rejected for several reasons, particularly at the start of the research work while exploring the best recipe and method to prepare a working MEA. Before presenting the performance and durability results, it is important to mention observations made during MEA fabrication which was used as a guide to developing a standardized method for the MEA fabrication which is mentioned section 4.3.

Catalyst Spreading

The hand painting method described in the literature proved to be unsuccessful. Painting thin layers of catalyst ink onto a GDL, and dying the GDE at 100° C in between each layer caused cracking of the catalyst layer (as shown in Picture 6-3-a), which then caused the layer to peel off from the GDEs.

A new approach was taken (described in section 4.3.5) to get a crack-free electrode in which a coating process takes place on a heated hot plate at around 70 °C,

and when the desired loading is obtained, the electrodes are then oven dried at 120 °C for 20 mins. The resulting GDE with the crack-free surface after the modified approach can be seen in a picture in Figure 6-3-b.
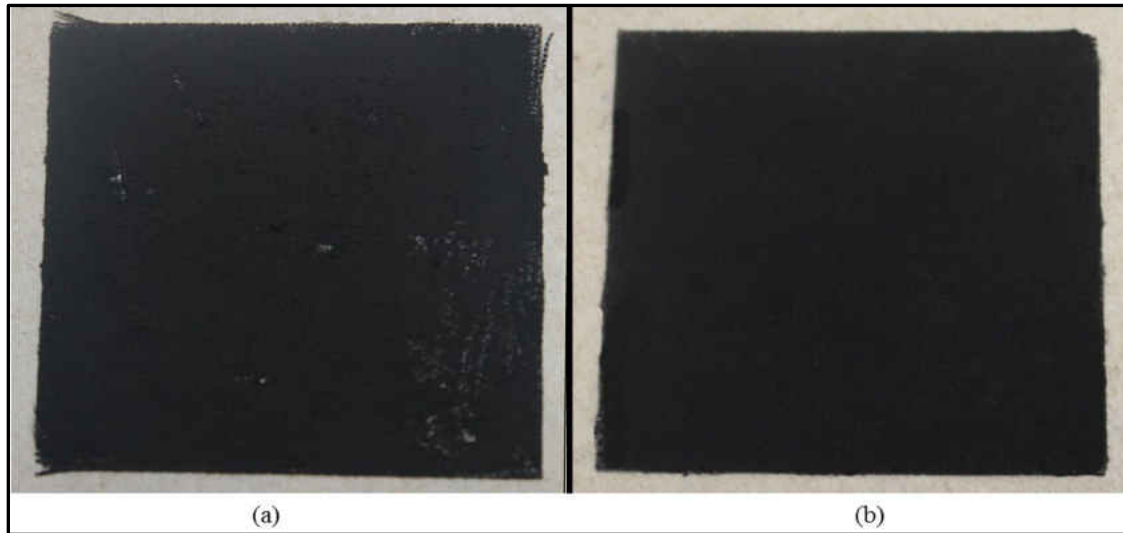
Figure 6-3 GDE fabricated using (a) literature approach (b) modified approach

Figure 6-4 In-house fabricated MEA rejected for (a) catalyst ink diffused through the GDL to the other side (b) improper alignment of the GDEs around the electrolyte membrane

The other reason for rejecting an MEA based on catalyst spreading was if the catalyst ink diffuses through the GDL to the other side. The picture of one of the MEAs

rejected, for this reason, is shown in Figure 6-4-a. The presence of the catalyst on the outer side due to diffusion could cause the reactants to react on the outer side of the MEA during operation in a fuel cell, and disrupt its performance.

The diffusion occurred when the paintbrush had excessive ink during the coating process. To avoid this problem the paintbrush was dipped into the catalyst ink, and then pressed against the side of the vial to remove excess liquid before each coat was applied.

Hot Press

During the replication of the hot-press procedure mentioned in literature, improper alignment of the GDE around the electrolyte membrane was observed in the fabricated MEA. The picture of one of the MEAs rejected, for this reason, is shown in Figure 6-4-b. Proper alignment is vital to ensure sealing, even distribution of the reactants to the catalyst layer and removal of the unwanted products from the catalyst layer.
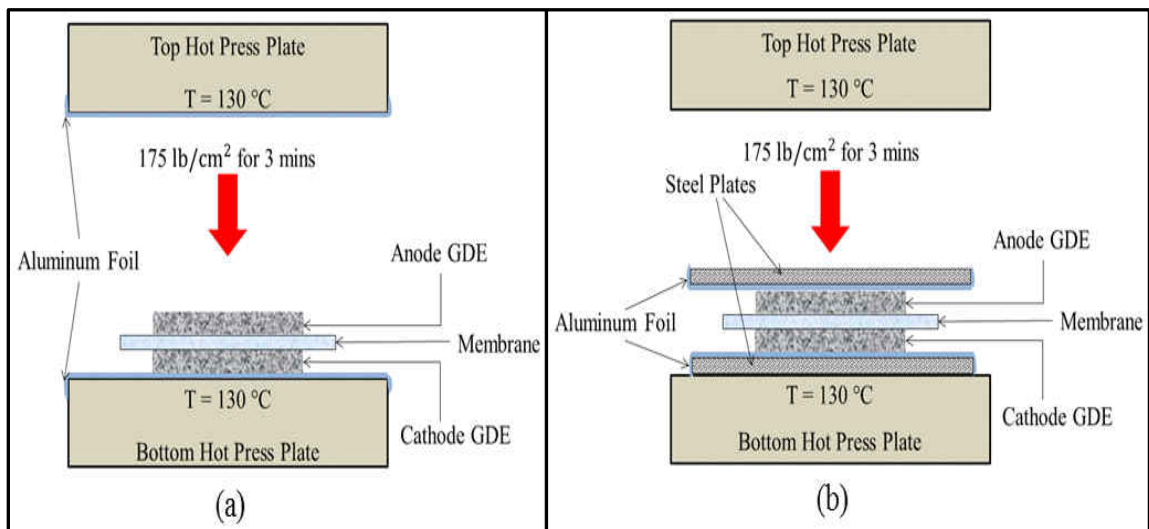
Figure 6-5 Illustration of hot press using (a) literature approach (b) modified approach

The improper alignment was the result of GDEs moving from its place after aligning with each other while placing it in the hot-press. To ensure proper alignment, the electrolyte membrane, and the two DGE were first aligned and placed between two separate flat metal plates (1 mm thick, 15 cm x 15 cm) before placing in the hot-press. Figure 6-5 illustrates the difference between the literature mentioned approach and the modified approach.

One of the other reasons for MEA rejection during hot-press was for discoloration of the electrolyte membrane after the hot press. As per the literature, after the hot press, the MEA was allowed to cool in the hot press for 30 minutes with the hot press pressure held, and the heat turned down. The discoloration of the electrolyte membrane is a result of degradation due to overheating, which could result in reduced proton conductivity of the membrane.
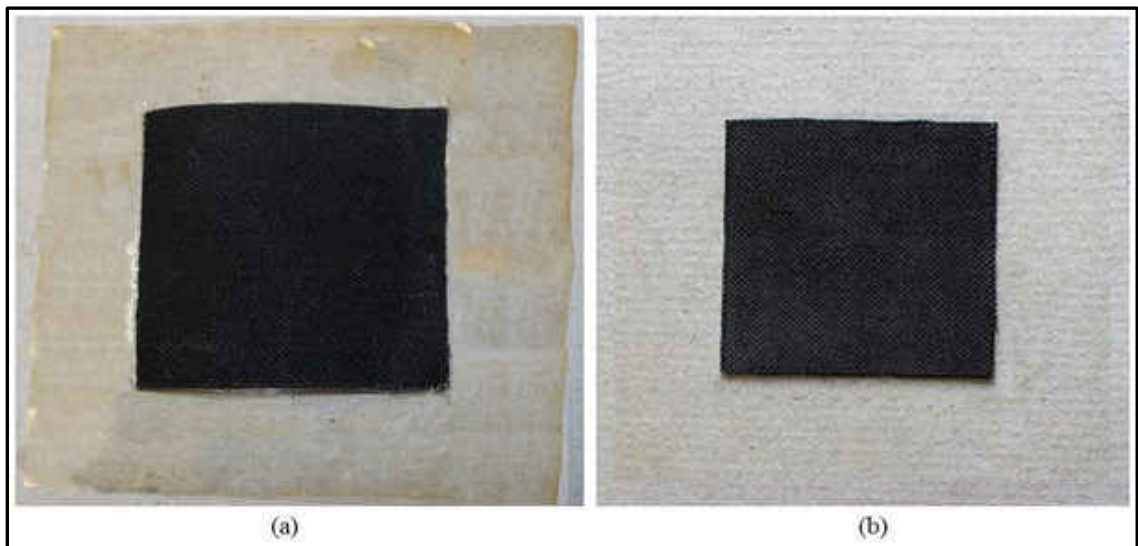
Figure 6-6 MEA cooling after Hot press using (a) literature approach (b) modified approach

To avoid this discoloration of the membrane, a new approach was taken in which the MEA was allowed to cool in the hot press for 30 minutes with the hot press pressure released, and the heat turned down. Figure 6-6-a shows the picture of the discolored MEA, and Figure 6-6-b shows a picture of the MEA with a new approach.

Type-BB MEA Developmental Work

The catalyst ink preparation method mentioned in section 4.3.4 however proved to be unsuccessful for preparing Type-BB MEA with carbon powder as an additive, in which 5 % carbon power was added to the catalyst ink. The 33 % Nafion ionomer was found to be insufficient to make a proper bonding of MEA layers. Therefore, to determine the minimum amount of ionomer (Nafion) content for Type-BB catalyst ink to prepare a workable MEA, higher ionomer content was used during Type-BB MEA fabrication. The ink compositions of these inks are listed in Table 6-1.

Table 6-1 INK1, INK2, and INK3 compositions for Type-BB MEA fabrication

	INK1	INK2	INK3
NFP (%)	33	35	37
Catalyst (Pt/SIlica)	75 mg	75 mg	75 mg
Carbon Powder	3.75 mg	3.75 mg	3.75 mg

Deionized water	As required to make catalyst wet (usually 4-5 drops total)	As required to make catalyst wet (usually 4-5 drops total)	As required to make catalyst wet (usually 4-5 drops total)
Solvent	3.15 g of isopropanol	3.15 g of isopropanol	3.15 g of isopropanol

Three different catalyst inks (INK1, INK2, and INK3) were prepared using the NFP (NFP as defined by equation 4.3) of 33%, 35%, and 37% respectively while keeping the catalyst loading and hot-press conditions constant. The amount of solvent in all three inks was 40 times the total amount of catalyst and carbon powder.

The resulting MEAs (MEA-INK1, MEA-INK2, and MEA-INK3) as shown in Figure 6-7 were first visually inspected and then mounted in unit-cell to ensure proper bonding of between the gas diffusion electrodes (GDEs) with the electrolyte membrane.

Bulge in the MEA

(a)   (b)   (c)
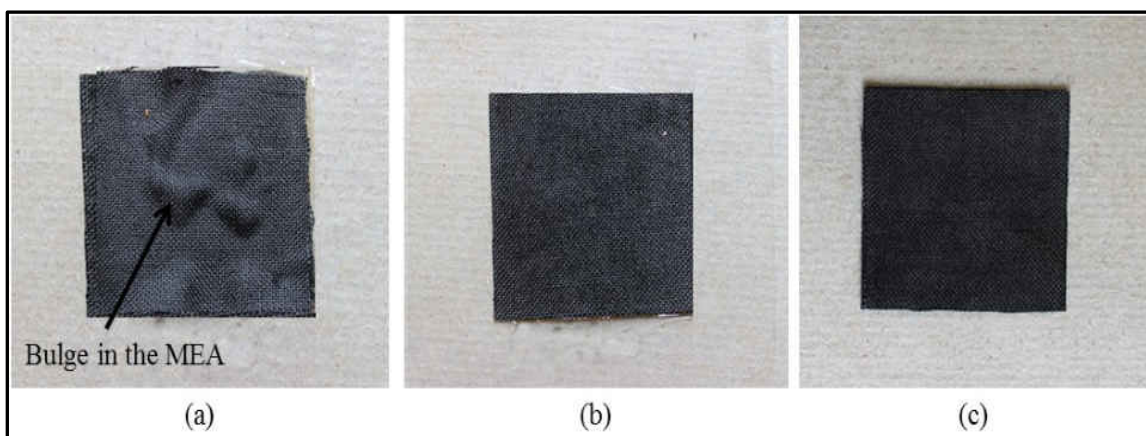
Figure 6-7 Effect of NFP on the Physical Appearance of type-AA MEA with (a) 33% NFP (b) 35% NFP (c) 37% NFP

The MEA-INK1 prepared using NFP of 33% (Figure 6.7-a) had the poorest bonding of the three, with some bulge visibly seen in the middle section of the MEA. The

reason for the bulge was that particular part of the GDE was not bonded to the electrolyte, which resulted in a non-workable MEA. Visibly there was very little difference between the MEA-INK2 prepared using NFP of 35% (Figure 6.7-b), and MEA-INK3 prepared using NFP of 37% (Figure 6.7-c). There was no bulge seen on either of these MEAs, though MEA-INK3 seemed to be more compact than MEA-INK2. MEA-INK2 and MEA-INK3 were then mounted in the unit-cell fixture for electrochemical evaluation.

During the conditioning process of MEA-INK2, catalyst particles were noticed in the anode and cathode side water collection bottles (Figure 6.8-a). The release of catalyst from the MEA was due to the inefficient binding of the catalyst ink to both the electrolyte membrane and GDLs. Since a considerable amount of catalyst was lost during the conditioning process, a performance test was not performed on MEA-INK2.

The conditioning and catalyst activation process were successfully carried out on MEA-INK3 without noticing any catalyst particles in product collection bottles (Figure 6-8-b). This MEA was then assembled in the unit-cell fixture for its performance evaluation, and the water produced by the electrochemical reaction in addition to the condensed water of humidification was collected in the product collection bottles. During the performance tests of MEA-INK3, the water collected in the cathode side product collection bottle (Figure 6-8-b) was without any catalyst particles in it. The absence of catalyst particles in both anode and cathode side bottles represents an excellent binding of the catalyst ink to both the electrolyte membrane and GDLs. Therefore 37% Nafion content was used for preparing Type-BB MEAs.

153
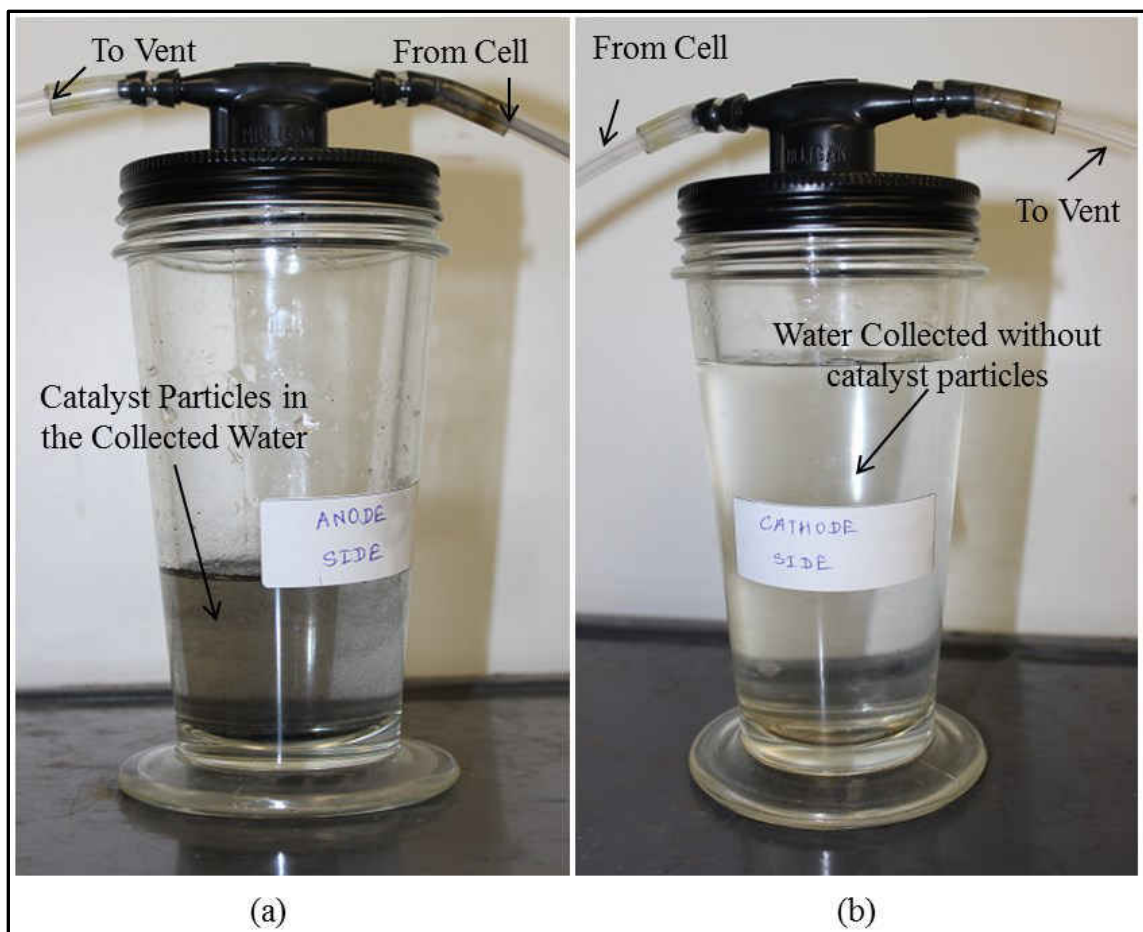
Figure 6-8 Water collected in one of the product collection bottles during (a) MEA-INK2 conditioning (b) MEA-INK3 conditioning and performance evaluation

6.2   Preliminary Evaluation

The performance results and observations made during preliminary studies are presented in this section.

6.2.1   MEA Reproducibility Study

The reproducibility of MEAs was first validated by fabricating four Type-A MEAs using the same catalyst ink composition and the identical hot press conditions. The quality of the MEAs fabricated in-house was then studied first by calculating catalyst loadings in each GDE using equation 4.6 and then by evaluating in-situ performance tests

using a unit-cell text fixture. The targeted catalyst loading for both anode and cathode electrode was 0.3 mg/cm^2.

Table 6-2 Calculated catalyst loadings of the MEAs (Type-A) fabricated for the reproducibility test

MEA #	Anode Pt Loading (mg/cm^2)	Cathode Pt Loading (mg/cm^2)	Average Pt Loading (mg/cm^2)
A017	0.329	0.283	0.306
A019	0.298	0.310	0.306
A020	0.305	0.320	0.313
A021	0.292	0.318	0.303

The MEAs fabricated for reproducibility testing have Pt loadings of 0.298-0.329 mg/cm^2 on anodes electrodes and 0.283-0.320 mg/cm^2 on cathodes electrodes, as shown in Table 6-2. Since the catalyst coating process was handled manually using a hand paint method, the coating consistency between MEA's loading was difficult to control. As a result, the Pt loadings of anode and cathode were not exactly as was targeted. For comparison, the greatest loading difference is less than ±0.05 mg/cm^2 (~16 %). The key to achieve the consistent catalyst loading was weighing the GDE after every layer of catalyst ink coating during catalyst application on the GDL.

The IV curves of the above MEAs are shown in Figure 6-9, and the power curves are plotted in Figure 6-10 for the reproducibility test. The polarization tests were conducted under identical operating conditions. Fully humidified reactants (ARH = CRH = 100) with anode stoichiometry of two (λ_{H_2}= 2) and cathode stoichiometry of 3.0 (λ_{O_2}=

3.0) were supplied to both the anode and cathode sides, and IV curves were recorded at cell temperature (T_{Cell}) 70 °C. The current and power densities were calculated based on the active areas (25 cm^2) of the MEA.
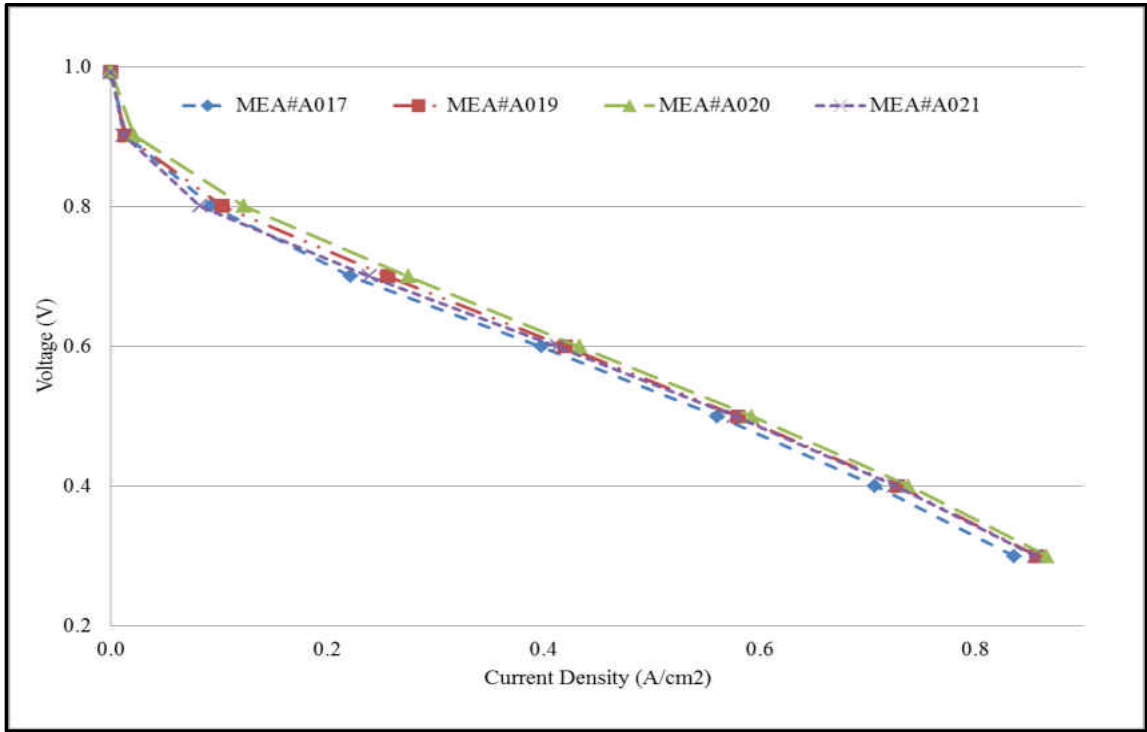
Figure 6-9 Reproducibility test IV curve at ARH = CRH = 100 %, λ_{H_2} = 2.0, λ_{O_2} = 3.0 and T_{Cell} = 70 °C.

The IV and power curves show that the performances of all four MEAs were very similar with less than 15 % difference for any given voltage at high current density. The MEA A020 extracted the maximum power density of 0.30 W/cm^2, while MEA A017 showed the lowest power density of 0.28 W/cm^2 out of the four MEAs. This variation is considerably lower than the differences in performance caused by handmade MEA fabrication in the literature.

The IV curve (Figure 6-9) also shows that the performances of MEA A019 and A021 are very similar with less than 10% difference for all operation voltages. The Pt loadings between these two MEAs only have ±0.012 mg/cm^2 differences between the anode GDEs and ±0.005 mg/cm^2 differences between the cathode GDEs. Hence, the performances of the MEAs are consistent with the Pt loadings on the MEAs. Furthermore, Figure 6-9 also showed that the performance of MEA A020 was further improved due to higher anode and cathode catalyst loading compared to other three MEAs.
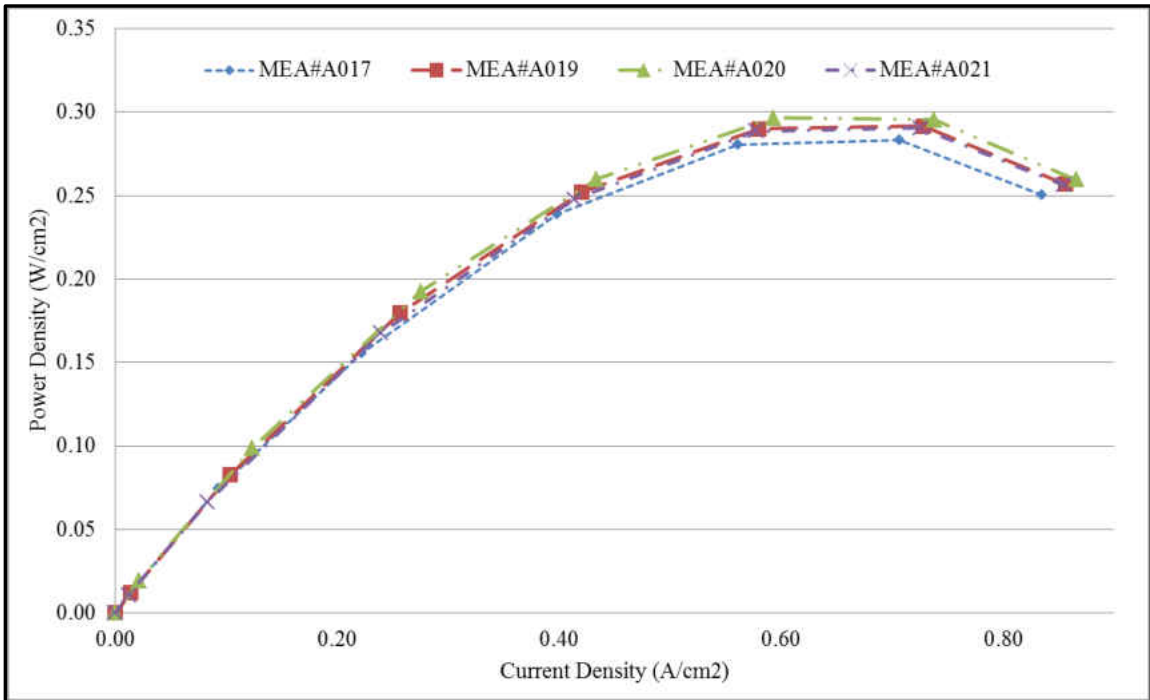
Figure 6-10 Reproducibility test power curve at $RH_{Anode} = RH_{Cathode} = 100$ %, $\lambda_{H_2} = 2.0$, $\lambda_{O_2} = 3.0$ and $T_{Cell} = 70$ °C

Using the data from Figure 6-9 and Figure 6-10, the relationship between the maximum power density and the average catalyst loading is illustrated in Figure 6-11. It shows that the power density increases with the Pt loading except for the MEA A017.

157

Although MEA A017 has very similar average Pt loadings as of A019, its performance was not as good as MEA A019. It has comparatively lower Pt loading on its cathode side than the other MEAs and has higher loading on the anode than the cathode side, which has resulted in its lower performance. The cathode side is considered to be very complicated due to the formation of heat and water during the electrochemical reaction. In order to keep the performance results to be consistent and be able to eliminate the effects of lower Pt loading on the cathode side, the GDE electrode, which has a higher Pt loading, was always selected as a cathode electrode during the MEA fabrication.
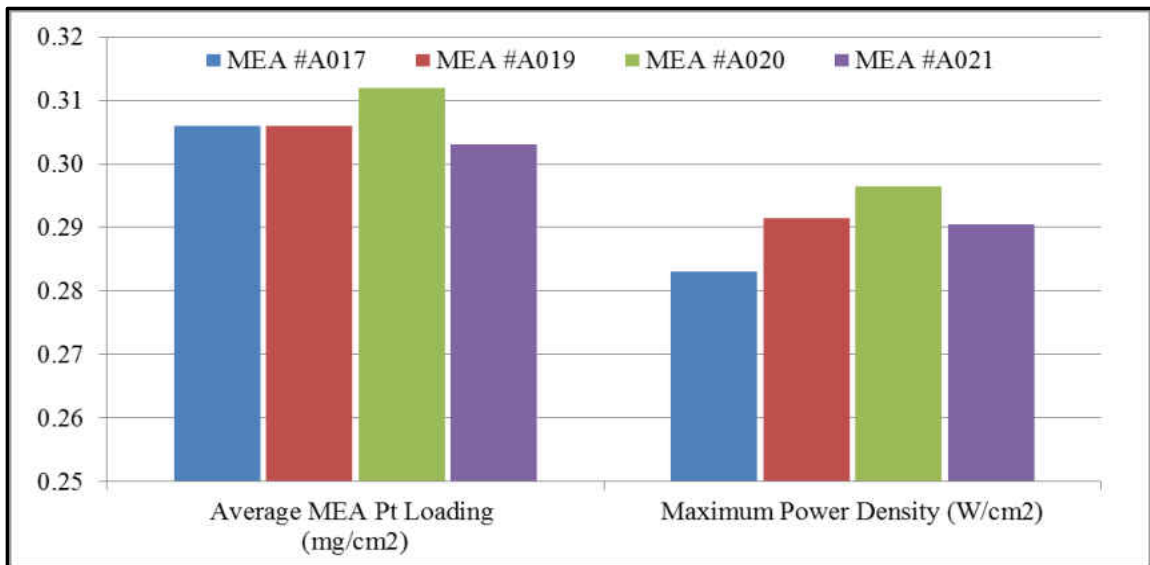
Figure 6-11 Relationship between the maximum power density and the average catalyst loading of in-house fabricated Type-A MEA

Although the MEA performance is closely related to the Pt loading, optimizing the Pt loading for optimum MEA performance was not the scope of this project. Therefore, the Pt loadings on MEAs throughout this work were not optimized, but the fabrication processes were followed consistently for all of the MEAs.

The results examined in this section show that the in-house fabrication method could be used to fabricate MEAs with consistent performance. This confirms the reproducibility of the standard MEA fabrication technique, and thus, the performance results of the in-house fabricated MEAs could be utilized as a basis for comparison.

6.2.2 Comparison Test (in-house fabricated MEA *vs.* commercial MEA)

A comparison test of in-house fabricated (Type-A) MEA with commercial (Type-C) MEA was performed by first mounting the MEA in a unit-cell for its performance evaluation followed by its conditioning. The actual amount of the catalyst loadings in both Type-A and Type-C MEAs are listed in Table 6-3.

Table 6-3 Catalyst loadings of MEAs used for comparison test between Type-A and Type-C MEAs

MEA	Anode Pt Loading (mg/cm^2)	Cathode Pt Loading (mg/cm^2)	MEA Pt Loading (Average) (mg/cm^2)
Type-A	0.309	0.317	0.313
Type-C	Unknown	Unknown	0.3

Figure 6-12 shows the conditioning time required for both MEAs. The current generated at the start of the conditioning for Type-C MEA was 6.64 A, which is about four times higher than the in-house fabricated MEA.
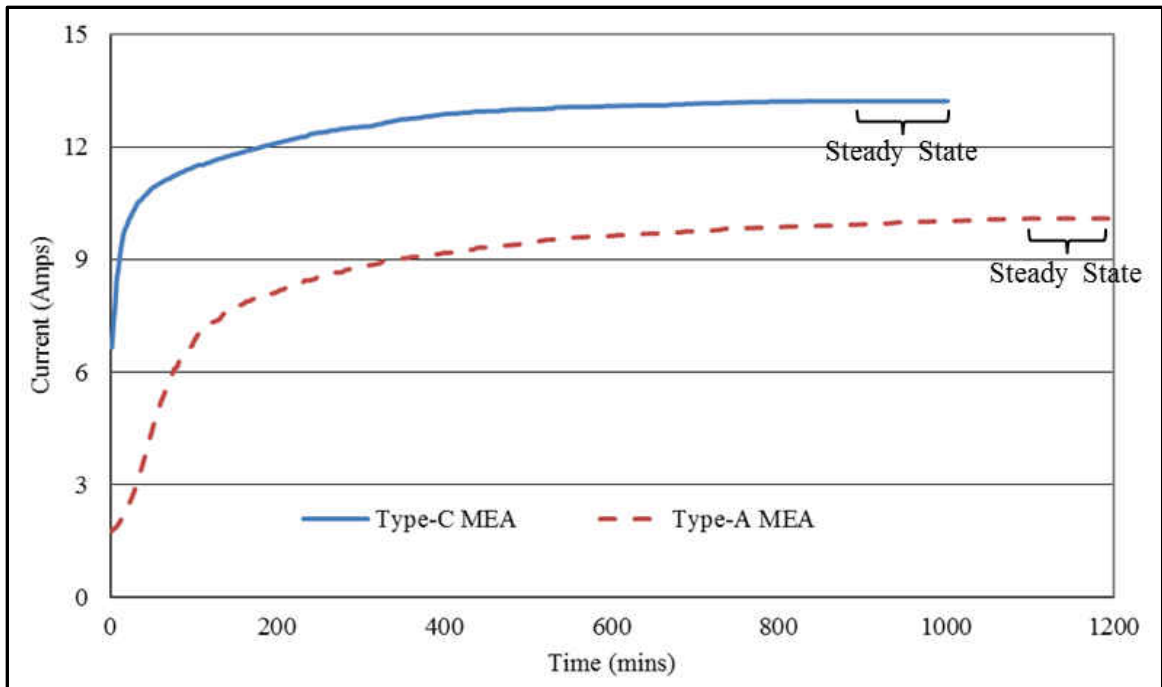
Figure 6-12 Conditioning curve for Type-C and Type-A MEA at V=0.6 V, ARH = CRH = 100 %, λ_{H_2}= 2.0, λ_{O_2}= 3.0 and T_{Cell} = 60 °C.

The Type-C MEA also took comparatively less time to reach a steady current at 0.6 V than the Type-A MEA. The differences in start current and conditioning time could be attributed to the difference in hot press procedures between the fabrications of these two MEAs. The difference in hot press procedure affects the membrane dehydration. Also, it was unknown if the Type-C MEAs had some post treatment after the hot press procedure. In addition, Type-A MEAs were tested within weeks after their fabrication, while Type-C MEAs were evaluated after longer (unknown) hold time. This holdup time may have helped the MEA relax and absorb more water from the environment.

Figure 6-13 and Figure 6-14 compares the performance of an in-house fabricated (Type-A) MEAs with a commercial (Type-C) MEAs. It is evident from the performance curves that the performance of the commercial (Type-C) MEA is superior to that of the in-house fabricated (Type-A) MEA. For both cases (Type-A and Type-C), the

160

experimental OCV was 0.994 and 1.035 V, which is very close to the expected value in the range of 1.0 to 1.10 V.
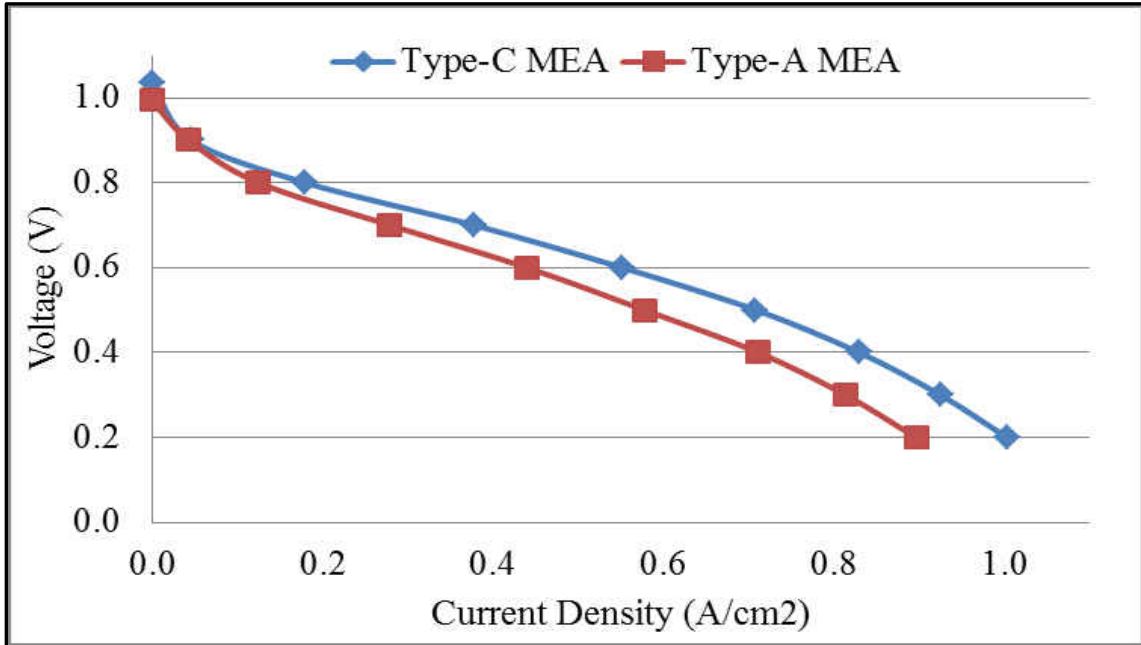
Figure 6-13 IV curve for Type-C and Type-A MEA at ARH = CRH = 100 %, λ_{H_2} = 2.0, λ_{O_2} = 3.0 and T_{Cell} = 70 °C
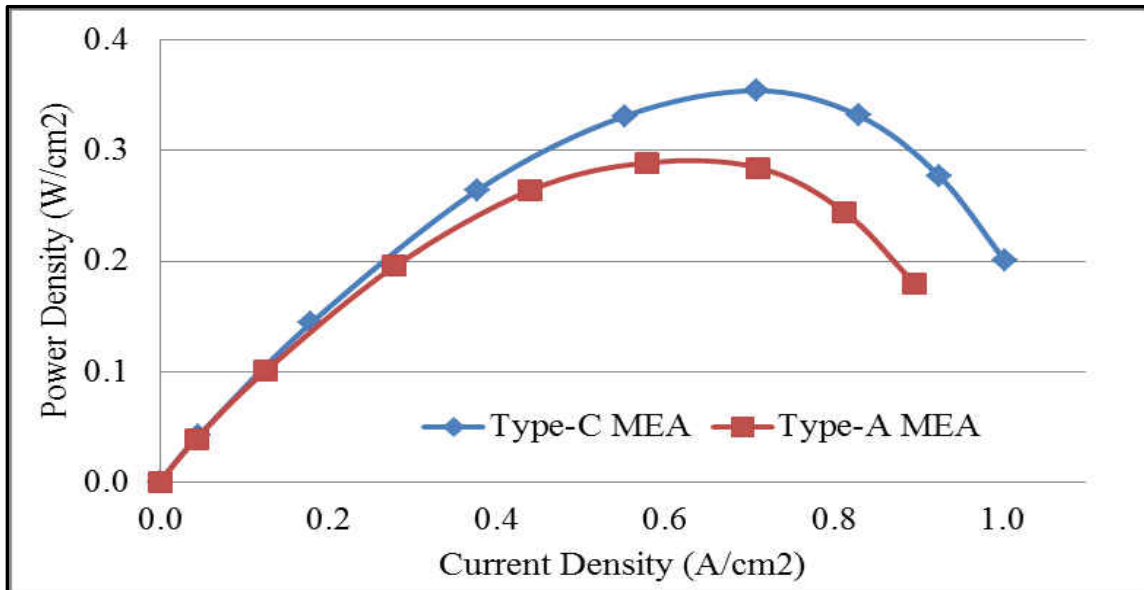
Figure 6-14 Power curve for Type-C and Type-A MEA at ARH = CRH = 100 %, λ_{H_2} = 2.0, λ_{O_2} = 3.0 and T_{Cell} = 70 °C

The commercial Type-C MEA varied in performance, with a difference of $0.11 \, A/cm^2$ (~20 % higher) in the maximum current density and $0.06 \, W/cm^2$ (~18 % higher) in the maximum power density as compared to the Type-A MEA. The in-house fabricated MEAs compared favorably with the commercial MEA up until 0.8 V. After 0.8 V, the performance of the manufactured MEA dropped below that the ElectroChem MEA. The in-house fabricated MEA (Type-A) showed an average decrease of 11 % in the maximum current density and 21 % in the maximum power density as compared to the ElectroChem MEA. The poorer performances of the in-house fabricated MEA may be caused by the inconsistent catalyst layer application during the catalyst ink application on the GDL to form GDE as their internal ohmic resistances determined by current interruption method at 0.6 V was 14 % higher than the commercial MEA as shown in Table 6-4.

Table 6-4 Performance comparison of Type-C and Type-A MEAs

| MEA Type | OCV (V) | Maximum | | Ohmic Resistance (Ω) |
		Power Density (W/cm^2)	Current Density (A/cm^2) at 0.3 V	
Type-A	0.994	0.290	0.810	0.724
Type-C	1.035	0.350	0.930	0.638

The details about the components and fabrication method used for the commercial (Type-C) MEA could not be obtained from ElectroChem Inc., since this was proprietary information, hence, a comparison of preparation methods, especially for electrode preparation, cannot be drawn. As a result, the lower performance of the in-house

fabricated MEA was attributed to (1) Electrochem Inc. using superior raw materials and (2) an improved fabrication procedure leading to increased performance.

6.3 Pt/Silica In-situ Performance Test (Hypothesis 01 Testing)

The IV performance and ECASA of in-house fabricated Type-A and Type-B MEAs were evaluated using a 25 cm^2 unit-cell under identical operating conditions and the results are summarized in this section. The results are presented on a current density and power density basis for a fair performance comparison.

6.3.1 Type-B (Pt/Silica electrodes) MEA performance against Type-A (Pt/Carbon electrodes) MEA

The actual calculated amount of the catalyst loadings in both Type-A and Type-B MEA for this test are listed in Table 6-5. The targeted loading was 0.3 mg/cm^2

Table 6-5 Catalyst loadings of MEAs used for comparison test between Type-A and Type-B MEA

MEA	Anode Pt Loading (mg/cm^2)	Cathode Pt Loading (mg/cm^2)	Average Pt Loading (mg/cm^2)
Type-A	0.3041	0.3097	0.3070
Type-B	0.3014	0.3048	0.3031

The steady-state polarization behavior and the power curves of Type-A and Type-B MEAs are presented in Figure 6-15 and Figure 6-16, respectively. For both (Type-A and Type-B) MEAs, the experimental open circuit voltage (OCV) was lower than the expected value but similar to each other at 0.962 and 0.948 V respectively. It should be noted that the OCV for a typical PEMFC catalyst is expected to be in the range of 1.0-1.1

163

V. Since it is of interest to compare the performance of commercial Pt/Carbon catalyst and the novel Pt/Silica catalyst, OCV baseline is considered less important than having similar OCVs.
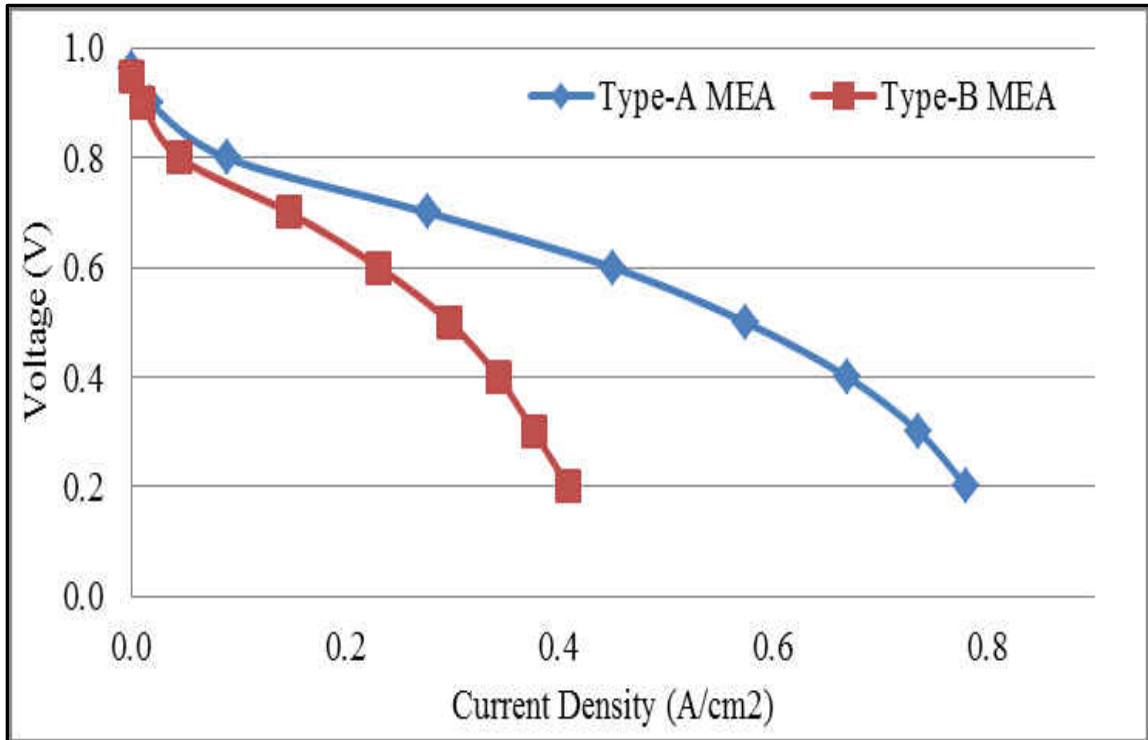
Figure 6-15 IV curve for *in-situ* performance comparison of Type- A and Type-B MEA at T_{Cell}= 70 °C, λ_{H_2}= 2.0, λ_{O_2}= 3.0 and Ld_{Pt}= 0.3 mg/cm^2

It can be noted from the IV curves presented in Figure 6-15, that the performance of the unit-cell with Type-A (Pt/Carbon electrodes) MEA was far superior to the Type-B (Pt/Silica electrodes) MEA under identical test conditions. The performance of the Type-B is comparable to the Type-A MEA till 0.8 V, which is the activation polarization region. Further, the Type-B MEA exhibits significantly lower current density at any given potential below 0.8 V than the Type-A MEA. This was due to the higher ohmic losses in Type-B MEA, which was 1.217 Ω compared to 0.652 Ω in Type-A MEA. At a fixed cell voltage of 0.6 V, the current density of novel Pt/Silica-based (Type-B) MEA is

0.23 A/cm^2 which is only 50% of the commercial Pt/Carbon based (Type-A) MEA, which was 0.45 A/cm^2.

The peak power of the cell with a Type-A MEA made using Pt/Carbon (0.29 W/cm^2) was meaningfully higher ($\sim$ 50 %) than that measured in the cell with Type-B MEA made using Pt/Silica, which was 0.15 W/cm^2, which is attributed to the better dispersion of Pt nanoparticles on the carbon surface. The power curve behavior also demonstrates that Pt/Carbon electrode has a higher limiting current density than the Pt/Silica electrode indicating that the mass transport properties of the Pt/Carbon electrodes are better than that of Pt/Silica electrodes.
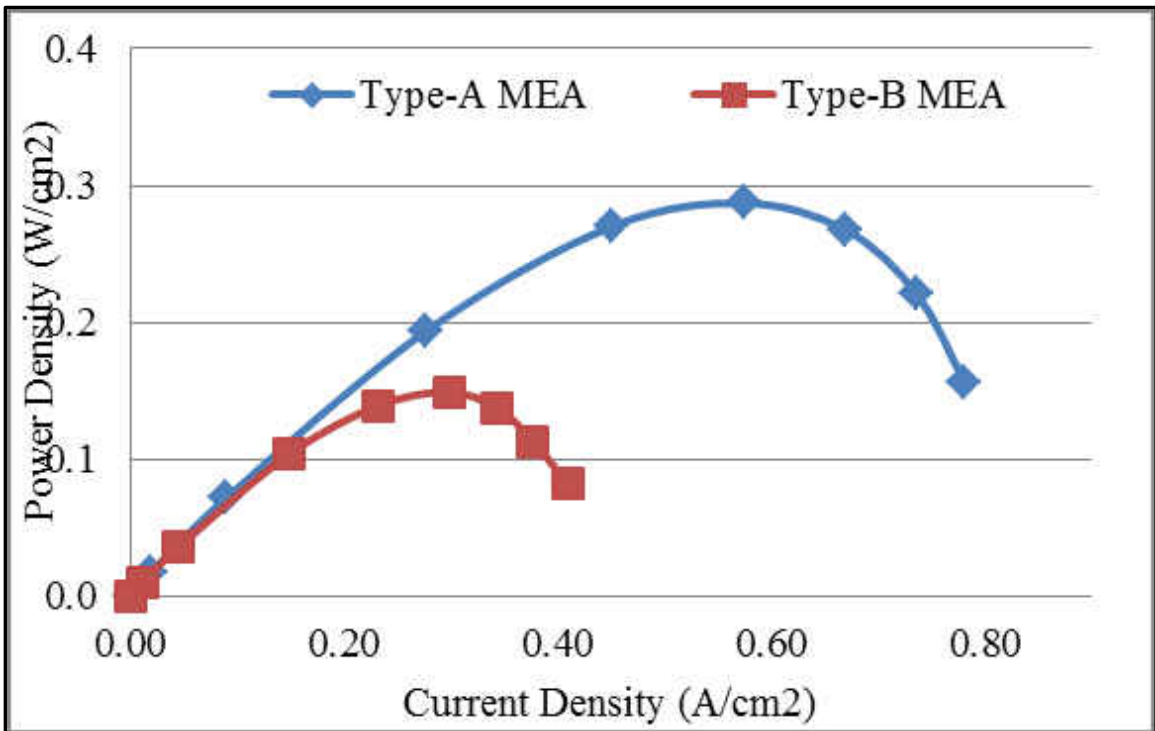
Figure 6-16 Power curve for *in-situ* performance comparison of Type- A and Type-B MEA at T_{Cell}= 70 °C, λ_{H_2}= 2.0, λ_{O_2}= 3.0 and Ld_{Pt}= 0.3 mg/cm^2

The results showed that the commercial catalyst exhibited better performance in fuel cells due to their higher mass activity. The mass activity of the Pt/Silica catalyst was found to be 0.034 A/gm$_{Pt}$, which was only 58 % of the commercial Pt/Carbon catalyst (0.059 A/gm$_{Pt}$). This shows that the activity of the in-house fabricated Pt/Silica catalyst was not as good as the commercial Pt/Carbon catalyst. The performance difference was consistent with the mass activity of the two catalysts used in these MEAs. The IV performance data of both Type-A and Type-B MEA are summarized in Table 6-6.

Table 6-6 Performance comparison of Type-A and Type-B MEAs using IV curve

MEA Type	OCV (V)	Maximum		Ohmic Resistance (Ω)	Mass Activity (A/gm$_{Pt}$)
		Power Density (W/cm^2)	Current Density (A/cm^2) at 0.3 V		
Type-A	0.96	0.29	0.74	0.65	0.059
Type-B	0.95	0.15	0.38	1.21	0.034

The two MEAs were then subjected to $in-situ$ ECASA measurements to determine the reason for the lower performance of Pt/Silica catalyst during IV measurements. Figure 6-17 shows the voltammogram of the two MEAs at a scan rate of 50 mV/s. The double-layer capacitance region (from 0.3 − 0.7 V) of Type-B MEA is wider compared to Type-A, this could be due to the absence of carbon in the Type-B MEA. In the voltammograms both the hydrogen adsorption and desorption regions of Type-B MEA seems larger than Type-B MEAs, however, the ECASA of Type-B MEA is smaller than Type-A MEA since Type-B MEA resulted in a wider double layer capacitance region.
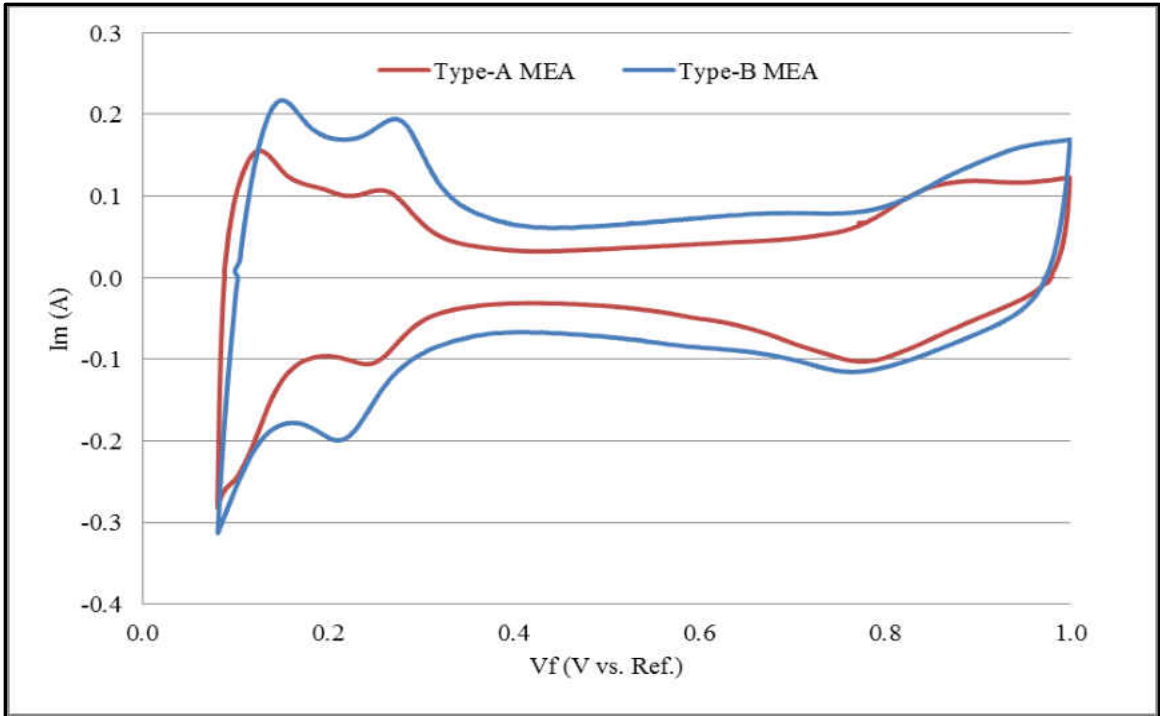
Figure 6-17 Cyclic voltammetry plots for in-situ performance comparison of Type- A and Type-B MEA at T_{Cell}= Room Temperature, scan rate of 50 mV/s and Ld_{Pt}= 0.3mg/cm^2
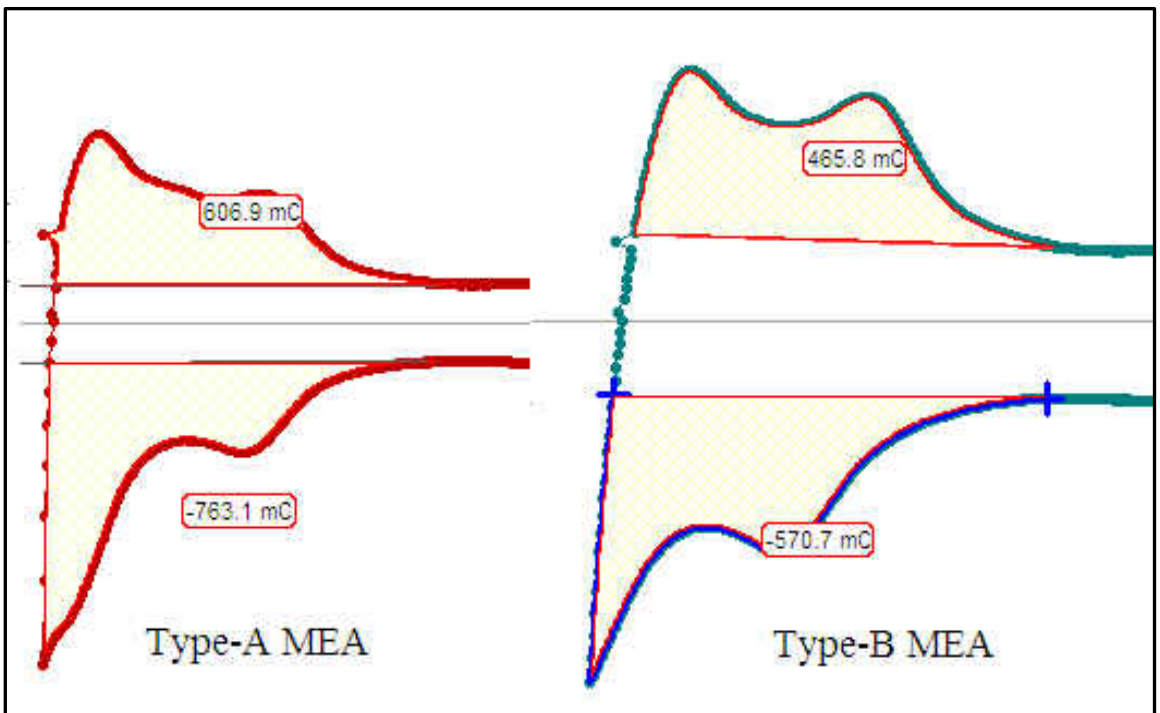
Figure 6-18 Cyclic voltammetry plots for Type A and Type B MEA with actual charge calculated

167

Figure 6-18 shows the picture of CV plots of Type-A and Type-B MEA with the estimated charge. The average of these two regions determines the ECASA. The ECASA of the novel Pt/Silica catalyst based electrode was found to be 0.329 cm^2/mg_{Pt}, which is ~25 % lower than that of novel Pt/Carbon based electrode (0.435 cm^2/mg_{Pt}), despite both the catalyst have a similar 10 wt. % Pt deposition on the support. The specific activity of Pt/Silica catalyst was found to be 0.106 A/m^2_{Pt}, which was only 75 % of the commercial Pt/Carbon catalyst (0.0.135 A/m^2_{Pt}).

The lower ECASA and specific activity of Pt in Type-B MEA suggest less number of platinum sites were available which leads to the dropped fuel cell performance seen in the polarization and CV test. That was due to the fact that the dispersion of Pt was less uniform in Pt/Silica catalyst noticed during the electron microscopy characterization. The calculated ECASAs were summarized in Table 6-7.

Table 6-7 Calculated ECASA values for the Type-A and Type-B MEA

Sample		Average Charge	ECASA	Specific Activity
MEA Type	Catalyst	(μC)	(cm^2/mg_{Pt})	(A/m^2_{Pt})
Type-A	Pt/Carbon	685.0	0.435	0.132
Type-B	Pt/Silica	518.3	0.329	0.106

Clearly, both the polarization and CV tests show that the performance of Pt/Silica catalyst was lower than the commercial Pt/Carbon catalyst, despite (1) both the catalyst have a similar 10 wt. % Pt deposition on the support and (2) both the MEAs use similar Platinum loading of 0.3 mg/cm^2.

To further identify the cause for the low performance of Type-B MEA, the performance of both type-A and type-B MEA was determined and analyzed in the activation and concentration overpotential regions.
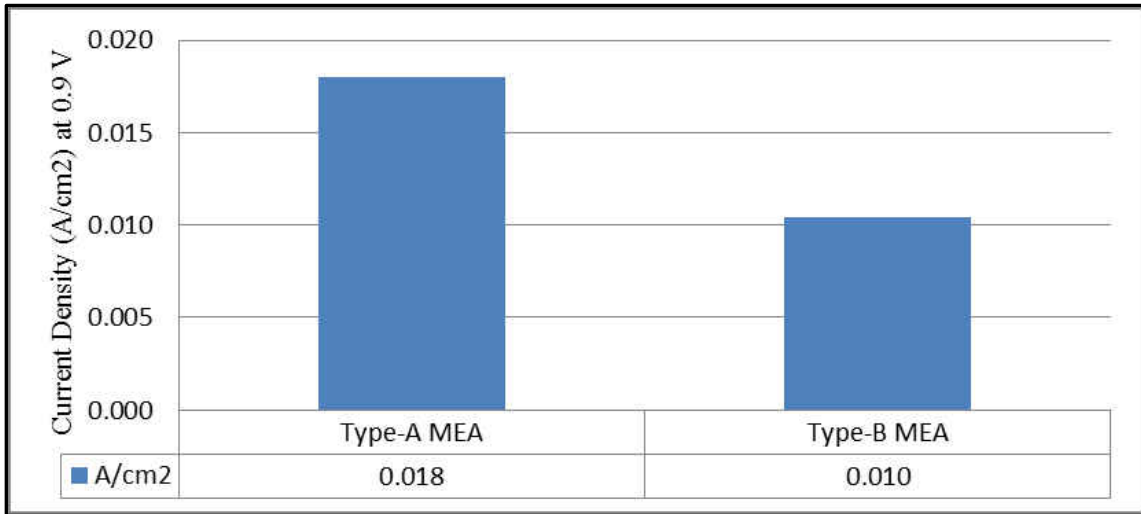
Figure 6-19 Current density at 0.9 V (low current density) for Type-A and Type-B MEA

At high voltage (~0.9 V), the cell performance is determined primarily by the activation overpotential. The activation overpotential originates from the limited rate of oxygen reduction reactions (ORR) at the active sites in the cathode catalyst layers. Figure 6-19 shows the current density at 0.9 V (low current density) for both MEAs, Type-B MEA has only 43 % of the current density at the same voltage for Type-A MEA in the activation region. Considering that the Platinum loading on both MEAs was uniformly controlled (0.3 mg/cm^2), the low performance of Type-B MEA is a result of lower platinum catalyst utilization than Type-A MEA.

The concentration overpotential, which is related to the mass transport of reactant gasses through the porous catalyst layers, is dependent on the cathode gas conditions, such as the oxygen partial pressure and the flow rates. By altering the cathodic flow rates

(stoichiometric ratio), variation in the current densities at low voltage could be confirmed for both MEAs, as shown in Figure 6-20.
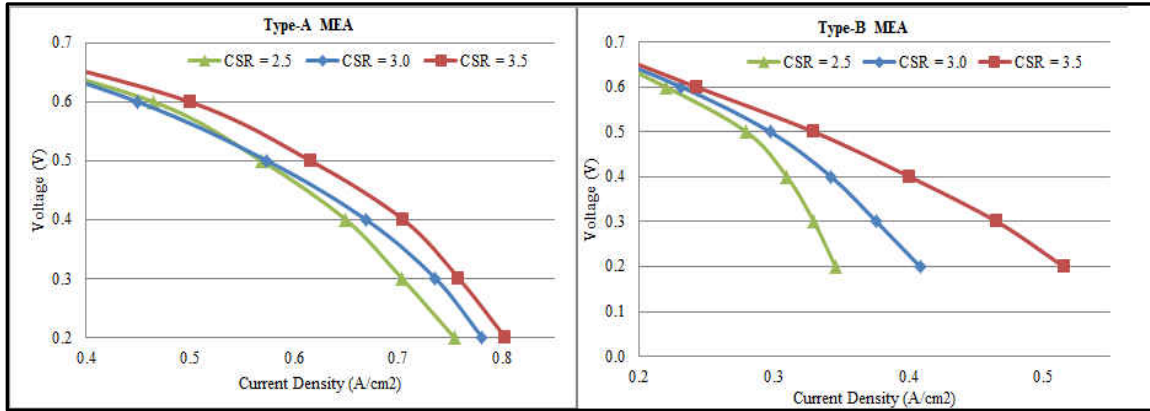
Figure 6-20 Performance of Type-A and Type-B MEA in concentration overpotential region

A comparison of the current density at lower cell voltage, where the concentration overpotential is dominant, is shown in Figure 6-21 as a function of the cathode stoichiometric flow rate. When the cathodic stoichiometric ratio was increased from 3.0 to 3.5, the maximum current density (at 0.3 V) of Type-A MEA (Pt/Carbon catalyst) increased only by 3 % (from 0.78 to 0.80 A/cm^2), suggesting that the gas channels were sufficiently developed so as to support oxygen transport at low voltage (high current density).

In contrast, for Type-B MEA (Pt/Silica catalyst), the current density increase was as high as 26% (from 0.41 to 0.52 A/cm^2), probably due to the flooding that occurred with more hydrophilic pores in the silica support. In addition, when the stoichiometric flow rate was decreased from 3.0 to 2.5, the decrease in current density was also much higher (~26%) for Type-B MEA. This result indicates that the mass transport limitation

was severe with Type-B MEA. As a result, the current density of Type-B MEA was lower than Type-A MEA at a low voltage (high current density) region.
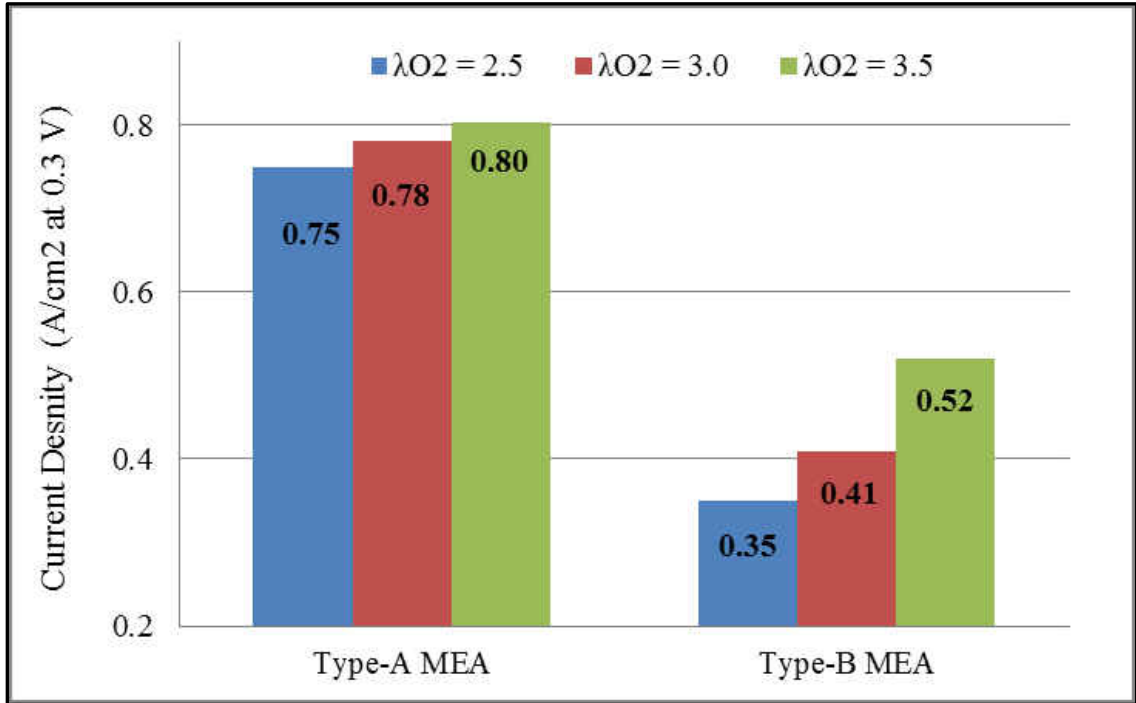
Figure 6-21 A comparison of current density of Type-A and type-B MEA at low cell voltage (0.3 V)

For the Type-A MEA, which has the larger ECASA value, the current density at 0.9 V (activation overpotential region) was also higher. This result demonstrates the correlation between the ECASA and the electrochemical activity. However, a more detailed analysis of Type-B MEA in the concentration overpotential region reveals that the silica supports due to its hydrophilic nature was able to retain a lot of water in the catalyst layer, and as a result, the electrodes were flooded. This behavior can be explained by less effective triple-phase-boundary within the catalyst layers. When resistance to the flow of ions and electrons within the catalyst layers is significant, the

overall catalyst/ionomer interface (ECASA), as measured by CV, cannot be fully utilized as active sites for electrochemical reactions.

Since both MEAs were fabricated using the same electrolyte membrane, similar catalyst ink composition, and identical hot-press conditions, the lower performance of Pt/Silica catalyst is related to the formation of less effective triple-phase boundaries on the Pt/Silica electrodes than the Pt/Carbon electrodes. Therefore it was hypothesized that the real cause for the less effective triple-phase-boundary in Pt/Silica electrodes was (1) *flooding of the catalyst layer in Pt/Silica electrodes at the testing environment (operating conditions), since the operating conditions chosen for this test were based on the Pt/Carbon catalyst from the literature* and (2*) the low electronic conductivity of silica support have caused the non-facile electronic and/or ionic flow path in the catalyst layer*, which has contributed to the lower performances. In addition to the relatively non-uniform dispersion of Pt on silica which could be seen in the section 6.1.1 has affected the performance of Type-B MEA.

Better performance of the Type-A MEA is also attributed to the superior conductivity of the Pt/Carbon catalyst due to the uniform Pt dispersion on the support of the optimized commercial catalyst, in addition to the relatively high conductivity of the carbon black support.

6.3.2 Effects of Operating Conditions on Pt/Silica Catalyst (Sub-hypothesis 01 Testing)

The results in this section provide a basis to test the first sub-hypothesis proposed to justify the lower performance of Pt/Silica catalyst. The proposed hypothesis was that

the electrode flooding was one of the causes of the lower performance of Pt/Silica catalyst, due to the silica support retaining water in the catalyst layer. It will also help understand the behavior of Pt/Silica catalyst in the unit-cell under various operating conditions. Since the lower performance of Pt/Silica catalyst was suspected due to the hydrophilic nature of the silica support, the experimental tests were designed to focus on the water management in unit-cell. Effects of stoichiometric flow rates of reactants, relative humidity (RH) of reactant gasses and the temperature of the unit-cell on the performance of Pt/Silica catalyst was examined using the unit-cell fixture. In order to identify the factors that affect in-situ Pt/Silica catalyst performance, a method of varying only one parameter at a time was adopted.

Effects of Cathode Stoichiometric Flow Rates

The stoichiometric flow rate is thermodynamically a mass flow rate of gas for generating one-Ampere current by one cell, which should be known according to Faraday's Law. However, the reactant flow rates for a fuel cell reaction must be equal to or higher than the stoichiometric flow rate (Barbir, 2005). Insufficient fuel will create fuel starvation which has damaging effects both on the catalyst and membrane. This state causes water electrolysis and carbon oxidation at the fuel cell anode in order to provide the required protons and electrons for the oxygen reduction reaction happening at the cathode.

The relationship between the cathode flow and the fuel cell performance was explained by Yan et al. (Yan et al., 2006). When an excess cathode flow rate was

173

supplied, the rate of water removal and the availability of oxygen at the cathode catalyst layer increased, and the fuel cell performance improved (Yan et al., 2006). However, too high cathode flow rate could result in rapid drying of the electrode. For this study the effects of varying cathode stoichiometry (λ_{O_2}) at 3.0, 3.5, 4.0 and 4.5 on the in-situ performance of Pt/Silica catalyst in a unit-cell were determined. The anode stoichiometry was kept constant at two ($\lambda_{H_2} = 2$) to avoid fuel starvation.
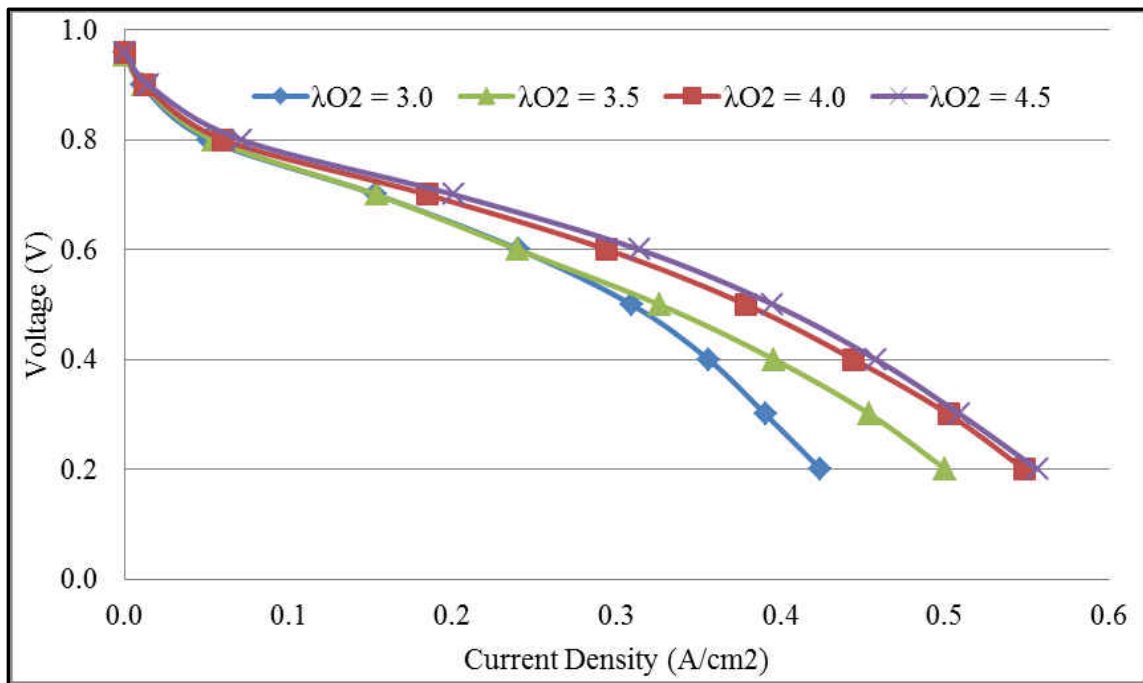
Figure 6-22 IV curve for the effects of stoichiometric flow on the performance of Type-B MEA at T_{Cell}= 70 °C, λ_{H_2}=2.0, ARH = CRH = 100 % and Ld_{Pt}= 0.3 mg/cm^2

One can clearly notice from Figure 6-22 and Figure 6-23 that the performance of Pt/Silica catalyst improves with an increase in cathodic stoichiometric flow rate. An increase in performance of almost 23% is caused by increasing the cathodic stoichiometric flow rate (λ_{O_2}) from 3.0 to 4.0. The higher flow rate forces more oxygen to the active catalyst sites and thus the reaction rate increases. Besides forcing more

174

oxygen into the cell, the higher oxygen flow rate also showed benefits related to water management. Liquid water that was generated on the cathode side could be pushed out more easily from the catalyst layer pores. At the exit, more water droplets exiting at higher stoichiometric flow rates than at lower rates were observed. A combination of both these aspects led to higher current densities.
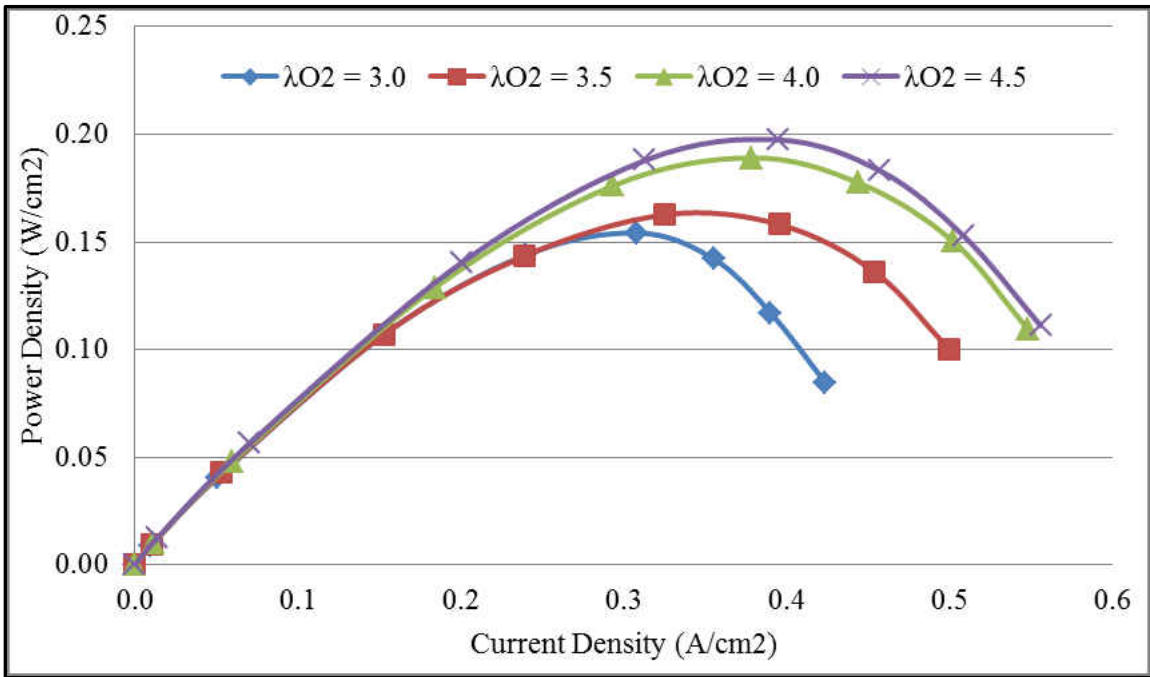
Figure 6-23 Power curve for the effects of stoichiometric flow on the performance of Type-B MEA at T_{Cell} = 70 °C, λ_{H_2} = 2.0, ARH = CRH = 100 % and Ld_{Pt} = 0.3 mg/cm^2

Further increase of stoichiometric flow rate (λ_{O_2}) from 4.0 to 4.5 increases the performance, particularly in the ohmic region. However, in the high current density region, the performance was slightly better for the stoichiometric flow rate of 4.5. Overall the cathodic stoichiometric flow rate (λ_{O_2}) of 4.5 gave the best performance.

The effects of cathode stoichiometric flow rate on Pt/Silica catalyst shows that the higher flow rate translates to the better performance. This effect also ascertains that the

175

Pt/Silica catalyst layer was flooded which was hindering its performance at a lower flow rate.

Effects of Humidity

The relative humidity (RH) of reactant gasses is important since it has profound implications on the operation of PEMFCs, in particular, on the unit-cell. The relative humidity keeps the electrolyte membrane hydrated to keep it performing at optimum level. This can be done easily by humidifying the reactant at the inlets, which results in the membrane humidification. However, the RH must not be to the level that it floods (excess water clogging) the electrodes, this can negatively affect the cell performance.

In order to determine the effects of humidity on Pt/Silica catalyst, the unit-cell temperature (T_{Cell}) was fixed at 70 °C; the anode stoichiometry flow rates was at two ($\lambda_{H_2} = 2.0$) and cathode stoichiometry flow rates was at 3.0 ($\lambda_{O_2} = 3.0$), and the cell performance was measured at three different humidity conditions of the reactant gasses on anode and cathode electrodes as listed in Table 6-8.

Table 6-8 Humidity levels to test effect of humidity of performance

Condition	Anode Side Relative Humidity (ARH)	Cathode Side Relative Humidity (CRH)
01	Dry Reactant	Dry Reactant
02	100 % RH	Dry Reactant
03	100 % RH	100 % RH

The first test condition was run with dry reactant on both cathode and anode side (ARH = CRH = 0 %) to determine if the Pt/Silica catalyst layer unit-cell generates and retains enough water into the catalyst layer to keep the electrolyte membrane hydrated during fuel cell operation. The second condition was run with dry reactant cathode side, and 100% RH of anode reactant (ARH = 100 and CRH = 0 %), and the third run was with 100% RH at both the cathode and anode side (ARH = 100 and CRH = 100 %). For the dry reactants case, the gas flow was bypassed from the humidifiers. For humidified reactants case gas flow was run through the humidifying bottle with the line temperature set 5 °C above cell temperature (T_{Cell}) to eliminate the condensation of humidified reactants in the lines.
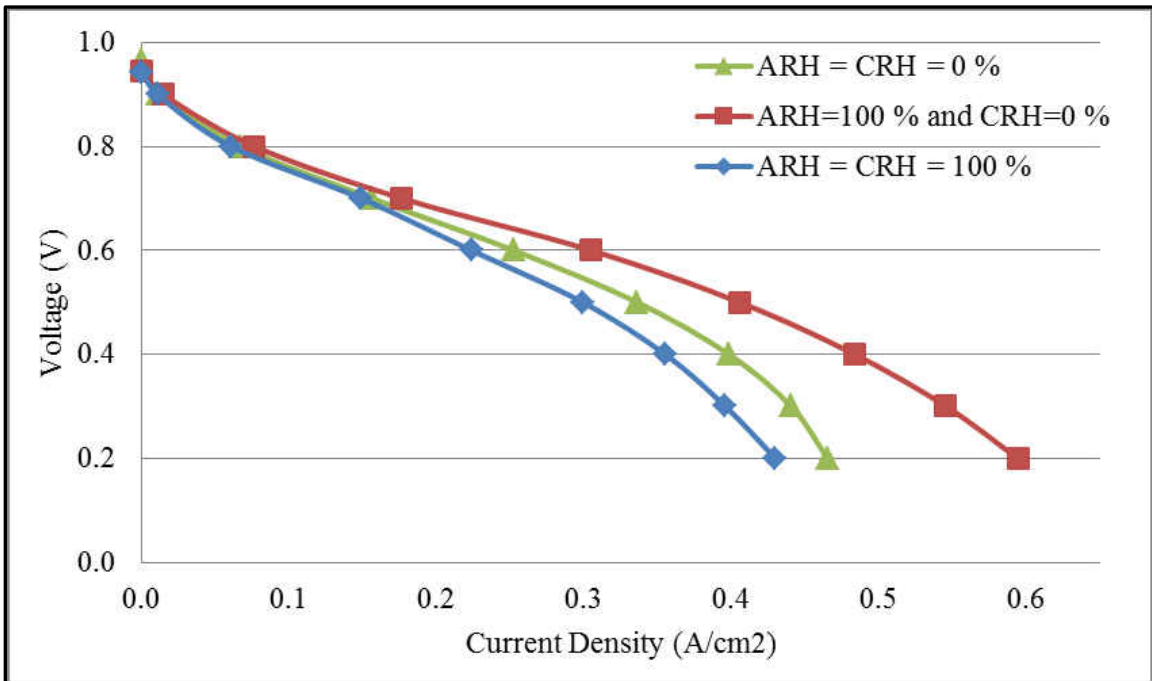
Figure 6-24 IV curve for the effects of humidity on the performance of Type-B MEA at T_{Cell}= 70 °C, λ_{H_2}=2.0 λ_{O_2}= 3.0 and Ld_{Pt}= 0.3 mg/cm^2

Figure 6-24 shows the polarization (IV) curve and Figure 6-25 shows a power curve of the Type-B MEA analyzed at three different humidity conditions and constant cell temperature (T_{Cell}) of 70 °C. It can be seen from both IV and power curves that unlike Pt/Carbon catalyst fully humidified reactant gasses on both anode and cathode side actually resulted is the reduced performance of Pt/Silica catalyst compared to the use of dry reactants. The resistance of the cell for Type-B MEA also increased at fully humidified reactants on both sides.
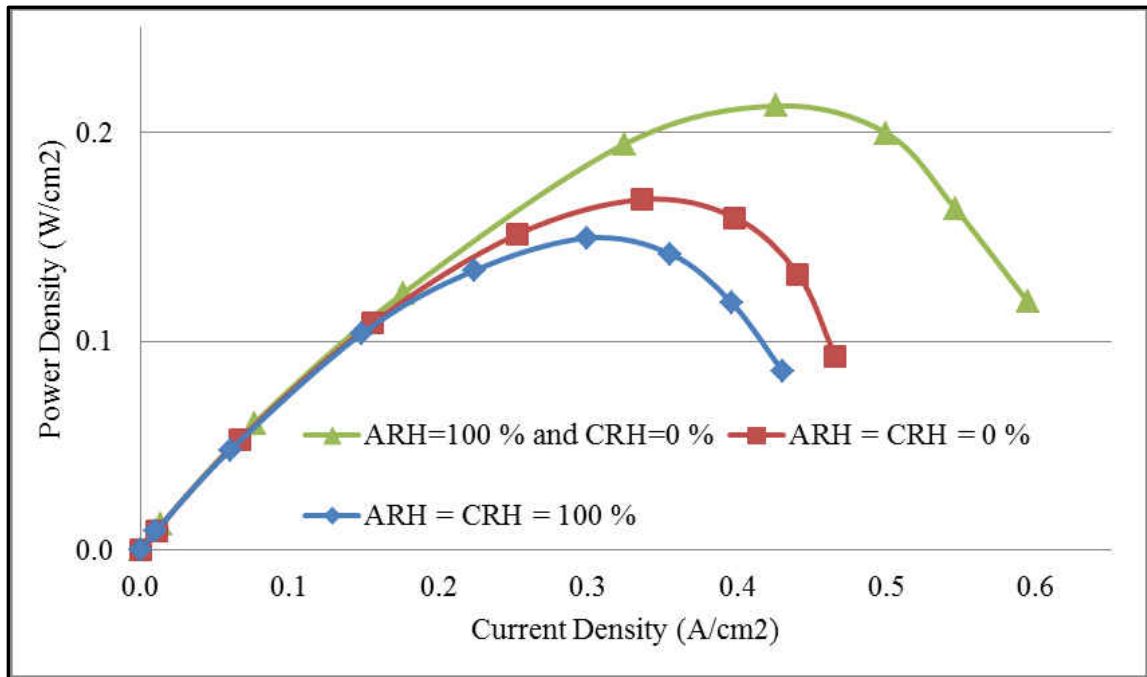
Figure 6-25 Power curve for the effects of humidity on the performance of Type-B MEA at T_{Cell}= 70 °C, λ_{H_2}=2.0 λ_{O_2}= 3.0 and Ld_{Pt}= 0.3 mg/cm^2

Out of the three conditions tested, Type-B MEA performed the poorest with fully humidified reactants (condition 03 in Table 6.8) on both the anode and cathode side (ARH = CRH = 100 %). The IV curve at fully humidified conditions also has a steeper slope compared to other two conditions, which represents a sudden drop in performance,

178

particularly at high current density. This result shows that the unit-cell electrodes with Pt/Silica catalyst were holding a lot of water, which led to electrode flooding, and resulted in a less effective triple-phase-boundary in the Pt/Silica catalyst layer.

The effect of humidification of only the anode reactant (ARH = 100 and CRH = 0 %), (condition 02 in Table 6-8) led to a 36 % increase (from 0.22 to 0.31 A/cm^2) in the maximum current density and (from 0.15 to 0.20 W/cm^2) the maximum power density. The improved performance can be explained by the higher electron and proton conductivity of the catalyst layer. The increased conductivity meant that the protons and electron were more easily conducted through the catalyst layer, and this decreased the cell losses and resulted in a higher cell performance.

Dry reactants on both anode and cathode side (ARH = CRH = 0 %) (Condition 01 in Table 6-8) resulted in a reduced MEA performance compared to the humidification of only anode reactant (ARH = 100 and CRH = 0 %). However, its performance was slightly better than fully humidified reactants. This shows that dry reactants (ARH = CRH = 0 %) (condition 01 in Table 6-8) do not provide adequate humidification to the electrolyte membrane. However, the presence of the smooth characteristic shape of the IV curve means that the electrolyte membrane had enough hydration to keep the cell operation going although at lower performance. During dry reactants run, the cathode side remains humidified by the liquid water generated by the electrochemical reaction, and the water generated in the cathode side seems to be not enough to keep the electrolyte membrane humidified.

Effects of Cell Temperature

The operating temperature has a significant effect on the performance of the PEMFC. Various properties such as kinetics of electrochemical reactions at the electrodes, the protonic conductivity of electrolyte membrane, the diffusivities of gasses, and cathode side water management depend on the cell temperature. At the higher temperatures, there are some advantages: better heat rejection, enhanced water management, and increased conductivity. However, increasing the temperature above a certain level can negatively affect its performance due to membrane dehydration and loss in ion conductivity which would eventually result in the quick drying of the cell membrane. An appropriate operating temperature for every fuel cell varies as it depends on the properties of its components. The effect of temperature of Pt/Silica catalyst was evaluated at a cell temperature of 70, 80, 85 and 90 °C, with fully humidified reactants (ARH = CRH = 100 %), anode stoichiometry flow rates at two (λ_{H_2}= 2.0) and cathode stoichiometry flow rates at 3.0 (λ_{O_2}= 3.0).

Figure 6-26 shows the effect of the operating temperature on the performance of the unit-cell. Inspection of the curves reveals that differences started to arise already at low current densities, reflecting the temperature dependence of the activation overpotential. The effect of ohmic overpotential in the middle region of the curve was very distinct.
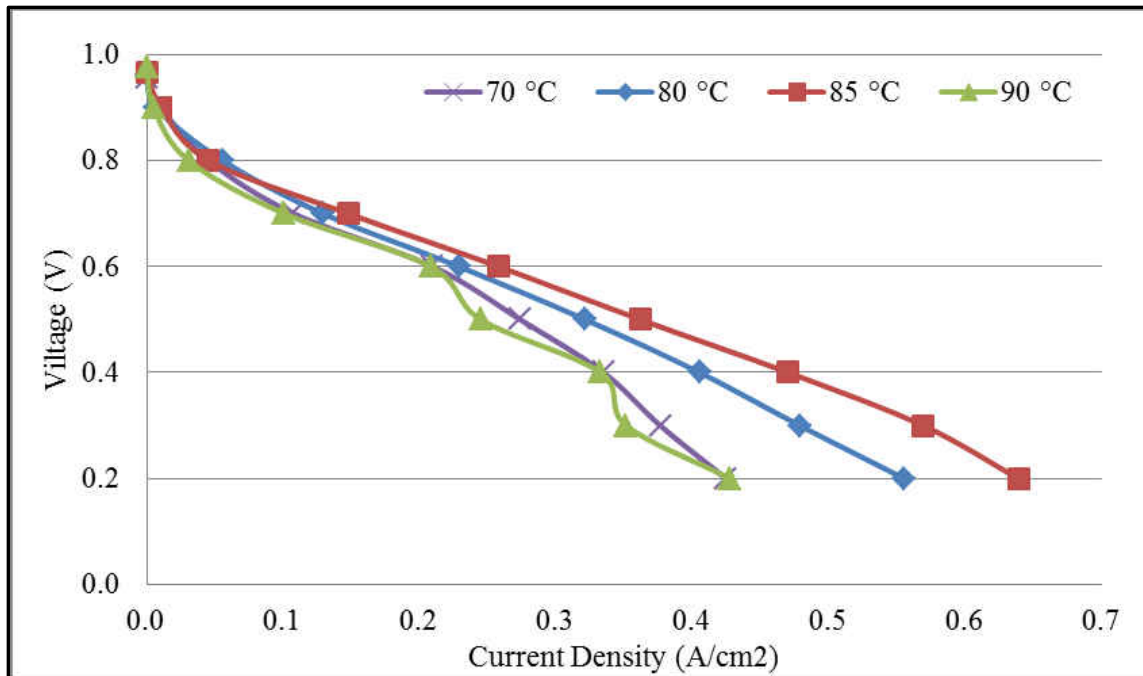
Figure 6-26 IV curve for the effects of cell temperature on the performance of Type-B MEA at T_{Cell}= 70 °C, λ_{H_2}=2.0 λ_{O_2}= 3.0, ARH = CRH = 100 and Ld_{Pt}= 0.3 mg/cm^2

It can be seen that a significant performance gain was achieved when the temperature was increased from 70 ℃ to 80 ℃. There was a 27 % increase in the maximum current density at 0.3 V and a 17 % increase in the maximum power density for a 10 °C increase in temperature from 70 to 80 °C. Further increase of 05-degree temperature resulted in the best performance at 85 °C. Higher temperature has helped increase the water evaporation and consequently reduced the flooding in the catalyst layer, which has resulted in performance enhancement. In addition, higher temperature reduces the fuel cell losses by increasing the reaction kinetics that has also resulted in improving the performance. Hence, the cell performance increased as temperature increased due to the decrease in the losses.
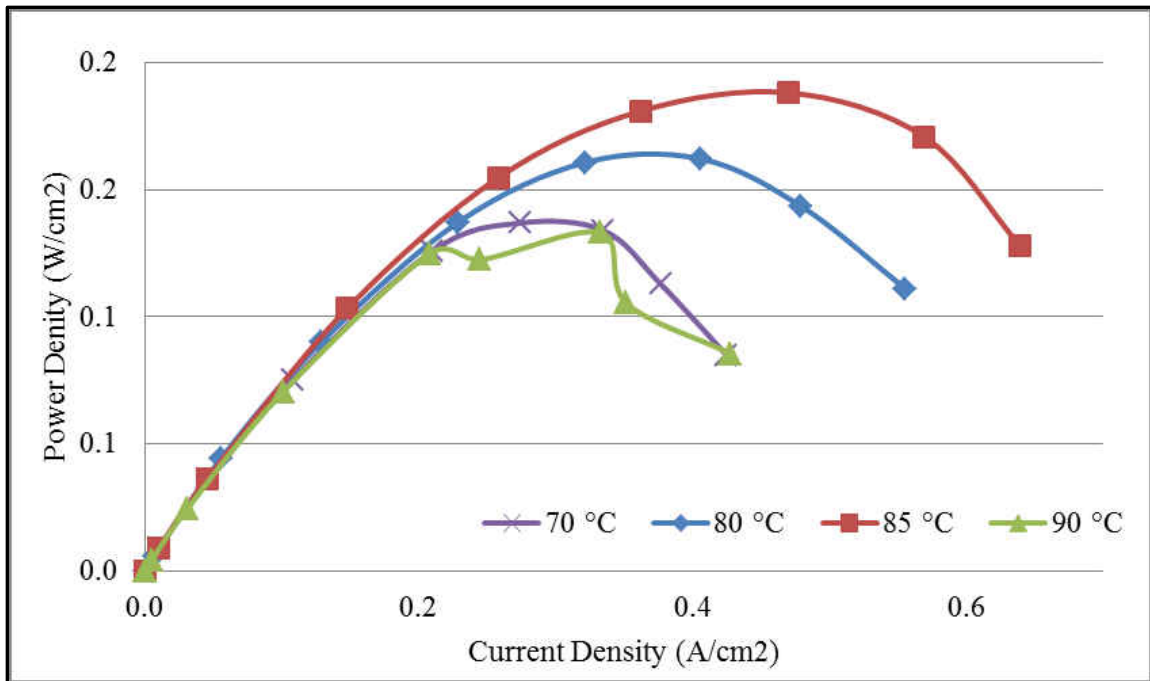
Figure 6-27 Power curve for the effects of cell temperature on the performance of Type-B MEA at T_{Cell}= 70 °C, λ_{H_2}=2.0 λ_{O_2}= 3.0, ARH = CRH = 100 and Ld_{Pt}= 0.3 mg/cm^2

However a temperature increase of another 5-degree from 85 °C to 90 °C, results in a significant deterioration in the MEA performance, especially at high current density. At high current densities, a substantial amount of heat is produced on the cathode electrode. An increase in the temperature in addition to the heat produced at high current density would have increased water evaporation and had led to drying of the electrolyte membrane. This increases the membrane resistance, which in turn again increases heat production. This composite effect cause further membrane drying and resulted in the significant performance deterioration at 90 °C.

6.3.3 Development of "Pt/Silica + Carbon powder" MEA (Sub-hypothesis 02 Testing)

The poor performance of Pt/Silica catalyst was thought to be because of low conductivity of silica. Therefore, to further improve the electronic path in the catalyst

182

layer carbon black powder was added to the catalyst ink. The results in this section provide a basis to test the second sub-hypothesis proposed to justify the lower performance of Pt/Silica catalyst. The proposed sub-hypothesis was that the low electronic conductivity of silica support had caused the non-facile electronic and/or ionic flow path in the catalyst layer, which has contributed to the lower performances.

Four MEAs were made for this study, each with a different carbon loading (Ld_{Carbon}) in the catalyst ink: 0, 5, 7.5 and 10 wt. %. The OCVs of the four Type-BB MEA are given in Figure 6-28. The OCV increased with increasing carbon loading at a constant Nafion content of 37 %, but a drop of OCV was observed at 10%.
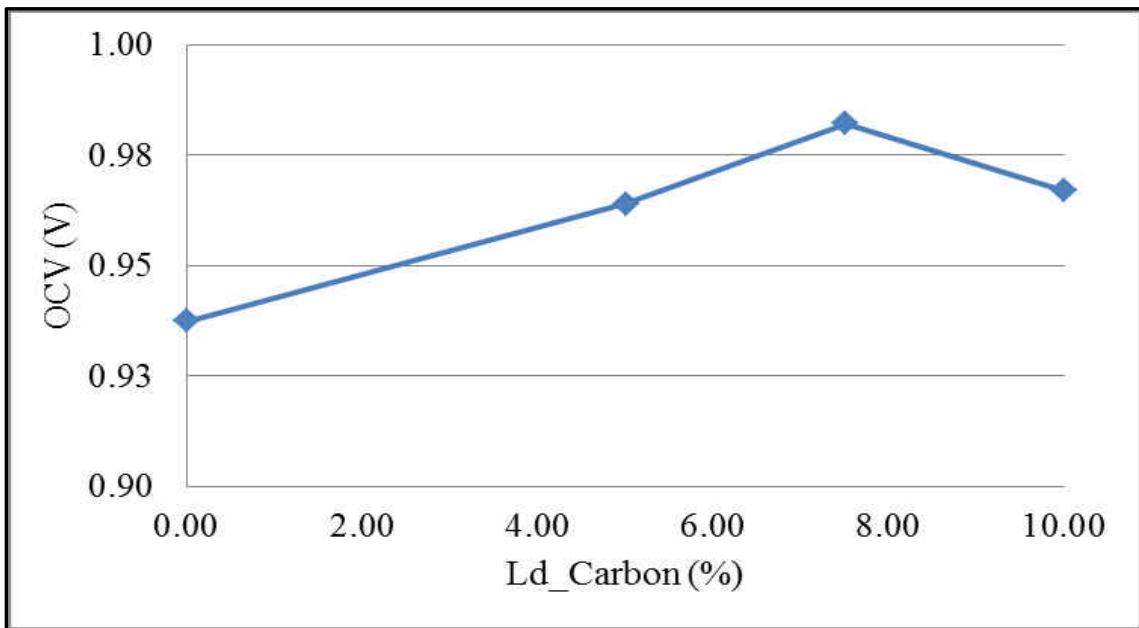
Figure 6-28 Type-BB MEA effect of carbon loading on OCV

Shown in Figure 6-29 are the polarization curves for the four Type-BB MEAs, in which the carbon loading of the anode and cathode GDEs were simultaneously changed.

An increase in current densities was observed with the addition of carbon powder in the catalyst ink

The cell performance started to rise already at low current densities. However, as the current increased, the MEAs with larger amounts of carbon loading (2.5, 5, and 7.5) showed a more rapid increase in current density at a given voltage. In contrast with OCV, huge current density changes were observed dependent on the carbon loading as shown in Figure 6-29. Overall, significant activity improvements were seen with an increase in carbon loading. The cell performance increases as the carbon loading increases from 0 to 7.5 %. A further increase up to 10 % of carbon loading resulted in a decrease in performance.
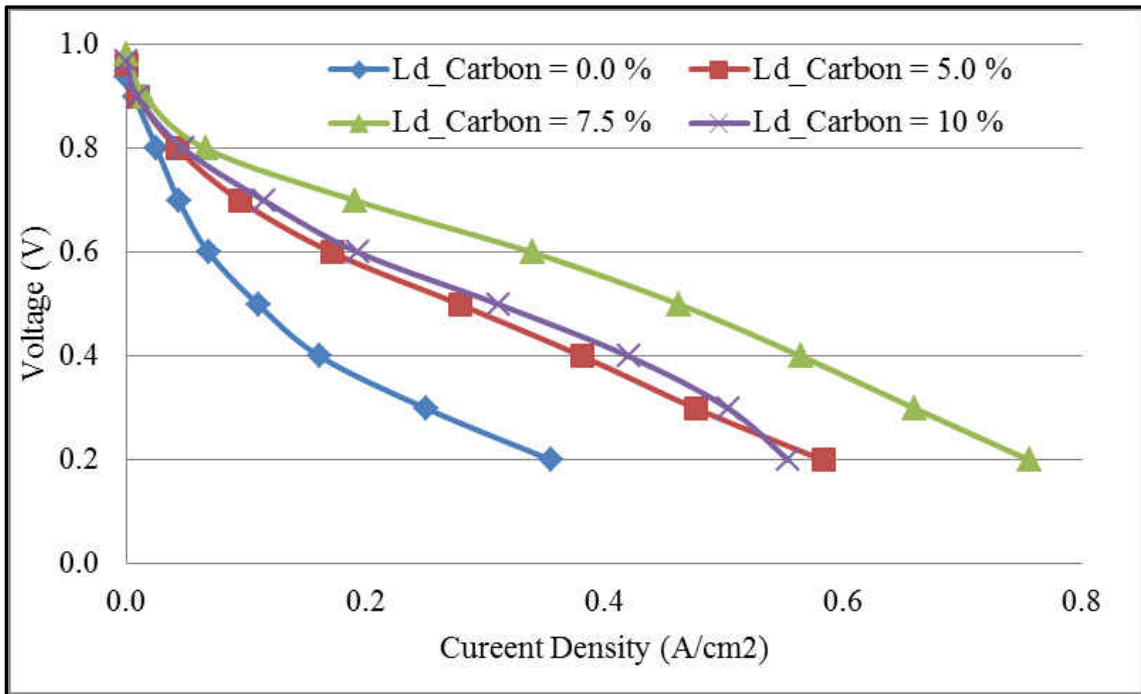
Figure 6-29 IV curve for effect of carbon loading on the performance of Type-BB MEA

Figure 6-29 shows that when the carbon loading (Ld_{Carbon}) was increased from 0.0 to 7.5 %, the maximum current density (at 0.3 V) increased significantly by 163 % (from 0.25 to 0.66 A/cm^2), suggesting that the addition of carbon powder has improved the electronic path in the catalyst layer. However a further increase of carbon loading from 7.5 to 10 %, on the other hand, results in a performance deterioration of 67 % (from 0.23 to 0.16 W/cm^2) in maximum power density. The decrease in maximum current density (at 0.3 V) was also much higher (~76 %) for 10 % carbon loading.
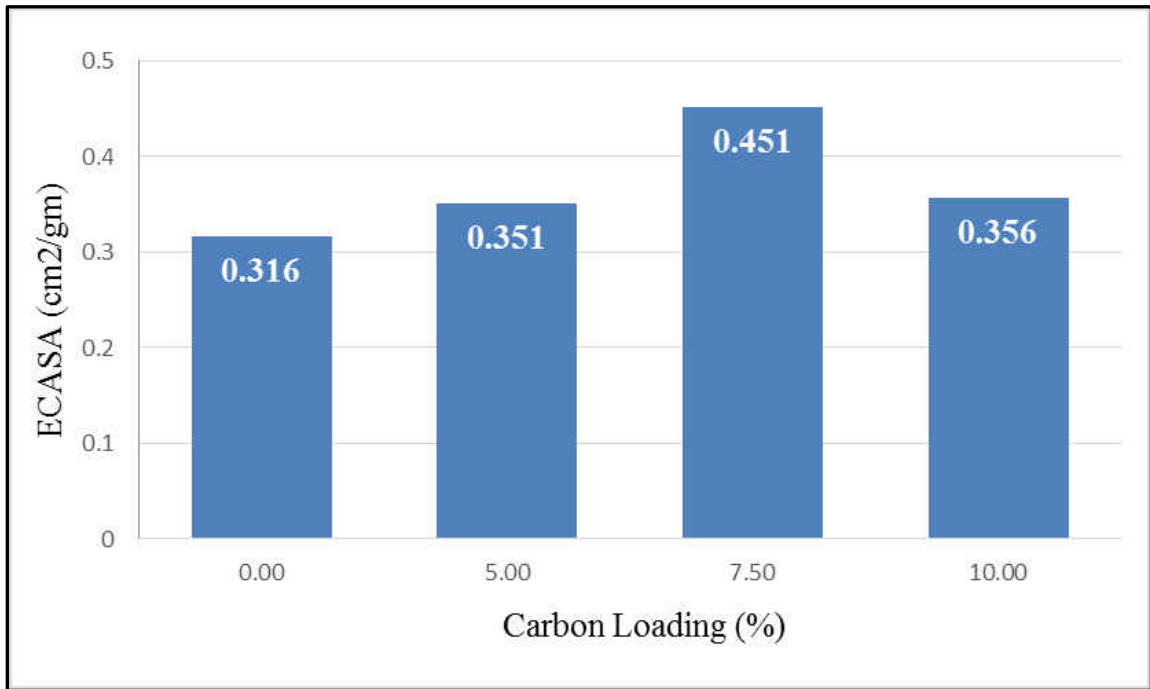
Figure 6-30 Effect of carbon loading on the ECASA, Scan Rate = 50mV/s, Voltage Sweep Range = 0.1 to 1.0 V, T_{Cell}= Room Temperature and $T_{Humidifier}$= 40 °C

The cyclic voltammograms were carried out to analyze the catalyst/ionomer/carbon interfacial area, and the corresponding ECASA with respect to the carbon loading is presented in Figure 6-30. The ECASA calculated were consistent with the cell performance trend of Figure 6-29. ECASA values increased with carbon

loading up to 7.5 % and then decreased with a further increasing the carbon loading to 10 % (Figure 6-30). This was probably due to the isolation of catalyst particles by excess ionomer and carbon powder.

The poor cell performance at low carbon loading (0 %) may be attributed to the low electrochemical active site due to high Nafion content of 37 % and the relatively low conductivity of silica support. In the case of 5 % carbon loading, there was a smaller performance enhancement compared to the other carbon loading samples, implying that 5 % carbon loading was not enough to connect the catalysts with the support to transfer electrons efficiently. Consequently, the additional catalyst might not participate in the reaction. High carbon loading (10%) electrodes also showed reduced performance. This could be deduced to an excess of carbon particles blocking the proton and the gas diffusion paths and reducing gas permeability and increasing mass transfer polarization in the catalyst layer. The best performance was observed at 7.5% carbon loading; at this carbon loading, a well-balanced percolating network was formed between the catalyst, the Nafion ionomer, and the catalyst support. Therefore, the electron, the proton, and the reactant gas can migrate easily throughout the network.

6.3.4 Comparison of Type-A, Type-B and Type-BB MEA at their Peak Performance

A comparison test of Type-BB (Pt/Silica + Carbon Powder) MEA with Type-A (Pt/Carbon catalyst), and Type-B (Pt/Silica catalyst) MEA was performed, and the findings are presented in this section. The actual amount of the catalyst loadings in MEAs are listed in Table 6-9.

Table 6-9 MEA composition of Type-A, Type-B and Type-BB MEA

MEA #	MEA Pt Loading (Average) (mg/cm^2)	Carbon Loading (%)	Nafion Loading (%)
Type-A	0.313	NA	33
Type-B	0.309	NA	33
Type-BB	0.312	7.5	37

Figure 6-31 compares the performance of these three MEAs. There are two curves for Type-B MEA, the dotted line curve is the performance at baseline conditions (i.e. ARH = CRH =100%, λh2 =2.0, λO2 = 3.0 and T_{Cell} = 70 °C). The solid line performance of Type-B MEA was its peak performance obtained at conditions where the flooding effect was minimal due the use of partial humidification and high stoichiometric flow on both anode and cathode side (i.e. ARH = 100%, CRH =0%, λ_{H_2} =3.0, λ_{O_2} = 4.5 and T_{Cell} = 70 °C).

Figure 6-31 shows that there was a performance improvement in the Type-B MEA with changing the operating conditions to minimize the flooding effects. The performance of Type-B MEA at baseline and peak conditions was comparable till 0.6 V, after which the performance at the peak condition improves considerably, particularly in the high current density region. The performance was improved by 15 % at the maximum power density (from 0.15 to 0.17 W/cm^2) and the maximum current density obtained at 0.3 V was 30% better (from 0.41 to 0.54 A/cm^2) than the baseline conditions. These results also successfully tested the first sub-hypothesis regarding the flooding effect at baseline condition.
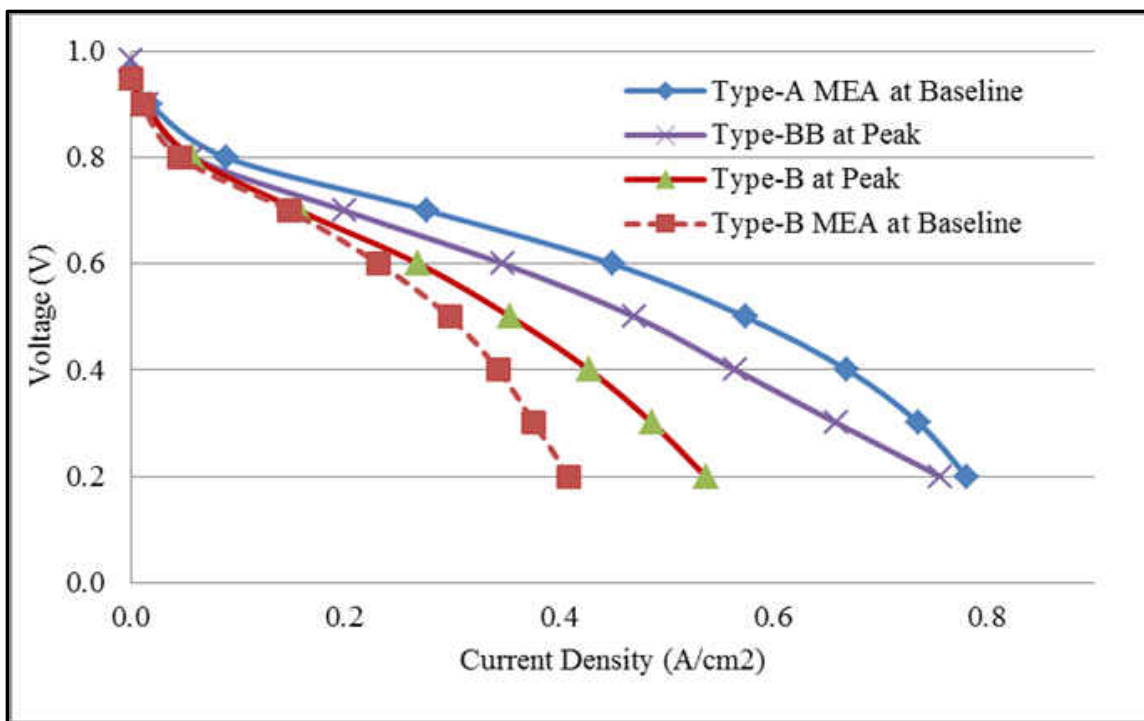
Figure 6-31Comparison of Type-A, Type-B and type-BB MEA

Figure 6-31 also shows that the performance of Type-BB MEA was improved by 58 % from the Type-B baseline conditions (from 0.15 to 0.24 W/cm^2) for the maximum power density despite using a higher amount of Nafion ionomer (37% compared to 33% in Type-B MEA). When the Type-B and Type-BB were compared at the same conditions (i.e. ARH = 100%, CRH =0%, $\lambda h2$ =3.0, $\lambda O2$ = 4.5 and T_{Cell} = 70 °C) the improvement in the performance was found to be 32 % (from 0.17 to 0.24 W/cm^2) for the maximum power density. The higher performance of Type-BB MEA was attributed to the addition of carbon powder into the catalyst ink, which has improved its performance by improving the electron flow path in the catalyst layer. These results have successfully tested the second sub-hypothesis that the lower conductivity of silica support was one of the causes of the reduced performance of Pt/Catalyst. The performance of Type-BB MEA was still

188

less than the commercial Pt/Carbon MEA (Type-A) by 18 %; it could be due to the fact that Type-BB MEA has a higher amount of Nafion ionomer than the Type-A MEA.

6.4 Pt/Silica In-situ Durability Tests (Hypothesis 02 Testing)

Conventional Pt/Carbon electrodes (Type-A MEA) and novel Pt/Silica electrodes (Type-A MEA) were subjected to two AST protocols, and the results are presented in this section. The durability of both Pt/Carbon and Pt/Silica catalysts in an MEA was investigated using an $in-situ$ AST tests in a unit-cell of 25 cm^2 electrode area.

6.4.1 Potentiostatic Hold (Support Stability Test)

Figure 6-32 shows IV curves of Type-B (Pt/Silica catalyst) MEA during an AST consisting of a potentiostatic hold at 1.2 V vs. RHE. Interestingly, the polarization curves show no degradation of the fuel cell performance following the first 8 hours of the test. The performance improved after the first 8 hours of the test, and the Pt/Silica catalyst generated 0.35 A/cm^2 (from 0.33 at baseline) at 0.6 V and a maximum power density of 0.22 W/cm^2, which were approximately 10 % higher than the baseline IV curve. This effect can be attributed to the additional proton conductivity of the ionomer, as it is the only component in the electrode that has the ability to change structure and morphology in such a reversible manner. Also, the presence of an amine group in the Pt/Silica catalyst can also be attributed to better performance since the AST test was run at high temperature (80 °C), and at which the amine groups gets highly protonated.

189
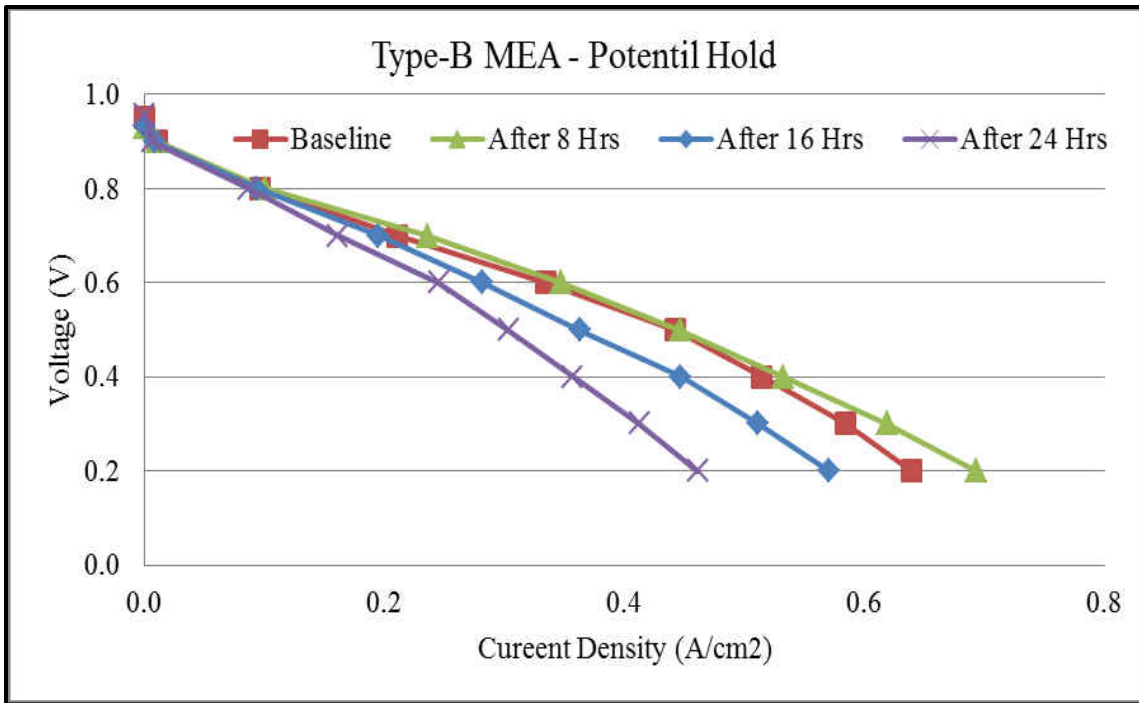
Figure 6-32 Effects of potentiostatic hold on the performance of Type-B (Pt/Silica) MEA
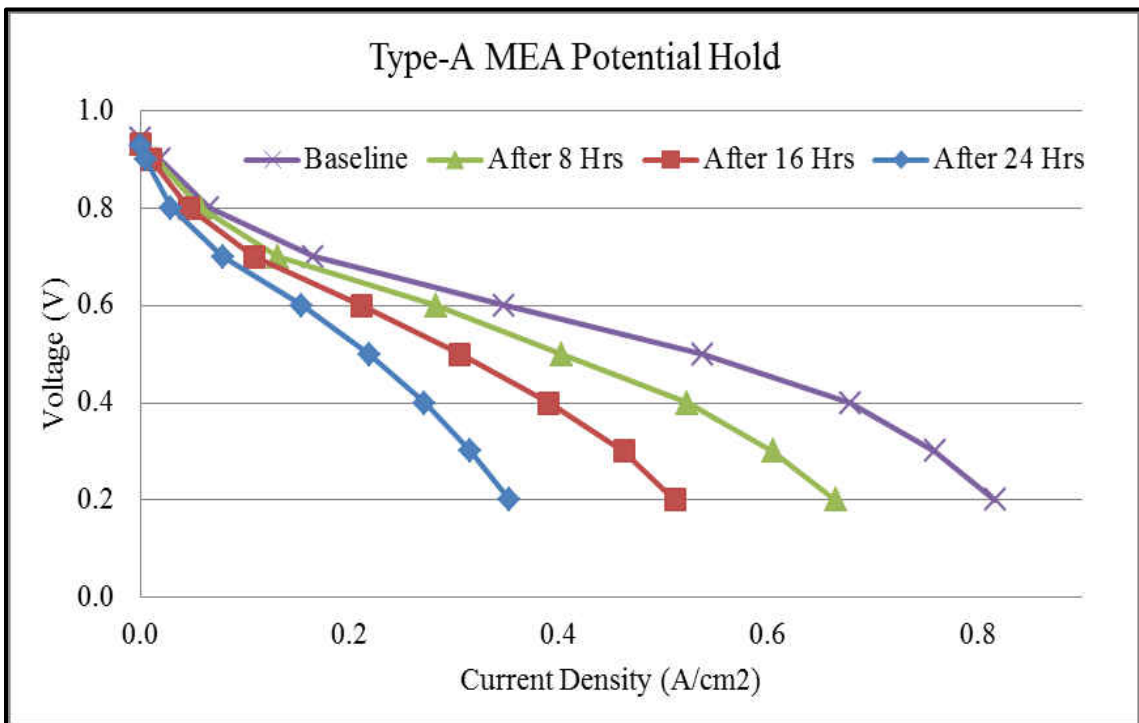
Figure 6-33 Effects of potentiostatic hold on the performance of Type-A (Pt/Carbon) MEA

The performance of Pt/Silica catalyst was reduced as testing time increased past 8 hours. The poorest performance was observed as expected after the 24 hours test. A lower performance was obtained for the current density at 0.6 V, 0.25 A/cm^2 vs. 0.33 at the baseline after the 24-hour test. The maximum peak power density of 0.15 W/cm^2 (0.22 at the baseline), which is 73 % of that generated for the baseline condition. These fuel cell results indicated that deposited Pt particles provided inadequate electron pathway and as a result, the electrical conductivity of the silica support seems to have reduced which results in degraded performance.

Figure 6-33 shows IV curves of Type-A (Pt/Carbon catalyst). Unlike Type-B MEA, there was a decrease in the performance after the first 8 hours of the test, which suggests that the start of the degradation at the early stage of the test in Type-A MEA compared to the Type-B MEA. Further, the performance of type-B MEA reduced significantly after 8 hours and like Pt/Silica catalyst; the poorest performance was observed after the 24 hours tests. A significantly lower performance was obtained for the current density at 0.6 V, 0.15 A/cm^2 vs. 0.35 at the baseline after the 24-hour test. The maximum peak power density of 0.11 W/cm^2 (0.27 at the baseline), is approximately 40 % of power density generated for the baseline condition.

Figure 6-34 compares the performance of Pt/Carbon and Pt/Silica catalyst at the baseline and at the end of the 24 hours test. Before the potential hold at the baseline conditions, the Pt/carbon catalyst showed higher overall performance than the novel Pt/Silica (max power density of 0.27 vs. 0.22 W/cm^2). However, after the potential hold tests their unit-cell performances were inversely related (0.11 vs. 0.15 W/cm^2).
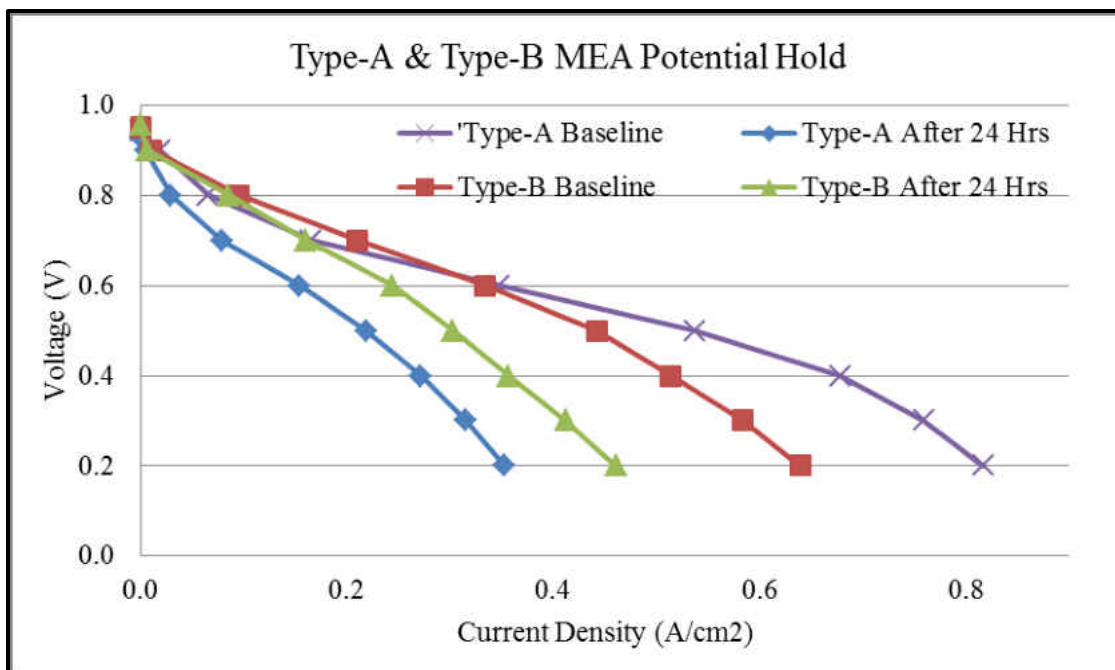
Figure 6-34 Comparison of the performance of Pt/Carbon and Pt/Silica catalyst at the baseline and the end of the 24 hours test

The observations in this work show that for the potentiostatic hold at 1.02 V and 80 °C, a significant decrease in maximum power density in Type-A MEA was observed with potential hold time. This leads to a loss of maximum power density in Type-A (Pt/carbon electrode) MEA of 60 % (from 0.27 to 0.11 W/cm^2) and in Type-B (Pt/Silica electrode) MEA by 31 % (from 0.22 to 0.15 W/cm^2) of the baseline test in a limited number of hours.

Figure 6-35 shows CVs of a Type-A MEA (Pt/Carbon electrode) after potential holding at 1.2 V. An apparent increase in the double layer current was observed. This current increase in the double layer region clearly indicates that the carbon support underwent surface oxidation. The increased double layer has traditionally been attributed to degradation of the support, e.g. increased oxygen functionalities on the surface of the carbon and increasing number of defects. Voltammograms of Type-A MEAs also shows

192

a decrease in the hydrogen adsorption and desorption-peaks attributed to a loss of Pt surface area. Fig.6-35 shows that after the end of the test (24 hours) there was a considerably larger increase in the double layer capacitance (0.3 to 0.6 V range) than the baseline test and an almost complete disappearance of the hydrogen desorption peak.
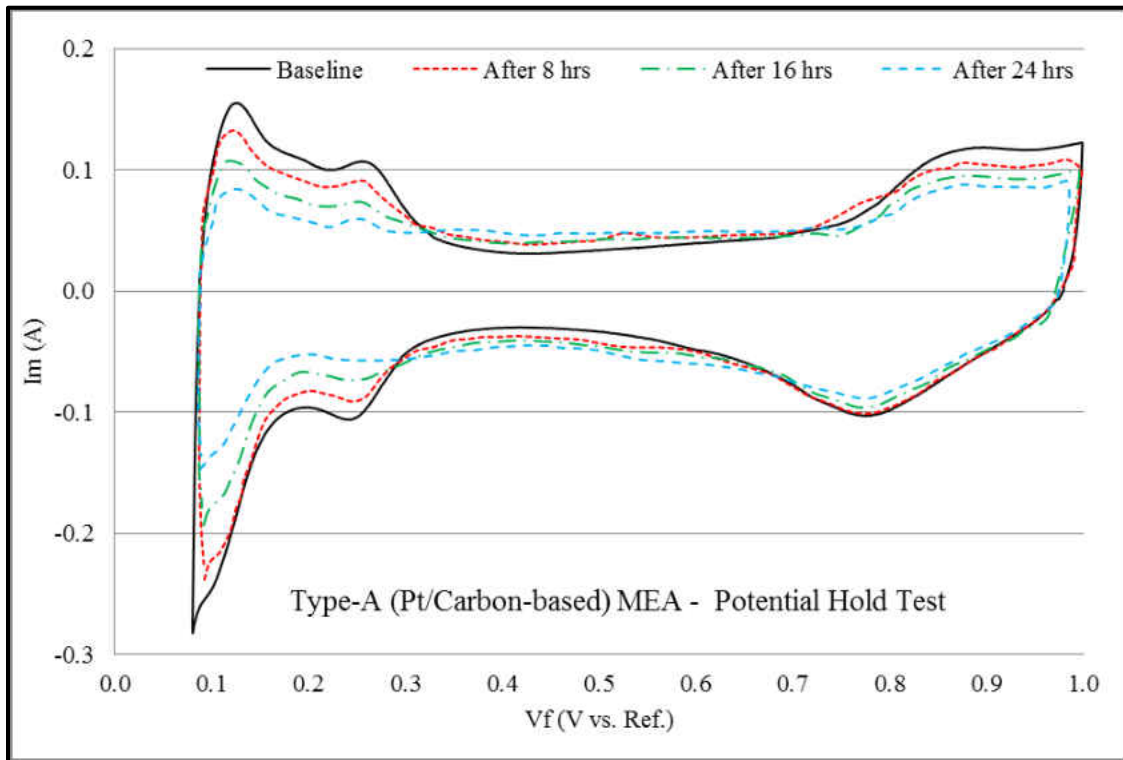
Figure 6-35 Effects of Potential Hold test on voltammograms of Type-A (Pt/Carbon-based) MEA

In contrast, the Pt/Silica electrode showed a different behavior from the Pt/Carbon, as illustrated in figure 6-36. Unlike the IV test, where a performance increase was observed after 8 hours potential hold, there was a small decrease in ECASA after the first 8 hours of the test. There was also very small difference between the double layer capacitance of the four CVs for the Pt/Silica catalyst. This suggests that the Pt/Silica catalyst has exceptional stability against high potential at 1.2 V, which is due to relatively

higher oxidation-resistant nature of the silica support. However, there was a decrease in the hydrogen adsorption and desorption peak with the potentiostatic hold time. This reduction in the hydrogen desorption peak suggests that Pt/Silica catalyst were also undergoing some degradation.
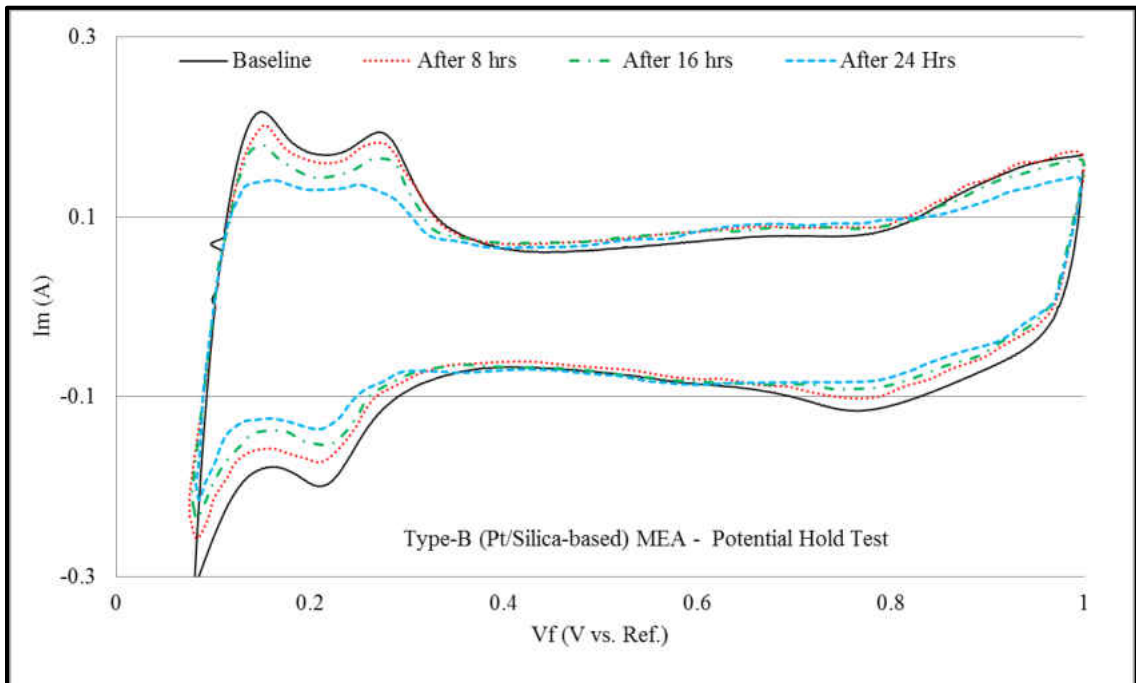
Figure 6-36 Effects of Potential Hold test on voltammograms of Type-B (Pt/Silica-based) MEA

The Pt surface area was then determined by integrating the peaks between $0.1 - 0.4$ V of the cyclic voltammogram. The calculated ECASAs were summarized in Table 6-10.

Table 6-10 Calculated ECASA for both Pt/Carbon and Pt/Silica catalyst during potential hold test

Number of Hours	ECASA (cm^2/mg$_{Pt}$)	
	Pt/Carbon Catalyst	Pt/Silica Catalyst

0 (baseline)	0.418	0.332
08	0.359	0.312
16	0.263	0.288
24	0.188	0.242

The ECASAs normalized by the initial values and were plotted against the time of the potential hold at 1.2 V as shown in Figure 6-37.
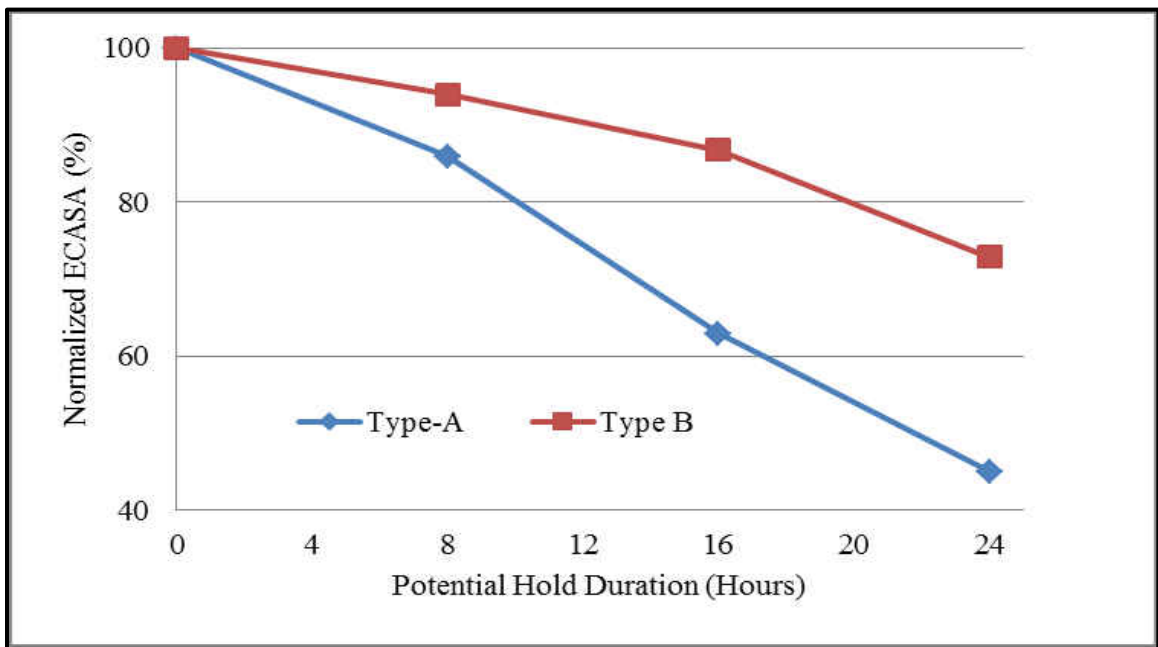
Figure 6-37 Comparison of loss of ECASA loss for the novel Pt/Silica with the commercial Pt/Carbon Catalyst

The ECASA and maximum power density of the two catalysts before and after the potential hold tests are summered in Table 6-11. As expected from the CVs, the significant decrease in ECASA of platinum in Type-A (Pt/carbon) catalysts was observed with potential hold time. This leads to a loss of approximately 55 % of the original ECASA in a limited number of hours. Such a loss of surface area is reported in many

papers occurring during the potentiostatic hold. Whereas only 27% loss is observed for Pt/Silica, this shows that silica support was relatively stable within the potential hold time. Furthermore, most of the surface area loss (~16%) for the case of Pt/Silica occurs within the last 8 h, indicating that silica support could potentially provide much higher durability than carbon support.

The results showed that the loss of the specific activity of novel Pt/Silica catalyst at the end of the potential hold test was 17 % from its baseline condition. Whereas the corresponding loss in commercial Pt/Carbon catalyst was found to be 36 %.

Table 6-11 Durability in terms of ECASA and Maximum power density of the two catalysts

Sample	Maximum power Density (W/cm^2)			ECASA (cm^2/mg)			Specific Activity (A/m^2$_{Pt}$)		
	0 hrs	24 hrs	% loss	0 hrs	24 hrs	% loss	0 hrs	24 hrs	% loss
Pt/Carbon Based MEA	0.269	0.110	59.4	0.418	0.188	55.0	0.142	0.091	35.8
Pt/Silica Based MEA	0.221	0.152	31.4	0.332	0.242	27.1	0.104	0.087	16.8

The degradation of the silica-supported catalyst was minimal, whereas the carbon degradation was significant, as indicated by the respective ECASA. Intensive carbon corrosion at high potential could have lead to insufficient contact between Pt particles and the carbon support so that Pt catalysts lose electrochemical activity. This suggests that the surface of silica is harder to oxidize than carbon under the tested conditions. This

196

means silica could potentially be more corrosion resistant and durable when used in a fuel cell.

6.4.2 Potential Cycling (Catalyst Stability Test)

Harsh potential cycling tests were performed using a triangle wave potential between 0.6 V and 1.2 V vs. RHE at a 70 mV/s scan rate to evaluate the durability of Pt/Silica catalyst further under harsher conditions than the potential hold test.
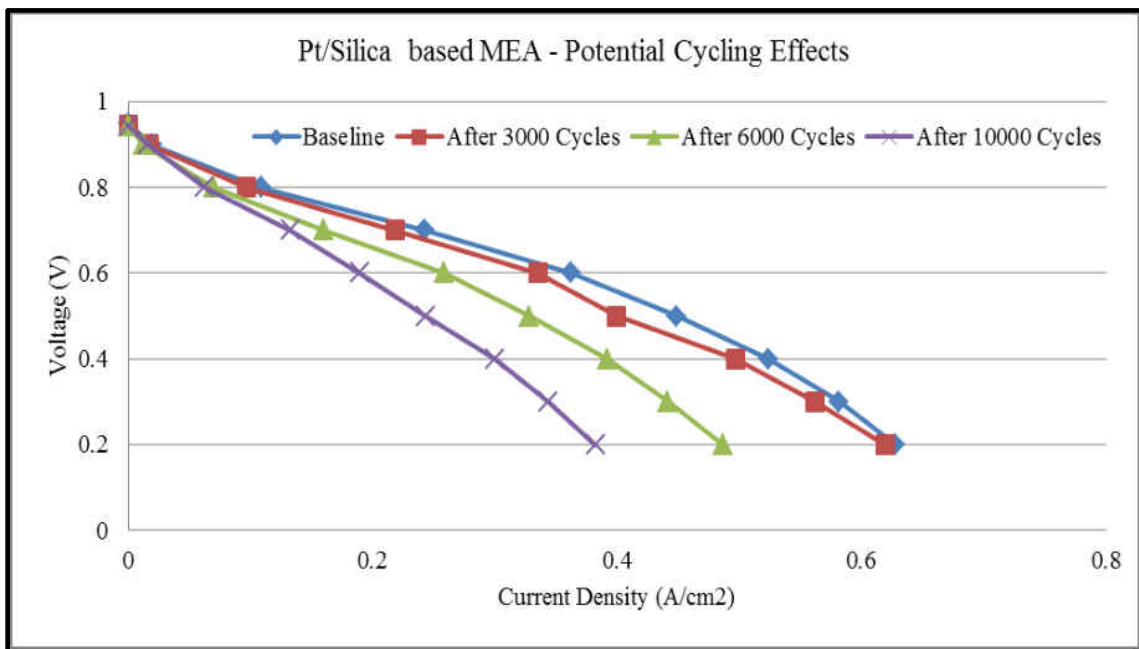
Figure 6-38 Effects of potential Cycling on the performance of Pt/Silica-based MEA

Figure 6-38 shows IV curves of Type-B (Pt/Silica catalyst) MEA during an AST consisting of a potential cycling at 80 °C. Unlike the potential hold test where the performance of Pt/silica catalyst was first improved and then declined, the polarization curves show degradation of the fuel cell performance following the first 3,000 cycles of the test. This suggests that the harsher environment has initiated the Pt/Silica catalyst degradation at the early stage of the cycling test compared to the potential hold test.

Interestingly there was a noticeable difference at 0.8 V performances until 3,000 cycles and after 3,000 cycles. Further, the performance of Pt/Silica-based MEA reduced after 3,000 cycles onwards, and the poorest performance was observed as expected after the 10,000 cycles. The current density at 0.6 V was 0.19 A/cm² vs. 0.36 at baseline after the 10,000-cycle test, which was 53 % of that generated for the baseline condition. The maximum peak power density of 0.12 W/cm² vs. 0.22 at baseline after the 10,000-cycle test, which was approximately 54 % of that generated for the baseline condition.
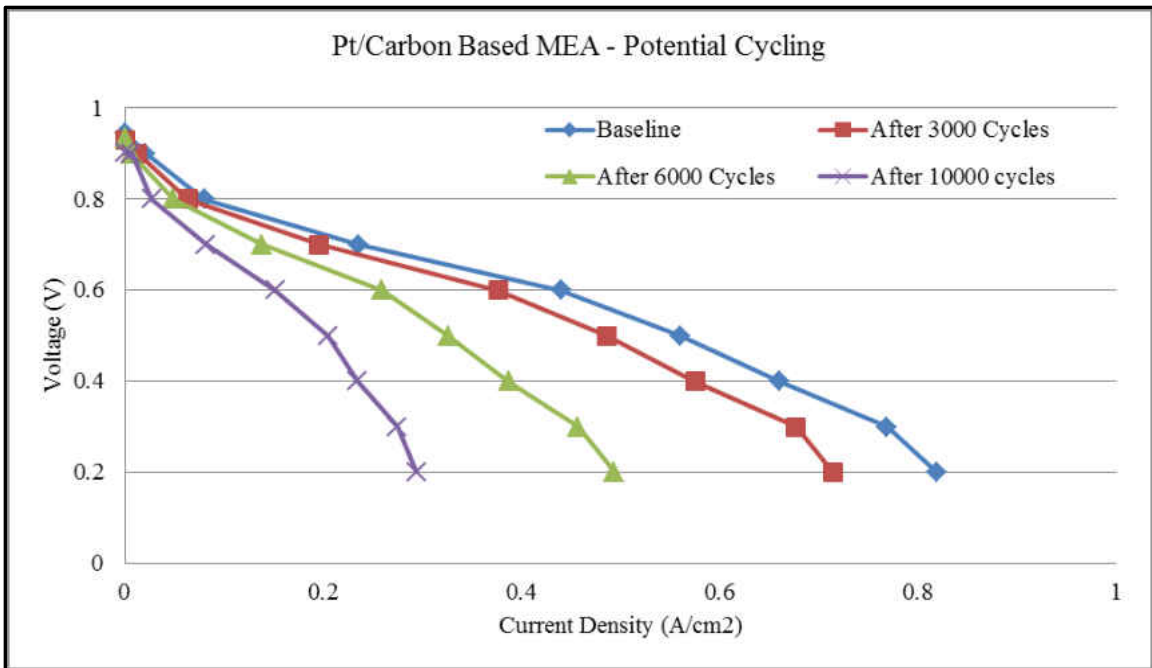
Figure 6-39 Effects of potential Cycling hold on the performance of Type-A (Pt/Carbon) MEA

Figure 6-39 shows IV curves of Type-A (Pt/Carbon Catalyst). There was a relatively small decrease in the performance after the first 3,000 cycles of the test, though the current densities are lowered in the potential region. The performance of Pt/Carbon catalyst dropped by 14 % compared to the 9 % decrease in Pt/Silica catalyst at 0.6 V after 3,000 cycles. The higher degradation in Pt/Carbon catalyst suggests that the degradation

rate was higher at the early stage of the test in Pt/Carbon based MEA compared to the Pt/Silica catalyst. Further, the performance of Pt/Carbon catalyst reduced significantly after 3,000 cycles, and the poorest performance was observed as expected at the end of the 10,000 cycles test. A significantly lower performance was obtained for the current density at 0.6 V, 0.15 A/cm^2 vs. 0.44 at the baseline after the 10,000-cycle test. The maximum peak power density of 0.10 W/cm^2 (from 0.28 at the baseline), was approximately 36 % of that generated for the baseline condition.

The observations in this work show that for the potential cycling between 0.6 – 1.2 V at 80 °C, a significant decrease in maximum power density was observed in both catalysts with a slightly larger degradation for the Pt/Carbon catalyst. This leads to a loss of maximum power density of Pt/Silica catalyst by 45 % (from 0.22 to 0.12 W/cm^2) and Pt/Carbon catalyst by 64 % (from 0.28 to 0.10 W/cm^2) of the baseline test in the limited number cycles (10,000). The potential cycling damages the porous surroundings of the platinum particles, making the gas pathways narrower and fewer. There can also be an agglomeration, diffusion and/or coarsening of the platinum catalyst particles during the potential cycling; that increases the mass transport losses because of a reduced active platinum surface area.

The polarization curves also indicate increased mass transport losses indicated by the performance drop at high current densities for the measurements performed after the potential cycles, compared to the baseline measurement. Since the transport losses were already minimized by using pure hydrogen and oxygen as reactant gasses, the mass transport losses originate from a worsened transport of produced water and to a reduced

electrochemically active platinum surface area. The rise in transport losses could have resulted from the affected produced water transport by the potential cycling.

Figure 6-40 and Figure 6-41 shows the CVs of Pt/Carbon based and Pt/Silica-based MEAs respectively, which were recorded before the test, and at 3,000, 6,000, 10,000 cycles. ECASA was evaluated from the CV curves as described in Section 4.5. The influence of potential cycling on both the catalyst was similar to that of the potential hold test, both the adsorption and desorption peaks for hydrogen in voltammograms decrease with the duration of the test.

Table 6-12 Calculated ECASA for both Pt/Carbon and Pt/Silica catalyst during potential cycling test

Number of Cycles	ECASA (cm^2/mg)	
	Pt/Carbon Catalyst	Pt/Silica Catalyst
0 (baseline)	0.423	0.321
3,000	0.347	0.285
6,000	0.266	0.267
10,000	0.113	0.217

The calculated ECASAs were summarized in Table 6-12. The ECASA of fresh Pt/Silica MEA (0.32 cm^2/mg) was smaller than that of commercial Pt/Carbon MEA (0.42 cm^2/mg); despite both the catalyst have a similar 10 wt. % Pt deposition on the support. That was because the dispersion of Pt was less uniform in Pt/Silica catalyst.
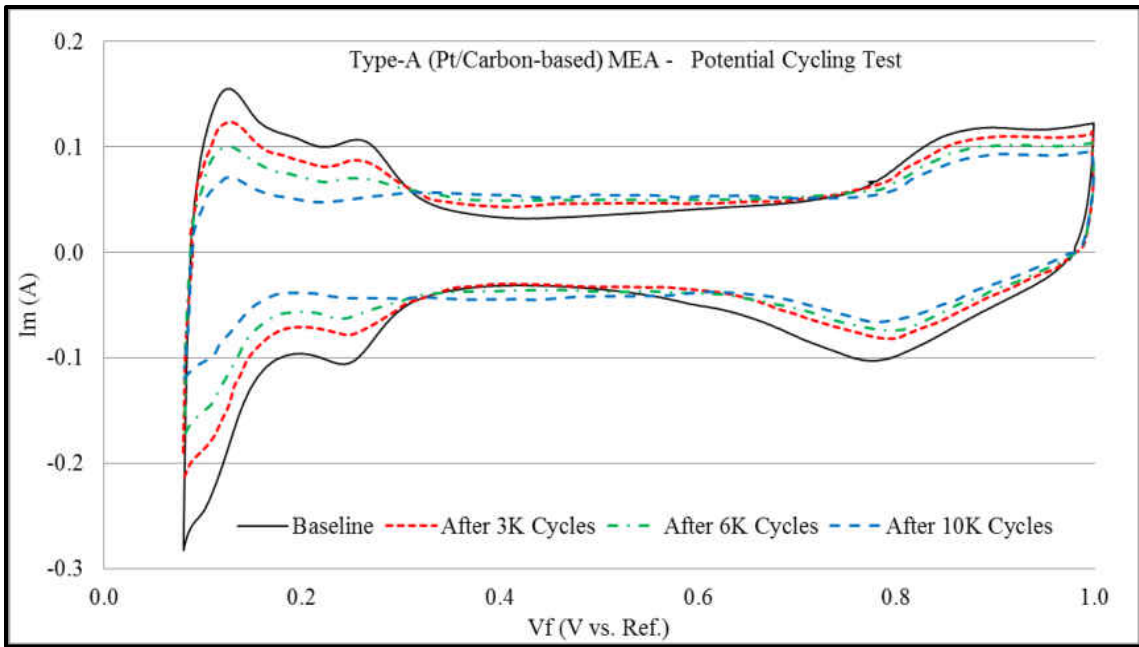
Figure 6-40 Effects of potential Cycling test on voltammograms of Type-A (Pt/Carbon-based) MEA
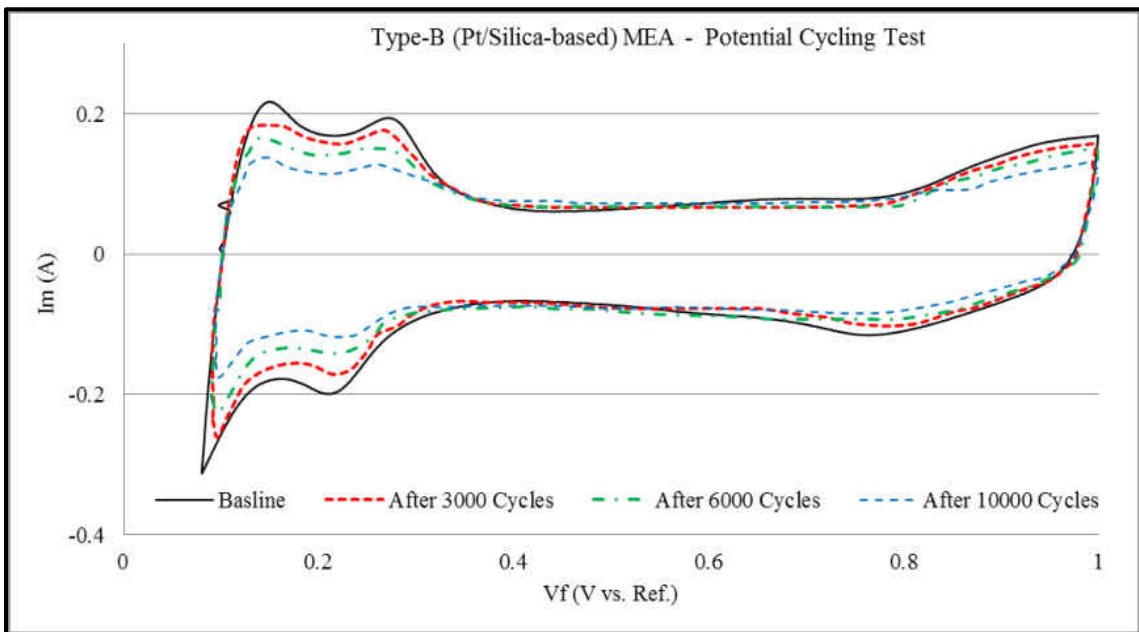
Figure 6-41 Effects of potential Cycling test on voltammograms of Type-B (Pt/Silica-based) MEA

As can be seen from Figure 6-41, no substantial change was observed in the CV of Pt/Silica even after 3,000 cycles. However, Pt/Carbon showed an apparent decrease in

the adsorption and desorption peaks after potential step cycles, as shown in Figure 6-40. These results were consistent with the potential holding experiments described above.

The ECASA of the novel Pt/Silica catalyst measured after the 10,000 cycles (0.217 cm2/ mg) was significantly higher than the commercial Pt/Carbon catalysts (0.113 cm2/mg). Moreover, the loss in ECASA of Pt/Silica was only by 33 % (from 0.321 to 0.217 cm^2/mg), while the loss in ECASA of commercial Pt/Carbon before and after potential cycling was 74 % (from 0.423 to 0.113 cm^2/mg). The ECASA and maximum power density of the two catalysts are summerized in Table 6-13.

Table 6-13 Durability in terms of ECASA and Maximum power density of the two catalysts

Sample	Maximum power Density (W/cm^2)			ECASA (cm^2/mg)			Specific Activity (A/m^2$_{Pt}$)		
	0 Cycles	10,000 Cycles	% loss	0 Cycles	10,000 Cycles	% loss	0 Cycles	10,000 Cycles	% loss
Pt/Carbon Based MEA	0.28	0.10	64	0.423	0.113	73	0.149	0.086	42.6
Pt/Silica Based MEA	0.22	0.12	44	0.321	0.217	32	0.111	0.087	25.9

Figure 6-42 shows normalized plots of ECASA vs. number of step cycles for Pt/Carbon and Pt/Silica electrodes. As expected from the CVs, the ECASA loss rate for Pt/Carbon is significantly large, whereas the ECASA of Pt/Silica was relatively stable within 10,000 step cycles under harsh conditions. The Pt/Carbon catalyst ECASA followed a steep linear decrease from 3,000 to 10,000 cycles. After 6,000 cycles, the

Pt/Carbon catalyst still shows higher decay rate (examined from the slopes as indicated in Figure 6-42), probably owing to smaller catalyst particle size compared to the silica supported catalyst. However, the in-house synthesized Pt/Silica is able to maintain its higher ECASA value even after the 6,000 potential cycles. Within the first 3,000 cycles, both catalysts have similar ECASA loss. However, the decay rate was slowed down for Pt/Silica catalyst at about 3,000 cycles.
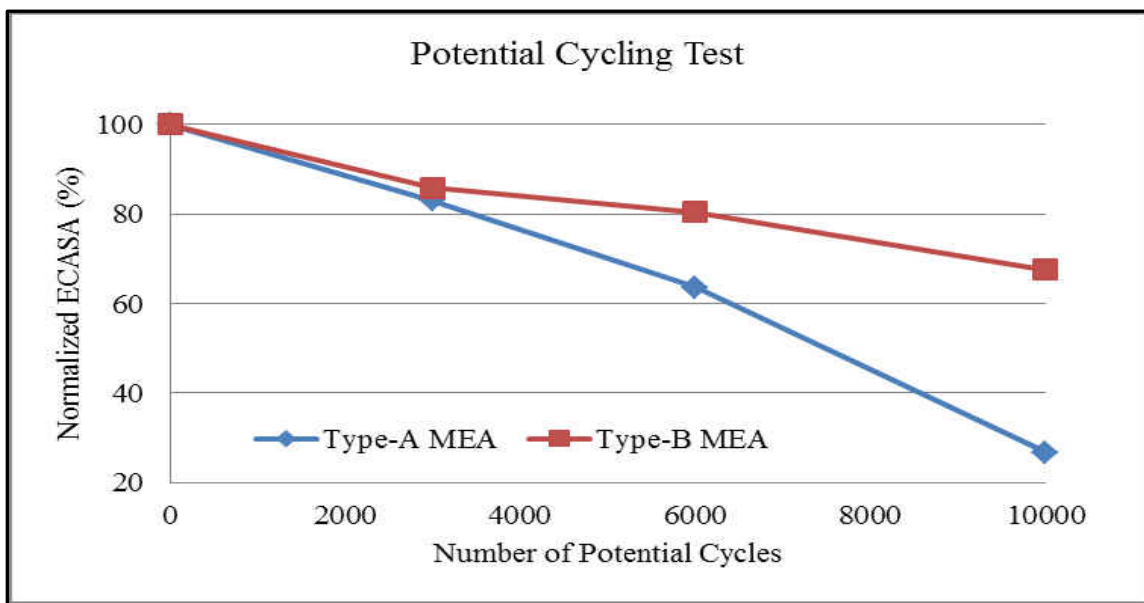
Figure 6-42 Comparison of loss of ECASA for the novel Pt/Silica with the commercial Pt/Carbon Catalyst

The results show that the Pt/Silica catalysts had the better stability since 68 % of the active Pt area was still available after 10,000 cycles. The Pt/Carbon catalyst deteriorated more severely compared to the silica support. The Pt/Carbon catalyst was able to retain only 27 % of the active Pt surface area after 10,000 cycles compared to the baseline area. The degradation on the ECASA after potential cycling can be ascribed to several factors, such as the size growth of Pt particle by $Pt-Pt$ aggregation, the

corrosion by oxidation of carbon support and the dissolving of Pt particles into the solution.

The results showed that the Pt/Silica catalyst sustained 74 % of its specific activity despite the harsh conditions of potential cycling. The specific activity of the Pt/Silica catalyst at the end of the 10,000-cycle test was found to be 0.082 A/m$^2_{Pt}$ vs. 0.111 A/m$^2_{Pt}$ at the baseline. The commercial Pt/Carbon catalyst sustained only 57 % of its specific activity.

Therefore, the silica-supported catalyst can be considered more electrochemically stable than the commercial carbon supported catalyst under the employed experimental conditions. The relatively high degree of stability of the silica support may also be attributed to the differences of the electronic conductivities associated with the two supports. The observed differences in performance and ECASA losses between the commercial Pt/C and Pt/Silica catalysts may be attributed to different surface morphologies. The results of this work show that the novel Pt/silica catalyst has less-pronounced decay rate in performance and ECASA than the commercial Pt/Carbon catalysts.

CHAPTER 7

7   EXPLORATORY STUDIES

The exploratory studies presented in this section were performed during this dissertation work. These studies were performed using the same unit-cell and the test-stand mentioned in section 4.3. MEA used in this study were commercial MEAs with 0.5 mg/cm^2 catalyst loadings purchased from FuelCell Store.

7.1   Novel Accelerated MEA Conditioning Protocol

The traditional procedures employed for MEA conditioning are classified as one step, and two step conditioning (Bi, Gray, & Fuller, 2007; Yuan, Zhang, Sun, & Wang, 2011; Yuan, Sun, Wang, & Li, 2012) with controlled cell voltage or current. In a one-step electrochemical conditioning, dry MEA is mounted in a fuel cell and exposed to fully humidified reactants on both anode and cathode side, followed by controlling the cell voltage or current at fuel cell operating condition until a steady state performance is achieved. In a two-step conditioning, first the MEA is hydrated off-line by submerging it in DI water for 60 minutes at 60 °C, and then it is mounted in PEMFC for on-line conditioning. The on-line fuel cell conditioning is done by controlling the cell voltage at 0.6 V until a steady state performance is achieved at fuel cell operating condition with fully humidified reactants.

Typically, during this conditioning period, the cell performance increases gradually, and then stabilized without further increase. Depending on the conditioning method used and the hot-press conditions employed during MEA fabrication, MEA conditioning can take hours and even days to complete. However, no standard measurement has been established to determine the effectiveness of a conditioning procedure. An ideal scenario is not only to have the highest possible power density after the conditioning procedure but also to minimize the activation completion time (Yuan et al., 2011).

Therefore an accelerated conditioning procedure was proposed, and its effectiveness was compared with the one-step and two-step conditioning procedures. In this novel two-step conditioning procedure, MEA was conditioned on-line after mounting in the fuel cell, first by flowing inert fluids on both electrodes of the fuel cell for 60 minutes. Deionized (DI) water was fed to the MEA anode side, and dry nitrogen gas was fed to the MEA cathode side. In the second step, the cell is maintained at a voltage of 0.6 V with fully humidified reactants (hydrogen and oxygen) until a steady current in obtained.

7.1.1 Experiments

A study was designed to investigate the effects of the proposed novel accelerated conditioning protocol on the activation completion time to attain a steady state current. During this study, the novel protocol was compared with the traditional one-step and two-step conditioning protocols. These three conditioning protocols were applied to identical MEAs (Type-C) with 0.5 mg/cm^2 of Platinum loading at same operation conditions.

In the novel method, Deionized (DI) water was fed to the MEA anode side, and dry nitrogen gas was fed to the MEA cathode side. DI water flow of 2.0 mL/min was archived using a mini-variable peristaltic pump (Fisher Scientific, Medium Flow: 0.4 to 85 mL/min). After the inert flow was established, the cell temperature (T_{Cell}) was brought to 50 °C, and these conditions were maintained for 60 minutes to ensure membrane humidification. During the MEA conditioning process, dehydrated electrolyte membrane and Nafion ionomer in the catalyst absorbs a lot of water to increase their ionic conductivities. Feed specifications for the novel MEA conditioning are listed in Table 7-1.

Table 7-1 Feed Specifications for the novel MEA Conditioning

Cell Condition	Anode Side	Cathode Side
Inert Fluid	DI Water	Dry Nitrogen
Flow (ml/min)	2.0	500
Cell Temperature (°C)	50	50
Duration (mins)	60	60

The electrodes were further activated to increase the extent of the triple phase boundary by operating the cell (T_{Cell}) at 60 °C. The cell was first purged with fully humidified nitrogen at 500 ml/min on both anode and cathode side for 15 min while heating the cell to reach 60 °C. The feed lines were set to at least 5 °C higher than the cell temperature. Once the set operating conditions were reached, nitrogen flow was switched to hydrogen and oxygen to the anode and cathode respectively. The operating conditions

used for all three conditioning protocols during electrode activation are summarized in the Table 7-2.

Table 7-2 Operating conditions for electrode activation for the three conditioning protocols

	Anode Side	Cathode Side
Reactants	Dry Hydrogen	Dry Oxygen
Cell Temperature (°C)	60	60
Stoichiometric Ratio (λ)	2.0	3.0
Relative Humidity (%)	100	100

All MEAs were subjected to the same conditions prior to testing and were tested at identical conditions on the same equipment to ensure a fair comparison. Before measurements, the MEA was mounted in a unit-cell as described in section 4.6 and was conditioned after the pre-integrity tests. Every MEA was preconditioned to hydrate fully, which allowed the fuel cell to reach its maximum performance that was determined by the steady state current at 0.6 V. After completion of the conditioning procedure, CV tests were conducted to evaluate the effectiveness of these protocol on the activation completion time to attain a steady state current

7.1.2 Results

Figure 7-1 illustrates the time required for an MEA activation to attain the steady state current at 0.6 V using the three MEA conditioning protocols. Clearly, the novel method is very effective in hydrating electrolyte membrane and activating the catalyst

layer. The novel method was 1.5 times faster than one step method and 1.3 times faster than two step method.

In one-step method, the water provided by the fully humidified reactants took almost 15 hours to hydrate the MEA fully and reach a steady state at 0.6 V. Since the MEA is under continuous operation, the flow of reactants forces the extra water on both reactants to push out of the cell, and as a result very limited amount of water is available to hydrate the membrane.
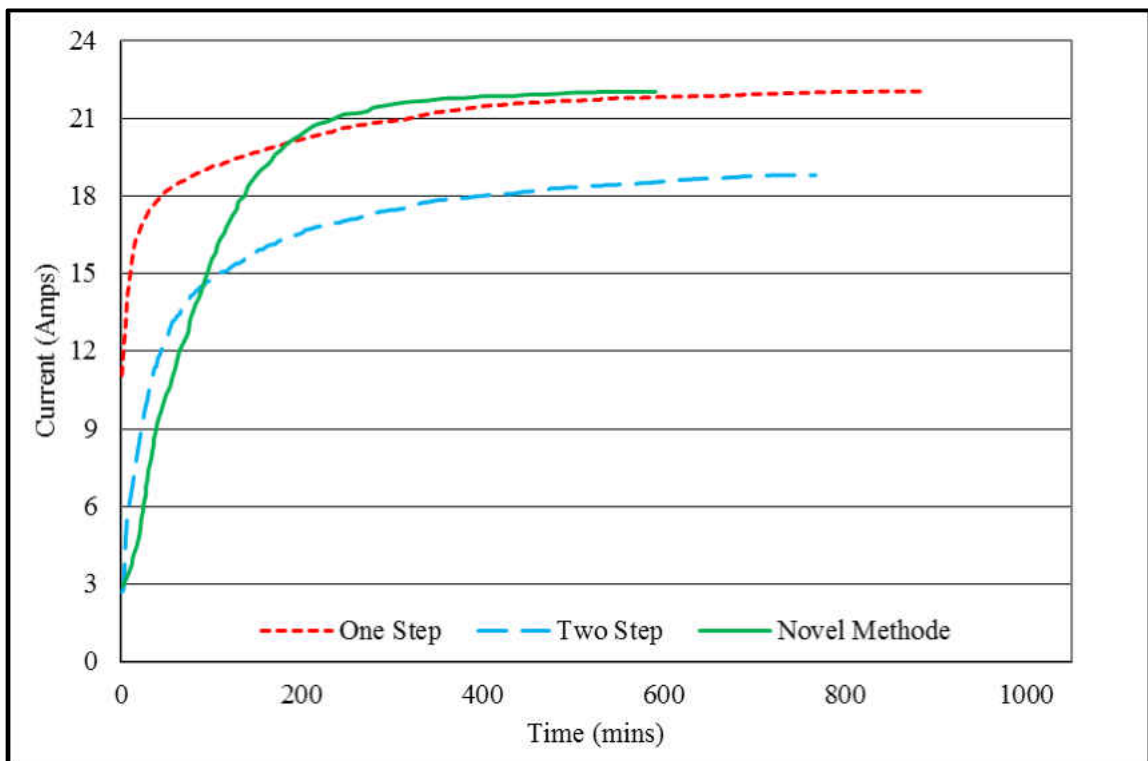
Figure 7-1 Time required for an MEA activation to attain the steady state current at 0.6 V using the three MEA conditioning protocols

In the two-step method, the current achieved at 0.6 V was 15 % less than both the one-step and novel method. It seems that immersing the MEA in DI water affects the intimate contact in the three-phase-boundary between the electrolyte membrane, catalyst

209

layer and gas diffusion layer. The electrolyte membrane swells with excess water during the immersion of MEA in DI water, which results in the less intimate contact between the electrolyte membrane and the electrodes.

The novel method gives the best performance in terms of both time and the steady-state current at 0.6 V after the test. Flowing DI water on only one side of the electrode, and dry nitrogen at a high flow rate on the other have affected positively. The flow of nitrogen on one side of MEA seems to have accelerated the MEA hydration process by dragging the water from one side of the MEA to the other side through the electrolyte membrane by convection. Also, since the MEA was held inside the cell under pressure before exposing to DI water, it has minimal effect of the intimacy between the various components of MEA when the electrolyte membrane swells. The time required for an MEA activation to attain the steady state current at 0.6 V with the steady state current using the three MEA conditioning protocols are summarized in Table 7-3.

Table 7-3 Time required for an MEA activation to attain the steady state current at 0.6 V with the steady state current using the three MEA conditioning protocols

Conditioning Method	Steady State Current at 0.6 V (A)	Time required to attain the steady state current (mins)
One Step	22.1	890
Two-Step	18.8	770
Novel Two Step	22.0	590

Although the highest performance was achieved by one-step method within 15 hours, similar performance could be yielded by the novel procedure within 10 hours.

Obtained results demonstrated that MEA conditioning under Novel method was an effective procedure that could significantly reduce the time of conditioning. However, the effect of the novel MEA conditioning procedure on the long-term performance and durability of the MEA needs to be studied in more details, because MEAs conditioning procedures can affect the microstructures of the conditioned MEA, which in turn, will affect its long-term behavior and durability.

7.2 Effects of freezing cycle on the performance and MEA durability of PEMFC

In order to meet automotive targets, PEM fuel cells must also be able to survive freezing temperatures. This section discusses the research efforts taken to conduct an investigation of the effects of sub-freezing conditions on a fuel cell performance and MEA durability. In this study, freezing temperature failure modes were investigated in PEM fuel cells using IV performance tests. The MEA was then removed from the cell and analyzed with electron microscopy to investigate its effect on MEA morphology. The obtained results under various freezing conditions are compared and discussed.

Due to the environmental chambers limitations, the experiments reported in this section were conducted at 0 °C and -10 °C.

7.2.1 Experiments

A fresh MEA was mounted in the cell and conditioned using the procedure outlined in section 4.5. Before the start of the cold experiment, a polarization curve was obtained at 70 °C as described in section (2.3) which serves as a baseline performance before cooldown. The unit-cell was then run at a steady state voltage of 0.6 V for 2 hours

to ensure that the MEA is fully saturated with water. The fuel cell load was then disconnected, and the dry nitrogen gas was used to purge both sides of the cell for 15 mins to remove excess water from the cell. The operating conditions used for the IV curve experiments are listed in Table 7-4.

Table 7-4 IV curve operating conditions for pre and post sub-freezing cycle

Variable	Anode Side	Cathode Side
Reactants	Dry Hydrogen	Dry Oxygen
Cell Temperature (°C)	70	70
Relative humidity (%)	100	100
Stoichiometric Flow Rate (λ)	2.0	3.0

The cell was then disconnected from the test stand and the reactant inlet, and outlet lines were sealed with Swagelok fittings as shown in Figure 7-2. The fuel cell inlet and outlet were sealed to ensure that no additional moisture from the environmental chamber enters the cell. The unit-cell was then kept inside the environmental chamber and cooled down to 0 °C. The cell was left at that temperature overnight before proceeding to the next step. During cooldown, the water content in the membrane was safely assumed to remain constant. This assumption can be justified by the fact that the cell stayed in the frozen state in the environmental chamber throughout. After the cooldown time, the cell was removed from the environmental chamber and kept on the bench top for 2 hours with the Swagelok fittings still on while warming up to the room temperature.
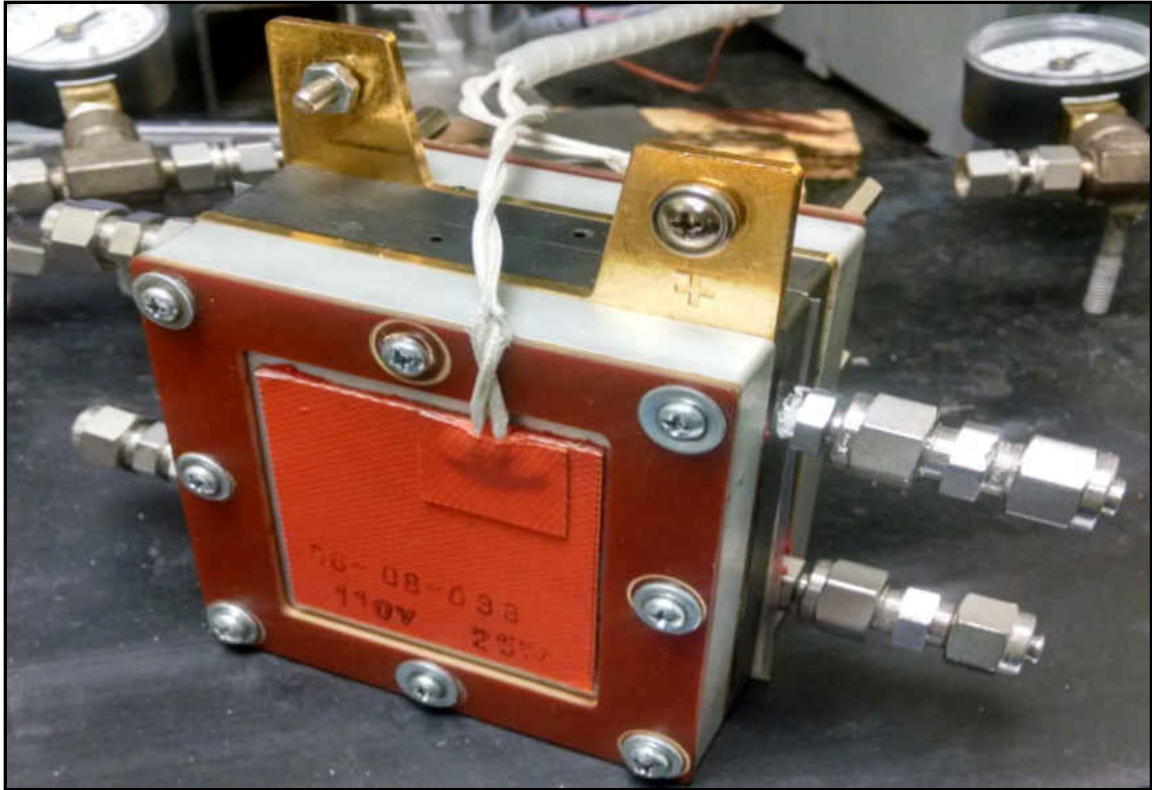
Figure 7-2 Unit-cell with inlets and outlets sealed with Swagelok fittings before keeping into the environmental chamber

The cell was finally mounted on the test stand and operated at 0.6 V for 2 hours to recover, and then the polarization curve was obtained. This IV curve characterizes the state of the electrode post-cooldown. The same procedure was followed to cool down the cell to − 10 °C using a fresh Type-C (commercial) MEA, and performance curves were obtained before and after the cool down procedures.

Research attempts were made to investigate the MEAs after cooldown experiment using electron spectroscopy. The microscopic analysis includes low magnification images to illustrate large-scale damage as well as high magnification images to determine if the damage is occurring to fine structures that would inhibit the electrochemical process or diffusion of reactants.

Since a piece an MEA had to cut as a representative sample of that MEA for electron microscopy investigation, a separate fresh MEA was used as a reference MEA. The images of this reference MEA was then used as a baseline MEA morphology.

7.2.2   Results

As mentioned in experimental procedure two IV curves were performed at 70 °C before and after each cooldown procedure. Electrochemical diagnostics found that the MEA cooled down to 0 °C does exhibit some performance degradation, and MEA cooled down to −10 °C suffers more performance degradation.
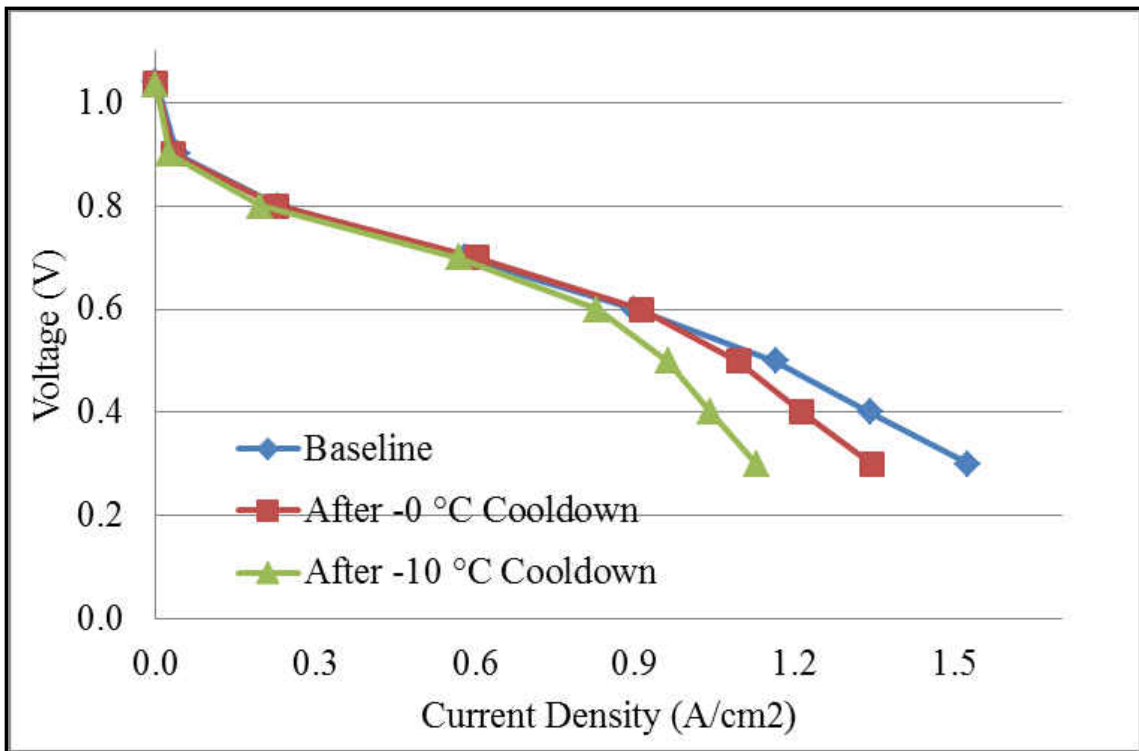
Figure 7-3 IV curves obtained during the cooldown cycle study

Figure 7-3 and Figure 7-4 are the IV curves and power curves obtained during this cooldown cycle study, and compare the baseline performance of the unit-cell with

cooldown temperature of 0 °C and -10 °C. Comparing to the baseline cell performance, there was very little difference between the three curves in the high voltage (low current density) region of 1.0 to 0.7 V. The difference in performance could be seen at 0.6 V for 0 °C cooldown temperature, while for -10 °C condition the performance difference started at 0.5 V. This polarization curve behavior indicate increased mass transport losses indicated by the performance drop at high current densities for the measurements performed after the cooldown procedure, compared to the baseline measurement. Since the mass transport losses were already minimized by using pure hydrogen and oxygen as reactant gasses, the mass transport losses could originate from the MEA structural damage caused by the effects of the cooldown cycle.
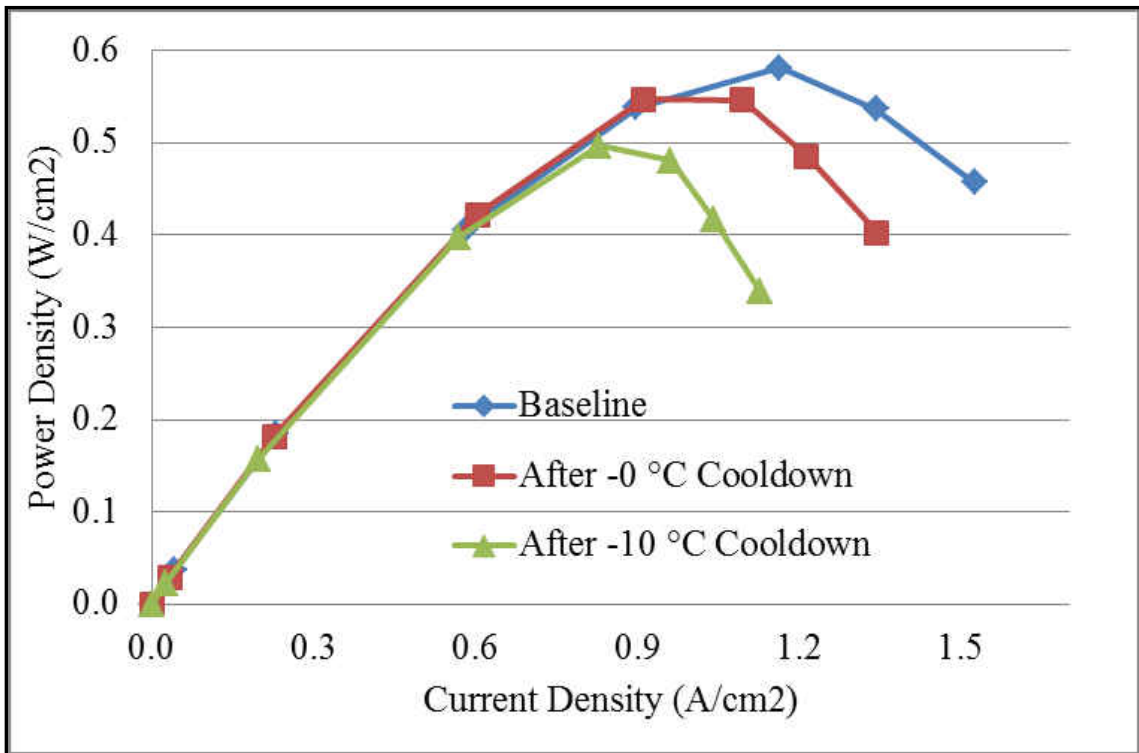
Figure 7-4 Power curves obtained during the cooldown cycle study

The performance loss was more evident, as the cooldown temperature decreased as shown in Figure 7-3 and Figure 7-4. For comparison, the performance decreased by 6 % at the maximum power density (from 0.58 to 0.55 W/cm^2) and the maximum current density obtained at 0.3 V was 11 % less (from 1.53 to 1.34 A/cm^2) than the baseline conditions for the 0 °C cooldown. A further 10-degrees decrease in cooldown cycle (-10 °C) resulted in a loss of 17 % of the maximum power density (from 0.58 to 0.48 W/cm^2) and the maximum current density obtained at 0.3 V was 26 % less (from 1.53 to 1.12 A/cm^2) than the baseline conditions.

Figure 7-5 is the SEM images for the fresh reference MEA, was used as th baseline MEA morphology. Images were taken from 35x to 350x magnification. The electrodes were not visible in this image since the catalyst layers were placed beneath the GDLs. The relatively flawless microstructure with smooth and uniformly distributed micro-porous layer (MPL) of Teflon and carbon on the GDL could be seen in Figure 7-5-a. The threaded woven layer is a GDL on which the MPL is deposited.
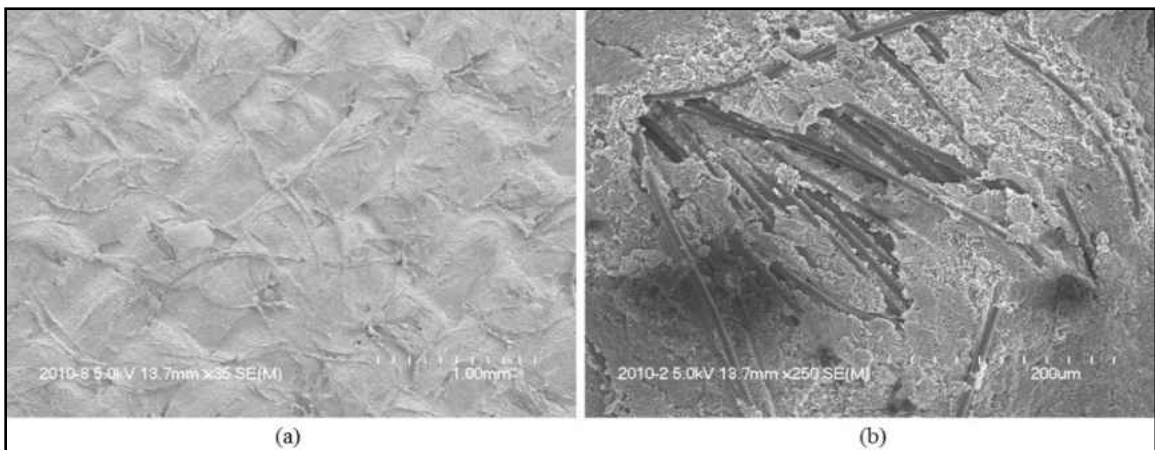
Figure 7-5 SEM images of the reference MEA (a) 35x magnification image (b) 250x magnification image

Figure 7-6 shows the SEM image of MEA after the cooldown experiment at 0 °C. The 35x magnification image of Figure 7-6-a shows a growing area of unwrapping MPL layer compared with that of Figure 7-5-a. MPL layer help retains water in the CL and also help uniformly distribute the reactants on the electrodes. The damage to the MPL resulted in the reduced performance. In Figure 7-7-b broken GDLs were noticed, but they were still intact in some regions of the MEA. These broken GDL were not observed in the reference images of Figure 7-5-b. This aged MEA indicates that there has been some degradation in this MEA; even after only one cooldown cycle, further degradation could be expected for repeated cooldown cycles.
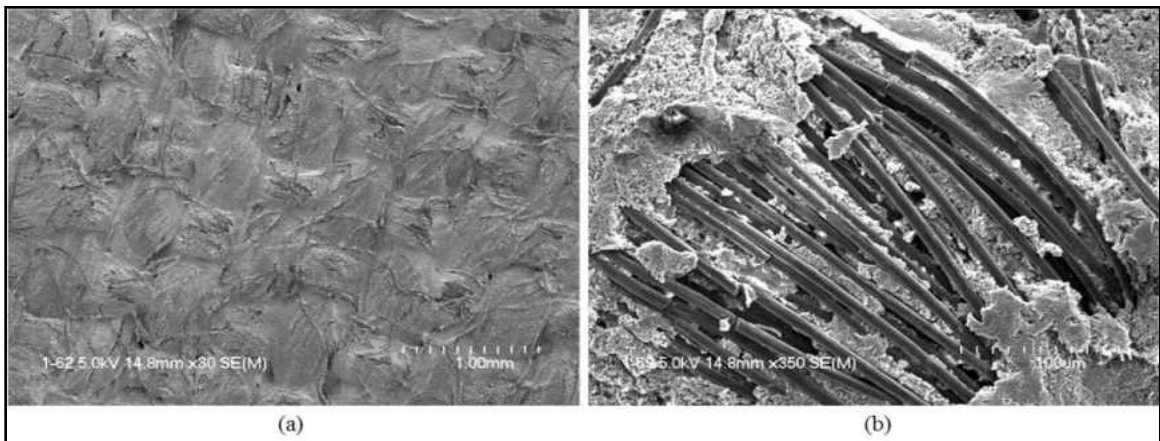
Figure 7-6 SEM images of MEA after the cooldown cycle at 0 °C (a) 30x magnification image (b) 350x magnification image

To verify the observations made during performance test cooldown experiment at -10 °C, images in Figure 7-7 show that cold temperature effects on the GDL were relatively significant. Figure 7-7-a shows a clear change in the MPL with increased unwrapped area as compared to the 0 °C experiment. High-magnification image (Figure 7-8-b) shows more severe damage to the GDLs which resulted in a significant drop in fuel cell performance in Figure 7-3 and Figure 7-4.
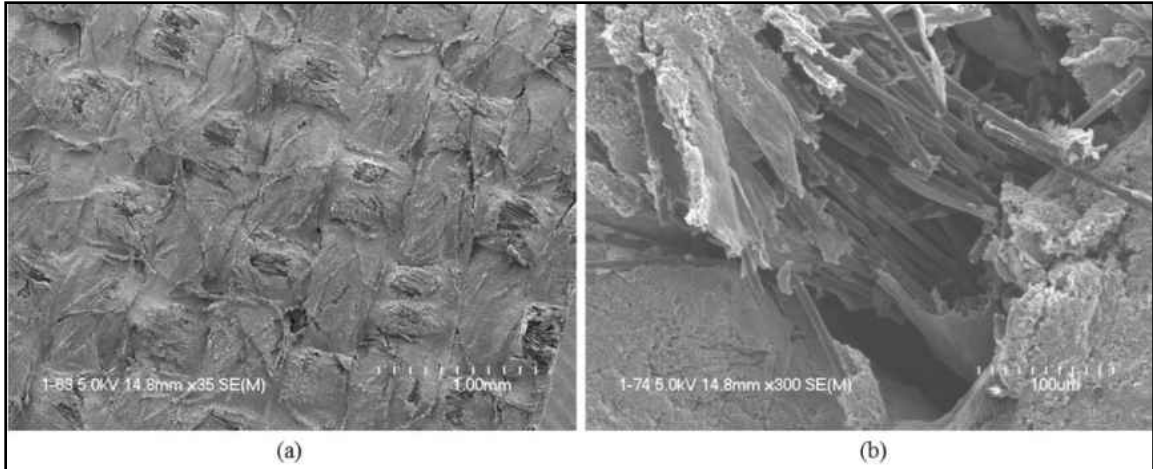
Figure 7-7 SEM images of MEA after the cooldown cycle at -10 °C (a) 30x magnification image (b) 300x magnification image

Even though further research is required to scrutinize the freezing temperature effects on MEAs, it can be concluded that fuel cell performance under sub-zero conditions would accelerate the MEA degradation. Moreover, this cooldown cycle (room temperature – subzero temperature – room temperature) is interesting as it represents a possible accelerated stress test (AST) protocol for the study of MEA degradation resulting from freezing conditions.

CHAPTER 8

8   SUMMARY AND RECCOMENDATIONS

This study was mainly focused on $in-situ$ characterization of a novel non-carbon support for platinum group metal (PGM) catalyst used in a PEMFC. The scope of this research work was related to improving the durability and lifetime, which will result in reducing the cost of the PEMFC technology. In this dissertation work, a series of experiments were conducted to evaluate the performance and durability of novel Pt/Silica catalyst using a 25 cm^2 active area unit-cell PEMFC.

The efforts of this work was focused on four primary tasks: (1) designing and fabricating a test station for controlled unit-cell characterization; (2) development of an MEA fabrication method to fabricate high performing MEAs in-house with consistent performance; (3) designing and conducting the performance tests to evaluate Pt/Silica catalyst in-situ performance in an MEA; and (4) designing and conducting the durability tests to evaluate Pt/Silica catalyst in-situ durability in an MEA. The results and contributions of the dissertation work are summarized below, and some personal opinions and suggestions for future work are provided.

A test stand was successfully designed and fabricated for a controlled unit-cell measurement; with a forced cathode gas supply, controlled humidification of the reactant gasses and precise temperature and gas flow rate control of the cell. Preliminary tests

with a commercial (Type-C) MEA and the experiments conducted on the sample (Type-A and Type-B) MEAs has successfully demonstrated that the test stand could reliably provide consistent conditions suitable for high-performance fuel cell operation and can reliably collect data. In addition to the control, the unit-cell characterization test-stand built for this research work is also capable of characterizing fuel cell stacks and water electrolyzer stacks.

A more challenging task of MEA fabrication method development to fabricate high performing MEAs in-house with consistent performance has been successfully completed. Cracking of the catalyst layer and catalyst ink diffusion through the GDL were the major problems faced during catalyst ink coating on GDL. A modified approach implemented a coating process on a heated hot plate at around 70 °C, and then oven drying the GDE after the coating process at 120 °C for 20 mins resulted in a crack-free surface. To avoid ink diffusion the paintbrush was dipped into the catalyst ink, and then pressed against the side of the vial to remove excess liquid before each coat was applied. Improper alignment of the GDE around the electrolyte membrane and discoloration of the electrolyte membrane during hot pressing were a major concern. Both of these concerns with the hot pressing were resolved with the modified method, which resulted in well aligned MEA with discoloration of the electrolyte membrane.

Experiments were conducted to validate the reproducibility of the in-house fabricated MEAs and their performance consistency. The reproducibility of the MEA was illustrated by the greatest catalyst loading difference of less than ± 0.05 mg/cm^2 ($\sim$16 %) with the targeted loading of 0.3 mg/cm^2. The key to achieve the consistent catalyst

loading was weighing the GDE after every layer of catalyst ink coating during catalyst application on the GDL. The performance results of the reproducibility test illustrated the consistency of the developed MEA fabrication processes. To verify the method developed to fabricate in-house MEA could produce high performing MEAs, a comparison study was performed with a commercial MEA with the similar loading of $0.3 \, \text{mg/cm}^2$. The in-house fabricated Type-A (Pt/Carbon electrodes) MEA was able to achieve 82 % power density of the commercial MEA at the same operating conditions.

A study was designed to investigate the performance of Pt/Silica catalyst in an MEA using a unit-cell, and its performance was compared with the commercial Pt/Carbon catalyst. The comparison was performed to test the first *hypothesis of this research that the Pt/Silica catalyst will achieve an equivalent power density of a Pt/Carbon catalyst in PEMFCs*. The performance of Pt/Silica catalyst, however, was found to be poor under the identical experimental setup and operating conditions. The Pt/Silica catalyst could only achieve 52 % of the maximum power density of the commercial Pt/Carbon catalyst. Similar results were demonstrated in CV testing, where the calculated ECASA of Pt/Silica catalyst was found to be 75 % of the commercial Pt/Carbon catalyst. The results indicated that the mass transport limitation was severe with Type-B (Pt/Silica catalyst) MEA. As a result, the current density of Type-B MEA was lower than Type-A (Pt/Carbon catalyst) MEA in the low voltage (high current density) region. Also, a more detailed analysis of Type-B (Pt/Silica catalyst) MEA in the concentration overpotential region reveals that the silica support due to its hydrophilic nature, was able to retain much water in the catalyst layer, and as a result, the electrodes

were flooded. Therefore it was hypothesized that the real cause for the less efficient triple-phase-boundary in Pt/Silica electrodes was (1) flooding of the catalyst layer in Pt/Silica electrodes at the testing environment (operating conditions), since the operating conditions chosen for this test were based on the Pt/Carbon catalyst from the literature, and (2) the low electronic conductivity of silica support caused a non-facile electronic and/or ionic flow path in the catalyst layer, which has contributed to the lower performances. In addition, there was a relatively non-uniform dispersion of Pt on silica, which was observed during the electron microscopy characterization.

Therefore, a study was designed and conducted to test the first sub-hypothesis that *the silica support in Pt/Silica catalyst was able to retain water in the catalyst layer which causes the electrode flooding*. The tests performed were focused on the water management in PEMFC. The effects of relative humidity of reactant gasses, the temperature of the unit-cell and stoichiometric flow rates on the performance of Pt/Silica catalyst were evaluated. A method of varying only one parameter at a time was adopted. Increasing the cathode stoichiometric flow rate by 33% (from 3.0 to 4.0) resulted in 23 % performance improvement. Similarly, humidification only on the anode side instead of the 100 % relative humidity on both sides increased the performance of the cell by 40 %. Increasing the cell temperature from 70 to 85 °C has resulted in an increase in the performance of the cell by 25 %. All these results clearly suggest that by managing the water content in the Pt/Silica catalyst layer, its performance could be improved.

The second sub-hypothesis for the lower performance of Pt/Silica catalyst was tested by designing a study to explore the possibility of using high conductive carbon

black as an additive in Pt/Silica catalyst ink. The incorporation of carbon black powder in the Pt/Silica electrodes with the catalyst deposited on the GDL turned out to be suitable for improving the performance of Pt/Silica catalyst by improving the electron flow path in the catalyst layer. The best results were obtained with a carbon loading of 7.5 % that has led to an increase in maximum power by 36 %.

Finally, two accelerated stress test (AST) studies were designed to investigate the durability of Pt/Silica catalyst in an MEA, and its durability was compared with the commercial Pt/Carbon catalyst. The comparison was performed to test the second hypothesis of this research that *the ECASA loss based on the AST test (potential hold and potential cycling) will be reduced for a Pt/Silica catalyst as compared to Pt/Carbon catalyst and thereby enhance the durability of PEMFCs*. The results of the 24-hour potentiostatic hold study showed that the loss of the specific activity of novel Pt/Silica catalyst at the end of the 24-hour test was 17 % from its baseline condition. The corresponding loss in commercial Pt/Carbon catalyst was found to be 36 %. The significant decrease in ECASA (55 %) of platinum in Type-A (Pt/carbon) catalysts was observed with potential hold time. Such a loss of surface area is reported in many papers, occurring during the potentiostatic hold. Whereas only 27% loss is observed for Pt/Silica, demonstrating that silica support was relatively stable within the potential hold time. Furthermore, most of the surface area loss (~16%) for the case of Pt/Silica occurs within the last 8 hours, indicating that silica support could potentially provide much higher durability than carbon support.

The results of the 10,000 cycles potential cycling test showed that the Pt/Silica catalysts had the better stability since 68 % of the active Pt area was still available after the 10,000 cycles test. The Pt/Carbon catalyst deteriorated more severely compared to the silica support. The Pt/Carbon catalyst was able to retain only 27 % of the active Pt surface area after 10,000 cycles compared to the baseline area. The Pt/Silica catalyst sustained 74 % of its specific activity despite the harsh conditions of potential cycling. The specific activity of the Pt/Silica catalyst at the end of the 10,000-cycle test was found to be 0.082 A/m^2_{Pt} vs. 0.111 A/m^2_{Pt} at the baseline. The commercial Pt/Carbon catalyst was managed to sustain only 57 % of its specific activity. The degradation on the ECASA after potential cycling can be ascribed to several factors, such as the size growth of Pt particle by $Pt-Pt$ aggregation, the corrosion by oxidation of carbon support and the dissolving of Pt particles into the solution.

During the durability testing, there was a loss in performance and ECASA observed in each case for both catalysts, consistent with platinum dissolution and agglomeration, and this was in line with expectations. Though silica has a relatively higher corrosion resistance, it was not designed to mitigate Pt dissolution. However, most interestingly, a relatively minimal detrimental impact on the performance of Pt/Silica catalyst was seen. The durability result suggests that the stability of the support is far more important than the stability of the platinum particles that are deposited onto the support in terms of avoiding cell failure. The fuel cell is likely to be much more forgiving of platinum dissolution and agglomeration.

8.1 Recommendations for Future Studies

It has been shown in this work that silica-supported platinum catalyst can be used to improve the *in-situ* durability of the PEMFC. However, the less uniform catalyst deposition on the support, hydrophilic nature and lower electronic conductivity of the silica support can pose a challenge in terms of obtaining a higher PEMFC performance.

Though lower electric conductivity issue has been dealt in this work by forming an MEA with "Pt/Silica + Carbon black powder", this technique does still use carbon which is the primary cause of catalyst degradation in PEMFC. Therefore optimizing "Pt/Silica + Carbon black powder" based MEA would not be a step in the right direction since this MEA would still be susceptible to carbon related degradation. One way to overcome this issue could be improving the electronic conductivity of the silica support by (1) doping it with some highly conductive material and/or (2) by making a composite support of silica with the highly conductive non-carbon material.

Using a higher amount of platinum content (> 10 % which was used in this study) could also be explored to see its effect on performance. A higher metal faction on the support could potentially help improve the electronic conductivity and reduce the water retention ability of Pt/Silica catalyst by reducing the amount of silica in the catalyst. Even though increasing the platinum fraction does not seem to fit in line with U.S. DOE target of reducing the total amount of catalyst in PEMFC, this could eventually result in reduced catalyst loading in an MEA. Therefore, the effect of the higher metal fraction on the performance is still worth evaluating.

CHAPTER 9

9 REFERENCES

1   A. V. D. Rosa. (2009). *Fundamentals of renewable energy sources* (2nd ed.) Elsevier Inc.

2   Agnolucci, P. (2007). Economics and market prospects of portable fuel cells. *International Journal of Hydrogen Energy, 32*(17), 4319-4328. doi:http://dx.doi.org/10.1016/j.ijhydene.2007.03.042

3   Andújar, J. M., & Segura, F. (2009). Fuel cells: History and updating. A walk along two centuries. *Renewable and Sustainable Energy Reviews, 13*(9), 2309-2322. doi:http://dx.doi.org/10.1016/j.rser.2009.03.015

4   Antolini, E. (2009). Carbon supports for low-temperature fuel cell catalysts. *Applied Catalysis B: Environmental, 88*(1–2), 1-24. doi:http://dx.doi.org/10.1016/j.apcatb.2008.09.030

5   Appleby, A. J., & Foulkes, F. R. (1993). *Fuel cell handbook*. Florida: Krieger Publishing Co.

6   Barbir, F. (2005a). CHAPTER 1 - introduction. In F. Barbir (Ed.), *PEM fuel cells* (pp. 1-16). Burlington: Academic Press. doi:http://dx.doi.org/10.1016/B978-012078142-3/50002-1

7   Barbir, F. (2005b). CHAPTER 3 - fuel cell electrochemistry. In F. Barbir (Ed.), *PEM fuel cells* (pp. 33-72). Burlington: Academic Press. doi:http://dx.doi.org/10.1016/B978-012078142-3/50004-5

227

8   Bi, W., Gray, G. E., & Fuller, T. F. (2007). PEM fuel cell Pt∕C dissolution and deposition in nafion electrolyte. *Electrochemical and Solid-State Letters, 10*(5), B101-B104. doi:10.1149/1.2712796

9   Borup, R. L., Davey, J. R., Garzon, F. H., Wood, D. L., & Inbody, M. A. (2006). PEM fuel cell electrocatalyst durability measurements. *Journal of Power Sources, 163*(1), 76-81. doi:http://dx.doi.org/10.1016/j.jpowsour.2006.03.009

10   Cengel, Y. A., & Boles, M. A. (2006). *Thermodynamics: An engineering approach* (5th ed., pp. 780) McGraw-Hill, New York.

11   Chen, J., Wang, M., Liu, B., Fan, Z., Cui, K., & Kuang, Y. (2006). Platinum catalysts prepared with functional carbon nanotube defects and its improved catalytic performance for methanol oxidation. *The Journal of Physical Chemistry B, 110*(24), 11775-11779. doi:10.1021/jp061045a

12   Cheng, X., Yi, B., Han, M., Zhang, J., Qiao, Y., & Yu, J. (1999). Investigation of platinum utilization and morphology in catalyst layer of polymer electrolyte fuel cells. *Journal of Power Sources, 79*(1), 75-81. doi:http://dx.doi.org/10.1016/S0378-7753(99)00046-4

13   Chunzhi He, Sanket Desai, & Garth Brown, and Srinivas Bollepalli. (2005). PEM fuel cell catalysts: Cost, performance, and durability. *The Electrochemical Society Interface, ,* 41-44.

14   Colmati, F., Paganin, V. A., & Gonzalez*, E. R. (2006). Effect of operational parameters of mini-direct methanol fuel cells operatingat ambient temperature. *Journal of Applied Electrochemistry, 36*(1), 17-23. doi:10.1007/s10800-005-9019-5

15 Darling, R. M., & Meyers, J. P. (2005). Mathematical model of platinum movement in PEM fuel cells. *Journal of the Electrochemical Society, 152*(1), A242-A247. doi:10.1149/1.1836156

16 de Bruijn, F. (2005). The current status of fuel cell technology for mobile and stationary applications. *Green Chemistry, 7*(3), 132-150. doi:10.1039/B415317K

17 Debe, M. K. (2011). Effect of electrode surface area distribution on high current density performance of PEM fuel cells. *Journal of the Electrochemical Society, 159*(1), B53-B66. doi:10.1149/2.032201jes

18 Fang, J., Qiao, J., Wilkinson, D. P., & Zhang, J. (2007). *Electrochemical polymer electrolyte membranes* CRC Press.

19 Feng, Y., Yao, R., & Zhang, L. (2004). Electronic properties of nanocrystalline tin oxide dispersed in monolithic mesoporous silica. *Physica B: Condensed Matter, 350*(4), 348-352. doi:http://dx.doi.org/10.1016/j.physb.2004.04.071

20 Fernandez, J. L., Walsh, D. A., & Bard, A. j. (2004). Thermodynamic guidelines for the design of bimetallic catalysts for oxygen electroreduction and rapid screening by scanning electrochemical microscopy. M−Co (M: Pd, ag, au). *J Am Chem Soc, 127*(1), 357-365.

21 Fernández, R., Ferreira-Aparicio, P., & Daza, L. (2005). PEMFC electrode preparation: Influence of the solvent composition and evaporation rate on the catalytic layer microstructure. *Journal of Power Sources, 151*, 18-24. doi:http://dx.doi.org/10.1016/j.jpowsour.2005.02.048

22   Ferreira, P. J., la O', G. J., Shao-Horn, Y., Morgan, D., Makharia, R., Kocha, S., & Gasteiger, H. A. (2005). Instability of Pt∕C electrocatalysts in proton exchange membrane fuel cells: A mechanistic investigation. *Journal of the Electrochemical Society, 152*(11), A2256-A2271. doi:10.1149/1.2050347

23   Frey, T., & Linardi, M. (2004a). Effects of membrane electrode assembly preparation on the polymer electrolyte membrane fuel cell performance. *Electrochimica Acta, 50*(1), 99-105. doi:http://dx.doi.org/10.1016/j.electacta.2004.07.017

24   Frey, T., & Linardi, M. (2004b). Effects of membrane electrode assembly preparation on the polymer electrolyte membrane fuel cell performance. *Electrochimica Acta, 50*(1), 99-105. doi:http://dx.doi.org/10.1016/j.electacta.2004.07.017

25   Gamburzev, S., & Appleby,A. (2002). Recent progress in performance improvement of the proton exchange membrane fuel cell (PEMFC). *Journal of Power Sources, 107*(1), 5-12. doi:http://dx.doi.org/10.1016/S0378-7753(01)00970-3

26   Gencoglu, M. T., & Ural, Z. (2009). Design of a PEM fuel cell system for residential application. *International Journal of Hydrogen Energy, 34*(12), 5242-5248. doi:http://dx.doi.org/10.1016/j.ijhydene.2008.09.038

27   Gittleman C, DM, Jorgensen S, Waldecker J, Hirano S, Mehall M. (2010). *Automotive fuel cell R&D needs.* (Workshop). Lakewood, Colorado: Department of Energy.

28   Greef, R., Peat, R., Peter, L., Pletcher, D., & Robinson, J. (1985). *Instrumental methods in electrochemistry*. Chichester,: Ellis Horwood Ltd.

29   Guilminot, E., Corcella, A., Charlot, F., Maillard, F., & Chatenet, M. (2007). Detection of pt z+ ions and pt nanoparticles inside the membrane of a used PEMFC. *Journal of the Electrochemical Society, 154*(1), B96-B105. doi:10.1149/1.2388863

30   Halder, A., Sharma, S., Hegde, M. S., & Ravishankar, N. (2009). Controlled attachment of ultrafine platinum nanoparticles on functionalized carbon nanotubes with high electrocatalytic activity for methanol oxidation. *The Journal of Physical Chemistry C, 113*(4), 1466-1473. doi:10.1021/jp8072574

31   Hamman, C. H., Hamnett. A., & Vielstich, W. (1998). *Electrochemistry* (1st ed.). Weinheim: Wiley-VCH.

32   Kangasniemi, K. H., Condit, D. A., & Jarvi, T. D. (2004). Characterization of vulcan electrochemically oxidized under simulated PEM fuel cell conditions. *Journal of the Electrochemical Society, 151*(4), E125-E132. doi:10.1149/1.1649756

33   Kirubakaran, A., Jain, S., & Nema, R. K. (2009). A review on fuel cell technologies and power electronic interface. *Renewable and Sustainable Energy Reviews, 13*(9), 2430-2440. doi:http://dx.doi.org/10.1016/j.rser.2009.04.004

34   Kocha, S. (2003). *Principles of MEA preparation, handbook of fuel cells, technology and applications* (3rd ed.) John Wiley & Sons.

35   Kordesch, K., & Simader, G. (1996). *Fuel cells and their applications*. Weinheim: VCH.

36   Kua, J., & Goddard, W. A. (1999). Oxidation of methanol on 2nd and 3rd row group VIII transition metals (pt, ir, os, pd, rh, and ru): Application to direct methanol fuel cells. *Journal of the American Chemical Society, 121*(47), 10928-10941. doi:10.1021/ja9844074

37   Kumpulainen, H., Peltonen, T., Koponen, U., Bergelin, M., Valkiainen, M., & Wasberg, M. (2002). *In situ voltammetric characterization of PEM fuel cell catalyst layers.* (No. VTT RESEARCH NOTES 2137).JULKAISIJA - UTGIVARE.

38   Küver, A., Vogel, I., & Vielstich, W. (1994). Distinct performance evaluation of a direct methanol SPE fuel cell. A new method using a dynamic hydrogen reference electrode. *Journal of Power Sources, 52*(1), 77-80. doi:http://dx.doi.org/10.1016/0378-7753(94)01943-6

39   Larminie, J., & Andrew, D. (2003). Proton exchange membrane fuel cells. *Fuel cell systems explained* (2nd ed., pp. 112). Chichester: John Wiley & Sons Ltd.

40   Larminie, J., & Dicks, A. (2000). *Fuel cell systems explained.* Chichester: John Wiley & Sons Ltd.

41   Lázaro, M. J., Calvillo, L., Celorrio, V., Pardo, J. I., Perathoner, S., & Moliner, R. (2011). *Study and application of carbon black vulcan xc-72r in polymeric electrolyte fuel cells.* ().Nova Science Publishers, Inc.

42   Lee, K., Zhang, J., Wang, H., & Wilkinson, P. D. (2006). Progress in the synthesis of carbon nanotube- and nanofiber-supported pt electrocatalysts for PEM fuel cell catalysis. *Journal of Applied Electrochemistry, 36*(5), 507-522. doi:10.1007/s10800-006-9120-4

43   Lee, S. J., Mukerjee, S., McBreen, J., Rho, Y. W., Kho, Y. T., & Lee, T. H. (1998). Effects of nafion impregnation on performances of PEMFC electrodes. *Electrochimica Acta, 43*(24), 3693-3701. doi:http://dx.doi.org/10.1016/S0013-4686(98)00127-3

44   LI, X. (2005). *Principles of fuel cells*. New York: Taylor & Francis.

45   Li, A., Zhao, J. X., & Pierce, D. T. (2010). Silica nanoparticles for template synthesis of supported pt and Pt–Ru electrocatalysts. *Journal of Colloid and Interface Science, 351*(2), 365-373. doi:http://dx.doi.org/10.1016/j.jcis.2010.07.068

46   Li, X., Geng, D., Zhang, Y., Meng, X., Li, R., & Sun, X. (2011). Superior cycle stability of nitrogen-doped graphene nanosheets as anodes for lithium ion batteries. *Electrochemistry Communications, 13*(8), 822-825. doi:http://dx.doi.org/10.1016/j.elecom.2011.05.012

47   Lim, D., Lee, W., Wheldon, J., Macy, N. L., & Smyrl, W. H. (2010). Electrochemical characterization and durability of sputtered pt catalysts on TiO2 nanotube arrays as a cathode material for PEFCs. *Journal of the Electrochemical Society, 157*(6), B862-B867. Retrieved from http://jes.ecsdl.org/content/157/6/B862.abstract

48   Lin, C., Cui, T., Chien, C., Tan, J., Chao, Y., & Van Zee, J. W. (2011). Dynamic mechanical properties of polymeric materials aged in PEM fuel cell conditions. In T. Proulx (Ed.), *Experimental and applied mechanics, volume 6: Proceedings of the 2011 annual conference on experimental and applied mechanics* (pp. 31-35). New York, NY: Springer New York. doi:10.1007/978-1-4614-0222-0_5

49   Lin, Y., Cui, X., Yen, C., & Wai, C. M. (2005). Platinum/carbon nanotube nanocomposite synthesized in supercritical fluid as electrocatalysts for low-temperature fuel cells. *The Journal of Physical Chemistry B, 109*(30), 14410-14415. doi:10.1021/jp0514675

50   Litster, S., & McLean, G. (2004). PEM fuel cell electrodes. *Journal of Power Sources, 130*(1–2), 61-76. doi:http://dx.doi.org/10.1016/j.jpowsour.2003.12.055

51   Mark F Mathias, Rohit Makharia, Hubert A Gasteiger, Jason J Conley, Timothy J Fuller, Craig J Gittleman, Shyam S Kocha, Daniel P Miller, Corky K Mittelsteadt, Tao Xie, SG Van, Paul T Yu. (2005). Two fuel cell cars in every garage. *Electrochem. Soc. Interface, 14*(3), 24-35.

52   Mennola, T., Mikkola, M., Noponen, M., Hottinen, T., & Lund, P. (2002). Measurement of ohmic voltage losses in individual cells of a PEMFC stack. *Journal of Power Sources, 112*(1), 261-272. doi:http://dx.doi.org/10.1016/S0378-7753(02)00391-9

53   Mert, S. O., Dincer, I., & Ozcelik, Z. (2012). Performance investigation of a transportation PEM fuel cell system. *International Journal of Hydrogen Energy, 37*(1), 623-633. doi:http://dx.doi.org/10.1016/j.ijhydene.2011.09.021

54   Millington, B., Du, S., & Pollet, B. G. (2011). The effect of materials on proton exchange membrane fuel cell electrode performance. *Journal of Power Sources, 196*(21), 9013-9017. doi:http://dx.doi.org/10.1016/j.jpowsour.2010.12.043

55   Minh, N. Q., & Takahashi, T. (1995a). Chapter 1 - introduction. In N. Q. M. Takahashi (Ed.), *Science and technology of ceramic fuel cells* (pp. 1-14). Oxford: Elsevier Science Ltd. doi:http://dx.doi.org/10.1016/B978-044489568-4/50002-5

56 Minh, N. Q., & Takahashi, T. (1995b). Chapter 5 - cathode. In N. Q. M. Takahashi (Ed.), *Science and technology of ceramic fuel cells* (pp. 117-146). Oxford: Elsevier Science Ltd. doi:http://dx.doi.org/10.1016/B978-044489568-4/50006-2

57 Nafion® material specification sheet. (2001). Retrieved from http://ion-power.com/nafion/naf001.html

58 O'Hayre, R., Lee, S., Cha, S., & Prinz, F. B. (2002). A sharp peak in the performance of sputtered platinum fuel cells at ultra-low platinum loading. *Journal of Power Sources, 109*(2), 483-493. doi:http://dx.doi.org/10.1016/S0378-7753(02)00238-0

59 Paganin, V. A., Ticianelli, E. A., & Gonzalez, E. R. (1996). Development and electrochemical studies of gas diffusion electrodes for polymer electrolyte fuel cells. *Journal of Applied Electrochemistry, 26*(3), 297-304. doi:10.1007/BF00242099

60 Park, J., Lee, J., Sauk, J., & Son, I. (2008). The operating mode dependence on electrochemical performance degradation of direct methanol fuel cells. *International Journal of Hydrogen Energy, 33*(18), 4833-4843. doi:http://dx.doi.org/10.1016/j.ijhydene.2008.04.060

61 Passalacqua, E., Lufrano, F., Squadrito, G., Patti, A., & Giorgi, L. (2001). Nafion content in the catalyst layer of polymer electrolyte fuel cells: Effects on structure and performance. *Electrochimica Acta, 46*(6), 799-805. doi:http://dx.doi.org/10.1016/S0013-4686(00)00679-4

62   Paul T. Yu, Wenbin Gu, Jingxin Zhang, Rohit Makharia, Frederick T. Wagner, Hubert A. Gasteiger. (2009). Carbon-support requirements for highly durable fuel cell operation. In Felix N. Büchi, Minoru Inaba, Thomas J. Schmidt (Ed.), *Polymer electrolyte fuel cell durability* (pp. 29-53). New York: Springer.

63   Pharkya, P., Alfantazi, A., & Farhat, Z. (2005). Fabrication using high-energy ball-milling technique and characterization of pt-co electrocatalysts for oxygen reduction in polymer electrolyte fuel cells. *ASME. J. Fuel Cell Sci. Technol., 2*(3), 171-178. doi:10.1115/1.1895985.

64   Qi, Z., & Kaufman, A. (2003). Low pt loading high performance cathodes for PEM fuel cells. *Journal of Power Sources, 113*(1), 37-43. doi:http://dx.doi.org/10.1016/S0378-7753(02)00477-9

65   Ralph, T. R., Hards, G. A., Keating, J. E., Campbell, S. A., Wilkinson, D. P., Davis, M., . . . Johnson, M. C. (1997). Low cost electrodes for proton exchange membrane fuel cells: Performance in single cells and ballard stacks. *Journal of the Electrochemical Society, 144*(11), 3845-3857. doi:10.1149/1.1838101

66   Rodgers, M. P., Mohajeri, N., Bonville, L. J., & Slattery, D. K. (2012). Accelerated testing of polymer electrolyte membranes in fuel cells containing pt/C and PtCo/C catalysts. *Journal of the Electrochemical Society, 159*(5), B564-B569. doi:10.1149/2.094205jes

67   Roen, L. M., Paik, C. H., & Jarvi, T. D. (2004). Electrocatalytic corrosion of carbon support in PEMFC cathodes. *Electrochemical and Solid-State Letters, 7*(1), A19-A22. doi:10.1149/1.1630412

68   Sasikumar, G., Ihm, J. W., & Ryu, H. (2004a). Dependence of optimum nafion content in catalyst layer on platinum loading. *Journal of Power Sources, 132*(1–2), 11-17. doi:http://dx.doi.org/10.1016/j.jpowsour.2003.12.060

69   Sasikumar, G., Ihm, J. W., & Ryu, H. (2004b). Optimum nafion content in PEM fuel cell electrodes. *Electrochimica Acta, 50*(2–3), 601-605. doi:http://dx.doi.org/10.1016/j.electacta.2004.01.126

70   Shin, S. -., Lee, J. -., Ha, H. -., Hong, S. -., Chun, H. -., & Oh, I. -. (2002). Effect of the catalytic ink preparation method on the performance of polymer electrolyte membrane fuel cells. *Journal of Power Sources, 106*(1–2), 146-152. doi:http://dx.doi.org/10.1016/S0378-7753(01)01045-X

71   Shui, J., & Li, J. C. M. (2009). Platinum nanowires produced by electrospinning. *Nano Letters, 9*(4), 1307-1314. doi:10.1021/nl802910h

72   Siroma, Z., Ishii, K., Yasuda, K., Miyazaki, Y., Inaba, M., & Tasaka, A. (2005). Imaging of highly oriented pyrolytic graphite corrosion accelerated by pt particles. *Electrochemistry Communications, 7*(11), 1153-1156. doi:http://dx.doi.org/10.1016/j.elecom.2005.08.014

73   Song, J. M., Suzuki, S., Uchida, H., & Watanabe, M. (2006). Preparation of high catalyst utilization electrodes for polymer electrolyte fuel cells. *Langmuir, 22*(14), 6422-6428. doi:10.1021/la060671w

74   Springer, T. E., Zawodzinski, T. A., & Gottesfeld, S. (1991a). Polymer electrolyte fuel cell model. *Journal of the Electrochemical Society, 138*(8), 2334-2342. doi:10.1149/1.2085971

75   Springer, T. E., Zawodzinski, T. A., & Gottesfeld, S. (1991b). Polymer electrolyte fuel cell model. *Journal of the Electrochemical Society, 138*(8), 2334-2342. doi:10.1149/1.2085971

76   Sun, L., Ran, R., & Shao, Z. (2010). Fabrication and evolution of catalyst-coated membranes by direct spray deposition of catalyst ink onto nafion membrane at high temperature. *International Journal of Hydrogen Energy, 35*(7), 2921-2925. doi:http://dx.doi.org/10.1016/j.ijhydene.2009.05.049

77   Sun, L., Ran, R., Wang, G., & Shao, Z. (2008). Fabrication and performance test of a catalyst-coated membrane from direct spray deposition. *Solid State Ionics, 179*(21–26), 960-965. doi:http://dx.doi.org/10.1016/j.ssi.2008.01.081

78   Tang, H., Wang, S., Jiang, S. P., & Pan, M. (2007). A comparative study of CCM and hot-pressed MEAs for PEM fuel cells. *Journal of Power Sources, 170*(1), 140-144. doi:http://dx.doi.org/10.1016/j.jpowsour.2007.03.062

79   Thanasilp, S., & Hunsom, M. (2010). Effect of MEA fabrication techniques on the cell performance of Pt–Pd/C electrocatalyst for oxygen reduction in PEM fuel cell. *Fuel, 89*(12), 3847-3852. doi:http://dx.doi.org/10.1016/j.fuel.2010.07.008

80   Therdthianwong, A., Ekdharmasuit, P., & Therdthianwong, S. (2010). Fabrication and performance of membrane electrode assembly prepared by a catalyst-coated membrane method: Effect of solvents used in a catalyst ink mixture. *Energy Fuels, 24*(2), 1191-1196. doi:10.1021/ef901105k

81   Ticianelli, E. A., Derouin, C. R., Redondo, A., & Srinivasan, S. (1988). Methods to advance technology of proton exchange membrane fuel cells. *Journal of the Electrochemical Society, 135*(9), 2209-2214. doi:10.1149/1.2096240

82   U. S. D. o. E. E. E. a. R. Energy. (2011). *Type of fuel cells.* ().

83   Uchida, M., Aoyama, Y., Eda, N., & Ohta, A. (1995). Investigation of the microstructure in the catalyst layer and effects of both perfluorosulfonate ionomer and PTFE-loaded carbon on the catalyst layer of polymer electrolyte fuel cells. *Journal of the Electrochemical Society, 142*(12), 4143-4149. doi:10.1149/1.2048477

84   Uchida, M., Fukuoka, Y., Sugawara, Y., Ohara, H., & Ohta, A. (1998). Improved preparation process of very-low-platinum-loading electrodes for polymer electrolyte fuel cells. *Journal of the Electrochemical Society, 145*(11), 3708-3713. doi:10.1149/1.1838863

85   Vogel, J. (2008). *U.S. DOE hydrogen program 2008.* (Annual Progress Report).

86   Wang, H., Yuan, X., & Li, H. (2011). *PEM fuel cell diagnostic tools* CRC Press.

87   Wang, J., Yin, G., Shao, Y., Zhang, S., Wang, Z., & Gao, Y. (2007). Effect of carbon black support corrosion on the durability of pt/C catalyst. *Journal of Power Sources, 171*(2), 331-339. doi:http://dx.doi.org/10.1016/j.jpowsour.2007.06.084

88   Wang, Y., Wilkinson, D. P., & Zhang, J. (2011). Noncarbon support materials for polymer electrolyte membrane fuel cell electrocatalysts. *Chemical Reviews, 111*(12), 7625-7651. doi:10.1021/cr100060r

89   Weaver. (2002). 4 - market and application analysis. In Weaver, (Ed.), *World fuel cells* (pp. 29-79). Oxford: Elsevier Science Ltd. doi:http://dx.doi.org/10.1016/B978-185617397-1/50004-6

90   Wilson, M. S., & Gottesfeld, S. (1992). High performance catalyzed membranes of ultra-low pt loadings for polymer electrolyte fuel cells. *Journal of the Electrochemical Society, 139*(2), L28-L30. doi:10.1149/1.2069277

91   Wu, J., Yuan, X. Z., Wang, H., Blanco, M., Martin, J. J., & Zhang, J. (2008). Diagnostic tools in PEM fuel cell research: Part I electrochemical techniques. *International Journal of Hydrogen Energy, 33*(6), 1735-1746. doi:http://dx.doi.org/10.1016/j.ijhydene.2008.01.013

92   Xiong, L., & Manthiram, A. (2005). High performance membrane-electrode assemblies with ultra-low pt loading for proton exchange membrane fuel cells. *Electrochimica Acta, 50*(16–17), 3200-3204. doi:http://dx.doi.org/10.1016/j.electacta.2004.11.049

93   Yan, X., Hou, M., Zhang, H., Jing, F., Ming, P., & Yi, B. (2006). Performance of PEMFC stack using expanded graphite bipolar plates. *Journal of Power Sources, 160*(1), 252-257. doi:http://dx.doi.org/10.1016/j.jpowsour.2006.01.022

94   Yasuda, K., Taniguchi, A., Akita, T., Ioroi, T., & Siroma, Z. (2006). Platinum dissolution and deposition in the polymer electrolyte membrane of a PEM fuel cell as studied by potential cycling. *Physical Chemistry Chemical Physics, 8*(6), 746-752. doi:10.1039/B514342J

95   Yoda, T., Uchida, H., & Watanabe, M. (2007). Effects of operating potential and temperature on degradation of electrocatalyst layer for PEFCs. *Electrochimica Acta, 52*(19), 5997-6005. doi:http://dx.doi.org/10.1016/j.electacta.2007.03.049

96 Yoshida, H., Kinumoto, T., Iriyama, Y., Uchimoto, Y., & Ogumi, Z. (2007). XAS study for degradation mechanism of pt/C catalyst during potential cycling test. *ECS Transactions, 11*(1), 1321-1329. doi:10.1149/1.2781045

97 Yu, P., Pemberton, M., & Plasse, P. (2005). PtCo/C cathode catalyst for improved durability in PEMFCs. *Journal of Power Sources, 144*(1), 11-20. doi:http://dx.doi.org/10.1016/j.jpowsour.2004.11.067

98 Yuan, X., Zhang, S., Sun, J. C., & Wang, H. (2011). A review of accelerated conditioning for a polymer electrolyte membrane fuel cell. *Journal of Power Sources, 196*(22), 9097-9106. doi:http://dx.doi.org/10.1016/j.jpowsour.2011.06.098

99 Zawodzinski, T. A., Springer, T. E., Uribe, F., & Gottesfeld, S. (1993). Characterization of polymer electrolytes for fuel cell applications. *Solid State Ionics, 60*(1), 199-211. doi:http://dx.doi.org/10.1016/0167-2738(93)90295-E

100 Zhang, J., Yin, G., Wang, Z., Lai, Q., & Cai, K. (2007). Effects of hot pressing conditions on the performances of MEAs for direct methanol fuel cells. *Journal of Power Sources, 165*(1), 73-81. doi:http://dx.doi.org/10.1016/j.jpowsour.2006.12.039